INVESTIGATION OF EMT-LIKE PHENOTYPES IN ESTABLISHED AND NOVEL MODEL SYSTEMS OF INVASIVE LOBULAR BREAST CARCINOMA

by

Emily Ann Bossart

B.S., Molecular Biology and Biochemistry, Penn State Erie, The Behrend College, 2012

Submitted to the Graduate Faculty of

the School of Medicine in partial fulfillment

of the requirements for the degree of

PhD in Molecular Pharmacology

University of Pittsburgh

2018

UNIVERSITY OF PITTSBURGH

SCHOOL OF MEDICINE

This dissertation was presented

by

Emily Ann Bossart

It was defended on

February 12, 2018

and approved by

Donald DeFranco, PhD, Professor, Pharmacology & Chemical Biology

Adam Feinberg, PhD, Professor, Materials Science & Engineering, Biomedical Engineering

Adrian Lee, PhD, Professor, Pharmacology & Chemical Biology

Timothy Burns, MD, PhD, Assistant Professor, Pharmacology & Chemical Biology

Dissertation Advisor: Steffi Oesterreich, PhD, Professor, Pharmacology & Chemical Biology

INVESTIGATION OF EMT-LIKE PHENOTYPES IN ESTABLISHED AND NOVEL MODEL SYSTEMS OF INVASIVE LOBULAR BREAST CARCINOMA

Emily Ann Bossart, PhD

University of Pittsburgh, 2018

Invasive Lobular Carcinoma (ILC) is an understudied, unique subtype of breast cancer. E-cadherin (*CDH1*) loss is a hallmark of ILC that contributes to its many observed epithelial to mesenchymal transition (EMT)-like features. Though ILCs predominantly express clinically actionable target estrogen receptor alpha (ERα), common late recurrences suggest a role for endocrine therapy resistance. We recently identified *de novo* resistance to the partial estrogen receptor antagonist/agonist Tamoxifen (4OHT) in MDA-MB-134-VI ILC cells that was accompanied by upregulation of EMT transcription factor (EMT-TF) SNAIL (*SNAI1*). We therefore hypothesized that 4OHT induction of SNAIL contributes to endocrine therapy resistance in a subset of ILCs. We demonstrated estrogen induction of *SNAI1* in multiple invasive ductal carcinoma (IDC) and ILC cell lines. In contrast, 4OHT induction of *SNAI1* was restricted to ILC cells tested, and was associated with recruitment of ERα to the *SNAI1* promoter. We observed upregulation of additional EMT genes in ILC cells, partially translatable to clinical samples. However, 4OHT regulation of SNAIL was unique, thus we pursued study of SNAIL-mediated phenotypes in ILC cells. Unfortunately, manipulation of SNAIL levels in ILC cells was challenging, with expression rebound in stable constitutive knockdown/overexpression attempts. Inducible SNAIL overexpression revealed unexpected repression of 2D and 3D proliferation. These data suggest a role for SNAIL in unexplored, critical ILC phenotypes (e.g. tumor dormancy). Lack of ILC models for these studies highlighted need for novel ILC cell lines. We therefore established and

characterized ILC cell line WCRC-25 from a pleural effusion from a patient with ER^+ ILC. WCRC-25 maintained phenotypes consistent with other ILC cells (e.g. slow proliferation, poor soft agar formation). We identified a somatic *CDH1* mutation (2240C>T, p.Q706*) in gDNA from WCRC-25 that we confirmed in liquid biopsies from the patient. DNA/RNA sequencing analyses are being performed using clinical samples from the patient. While loss of ER impeded testing endocrine therapy resistance in WCRC-25 cells, additional drug responses revealed sensitivity to a PI3K inhibitor. In summary, these studies provided the foundation for better understanding of the role of EMT-TF SNAIL in endocrine therapy resistance, and led to establishment and characterization of a novel ILC research tool.

TABLE OF CONTENTS

LIST OF TABLES

LIST OF FIGURES

PREFACE

So we do not lose heart. Though our outer self is wasting away, our inner self is being renewed day by day. For this light momentary affliction is preparing for us an eternal weight of glory beyond all comparison, as we look not to the things that are seen but to the things that are unseen. For the things that are seen are transient, but the things that are unseen are eternal.

-The Bible, 2 Cor. 4:16-18

Do not go where the path may lead, go instead where there is no path and leave a trail.

-Ralph Waldo Emerson

As I reflect upon my years in graduate school and look at the culmination of the efforts in this time, I have many people to thank. First, I would like to thank my dissertation advisor, Dr. Steffi Oesterreich. I had limited bench experience when I joined Steffi's lab in 2013, but Steffi provided many opportunities for me to learn and grow as a scientist. These opportunities often extended beyond the bench, and I am thankful that Steffi afforded me so many experiences that contributed to a well-rounded education. In addition, Steffi fueled our shared passion for cancer research, and I will always remember these days as I continue to pursue a career in this field.

I must also give many thanks to my postdoctoral mentor, colleague, and friend, Dr. Nilgun Tasdemir. Nilgun has been a wonderful role model and an inspiration for many of the studies pursued in this work. She gave much of her time to me, and deserves the best in all her future endeavors. Additionally, Dr. Susan Farabaugh provided much guidance in the studies from Chapter Two. She never turned down the opportunity to discuss my project with me and

always helped me think through my experiments. Special thanks must also be given to my medical fellow mentor, Dr. Shweta Nayak. Shweta trained me in many laboratory techniques and provided invaluable guidance in my first projects in Steffi's lab.

I next thank my thesis committee members Dr. Don DeFranco, Dr. Timothy Burns, Dr. Adrian Lee, and Dr. Adam Feinberg for their guidance and patience with this work. Your suggestions and support were always appreciated. I must also thank the entire Women's Cancer Research Center (WCRC) at the Magee-Womens Research Institute (MWRI), particularly Dr. Carola Neumann for her commitment to my dissertation project. The entire WCRC provided a welcoming environment of constructive feedback and phenomenal collaboration. This includes everyone on the fourth floor of MWRI, and particularly my colleagues and friends in the shared Oesterreich-Lee labs. There are far too many individuals who have come and gone to name, but please know that I am grateful for all your assistance and am honored to call you colleagues and friends. I would not be in graduate school if it were not for the opportunity to join the Molecular Pharmacology program. Dr. Patrick Pagano, Dr. Bruce Freeman, Dr. Guillermo Romero, and many others are to thank for their invitation to join this wonderful group, as well as their constant support during my training.

This work would not have been possible without the extensive collaborative relationships that were developed. Dr. Timothy Burns provided assistance by sharing materials for the studies in Chapter Two, and offered great feedback during troubleshooting efforts. Dr. Adam Feinberg welcomed me into his lab and provided resources and training for the micropatterning experiments performed in Chapter Two. Li Zhu, MS assisted with many of the clinical characterization studies, as did Kevin Levine, BS and Ahmed Basudan, BS. Ahmed continues to collaborate with me extensively on the project described in Chapter Three, and I am very

thankful to work with him during this special opportunity. Kevin also deserves extra credit for his consistent support and time in discussing these projects. The “Kemily Bay” will always hold a special place in my heart. Dr. Nancy Davidson, Dr. Yi Huang, and Shauna Vasilatos, MS provided feedback and technical assistance for LSD1 studies in Chapter Two, and inspired the pursuance of the SNAIL-LSD1 axis in our studies. Many of these individuals (Dr. Steffi Oesterreich, Dr. Nancy Davidson, Dr. Timothy Burns, Dr. Don DeFranco, Dr. Adrian Lee, Dr. Yi Huang) also deserve thanks for their personal support in the submission of my F31 grant application. Without your assistance, this application would not have been possible. Thank you to Jian Chen, MS, Ms. Kara Burlbaugh, Ms. Caro Meier, and Ms. Jasmine Lee for all your technical assistance in these works. I had the pleasure to mentor Kara, Caro, and Jasmine, and I hope that their time in the lab was as fruitful and inspirational as it was for me. Tanya Minteer, MS and Julie (Arlotti) Scott are to thank for their tireless efforts in the project in Chapter Three. Thank you for all that you did to make this work possible.

I must thank the many clinicians, clinical staff, and patients who were involved in the accrual and generous donation of tissues used in studies. Patient WCRC-25 is to thank for all of the work in Chapter Three, and the addition of a novel cell line to the Invasive Lobular Carcinoma (ILC) research field. Though she is no longer with us, her selflessness transcended her suffering. She will live on through the research presented herein, as well as through any efforts taken by other researchers to further progress for patients afflicted with ILC and in the larger field of cancer research. I am humbled to have been selected to work on this project, and am grateful for the collaborative efforts taken by all to ensure its success.

On a personal note, I would be remiss if I did not thank every single friend who helped me through my graduate studies. That list would take pages, but please know that whether you

were in the field of science, or a friend outside of the field of science, I will be eternally grateful for your support and guidance. Thank you to Dr. Michael Campbell, my first mentor, who invited me to work in his lab the day I switched majors from bioengineering to biology. Your dedication and belief in my passion and abilities granted me more opportunities than I can ever thank you for. To my parents, Patricia and Michael Harrington, thank you for instilling the "Harrington" work ethic and morals in me, and for making sure that I had every opportunity to grow from a child in our one-stoplight town to the woman I am today in a life beyond "Mayberry." Thank you to my brothers, Dr. Ryan Harrington and Christopher Harrington, MS, for inspiring me to be a scientist-among-scientists in our family. Ryan, you told me I had ten years to catch up to you in *your* dissertation preface and on the night of my graduation from high school in 2008. Thank you for giving me the challenge to reach this place. Chris—looks like you are next!

There are many people who are no longer with me on this earth who are to thank for the person I am, but two people need to be acknowledged. Mary Near Beckman was a family friend who I learned was diagnosed with metastatic ILC toward the beginning of the Chapter Two studies. Her struggles and upbeat mentality in the face of severe illness were truly inspirational, and I dedicate my efforts in Chapter Two to her. Second, my grandfather, Joseph Baron, was the first person I lost in my life. Grandpa Joe, my "buddy," passed away from lung cancer, and this loss spurred me to pursue a career in cancer research. I will always work for a day when no one will have to lose their loved one the way that I lost him.

Finally, thank you to my husband Gregory Bossart, MS. You were there for me every time I wanted to give up, supported me in more ways than I could possibly list, and have been my rock since we fortuitously met in math class in college. I sometimes cannot believe the kinds

of challenges that we have already faced together, and I know that I could not make it through without you by my side. Your love and encouragement have greatly shaped me, and I thank you for always keeping me grounded with faith. Thank you.

This work has been supported financially by NIH Ruth L. Kirschstein National Research Service Award F31 CA203055 (“Targeting the EMT-like Phenotype in Invasive Lobular Carcinoma”), a fellowship from the University of Pittsburgh Department of Pharmacology, the John S. Lazo Cancer Pharmacology Fellowship, the Nicole Meloche Memorial Breast Cancer Fund, the Magee-Womens Research Foundation, and the University of Pittsburgh Cancer Institute.

LIST OF ABBREVIATIONS

ILC	Invasive Lobular Carcinoma
IDC	Invasive Ductal Carcinoma
LCIS	Lobular Carcinoma *in situ*
ERα	Estrogen Receptor Alpha
SERM	Selective Estrogen Receptor Modulator
SERD	Selective Estrogen Receptor Downregulator
AI	Aromatase Inhibitor
E2	17beta-estradiol
4OHT	4-hydroxytamoxifen
ICI	ICI 182,780 (Fulvestrant)
FDA	Federal Drug Administration
pCR	Pathologic Complete Response
PFS	Progression Free Survival
FBS	Fetal Bovine Serum
CSS	Charcoal Stripped Serum
FS	Full Serum (Either FBS or CSS)
EMT	Epithelial to Mesenchymal Transition
EMT-TF	Epithelial to Mesenchymal Transition Transcription Factor
FC	Fold Change
Veh	Vehicle
qRT-PCR	Quantitative Real-Time Polymerase Chain Reaction

IB	Immunoblot
IP	Immunoprecipitation
IF	Immunofluorescence
ChIP	Chromatin Immunoprecipitation
2D	Two-Dimensional
3D	Three-Dimensional
ULA	Ultra-Low Attachment
TCGA	The Cancer Genome Atlas
LOH	Loss of Heterozygosity
STDEV	Standard Deviation of the Mean
SEM	Standard Error of the Mean
Dox	Doxycycline Hyclate
Scr	Scramble
Ren	Renilla
GFP	Green Fluorescent Protein
RFP	Red Fluorescent Protein
P	Passage

1.0 INTRODUCTION

1.1 BREAST CANCER

Breast cancer is the most common cancer among women in the United States, and the second leading cause of cancer-related death[1]. In 2018, an estimated 268,670 patients will be diagnosed with breast cancer, and approximately 41,400 will succumb to the disease. Most of these patients are female, and thus are the focus of this work. The incidence of breast cancer has remained relatively stable over the past two decades, largely attributed to the multitude of environmental and physical factors that drive disease progression[2]. Epidemiologic studies have revealed that increasing rates of obesity among American women, as well as uses of postmenopausal hormonal therapy replacement, are linked to increased risk for breast cancer[3-5]. Beyond these factors, age, parity, lifestyle choices, and genetics also can play a role in the onset of disease[6]. These disparate entities all contribute to a disturbing reality: each woman in America faces a 1-in-8 risk in her lifetime of developing breast cancer.

Various therapeutic agents are available for breast cancer patients, which will be described in detail in this work. Although these therapeutic classes available for breast cancer patients have been heralded as some of the most successful targeted therapies of all cancer treatments, recurrences due to resistance to these therapies remain the greatest clinical challenge[7, 8]. It is well understood that it is not the primary cancer that leads to a patient's passing, but instead the

metastatic burden that infiltrates into various organ systems. For this reason, studies on recurrence, resistance, and metastatic disease have been central to the field of breast cancer research for decades. Beyond these molecular studies of disease, unique pathology within breast cancer has become an important focus in delineating patient subsets who should receive certain targeted therapies[9]. The work in this dissertation attempted to assess all of the aforementioned points: (1) to better understand the differences in therapeutic response in two major histological subtypes of breast cancer, (2) focus on the potential negative impacts of a widely used targeted therapy within one of these breast cancer subsets, and (3) generate and characterize a novel model for this subset to further the understanding of disease progression and resistance to therapeutics, providing a preclinical tool for breast cancer researchers to employ in future endeavors.

1.1.1 Breast Cancer Development and Progression: A Historical and Ongoing Perspective

Breast cancer is most adequately described as the malignant outgrowth of epithelial cells in the breast[6]. The first descriptions of breast cancer can be traced to approximately 3500 B.C. when ancient Egyptian physicians were stated to have removed breast tumors or ulcers by primitive burning methods[10]. Though various other citations regarding the disease have been found scattered across the subsequent few thousand years, the first postulations regarding origin of the carcinoma were not made until circa 200 A.D. by Greek physician Galen. Building off Hippocrates' theory that all diseases are caused by an imbalance of four "humours" (blood, phlegm, yellow bile, and black bile), Galen suggested that an excess of black bile was the cause of breast cancer. This accepted paradigm remained unchallenged for nearly one thousand three hundred years, much to the disservice of afflicted individuals.

As interest in medicine gained ground in the 1600-1900s, new viewpoints arose from various physician scientists to describe the origin of breast cancer. The Lymph Theory proposed that an outgrowth of lymph from blood led to carcinoma[11]. Humours and lymph were finally discredited as sources of carcinoma in the mid-1800s when Muller first showed scientific evidence that carcinoma is derived from cells, and his student Virchow confirmed that cancer cells derive from other cells[12]. Virchow's *Omnis cellula e cellula*, or "All cells come from cells," became the paradigm shift that was required to move the fields of biology, pathology, and oncology in a forward trajectory. This Blastema Theory, as it was called, gave rise to three additional theories: Virchow and Dvorak's Chronic Irritation Theory (cancer is a wound that does not heal), Ribbert's Trauma Theory (cancer cells become free from tissues of origin by mechanical disruption), and Gye and Barnard's Parasite Theory (viruses and other microbes cause cancer)[13-15]. While all theories held scientific merit in their approaches and syntheses of available evidence to describe the complex disease before them, it was not until the structure of DNA was solved by Wilkins, Franklin, Watson, and Crick that the opening floodgates of research in the burgeoning field of molecular biology could lay these theories to rest[16-18].

Anatomically, fully developed breasts are superior to the pectoral muscles[19]. Internally, each breast is comprised of approximately fifteen to twenty lobes. Each lobe contains twenty to forty lobules, in which milk is produced. From these lobules, ducts extend in intricate networks toward the nipple. In addition to these main components, the normal breast is filled with arteries, veins, nerves, connective tissue, and a large amount of adipose. As breast cancer arises from epithelial breast cells, the entire terminal ductal lobular unit (TDLU) is a site of origin for breast cancer.

Pathologically, breast cancer follows a progression from flat epithelial atypia (FEA) to atypical hyperplasia (AH) to carcinoma *in situ* (CIS) to carcinoma[20]. Each condition is a non-obligate precursor to the next and, as such, the penultimate condition of CIS is a non-obligate precursor to the final state of carcinoma. Each transition is accompanied by increasing epithelial aberrancies, altered proliferation, and morphological changes. Epithelial cell infiltration of the surrounding stromal milieu marks the presence of carcinoma, as distinct or non-distinct tumors take form.

Beyond these observations, much controversy remains regarding the specific cell origin of breast cancer[21, 22]. Two main hypotheses exist: (1) the Clonal Hypothesis and (2) the Stem Cell Hypothesis. In the former, a multitude of breast cancer cells are affected by mutations and those with the advantageous mutations are selected for to contribute to tumorigenesis. In the latter, a rare population of stem and progenitor cells initiates the tumor and potentiates its formation. These hypotheses have also been proposed to not exist in a vacuum, but to instead be a combined, dynamic model. To this end, no single cell of origin for breast cancer can currently be identified. The complexity of breast cancer begins to increase at the cellular level, as scientists now understand that each tumor is comprised of a heterogeneous population of cells that may each contribute to the lesion in different ways.

The most complicated level of study within breast cancer, molecular development and progression of disease, is also the most recently investigated. Various somatic and germline aberrations have been identified that contribute to the development and progression of breast cancer[23, 24]. For example, from a developmental standpoint, *BRCA1* and *BRCA2* mutation carriers are susceptible to breast cancer, obtained from either somatic or germline events[25]. These genes both generate protein products, BRCA1 or BRCA2, that control DNA repair mechanisms. Without

these pertinent proteins operating in their normal capacity, cells become susceptible to genomic aberrancies that can allow for uncontrolled proliferation, evasion of apoptosis, and other mechanisms that lead to carcinogenesis. Mutations in the tumor suppressor gene, *TP53*, have been identified in nearly half of all cancers, and *TP53* is among the most highly mutated genes in breast cancer[26]. Individuals afflicted with germline *TP53* mutations are commonly diagnosed with Li-Fraumeni cancer susceptibility syndrome, a disease that is known to confer a higher risk for breast cancer. *TP53* functions revolve around control of apoptosis in response to various stimuli in the cell, including accumulated DNA damage. Loss of the protein product of *TP53*, p53, leads to evasion of apoptosis for genomically unstable cells.

Additional genes that may contribute to the development and progression of breast cancer have been thoroughly studied. A highly notable gene includes epithelial marker *CDH1*, which encodes the protein for E-cadherin, a major focus of the second chapter of this dissertation[27, 28]. E-cadherin is a transmembrane protein that tethers neighboring cells together through a homotypic interaction with an adjoining E-cadherin protein. Further, E-cadherin is a master regulator of the continued connection between cells by binding to catenin molecules, which are secured to the internal actin cytoskeleton. This comprehensive interaction comprises what is known as the adherens junction. The functions of E-cadherin are imperative both in general anatomical development, as well as in carcinogenesis. Developmentally, E-cadherin expression is downregulated to alter polarity in epithelial cells during a controlled process called epithelial to mesenchymal transition (EMT). This controlled EMT leads to formation of the mesoderm, neural crest, and directs many other processes that contribute to proper development of an embryo. However, EMT is also utilized by cancer cells to disseminate from primary lesions to metastatic sites[29]. Loss of E-cadherin expression has become an important focus in breast cancer

development, particularly for major histological subtype Invasive Lobular Carcinoma (ILC), as described loss can be found predominantly in both ILC and its non-obligate precursor, Lobular Carcinoma *in situ* (LCIS)[30]. E-cadherin loss is observed less frequently in counterparts Ductal Carcinoma *in situ* (DCIS) and Invasive Ductal Carcinoma (IDC). This depletion of E-cadherin from LCIS/ILC cells is highly notable and unique within breast cancer, and suggests an EMT-like nature for these cells.

Ongoing studies continue to probe the complicated biological consequences of various genetic and cellular abnormalities that drive development and progression of breast cancer. These elaborate mechanisms continue to provide evidence that the complexity of cancer is beyond the initial theories of humours that were first described many thousand years ago. Though an entire dissertation could be devoted solely to the discussion of further molecular abnormalities that contribute to breast carcinogenesis and maintenance, only one other major protein (Estrogen Receptor Alpha, ERα) is pertinent to the focus of this compiled work and will be expounded upon in the next section.

1.1.2 Estrogen Receptor and its Role in Breast Cancer

Estrogen Receptor (ER) is the most commonly overexpressed entity in breast cancer, identified in 60-70% of all tumors[31]. ER consists of two major forms, alpha (α) or beta (β), which are hormonally driven transcription factors[32, 33]. ERα and ERβ are encoded by two separate genes, *ESR1* and *ESR2*, respectively. Though both genes/proteins are highly related in their structures and share some genomic targets, their chromosomal loci and patterns of tissue expression are different[34, 35]. In addition, ERα is the most commonly overexpressed form and is the focus of this work.

17β-estradiol, or estrogen (E2), is the natural steroid hormone ligand for ERα[34]. It is sourced primarily in premenopausal ovaries, or in postmenopausal women in adipose tissues from aromatization of the male sex hormone testosterone. Upon diffusion into a cell, E2 binds to ERα leading to activation of the transcriptional activator domain and causes rapid alterations in downstream associated target gene expressions[36-38]. This can happen either via genomic or non-genomic mechanisms. In genomic signaling, E2 binds to ERα, which dimerizes in the nucleus and associates directly to Estrogen Response Elements (EREs) or indirectly through other proteins to non-EREs[39]. Either interaction occurs in combination with various coactivator or corepressor proteins and the general transcriptional machinery. In non-genomic signaling, E2 binds to ERα that is located near the plasma membrane and activates downstream signaling via various signaling pathways (e.g. PI3K/MAPK)[40]. Alternative signaling pathways may also influence ERα signaling. Genomic and non-genomic signaling can influence the expression of thousands of genes in each cell (Figure 1).

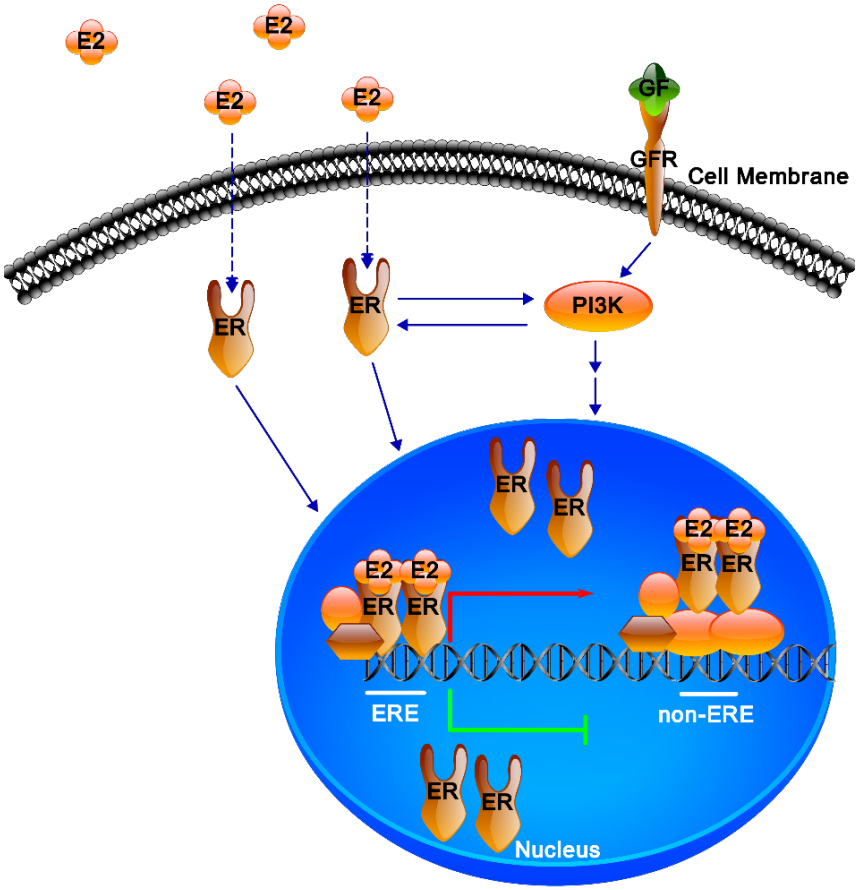

Figure 1: ERα Signaling is a Major Driver of Breast Cancer
A simplified version of ERα signaling is displayed. E2 diffuses into a cell, and binds to ERα, which dimerizes in the nucleus of the cell to promote downstream transcription programs via direct interactions at EREs or indirectly through non-EREs. Additionally, ERα can be activated through cross-talk with other signaling pathways, such as those driven by growth factors (GFs) and growth factor receptors (GFRs). An example of downstream cross-talk with PI3K is displayed.

In breast cancer, two main fields of thought exist to explain the implications of E2 in driving ERα-promoted carcinogenesis. First, ERα can promote proliferation in breast cancer cells[41, 42]. By inducing the expression of genes that drive the cell cycle (*PCNA*/*MKI67*) and repressing genes that normally contribute to cell cycle arrest (*TP53*/*CDKN1A*), ERα can push a cell into a cycle of uncontrolled proliferation. During uncontrolled proliferation, additional mutational events occur, leading cells to continue to contribute to tumor growth. Another understudied and controversial mechanism that may contribute to E2-driven breast cancer is the

metabolism of E2 itself, which has been shown to lead to both DNA adducts and oxygen free radicals[43]. These genotoxic metabolites are linked to DNA damage and eventual neoplasm formation. Both ERα-driven pathways lead to the formation of ERα-positive ($ER\alpha^+$) tumors. Therapeutic agents that are used to target the addiction of breast cancer cells to this oncogene will be covered in a later section of this chapter.

1.2 SUBTYPES OF BREAST CANCER

While $ER\alpha^+$ tumors encompass most breast cancers, other molecular subtypes also exist. Beyond these molecular subtypes, major histological subtypes can also be differentiated among breast tumors. Altogether, these heterogeneous populations of tumors are composed of further heterogeneous populations of cancer cells that make the overarching nomenclature of "breast cancer" seem an oversimplification for a collection of unique diseases. The identification of these tumor types is imperative for informing treatment options for patients, and for determining potential behaviors of tumors. Unfortunately, one major subtype, ILC, has been grossly understudied.

1.2.1 Molecular Subtypes of Breast Cancer

Recognition of the multitude of transcriptional and signaling programs that are observed as patterns in tumor subtypes have been made[44, 45]. However, it was not until 2000 that Perou and colleagues performed the first comprehensive expression analysis of sixty-five breast or breast metastatic specimens[46]. They analyzed the expression of 8,102 genes, and delineated the samples

into four major molecular subtypes. The first major subtype described was named luminal epithelial/ERα. The gene expression profile of this tumor subset was largely driven by ERα expression and related gene expression targets. The second subtype was comprised of tumors that were driven by overexpression of the growth factor receptor *ERBB2*, or HER2. The last two subtypes described in this original analysis were both basal in nature: one strictly deemed basal-like, and the other more normal-like in patterns of gene expression. Only the luminal subtype was related to expression of ERα, while the remaining three subtypes were devoid of the expression of ERα.

These subtypes have been further evaluated to test stability of clusters that were initially observed[46]. The first attempt at this expanded analysis occurred in 2001 by Sorlie and colleagues[47]. Not only were the original four clusters replicated in these analyses (Luminal/HER2/Basal/Normal), but luminal was further differentiated into two additional subtypes: Luminal A and Luminal B. The two luminal subtypes were separated primarily by outcome; patients with Luminal A tumors had better survival outcome than those with Luminal B tumors. An additional analysis was completed in 2012 and contained clinical specimens from 825 patients quantified on five platforms covering mRNA expression, DNA methylation, Single Nucleotide Polymorphisms (SNPs), miRNA, and whole-exome sequencing[48]. 348 of the samples were also subjected to reverse-phase protein array (RPPA) analyses. Luminal tumors were overall more highly associated with increased rates of *PIK3CA*, *GATA3*, and *FOXA1* mutations. Luminal A could be differentiated from Luminal B by many factors including, but not limited to, lower frequencies of *TP53* mutations (12% versus 32%), cyclin D1 amplification (29% versus 58%), and high estrogen signaling (Luminal A > Luminal B). Their conclusions aligned with what has been

clinically observed: Luminal A is associated with less aggressive breast cancers, while Luminal B is associated with more aggressive breast cancers, when comparing both subtypes directly.

Analyses related to the remaining three subtypes revealed additional details not uncovered by the first study. The HER2 subtype was found to have a specific HER2/EGFR gene expression signature that could separate the tumors into responders to HER2-targeted therapies, and those that would likely not respond[48]. Finally, the basal-like, largely comprised of triple negative breast cancers (TNBCs), had the highest rates of *TP53* mutations (80%) and widespread genomic instability that was more commonly related to serous ovarian cancers as opposed to the other molecular breast cancer subtypes. Additional follow-up studies have concluded that basal-like tumors can also be further subdivided into other classes such as Claudin-Low, which are associated with upregulations of transcription factors *SNAI1*, *TWIST1*, and *ZEB1*, and are noted to have high immune infiltrate[49].

The clinical implications of these molecular subtypes were noted after the first definitions of Luminal A/Luminal B/HER2/Basal/Normal were defined and are now commonly called the PAM50-based subtype classifier for the original 50 genes used to delineate the intrinsic subtypes[46-50]. Beyond survival differences (Luminal A > Luminal B > HER2 > Basal), the implications of these intrinsic breast cancer subtypes continue to be studied[51-54]. PAM50 was the first comprehensive test to give insight into personalized medicine in the field of breast cancer, and has inspired the use of subtyping in the clinical tailoring of treatments to tumors. From these subtypes, clinicians can now predict response to therapeutics based on the subtyping of a given tumor, whether in response to chemotherapy or targeted therapy.

1.2.2 Histologic Subtypes of Breast Cancer: A Comparison of ILC and IDC

Though molecular subtyping is novel, it has not replaced the pathological subtyping that has been performed on breast tumors for nearly one hundred years. Breast cancer can be subdivided into two main histological subtypes: ILC and IDC[55-57]. ILCs account for 10-15% of all invasive breast carcinomas, and IDCs account for 80%. There are roughly 22 remaining histological subtypes which are much less frequent, and not a focus of this work[58]. After clinical sample acquisition, classical Hematoxylin and Eosin (H&E) staining can help pathologists to identify the subtype of tumor with which a patient is afflicted.

ILCs have a unique growth phenotype consisting of small, discohesive cellular growth throughout surrounding stroma (Figure 2)[59-61]. This linear growth pattern is caused by loss of the epithelial protein E-cadherin, a calcium-dependent transmembrane protein imperative for cell-cell interactions at adherens junctions[28, 62, 63].

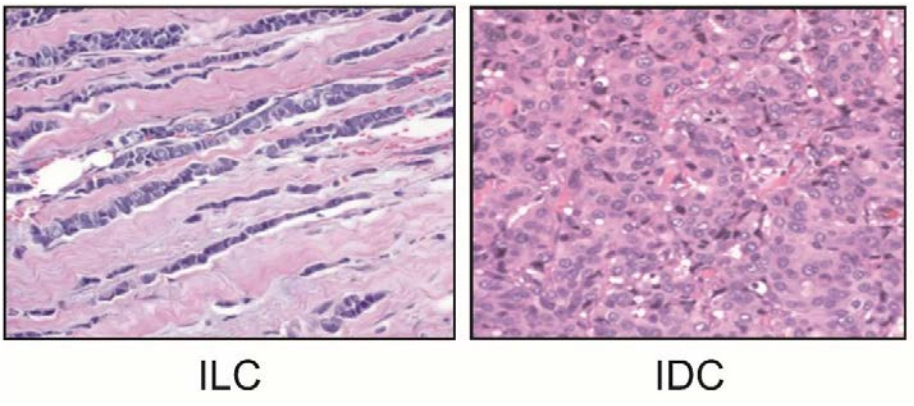

Figure 2: ILC and IDC Have Different Presentations in Breast Tissue
H&E stains for ILC and IDC were performed on primary tumors. The ILC lesion displayed a classic discohesive growth pattern, while IDC cells filled the section of interest.

Previous studies have defined this loss of E-cadherin protein in 90-100% of primary ILCs by Immunohistochemistry (IHC) staining methods[64-66]. A more recent and comprehensive study performed by The Cancer Genome Atlas (TCGA) ILC working group utilized a cohort of n = 127 primary ILCs to identify *CDH1* mutations leading to truncated or missense mutated protein in 65% of all cases[67]. In addition, these *CDH1* mutations often coincided with loss of heterozygosity (LOH) of 16q22, the chromosomal location of *CDH1*. Including the TCGA ILC working group's studies regarding mutations, copy-number alterations (CNAs), mRNA downregulation, and protein downregulation, loss of E-cadherin was found in 95% of the tumors studied. Mechanisms of loss and other postulations regarding E-cadherin will be covered in depth in the second chapter of this dissertation. This loss of E-cadherin largely contributes to the unique growth pattern of ILCs, making the tumors more difficult to detect by palpation and standard mammographic methods[68-70]. As such, ILCs are often diagnosed at later stages, when at larger sizes. Approximately 90-95% of ILCs are ERα$^+$, giving clinicians a choice of endocrine therapies for treatment of patients[71, 72]. IDCs, in contrast, do not tend to have loss of E-cadherin or a linear growth pattern[73]. Instead, they form classic palpable masses, more easily detected at early stages[74]. Loss of E-cadherin can occur in IDCs, but is more often associated with poorly differentiated or highly metastatic lesions[75-77]. A large proportion of IDCs also express ERα, making these tumors susceptible targets for endocrine therapy treatments.

Beyond the differences in E-cadherin expression and pathology in ILC compared to IDC, recent studies have focused on differences in metastatic lesion sites for the two diseases. Due to the abundance of ERα expression in both subtypes, bone is the most common metastatic site for both diseases[78, 79]. However, other sites of metastases can differ vastly between the two subtypes. While IDCs more commonly form secondary lesions in the lung or liver, ILCs are often found in

ovaries or the gastrointestinal tract[80-82]. Though these differences have been noted, the molecular mechanisms behind these unique metastatic sites have yet to be elucidated. These diverse presentations give further evidence to the uniqueness of ILC as compared to IDC as a subtype of breast cancer.

Other clinical differences have been noted between ILC and IDC. As mentioned previously, larger ILCs are often found at later stage of diagnosis. The combination of larger size and E-cadherin loss can lead ILCs to present with spiculated or poorly-defined margins[83-86]. These diffuse margins, also present in early lesions, can be difficult for detection in imaging, and for surgeons to navigate in excision. This can lead to aggressive measures of mastectomy, which has been discovered to have similar rates of breast cancer-specific survival as breast conservation surgery in early-stage ILC patients[87]. Another clinical observation is that early lesions are often missed by typical mammographic or ultrasound methods, due to lack of desmoplastic reaction in surrounding stroma and the unique proliferation pattern of ILC[68, 88]. ILC patients are more likely to be afflicted with multicentric or multifocal disease and have prevalence of contralateral episodes of disease[89, 90]. These clinical presentations contribute to difficulty detecting ILC and can hinder the timely treatment of afflicted patients.

At the molecular level, ILCs tend to have low mitotic indices and histological grade compared to IDCs, correlating with their lower rates of proliferation[65]. ILC nuclei can be proportionally larger and may exhibit hyperchromatism[91]. Ki67 levels are overall lower in ILC compared to IDC, contributing to lower proliferation rates[92]. The combination of $ER\alpha^{+}/Ki67^{low}$ status in ILCs translates to their predominant Luminal A subtyping, suggesting that these lesions are overall less aggressive and have increased survival compared to other breast cancer subtypes[67]. However, retrospective analyses regarding survival in relation to therapeutic regimen

have revealed a potentially different story; this will be detailed in the next section of this chapter. Loss of *PTEN* and alterations in PI3K/AKT/mTOR signaling have also been noted as driving pathways in ILC[67, 93, 94]. However, the molecular intricacies of ILC remain undefined, and are a leading rationale for this body of work.

In summary, ILC and IDC are distinct diseases within breast cancer, with some clear clinical, morphological, and molecular differences largely defined in the last decade (Table 1). With approximately 39,000 new cases of ILC projected to be diagnosed in 2018 in the United States, ILC is the sixth most common type of cancer for women[1]. This prevalence and all the unique aspects of this breast cancer subtype merit an enhanced interest in treating patients afflicted with ILC differently than those affected by IDC. However, the research regarding these treatments and their implications for specific histological subtypes is in its infancy. Further recognition of the uniqueness of ILC will assist in informing clinical decisions related to treatment regimens that are prescribed to patients. Better distinction between the two major subtypes could promote better patient outcomes, which is covered in the next section.

Table 1: Overview of Characteristics of ILC and IDC

		ILC	IDC
Percent of Breast Cancers (%)[1, 27]		10 – 15	80
Patients Annually Diagnosed in U.S.[1] ***Numbers Calculated from 2018 Diagnoses Projections***		26,867 - 39,918	212,896
Average Age of Patient Diagnosed[27, 95]		63.4 ± 12.7	59.5 ± 13.6
Tissue Presentation (see Figure 2)		Discohesive linear cords	Distinct masses
Detection[83-86]		Less palpable until at later stages, difficult to observe with mammographic methods	More often palpable during self-examination, more obvious masses during mammography
Metastatic Sites[78-82]	***Major:***	Bone > CNS, Lung > Liver	Bone > Lung > Liver > CNS
	Unique:	GI Tract, Ovary	--
ERα Expression[67, 71, 72]		+ 90-95%	+ 60-70%
Molecular Subtype[67]		Predominantly Luminal A	Luminal A Luminal B HER2 Basal
E-cadherin Expression[64-67]		-	Predominantly +
TCGA CDH1 Mutation Significances[67] ***ILC versus IDC Comparisons Displayed***		3.40E-12	7.63E-03
Selected Top Mutated Genes from TCGA Study[67] ***Data are Adapted from the Above Publication*** ****Significant Differences in Mutation Frequencies When Directly Comparing Luminal A Subtypes***	***PIK3CA***	9.18E-13	6.79E-13
	RUNX1	9.18E-13	1.32E-05
	TP53	2.22E-04	**6.79E-13***
	TBX3	**4.01E-06***	*NS*
	PTEN	**8.86E-09***	5.63E-03
	FOXA1	**6.53E-04***	*NS*
	GATA3	*NS*	**6.79E-13***
Primary Therapeutic Modalities (ERα+)		Endocrine Therapies	Endocrine Therapies

1.3 BREAST CANCER TREATMENT REGIMENS

Breast cancer treatments have evolved from the primitive burning methods of medieval times to targeted therapeutics that are on the cusp of the personalized medicine movement[96]. From classic methodologies that have been utilized for centuries (e.g. surgery), to the class of endocrine therapies that can be selected for patients' tumors expressing ERα, the therapeutic landscape for breast cancer patients is a constantly evolving or changing entity. Further, differences in indications (e.g. ILC versus IDC) have the potential to influence the treatment course for a given patient. Herein, we give a brief overview of the major classes of treatment regimens and examples of some pertinent clinical study outcomes for breast cancer patients with a focus on ILC patient populations.

1.3.1 Endocrine Therapies and Selected Clinical Studies

Endocrine therapies are a class of targeted therapies that directly or indirectly inhibit ERα[97-99]. The major subclasses of endocrine therapies include Selective Estrogen Receptor Modulators (SERMs), Selective Estrogen Receptor Downregulators (SERDs), and Aromatase Inhibitors (AIs) (Figure 3). Each class is rationally chosen for patients based on their menopausal status, prior treatments, and progression of disease. Overall, these therapeutics have successfully contributed to the standard of care for millions of breast cancer patients, by curing disease or extending survival[100].

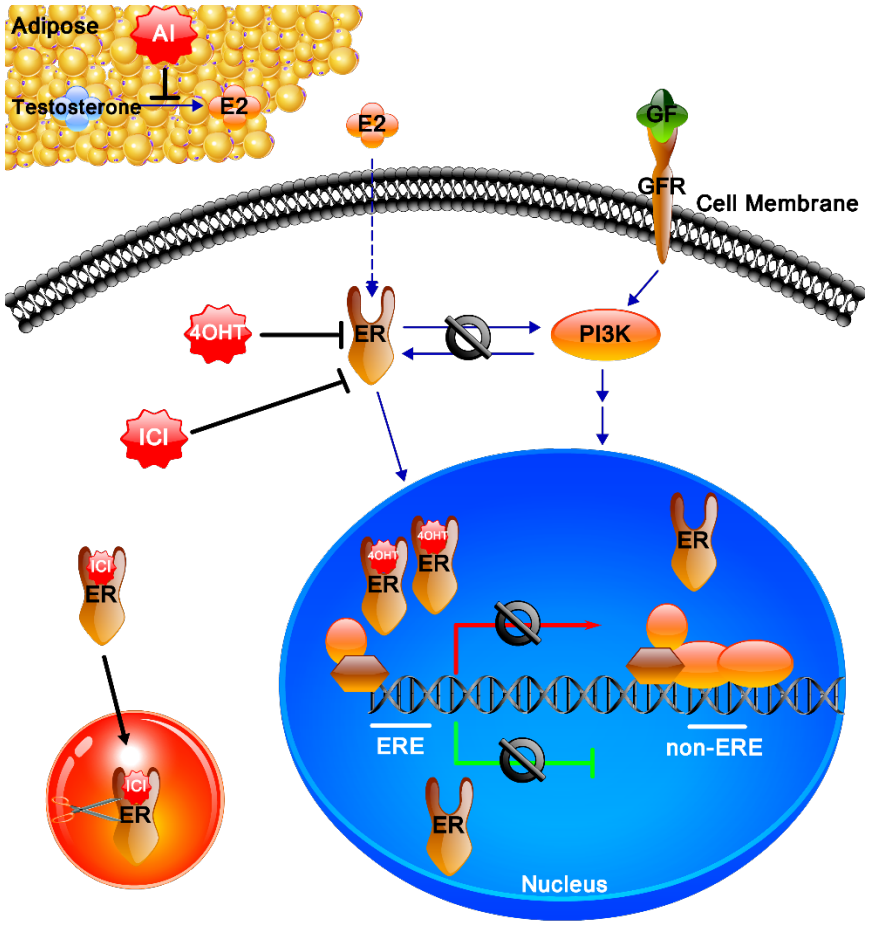

Figure 3: Endocrine Therapies Target ERα in Breast Cancer
Three commonly used endocrine therapies and their simplified mechanisms are shown above as a modification of a similar scheme in Smith *et al*[98]. SERMs (4OHT), SERDs (ICI), and AIs all work to decrease ERα signaling in breast cancer through different mechanisms. 4OHT can directly bind to and inhibit ERα signaling by competing with E2. ICI prevents downstream signaling by inciting degradation of ERα in the proteasome. AIs inhibit aromatase in subcutaneous tissues (e.g. fat) to prevent conversion of testosterone to E2. It should be noted that alternative signaling pathways are still able to regulate their own downstream targets that may be shared by ERα.

1.3.1.1 SERMs

SERMs include molecules that directly interact with ERα as partial agonists or partial antagonists, depending on the physiological context[97, 101]. There are currently 11 Federal Drug Administration (FDA)-approved SERMs, and an additional 22 or more that are under development or not currently approved for medical use[102, 103]. Despite this lengthy list, only two SERMs are currently indicated

for the treatment of breast cancer: Tamoxifen and Toremifene. However, the approved patient subset for Toremifene is limited in the U.S., as it is given only to postmenopausal women with advanced metastatic ERα^{+} or unknown status tumors[104]. An additional SERM, Raloxifene, is FDA-approved; however, the current indications of use are only for prevention of breast cancer[105]. Thus, Tamoxifen remains the drug of choice for the class of SERMs. It is also the focus of the second chapter of this dissertation.

Tamoxifen was first generated by scientists at Imperial Chemical Industries in 1966 under the name ICI 46,474[106]. The rationale for its generation was to find novel emergency contraceptives, but Tamoxifen failed to produce the results desired by Imperial Chemical Industries. Instead, nonsteroidal Tamoxifen's estrogen-mimic molecular structure made it a ligand for ERα[107]. Tamoxifen is normally ingested as a tablet preparation in this prodrug state. Once in the liver, cytochrome P450 enzymes (CYP2D6 and CYP3A4) convert Tamoxifen into metabolites 4-hydroxytamoxifen (4OHT), afimoxifene, and endoxifen[108]. The metabolites have a significantly higher affinity for ERα than does Tamoxifen itself, and are the primary molecules in competition with E2 for binding[109]. For the studies described in this dissertation, only 4OHT was utilized and will be the only metabolite mentioned from this point forward. The binding of 4OHT induces a conformational change in the receptor, preventing appropriate interaction with coactivators or corepressors and reducing interactions with DNA[110]. Thus, 4OHT leads to decreased ERα activity, arrest in G_0/G_1, induction of apoptosis, and inhibition of a multitude of other tumorigenic behaviors[111, 112]. The activity of SERMs is not restricted to ERα, but can also influence ERβ, a molecule not further covered in this dissertation[113]. Additionally, these therapeutics have a mixed antagonist-agonist nomenclature due to their ability to act as antagonists in tissues such as the target tissue of the breast, but as agonists in tissues such as bone,

endometrium, and uterus[114]. This mixed behavior can be beneficial (e.g. strengthening bone) or deleterious (e.g. increased risk for endometrial, uterine cancers, side effects including hot flashes or potential blood clots), but is still insufficient to detract from the clinical benefits of Tamoxifen for primarily premenopausal breast cancer patients.

Tamoxifen is a common therapeutic for ILC and IDC ERα$^+$ lesions in premenopausal women[115]. However, its utility in ILC has been questioned and pursued in recent clinical studies. A retrospective study by Smith and colleagues in 1987 observed n = 33 ILC versus n = 264 IDC advanced patient clinical data, and assessed that the survival outcomes between the two groups were not significantly different[116]. However, this study covered the broad class of endocrine therapies, and was not specific to Tamoxifen. Also, though 90% of the ILCs and 67% of the IDCs in this study expressed ERα, all patients were stated to have received endocrine therapy at relapse, regardless of receptor status. Patients only received chemotherapy if "life threatening disease dictated" necessity. A more focused retrospective study regarding Tamoxifen treatment was undertaken by Jïrstrom and colleagues with n = 43 ILC versus n = 411 IDC patients with multivariate analysis revealing no significant difference in survival for the two groups[117]. Interestingly, a small subgroup of the ILCs did not appear to respond effectively to Tamoxifen, but it was concluded that a more comprehensive meta-analysis was required to appropriately power the question of ILC versus IDC in relation to specific treatments. Shortly following this study, Rakha and colleagues utilized well-characterized clinical data with long-term follow-up from n = 415 ILC and n = 2,901 IDC patients to first reveal a worse long-term outcome for ILC patients who took endocrine therapies compared to IDC patients[118]. A few months after the release of this study, Pestalozzi and colleagues performed a larger retrospective study using clinical data obtained from outcomes from pure ILCs and IDCs (ILC n = 767; IDC n = 8,607), and uncovered a

significant early advantage in disease-free and overall survival for ILC versus IDC patients ($p < 0.01$) that was reversed at 6-10 years[119]. These patterns were observed in cohorts defined by ER status, suggesting a role for late endocrine therapy resistance in ILC patients. Patients in these latter two studies were classified as having received endocrine therapy, with no specific analyses applied to patients who received Tamoxifen exclusively, and conclusions thus are a broader observation regarding endocrine therapy resistance in ILC.

Few other studies have reported direct comparisons between ILC and IDC patient outcomes, and only one study is currently completed that addresses the outcomes of ILC patients in relation to Tamoxifen. Metzger-Filho and colleagues recently completed retrospective BIG 1-98 trial analyses to compare outcomes in ILC (n = 324) and IDC (n = 2,599) for patients who received Tamoxifen, AI Letrozole, or sequential treatments[120]. Overall outcomes revealed that there was greater survival benefit for ILC patients who received Letrozole compared to Tamoxifen, regardless of Luminal A or B subtype. In contrast, a survival benefit for IDC patients was apparent in the Luminal B subtype tumor group, but not the Luminal A. However, caution was noted in interpretation of these results until a validation cohort has been observed with similar outcomes prior to implementation in clinical practice.

Two ongoing clinical trials will continue to assess the implications of Tamoxifen in the ILC subset of patients. At the University of Pittsburgh, Jankowitz and colleagues are actively recruiting patients with ER^+ ILC to a three-armed endocrine therapy window trial (Tamoxifen, Anastrazole, Fulvestrant) to assess reductions in Ki67 and ER-regulated gene target expressions[121]. Metzger-Filho and colleagues are continuing to pursue differences in Tamoxifen and Letrozole for ILC and IDC patients with a new trial that appends newly FDA-approved CDK4/6 inhibitor Palbociclib (PELOPS)[122]. As both trials were initiated in 2014 and 2016,

respectively, and are still recruiting, it will take some time until the outcomes of these trials are known. Currently, our knowledge allows us to hypothesize a role for potential endocrine therapy and, exclusively, Tamoxifen resistance in ILC patients.

1.3.1.2 Mechanisms of Tamoxifen Resistance

Though Tamoxifen is often a successful treatment for ER^+ breast cancers, multiple resistance mechanisms have been discovered in breast cancer cells that allow cancer to alleviate or inhibit the impacts of the therapeutic[122-126]. Some of the common mechanisms of resistance to Tamoxifen include (1) alterations in ERα expression levels (e.g. loss of ERα to prevent binding of Tamoxifen to target), (2) aberrancies in coregulatory protein expression/activity (e.g. upregulation of coactivators SRC1 or AIB1; downregulation of corepressor SMRT), and (3) implications of alternative signal transduction pathways to drive tumorigenesis (e.g. PI3K/AKT/mTOR signaling)[126-128]. This list is not inclusive of all mechanisms of resistance, as novel mechanisms including mutations in ERα or upregulation of EMT proteins (e.g. SNAIL, TWIST1, ZEB1) have also recently been implicated[129, 130]. However, most of these studies have been performed in IDC breast cancer cell lines and Tamoxifen-resistant derivatives (e.g. MCF-7, MCF-7^{TAMR}, T47D)[131]. Understanding the role of Tamoxifen resistance and mechanisms in different histological contexts is imperative to generating better therapeutic options for patients, and thus, studies must also be extended to other major histological contexts, such as ILC.

To this end, our lab recently identified a role for *de novo* Tamoxifen resistance in an ILC cell line, MDA-MB-134-VI[132]. We performed dose response assays for E2 and 4OHT to uncover a unique phenotype for MDA-MB-134-VI cells treated with 4OHT; instead of inhibiting growth, or having no influence without competition provided by E2, 4OHT promoted the 2D proliferation of these cells (refer to Figure 5C within [132]). Additionally, we observed 4OHT upregulation of

SNAI1, suggesting that EMT may contribute to the 4OHT partial agonist-driven phenotypes observed (refer to Figure 6A within citation [132]). This striking and concerning observation, opposite of the intended roles of Tamoxifen in ER^+ breast cancer cells, led to the follow-up studies provided in Chapter Two of this dissertation. The initial study suggested that differential ERα-regulated gene expression and phenotypic programs exist in different histological subtypes of breast cancer (ILC versus IDC), and encourages researchers and clinicians to further examine the role for Tamoxifen in different subtype contexts.

1.3.1.3 SERDs and AIs

SERDs and AIs are two additional major classes of endocrine therapies that were not employed in this work, but are essential for any discussion regarding ER^+ breast cancer. The most widely used SERD is Fulvestrant, or ICI 182,780 (ICI)[133]. ICI has a molecular affinity for ERα that is one hundred times greater than that of Tamoxifen, and upon binding causes rapid degradation of the receptor as a pure antagonist. While it may then seem more feasible to utilize ICI instead of Tamoxifen for the treatment of ER^+ breast cancer, ICI is not currently FDA-approved as a first-line therapy for breast cancer. The SWOG 0026 Phase III clinical trial recently evaluated the efficacy of ICI with the AI Anastrazole as a combination therapy in endocrine therapy-naïve patients and found that there was a significant improvement in progression free survival (PFS) in comparison to Anastrazole alone for postmenopausal ER^+ patients[134]. Additionally, the FIRST Phase II and FALCON Phase III studies suggested a role for ICI as a first-line monotherapy compared to AIs[135, 136]. Despite these new clinical trials, it should be noted that the delivery route (painful intramuscular injection), slow absorption, and short maximum plasma concentration (5 days) require patients to go to a treatment facility, usually monthly, for treatments[137]. In addition, ICI is not exempt from promoting its own mechanisms of resistance[138]. Ongoing development of

oral SERDs aims to combat the previously mentioned issues, but require much research to pursue their clinical development[139]. Though specific impacts for ILC in relation to ICI are not currently known, the previously described window trial by Jankowitz and colleagues will assess the effects of ICI in comparison to Tamoxifen or Anastrazole[121].

AIs provide a different mechanism of targeting ERα as compared to Tamoxifen or ICI by inhibiting the enzyme aromatase that is responsible for the conversion of testosterone into E2[98]. Currently, third-line AIs include nonsteroidal Letrozole or Anastrazole, and steroidal Exemestane[140]. Nonsteroidal inhibitors prevent the binding of testosterone to aromatase by reversibly binding the enzyme, while steroidal inhibitors irreversibly bind to aromatase. The mechanism of AIs supports their utility in postmenopausal women in whom E2 is sourced from androgens in subcutaneous tissues. Though either Tamoxifen or AIs are acceptable modalities for postmenopausal women afflicted with ER^+ breast cancer, the ATAC trial showed that Anastrazole significantly increased disease-free survival, time-to-recurrence, and reduced distant metastasis compared to Tamoxifen[141]. High levels of competing E2 in premenopausal women hinder the use of AIs in this patient subset, unless ovarian suppression is concomitantly administered by treatment with luteinizing hormone-releasing hormone (LHRH) therapy (e.g. Trelstar) or Salpingo-oophorectomy[142, 143]. Oophorectomy is an irreversible ovarian ablation method, and many premenopausal women may not desire to either enter menopause prematurely or end their reproductive lives. Chemical suppression is beneficial, as it is reversible; recently completed clinical trials SOFT and TEXT have probed the combination of Tamoxifen/AIs and Trelstar in premenopausal women, and future studies will likely continue to evaluate the feasibility of these combinations. Beyond the previous clinical trials mentioned that included AI arms (BIG 1-98, ongoing PELOPS, and Jankowitz *et al* window trial), data obtained from AI window trial POETIC

will continue to yield both short-term information about ILC and IDC response to AIs and long-term survival benefit with a follow-up of 10 years[120-122, 144].

1.3.1.4 Reflections on Endocrine Therapy Clinical Studies Discussed and Overview

Few clinical studies have been completed that adequately describe the specified outcomes for ILC patients who receive endocrine therapies. Data from retrospective studies have suggested worse long-term survival for ILC patients who receive endocrine therapy (Rakha *et al*, Pestalozzi *et al*), and outcomes may be worse for ILC patients who receive Tamoxifen as opposed to other endocrine modalities (BIG 1-98)[118-120]. These observations suggest a necessity for more clinical trials addressing the specific needs for this patient cohort, as well as long-term follow up to evaluate differences in survival and appropriate treatment during recurrence. The culmination of the ongoing clinical trials involving endocrine therapies of multiple classes will give the first information regarding the impacts of Tamoxifen, ICI, and AIs in ILC in new cohorts (Jankowitz *et al* window trial, PELOPS)[121, 122]. These data will be invaluable to our understanding of therapeutic resistance in ILC and will continue to influence future studies (Table 2).

Table 2: Summary of Described Clinical Studies Involving Tamoxifen and ILC

	Citation	Study Type	Number of ILC/IDC Patients		Outcome
Endocrine Therapy, Not Specified	Smith *et al*[116]	Retrospective	33	264	*NS* difference between ILCs and IDCs
	Rakha *et al*[118]	Retrospective	415	2901	Worse long-term outcome in ILCs v IDCs
	Pestalozzi *et al*[119]	Retrospective	767	8607	Significant early survival advantage in ILC v IDC ($p < 0.01$) followed by significant late survival advantage IDC v ILC ($p < 0.01$)
Studies Including Exclusive Tamoxifen Treatment Outcomes	Jïrstrom *et al*[117]	Retrospective	43	411	*NS* difference between cohorts; however, ILCs had early survival advantage that later converged with IDCs
	Retrospective BIG 1-98[120]	Retrospective	324	2599	Significant survival benefit for ILC patients who received Letrozole v Tamoxifen
	Jankowitz *et al*[121]*	Neoadjuvant Window Trial	*Recruiting**		Three arms of Tamoxifen, Anastrazole, and ICI will be compared for ILC patients with Ki67 and ER-regulated gene targets as measurable outcomes
	PELOPS[122]*	Phase II Neoadjuvant Clinical Trial	*Recruiting**		Combination of Palbociclib with endocrine therapies with Ki67 and pathologic complete response (pCR) measurement outcomes

1.3.2 Other Chemotherapies/Targeted Therapies

In contrast to IDCs, chemotherapy is rarely given as a primary monotherapy due to the predominance of ER^+ lesions in ILC. Various clinical studies have indicated that ILCs can be less responsive to chemotherapy compared to IDCs[145-147]. Lips and colleagues further investigated this observation by combining retrospective data from two clinical trials, including n = 75 ILC patients[147]. Unlike previous studies, which focused on the definition of lobular histology as the

rationale for lower pCR, Lips *et al* adjusted for hormone receptor and HER2 status ($ER^+/HER2^-$) and found that this group of tumors was driving lower pCR for *both* ILC and IDC. As ILC is enriched for $ER^+/HER2^-$, this study identified the molecular phenotype, rather than lobular histology, as the rationale for ILC's lower pCR. Many other retrospective studies have made these same observations, and thus, clinical recommendation has been to reserve chemotherapy monotherapy for ER^- ILCs[148]. In the largest retrospective ILC versus IDC study by Chen and colleagues in 2017 (n = 85,048 ILCs; n = 711,287 IDCs), the observation of increased distant metastasis at late stage diagnosis for ILCs led to their suggestion that combination endocrine therapy and chemotherapy may be more beneficial for patients with ILC[30].

Chemotherapy or alternative targeted therapies as primary monotherapy may not be feasible for most ILC patients; however, combination of targeted therapy with endocrine therapy is currently under investigation. For example, the PELOPS trial by Metzger-Filho and colleagues will provide information regarding the combination of the CDK4/6 inhibitor, Palbociclib, with various endocrine modalities[122]. The rationale for use of CDK4/6 inhibitors lies in the need to combat endocrine therapy resistance[149]. Palbociclib directly inhibits the enzymes cyclin-dependent kinases CDK4 or CDK6, master regulators of the transition through the restriction checkpoint and through G_1 phase of the cell cycle. The pathways associated with CDK4/6 and cyclin D1 (*CCND1*) amplification have been uncovered as mechanisms of endocrine therapy resistance[150]. To this end, the PALOMA trials were performed to combine AI Letrozole with Palbociclib in $ER^+/HER2^-$ advanced breast cancers. An ILC cohort was included in this study, however, the sample size was small and therefore result interpretation was limited ($n_{ILC\ Letrozole}$ = 19; $n_{ILC\ Letrozole\ +\ Palbociclib}$ = 18). The success of these trials led to the FDA approval of combination Letrozole/Palbociclib in an accelerated manner and have now become a standard of care option in

the first and second-line setting. Interestingly, a role for CDK4/6 and *CCND1* amplifications was also noted by our lab in the MDA-MB-134-VI *de novo* Tamoxifen resistance study, suggesting Palbociclib may influence mechanisms in ILC cells that display endocrine therapy resistance[132].

Another emerging pathway of interest to concurrently target in ILC ER^+ tumors is PI3K/AKT/mTOR. The TCGA ILC working group previously described that ILCs have the highest PI3K/AKT activation signature of the breast cancer histological/molecular subtypes[67]. Oncogenic mutations in *PIK3CA* have also been described in ILC[94]. Various inhibitors for these pathways are currently under development by companies such as Novartis (BKM120, BYL719)[151]. Considering the observations made by the TCGA ILC working group and others, clinical trial design should include a focus on ILC patients. One pertinent analysis of an ILC cohort of notable importance to this pathway comes from the Phase III BOLERO-2 trial comprised of combination Exemestane and Everolimus (mTOR inhibitor) treatment of ER^+ locally advanced or metastatic breast cancer patients with AI-refractory disease[152]. ILC patients in this study benefited from significantly increased PFS, suggesting rationale for follow-up studies with these inhibitors.

Additional preclinical research and clinical trials are needed to assess the use of these and other inhibitors specifically in ILC. Increasing interest in ILC as a unique histological subtype with endocrine therapy resistance mechanisms will likely benefit ILC patients in the upcoming decades of clinical trials that have yet to be designed.

1.3.3 Surgery and Radiation

Surgery and radiation are common treatments for early-stage (stage I-III) breast cancer patients. For early-stage patients with ILC, breast conservation surgery (BCS) has been described to be as effective as total mastectomy, leading to no significant differences in survival[89, 153, 154]. Despite

these observations, late local recurrence is still an issue for patients who decline mastectomy[154, 155]. This may be due to the significantly increased rate of positive margins often observed in ILC, which leads to re-excision of tissue or complete mastectomy upon recurrence[155]. Increased rates of mastectomy have been observed in the ILC subtype, as well as increased multifocal, multicentric, and contralateral occurrences[30, 89, 90]. A 15-year retrospective study performed by Fodor and colleagues observed the comparison of BCS in combination with radiation therapy and total mastectomy and concluded the same as studies performed since the 1990s[87, 89, 153, 154]. Radiation therapy is often combined with local resection of the primary ILC lesions, and offers an additional survival benefit to patients[156]. This may be due to the observation that ILCs have a higher radiosensitivity than IDCs[157-159]. Still, late recurrence continues to remain a clinical problem for ILC patients, suggesting that beyond the excision and radiation of disease, molecular control of these tumors is imperative to combatting disease progression, metastasis, and death.

1.4 UNDERSTANDING THE IMPLICATIONS OF ENDOCRINE THERAPY RESISTANCE IN INVASIVE LOBULAR CARCINOMA

Though understudied, the unique histological subtype of ILC has been observed as a separate disease from IDC within the overarching context of breast cancer. Differences in growth patterns (linear, discohesive; refer to Figure 2), molecular marker expressions (predominantly ER^+), and responses to therapy (for endocrine therapy, refer to Table 2) are all paramount to understanding the clinical implications of appropriately treating ILC. Studies of the molecular controls for Tamoxifen resistance will contribute to informed clinical decisions that will likely influence

survival outcomes for patients[67, 71, 72]. This concept challenges the use of standard endocrine therapies for a large patient cohort, and required further investigation.

As previously described, we observed 4OHT upregulation of *SNAI1* in ILC cell line MDA-MB-134-VI[132]. This upregulation of a vital component of the EMT program and the known loss of E-cadherin in this disease led us to consider the role of Tamoxifen in contributing to the EMT-like phenotypes observed in ILC. **We hypothesized that Tamoxifen resistance in ILC is driven by 4OHT upregulating resistance pathways that contribute to EMT-like phenotypes that have been observed in ILC, and hence metastatic progression. In addition to this hypothesis, we recognized the lack of research models available for ILC and undertook the task to establish and characterize a novel ILC cell line for use in current and future research endeavors.**

In the subsequent chapters, I describe studies performed to understand the upregulation of an EMT program in ILC, both basally and driven by 4OHT. We evaluated the feasibility of targeting this program, and suggest an alternative, understudied role for a well-studied protein involved in EMT. In the second part of this dissertation, we characterized a novel ILC cell line to assess its utility as an additional tool in the field of ILC research. Though outcomes of the testing of the initial hypothesis were unanticipated, these findings cumulatively represent a foundation for endocrine therapy resistance studies in ILC that will likely contribute to further development of appropriate treatments for this unique patient subset.

2.0 TARGETING THE EMT-LIKE PHENOTYPE IN INVASIVE LOBULAR CARCINOMA

2.1 INTRODUCTION

Loss of E-cadherin expression is the most common feature of ILC, and is highly characteristic of EMT, a major process in development and cancer[160, 161]. The transmembrane epithelial protein E-cadherin is a calcium-dependent cell adhesion molecule that interacts with cadherin molecules on neighboring cells to create cell-cell contacts[29, 162-164]. E-cadherin is linked to the internal cytoskeleton through interactions with p120, β-catenin, and α-catenin, all components of the adherens junction. Loss of the components of the adherens junction leads to a loss of cell polarity and decreased cell-cell interactions, as well as mesenchymal phenotypes and tumorigenic behaviors.

Recently, EMT has been associated with endocrine therapy resistance in breast cancer[165]. When IDC cell line MCF-7 is exposed to Tamoxifen to produce an outgrowth of resistant cells (MCF-7^{TAMR}), crosstalk between ERα and growth signaling pathways (PI3K/AKT/mTOR) is upregulated; this upregulation drives resistance to endocrine therapies and promotes mesenchymal phenotypes[166]. Though this pathway crosstalk has been identified, the precise mechanism that drives the upregulation of this pathway remains to be elucidated. Other studies have also shown that Wnt/β-catenin signaling can be aberrantly driven in endocrine therapy resistant breast cancer, but these studies are restricted to IDC[167, 168]. These two facets have already been explored in ILC; mutations in *PIK3CA* and increased PI3K/AKT signaling have been described as major perturbations in ILC, and β-catenin is often not expressed in primary ILC tumors (Appendix B

Figure 64)[64, 67]. Further elaborations regarding these observations are currently ongoing in the ILC research field; for example, our lab has recently identified an increase of β-catenin mRNA expression in ovarian metastases from ILC patients relative to matched primary samples (*Ahmed Basudan, MS unpublished results*). However, the underlying mechanisms of Tamoxifen resistance that have been observed clinically, and pre-clinically by our group (see Chapter One), have overall remained unexplored. Further, the implications of EMT due to the genetic loss of E-cadherin in ILC have been unresolved.

2.1.1 Loss of E-cadherin is a Key Step in EMT

The generation of the neural crest during embryonic development is a prime example of appropriately timed EMT. This highly conserved process is observed from *Xenopus* to humans, and involves the direction of EMT transcription factor (EMT-TF) proteins such as SNAIL, SLUG, TWIST1, and ZEB1 to concomitantly downregulate the expression of epithelial marker E-cadherin while upregulating mesenchymal marker expressions (e.g. N-cadherin) to allow for cell migration and invagination of the early embryonic central nervous system[169]. However, cancer often hijacks this developmental process; in carcinogenesis and progression, EMT is a process by which tumor cells found in the primary lesion downregulate these same epithelial and upregulate these same mesenchymal programs to form a lesion[170]. This highly complex process allows for transition to a mesenchymal state by which cells lose cell-cell contacts, become more spindle-shaped, and gain phenotypes such as motility, migration, and invasion. Upon establishment at a metastatic site, cells will undergo the reverse process called mesenchymal to epithelial transition (MET) and will then continue to grow. This process, once thought to be fixed is instead plastic[161]. Cells can transition

from EMT to MET, and back again, or remain in an EMT-like state where certain beneficial EMT properties are consistently maintained by the cell.

Loss of E-cadherin is key to EMT because it is the molecular glue that holds cells together, whether normal or cancer. IDC cells often retain E-cadherin expression enabling them to grow together in clusters and to easily form cohesive masses[171]. As described previously, IDC cells undergo the typical EMT process to disseminate the cancer. However, as stated in Chapter One, ILCs do not express E-cadherin[71, 72, 172]. Unlike the epigenetic downregulation of E-cadherin that occurs during EMT, E-cadherin is lost at the genetic level in ILC. Typically, ILCs have mutations in *CDH1* that lead to premature termination codons (PTC) or truncated forms of proteins that are degraded by the nonsense mediated decay (NMD) pathway[65, 172, 173]. Additionally, many ILCs harbor a deletion in one of the two alleles for *CDH1*, causing a LOH. This genetic loss and subsequent mRNA and protein losses of E-cadherin suggest that ILC cells are continually in an EMT-like state. The EMT-like phenotypes and mechanisms in ILC have not yet been detailed and, in the few studies available, are debated[64, 174]. Thus, we attempted to better define these entities in ILC, particularly in their relationship to commonly used therapeutic Tamoxifen.

2.1.2 EMT is Known to Contribute to Tamoxifen Resistance via EMT-TFs Such as SNAIL

Upregulation of EMT pathways has been shown to contribute to Tamoxifen resistance[175, 176]. Some studies have shown this upregulation contributes directly to metastatic phenotypes, while others have shown that this upregulation of programs causes stem-cell like phenotypes where cells are resistant to therapeutics given. A major driver of EMT, SNAIL, has also been shown to contribute to Tamoxifen resistance in breast cancer cells[130]. SNAIL is an evolutionarily conserved

29 kDa transcription factor that interacts with DNA at conserved E-box sites (CANNTG), often in conjunction with epigenetic repressor proteins such as lysine demethylase 1 (LSD1, *KDM1A*) to repress epithelial gene *CDH1*[177, 178]. SNAIL is also able to repress the expression of *ESR1*, which can lead to 4OHT-resistant phenotypes[179]. Outside of EMT, SNAIL has been observed to upregulate EGFR/ERK pathways in T47D^{TAMR} cells to drive 4OHT resistance[130]. The direct mechanism of this upregulation remains unclear, but is not sufficiently recapitulated by repression of E-cadherin expression in T47D cells. These data suggest that SNAIL can also promote 4OHT resistance in EMT-independent manners. The implications of SNAIL in ILC have not been highly studied, and warranted further investigation in *lieu* of the observed 4OHT agonist promoting phenotypes in ILC cells[132].

2.1.3 Lack of Clarity in Role of EMT in ILC

To date, only two studies have attempted to evaluate the expressions of EMT proteins in ILC. The first study, performed by King and colleagues, involved IHC staining of n = 36 patient mastectomy samples of pure LCIS (n = 11), concurrent LCIS/ILC (n = 18), or concurrent LCIS/IDC (n = 7) for EMT proteins SNAIL and TWIST1, along with other markers of interest[64]. One of their major conclusions included observing a significant increase from LCIS to LCIS/ILC to pure ILC for TWIST1 expression ($p < 0.001$). Although this pattern of increased expression was not present for SNAIL, they did note that most of these same lesions stained with 50%+ nuclear intensity, and that mRNA expressions for *SNAI1* were higher in ILC than in IDC lesions. Due to their small sample size and inconclusive results, they concluded that further work was necessitated to evaluate the role of *SNAI1* in ILC.

A more recent study performed by Simpson and colleagues also performed IHC staining on n = 148 primary ILC lesions for a panel of EMT markers including SNAIL, TWIST1, Fibronectin, Vimentin, N-cadherin, and others[174]. This study revealed that SNAIL expression was present in only 2.2% and TWIST1 expression in 3.8% of epithelial cells from tumors stained. However, it was noted that TWIST1 expression was present in stromal fibroblasts in lesions. In addition to their IHC, a meta-analysis of TCGA ILC tumor RNA expression was performed, and did not show a relationship between *SNAI1* or *TWIST1* expression and presence of WT *CDH1* allele. These highly opposing results to the study by King (high EMT-TF staining) and contradiction to a study by Yang and colleagues (70% of ILCs have high *TWIST1* mRNA expression), created a lack of clarity for the expression of and potential role of EMT-TFs in ILC[180].

With few studies regarding EMT proteins in ILC currently published, and the observed EMT-like phenotype of ILC cells, we felt it imperative to pursue a project to elucidate the expressions of these markers in ILC, understand their contribution to EMT-like phenotypes, and assess their potential role in endocrine therapy resistance.

2.2 MATERIALS AND METHODS

2.2.1 Tissue Culture

MCF-7, T47D, MDA-MB-231, CAMA-1, ZR-75-30, SKBR3, MCF-10A, MDA-MB-134-VI, MDA-MB-330, HEK293T, and GP2-293 cells were obtained from the American Tissue Culture Collection (ATCC). BCK4 cells were generously given by the lab of Britta Jacobsen, PhD

(University of Colorado at Denver)[181]. Sum44PE cells were obtained from Asterand. IPH-926 cells were obtained from Ulrich Lehmann, PhD (Hannover Medical School, Germany)[182]. Sum44/LCCTam (abbreviated Sum44^{TAMR}) cells were provided by Rebecca Riggins, PhD (Georgetown University)[183]. T47D sh*Renilla* and sh*CDH1* cells were generated by Tiffany Katz, PhD (*unpublished*). Briefly, cells were infected with retroviral miRE-LEPG containing sh*Renilla*713 (referred to by Dr. Katz as "sh*Renilla*") or sh*CDH1* constructs (see Appendix A Table 9 for sequences). MDA-MB-134-VI rtTA cells were generated from retroviral infection of the rtTA construct by Kevin Levine, BS (a gift from Scott Lowe, PhD; Addgene#18782; modified by Dr. Lowe's laboratory). The retroviral infection protocol is detailed in upcoming section 2.2.10.

Cultures were maintained as follows: MCF-7 and MDA-MB-231 cells were cultured in Dulbecco's Modified Eagle Medium (DMEM) (Gibco#11965-092) supplemented with 5% Fetal Bovine Serum (FBS) (Gibco#26140-079), T47D and ZR-75-30 in Roswell Park Memorial Institute (RPMI) 1640 Medium (Gibco#11875-093) supplemented with 10% FBS, SKBR3 in McCoy's 5A Modified Medium (Gibco#16600-082) supplemented with 10% FBS, MCF-10A in a 1:1 mixture of DMEM and Ham's F-12 sans phenol red (Gibco#11039-021) supplemented with 5% Horse Serum (Sigma#H1270), 20 ng/mL EGF (Fisher#EA140), 0.5 mg/mL Hydrocortisone (Sigma#H6909-10ML), 100 ng/mL Cholera Toxin (Sigma Aldrich#C8052-1MG), and 10 µg/mL Insulin (Sigma#I2643-250MG), BCK4 in Modified Eagle Medium (MEM) (Gibco#11095-080) supplemented with 5% FBS, 1% Non-Essential Amino Acids (Thermo Fisher Scientific#11140-050), and 1 nM Insulin, MDA-MB-134-VI in a 1:1 mixture of DMEM with Leibovitz-15 (L-15) (Gibco#11415-064) media supplemented with 10% FBS, MDA-MB-330, HEK293T, GP2-293, and CAMA-1 in DMEM supplemented with 10% FBS, Sum44PE in a 1:1 mixture of DMEM and Ham's F-12 (F-12) (Gibco#11330-032) media supplemented with 2% dextran charcoal stripped

fetal bovine serum (CSS; Gibco#12676-027, Lot#1747185 or Gemini#100-119, Lot#A67F02H), 5 mM Ethanolamine (Sigma#E0135-100ML), 1 µg/mL Hydrocortisone, 5 µg/mL Transferrin (Sigma#T2252-100MG), 10 nM Triiodothyronine (Sigma#T5516-1MG), 50 nM Sodium Selenite (Sigma#S9133-1MG), and 5 µg/mL Insulin, and IPH-926 in RPMI-1640 supplemented with 20% FBS, 10 mM HEPES (Fisher#15630080), 1 mM Sodium Pyruvate (ThermoScientific Hyclone#SH3023901), 2.5 g/L Glucose (Gibco#A2494001), and 10 µg/mL Insulin. Sum44^{TAMR} cells were maintained in Modified Eagle's Medium without phenol red (IMEM PRF) (ThermoFisher#A10488-01) supplemented with 2% CSS, 1 µg/mL Hydrocortisone, 5 µg/mL Insulin, and 500 nM 4-hydroxytamoxifen (4OHT, Sigma#H6278, dissolved in Dimethylsulfoxide (DMSO) (ATCC#4-X-5)). Tetracycline-Free FBS was a gift from Timothy Burns, MD, PhD.

Routine culture was performed by removal of media, gentle rinsing of cells in 1X DPBS (Corning CellGro#21-031-CV), and treatment with 0.25% Trypsin-EDTA (Gibco#25200-056) until cells were in single-cell suspension. Trypsin was deactivated with base media, except for Sum44PE which were deactivated in DMEM supplemented with 5% FBS. Cells were always centrifuged at 14,000 rpm for 4 minutes at room temperature to completely remove trypsin prior to plating. Plating densities for given assays are included in each respective section, while routine maintenance was performed with no harsher than 1:2 or 1:3 splits for ILCs and 1:5 to 1:20 cells for IDC or control cell lines, as deemed necessary. Cells were authenticated at the University of Arizona Genetics Core by Short Tandem Repeat (STR) profiling, comparisons were made to available cell line profile databases, and cells used were taken from authenticated stocks stored in liquid nitrogen.

2.2.2 Estrogen Deprivation Studies

Estrogen deprivation was performed as previously described[132]. Briefly, cells were either grown to 70-90% confluence and bulk deprived in T75 or T150 flasks, or plated directly into 12 (IDC: 90,000 cells/well; ILC: 270,000 cells/well) or 6 welled (IDC: 1,000,000 cells/well; ILC: 2,000,000 cells/well) plates for estrogen deprivation after seeding at set densities. Once cells were adherent for minimum 1.5 days in respective growth environments, they were washed 3-5 times per day, twice at each wash with half total volume of each container size (e.g. 1 mL wash in 6 welled plate, 0.5 mL wash in 12 welled plate, etc.) with IMEM/PRF (ThermoFisher#A10488-01). Cells were then incubated in IMEM/PRF supplemented with 10% CSS with minimum one hour between wash sets. This was repeated for three days total. Splitting of cells was performed with phenol red free 0.05% trypsin (Gibco#15400-054). Estradiol (E2) (Sigma#E2758) and 4OHT (described in 2.2.1) were dissolved in DMSO. ICI 182,780 (ICI) (Tocris Bioscience#1047) was dissolved in 100% Ethanol (Decon Laboratories#2701).

2.2.3 Dose Response Assays

Cells were seeded at 5,000 cells/well for IDCs or 15,000 cells/well for ILCs in six replicate wells of a 96 welled 2D (Fisher#353072) or flat bottomed ultra-low attachment (ULA) (Corning#3473) plate for each concentration of drug tested. Vehicle controls were always included, as well as media blank wells, and unused wells were given equal volume 1X DPBS to keep consistent surface tension across the plate, and to avoid evaporation of inner wells. Cells were seeded 1 to 1.5 days prior to treatment and typically collected at day 7 (D_7) unless otherwise noted. Upon time point of collection, media was flicked off of 2D plates, extraneous media was wicked with a paper towel,

and plates were promptly frozen at -80°C. Plates were then thawed to room temperature and osmotic pressure was applied across entire plates at 100 µL/well water, with incubation at 37°C for one hour, and freezing plates again at -80°C. Plates were again thawed, and then Hoechst dye was applied and measurements assessed for fluorescence per manufacturer's protocol of the FluoReporter Blue Fluorometric dsDNA Quantitation Kit (ThermoScientific#F2962) on a PerkinElmer 2030 Multilabel Reader with VictorX software. For ULA assessment, experimental plates were obtained from the incubator and brought to room temperature without exposure to light for approximately 30 minutes. Then, room temperature reagent from the CellTiter-Glo Luminescent Cell Viability Assay kit (Promega#PR-G7573) were prepared, applied, and stored per manufacturer's protocol and added in a 1:1 ratio to well contents with rocking at 2 minutes without exposure to light to lyse cells, and further incubation at room temperature for 10 minutes to stabilize luminescence. Contents were then transferred to white walled luminescent plates (Corning#3912) and were measured on a Promega Glo-Max Microplate Reader. Data were corrected for each experiment by subtracting average background fluorescence (2D) or luminescence (ULA) from values, and normalizing to respective vehicle controls as "1." Outliers were removed using Grubb's Test at $\alpha = 0.05$. Error was displayed as standard deviation of the mean (STDEV).

2.2.4 Reverse-Phase Protein Array (RPPA)

MDA-MB-134-VI and Sum44PE cells were seeded at 70-80% confluence and were incubated in media supplemented with serum or were deprived and treated for 24 hours ± 1 nM E2. Samples were collected in MD Anderson RPPA lysis buffer (1% Triton X-100 (Sigma#T8785-50ML) , 50 mM HEPES, pH 7.4, 150 mM NaCl, 1.5 mM $MgCl_2$, 1 mM EGTA, 100 mM NaF (New England

Biolabs#P0759L), 10 mM NaPyrophosphate, 1 mM Na_3VO_4 (New England Biolabs#P0758S), 10% Glycerol (Fisher#BP2291)), supplemented with 1X Halt™ Protease Phosphatase Inhibitor Cocktail (PPis) (Thermo Fisher Scientific#78430) by rocking samples on ice for 20 minutes. Samples were scraped into tubes and centrifuged for 10 minutes at 14,000 rpm at 4°C. Supernatant fractions were saved, quantified by BCA (Thermo Scientific#23225), and mixed with 1X final concentration 4X SDS sample buffer (40% Glycerol, 8% Sodium Dodecyl Sulfate (SDS) (Fisher#O2674-25), 0.25M Tris-HCl, pH 6.8, 1% β-mercaptoethanol (Sigma#M6250-100ML)) prior to freezing at -80°C. Samples were quantified for expression of 200 proteins or phospho-proteins at the Functional Proteomics Core of MD Anderson. Data were measured as log_2-normalized, median centered values, and plotted with Multi Experiment Viewer v4.8.1.

2.2.5 Quantitative Real Time Polymerase Chain Reaction (qRT-PCR)

Triplicate samples of mRNA were isolated using manufacturer's protocols of either the illustra RNAspin Mini Kit (GE Healthcare#25-0500-72) or NucleoSpin RNA Kit (Takara Clontech#740955.250) and quantified by NanoDrop Spectrophotometer (ThermoScientific). For deprivation studies, 250 ng of mRNA were converted to cDNA, and for endogenous studies 500 ng of mRNA were converted, both using 1X iScript (BioRad#1708891) manufacturer's protocol. Samples were assessed by qRT-PCR using SsoAdvanced™ Universal SYBR® Green Supermix (BioRad#1725274), Nuclease Free Water (Ambion#AM9938), and primers listed in Appendix A Table 5 with 0.5 μM final concentrations per reaction. All qRT-PCRs were performed in two to three independent experiments with data corrected to internal control gene *RPLP0*, outliers removed using Grubb's Test for Outliers (standard $\alpha = 0.05$), and shown relative to MCF-7 (endogenous comparisons), Vehicle (deprivation studies) or *Scramble*/*Renilla* controls, if required.

2.2.6 Immunoblotting (IB)

Protein was isolated according to experimental design. In deprivation studies, lysates were isolated using the MD Anderson RPPA protocol. Whole cell lysates in proteasomal degradation studies received vehicle (DMSO) or 5 µM MG132 (Sigma#M8699-1MG) (denoted in figure legend, as appropriate) for 2 hours prior to isolation. Protein in basal expression studies were isolated using RIPA buffer (50 mM Tris, pH 7.4, 150 mM NaCl, 1 mM EDTA, 0.5% Nonidet P-40 (Sigma Aldrich#21-3277 SAJ), 0.5% NaDeoxycholate, 0.1% SDS) supplemented with 1X PPis, sonicated in a 4°C cup horn sonicator at amplitude 100 for 5-10 minutes total with 1-minute pulses and 30 second pauses, and centrifuged for 10 minutes at 14,000 rpm at 4°C. All samples were quantified for protein concentration using BCA Assay and 25-50 µg per sample (noted in figure descriptions) were run on 15% or 4-15% gradient homemade SDS-PAGE gels with transfer to PVDF membranes (Millipore#IPFL00010). When utilizing the Odyssey system (LiCor), membranes were blocked using Odyssey PBS blocking buffer (LiCor#927-40000) for one hour and probed with primary antibodies listed in Appendix A Table 6. After removal of primary antibodies, blots were washed with 1X PBS-Tween 20 (0.1%) for 10 minutes, three times, followed by incubation in 1:10,000 secondary antibodies (anti-mouse 800CW: LiCor#925-32210; anti-rabbit 800CW: LiCor#925-32211). Blots were again washed prior to imaging on the Odyssey Infrared Imaging system (LiCor). When using film methods, membranes were blocked in 5% BSA (Sigma Aldrich#A9647-500G) or 5% milk (Fisher#NC9121673) for one hour, and probed with primary antibodies as previously described. After removal of primary antibodies, blots were washed as previously, followed by incubation in 1:10,000 secondary antibodies (anti-mouse: anti-Mouse IgG, HRP-linked Ab Cell Signaling#7076; anti-rabbit: anti-Mouse IgG, HRP-linked Ab Cell Signaling#7074). Bands were visualized after application of Clarity Western ECL Substrate

(BioRad#170-5061) or Thermo SuperSignal West Femto Chemiluminescent Kit (Fisher#PI-34094) per manufacturer's protocols, and exposure in a dark room to standard film (HyBlot CL Autoradiography Film, Denville Scientific#E3018), with standard film processing. Blots were stripped after two washes with rocking at room temperature in 1X PBS-Tween 20 (0.1%) for 5 minutes, each, followed by application (with rocking) of 1X Newblot PVDF Stripping Buffer (LiCor#928-40032) diluted in water for 15 minutes, and washed again prior to blocking. Stripping was never performed more than twice, and Actin was always probed at the final step.

2.2.7 Chromatin Immunoprecipitation (ChIP), IP Validation, and ChIP qRT-PCR

For ERα ChIPs, MDA-MB-134-VI cells were 80-90% confluence prior to deprivation. After deprivation, cells were treated to ten-fold molar excess of top dose-response concentrations assessed for E2 or 4OHT. At the treatment time point, media was removed prior to further processing. At time of processing, cells were fixed in 1% Formaldehyde (Polysciences#18814) for 10 minutes while rocked at room temperature. Quenching was then performed with 0.125 M Glycine for 5 minutes with rocking at room temperature, samples were washed three times in cold 1X DPBS supplemented with 1X PPis, were scraped into tubes, and centrifuged at 2,500 rpm for 5 minutes at 4°C. Supernatant were aspirated and pellets were resuspended in 1 mL Nuclei Preparation Buffer (5 mM PIPES, 85 mM KCl, 0.5% NP-40, pH 8.0, 1X PPis) with rotating at 4°C for 30 minutes. Samples were centrifuged at 2,500 rpm for 5 minutes at 4°C. Supernatant were again aspirated, and pellets were resuspended in 300 µL TE Buffer (10 mM EDTA, 50 mM Tris-HCl, pH 8.1, 1X PPis, 1% final concentration SDS). Samples were sonicated at amplitude 100 for 25 minutes total with 1 minute pulses and 30 second pauses, and then centrifuged at 14,000 rpm for 10 minutes at 4°C. Supernatant were collected and portions of samples were checked for DNA

shearing between 200-700 base pairs. Briefly, 10 µL of sample were combined with Elution Buffer (1% SDS, 0.1 M $NaHCO_3$), boiled for 15 minutes at 100°C, cooled to room temperature, incubated with 1 µL of 10 mg/mL RNase A (Qiagen) for 15 minutes at room temperature, purification of DNA using manufacturer's protocol of the QiaQuick PCR Purification Kit (Qiagen#28106), and 15 µL of DNA product were run on a 1% agarose gel supplemented with 1X SYBR Safe (Thermo Scientific#S33102) with 1X final concentration DNA Loading Buffer (Thermo Scientific#R0611) against GeneRuler 1 kb Plus DNA Ladder (Thermo Scientific#SM1331) by standard electrophoresis, with assessment of smears by ultraviolet (UV) light. Upon confirmation of shearing, samples were quantified by BCA as previously described, portions of samples were saved for input use, and remaining samples were diluted 1:10 in Dilution Buffer (1% Triton X-100, 2 mM EDTA, 150 mM NaCl, 20 mM Tris-HCl, pH 8.1, 1X PPis) and were precleared with 5 µg Rabbit Immunoglobulin G (IgG) and 135 µL Protein G-Sepharose (Thermo Fisher#10-1243) by rotating at 4°C for 2 hours. Beads were pelleted by centrifugation at 1,000 rpm for 1 minute at 4°C, and supernatant were collected. Samples were split into fractions for IgG or antibody of interest (Appendix A Table 7) for immunoprecipitation (IP) or chromatin immunoprecipitation (ChIP) with rotation overnight at 4°C. Samples were given 55 µL Protein G-Sepharose beads the next morning, and samples were rotated for 1 hour at 4°C prior to centrifugation at 1,000 rpm for 1 minute at 4°C. For IP sample verification, samples were washed three times in 1X DPBS supplemented with 1X PPis by rotating at 4°C for 5 minutes, and centrifugation at 1,000 rpm for 1 minute at 4°C; upon completion of washes, protein were eluted from beads and samples were processed as previously described by standard immunoblotting technique against 10% input. For ChIP samples, pelleted samples were washed sequentially by rotating at 4°C for 5 minutes each, followed by centrifugation as previously with the following: TSE I (1% Triton X-100, 2 mM

EDTA, 20 mM Tris-HCl, pH 8.1, 150 mM NaCl, 1X PPis), TSE II (1% Triton X-100, 2 mM EDTA, 20 mM Tris-HCl, pH 8.1, 500 mM NaCl, 1X PPis), Buffer III (0.25 M LiCl, 1% NP-40, 1% Deoxycholate, 1 mM EDTA, 10 mM Tris-HCl, pH 8.1, 1X PPis) and twice with TE Buffer. ChIP samples were then combined with 100 µL Elution Buffer, vortexed, and incubated at 65°C for 30 minutes with rotation. Samples were centrifuged and supernatant were collected. Eluates were heated at 65°C for 6 hours along with input fractions that were combined with Elution Buffer. DNA was isolated using the Qiagen PCR Purification Kit protocol. ChIP qRT-PCR were performed using input samples diluted 1:5 and samples diluted 1:3, with 5 µL per technical replicate well. ChIP qRT-PCR Primers used are listed in Appendix A Table 8. ERα ChIPs were performed twice, independently. Data were analyzed using fold enrichment over IgG controls with removal of outliers by Grubb's Test ($\alpha = 0.05$), and displayed with STDEV for technical triplicates.

2.2.8 Transient si*RNA* Knockdown Assays

Cells were reverse transfected by Lipofectamine™ RNAiMAX manufacturer's protocol (Thermo Fisher Scientific#13778-150). For preliminary assessments, 10, 25, 50, or 100 nM were utilized to assess best dose. For subsequent assays, 10 nM were utilized for *SNAI1* or *KDM1A* knockdown assays, and 25 nM were used for *CDH1* (previously assessed by others in lab to be effective). For si*SNAI1* assays, ON-TARGETplus Non-targeting Pool (Dharmacon#D-001810-10-05) or ON-TARGETplus Human *SNAI1* siRNA (Dharmacon#L-010847-01-0020) were used. For si*KDM1A* assays, the same si*Scramble* was used as in si*SNAI1* assays, and ON-TARGETplus Human *KDM1A* si*RNA* (Dharmacon#J-009223-07 or J-009223-08) were used. For si*CDH1* assays, siGENOME Non-targeting si*RNA* Pool#2 (Dharmacon#D-001206-14-50) or siGENOME Human *CDH1* si*RNA* Pool (Dharmacon#M-003877-02-0010) were used. In basal expression assays, si*RNA*

complexes were generated in Opti-MEM® I (Gibco#31985-070) for 24-48 hours prior to assessment of downstream applications. In deprivation assays, si*RNA* complexes were generated in Opti-MEM® I without phenol red (Life Technologies#11058-021).

2.2.9 2D, ULA Proliferation Assays

Cells were seeded at densities previously assessed to be appropriate given cell size and doubling time (*Matthew Sikora, PhD unpublished data*). Cells were plated in technical replicates of 3-6 at 15,000 (ILC) or 5,000 (IDC) cells/well, and plates were collected at appropriate time points for each assay as previously described. Data were plotted after correction to background media fluorescence relative to initial day values, outliers were removed by Grubb's Test ($\alpha = 0.05$), and error displayed with STDEV. Non-linear exponential regressions were fitted to each data set and were used to test differences in rates of growth. ULA proliferation was performed as previously described with data processing as performed in this section. Inducible cells were treated to Doxycycline Hyclate (Dox; Sigma-Aldrich#D98981-1G; dissolved in water) in doses indicated in experimental legends.

2.2.10 Generation of Virus for Stable Knockdown/Overexpression Cell Lines or Transient Virus Studies

Plasmid information for Lentiviral sh*Scramble*/*SNAI1*, miRE-LEPG Retroviral sh*Renilla*/*SNAI1*, LT3GEPIR sh*Renilla*/*SNAI1*, pENTR221 *SNAI1* ORF 124, Lentiviral W118, pINDUCER20-*SNAI1*, and information regarding packaging plasmids are available in Appendix A Table 9, 10. Standard restriction enzyme digests were performed to generate backbones of interest and products

were ligated with T4 DNA Ligase (New England Biolabs#M0202M). Gateway Cloning was performed by manufacturer's protocols using Gateway LR Clonase II Enzyme Mix (Invitrogen#11791-020). Third generation packaging systems were utilized in HEK293T (Lentiviral) or HEK293T-GP2 (Retroviral) cells by polyethylenimine (PEI) transfection (1 µg/mL; Polysciences#23966-2) with a 3:1 ratio of PEI to transfected DNA constructs. sh*PASHA* was always transfected with sh*RNA* of interest to inhibit the transfected cells' capability of degrading potentially lethal sh*RNA* complex generation. Target media for each respective cell line was placed on virus producing cells and collected at the 36- and 48-hour time points, filtered through 0.45 µm filters (Fisher#09-754-21), and combined with 1 µg/mL Polybrene (Sigma#107689-10G) to infect target cells. Target cells were recovered after two infections in media without antibiotics for two days, and then split into 1 µg/mL Puromycin (Life Technologies#A11138-03) or 1.25 mg/mL Geneticin G418 (Invitrogen#10131-035), depending upon the backbone of interest. Cells were always maintained in selection antibiotic.

For transient virus assays, virus containing media were generated as in the previous paragraph, but were only placed on cells at the 24- to 36-hour time point post PEI transfection, and were removed 24 hours post infection of target cells with appropriate BSL2+ protocol. Downstream assays for mRNA, protein, and proliferation were performed as previously described (see 2.2.5, 2.2.6, and 2.2.9).

2.2.11 Matrigel, Collagen I Assays

For Matrigel (BD Biosciences#354230) assays, cells were seeded at 2,500 cells/well (MDA-MB-231), 5,000 cells/well (MCF-7), or 15,000 cells/well (ILCs) in single wells of 8-welled LabTek Chambered Coverglass slides (Fisher#155409). Media was supplemented with

Penicillin/Streptomycin (Hyclone#SV30010). Media were changed every four days, and "on top" cultures were supplemented with 2% Matrigel each time a change occurred. ILC wells were additionally treated to control or Dox (0.5 µg/mL). Collagen I (Corning#354249) was utilized for Collagen assays in 24-welled plate formats with duplicate wells for each embedded cell type/treatment. Colonies were imaged on a Nikon Hammamatsu camera under phase microscopy of an Olympus IX83 (Olympus) inverted microscope.

2.2.12 Mammosphere Assay

Mammosphere media was composed of the following: 1:1 DMEM/Ham's F-12 media, 20 ng/mL bFGF (BD Biosciences#354060), 20 ng/mL EGF (BD Biosciences#354001), B27 (Gibco#17504), 2.5 mL Penicillin/Streptomycin, and 4 µg/mL Heparin (Sigma#H4784). Cells were cultured in triplicate wells of six welled ULA Plates (Corning#3471). Cells were trypsinized as previously described, centrifuged, and resuspended in 1X DPBS to remove serum from base media. Cells were then counted by Hemacytometer and were plated in single-cell suspensions for primary cultures; MCF-7 cells were plated at 20,000 cells/well in each of the replicate wells, and inducible ILC cells were plated at 60,000 cells/well in each of the replicate wells for control or Dox (0.5 µg/mL) treatment. Plates were agitated by brief shaking every three days to prevent clumping of spheres, and 1 mL media (with or without Dox) were replenished every three to four days. Secondary and tertiary cultures were generated by hand-counting, collecting spheres, centrifugation at 1,000 rpm, trypsinization with 0.05% trypsin (Gibco#25300-054) for 10 minutes with refluxing of cells every 5 minutes, deactivation of trypsin with mammosphere media, and centrifugation at 1,000 rpm. Cells were counted with a Hemacytometer and plated for subsequent cultures at 2,000 (MCF-7) or 6,000 (ILCs) cells/well to enrich for stem-like cells. Spheres were

imaged on days 4, 10, 17, 24, and 34 using a Nikon Hammamatsu camera under phase microscopy of an Olympus IX83 (Olympus) inverted microscope. Spheres larger than ~50 µm were hand-counted on days 10 (primary), 20 (secondary), and 34 (tertiary) using a standard bright field microscope.

2.2.13 Flow Cytometry Assays

Cells were plated in triplicate at 300,000 cells/well in 6 welled plates, treated per experimental design ± 0.5 µg/mL Dox, and were collected by standard trypsinization and centrifugation, diluted to 1 x 10^6 cells/mL in standard media, with pellets were treated to 20 µg/mL Hoechst 33342 (Life Technologies#H3570) at 37°C, 5% CO_2 while protected from light for 30 minutes. Just prior to measuring, 2.5 µg/mL Propidium Iodide (PI; Sigma#P4170) were spiked into the mixture. Cells were quantified on a BD LSR II Flow Cytometry machine with compensation controls previously provided for BCK4 cells by Nilgun Tasdemir, PhD. ALDH Flow Cytometry was performed by Jian Chen, MS, using the ALDEFLUOR protocol (STEMCell Technologies#01700).

2.2.14 Immunohistochemistry (IHC)

Formalin fixed paraffin embedded (FFPE) pellets were generated for BCK4 pINDUCER20-*SNAI1* ± Dox and MDA-MB-134-VI as follows: upon collection of cells, media were removed, and cells were washed with 1X DPBS twice. Cells were then fixed in 10% neutral buffered formalin (Sigma Aldrich#F554-4L) for three hours at 4°C. Formalin was decanted to half-volume, and cells were scraped into a conical for centrifugation at 1,400 rpm for 4 minutes at room temperature. Pellets were transferred in small volumes of formalin to 1.5 mL centrifuge tubes and were centrifuged as

previously, with removal of all formalin prior to freezing at -80°C for one hour. Samples were processed for embedding in paraffin by the Magee-Womens Research Institute Histology and Microimaging Core facility and were cut at 5 µm sections on a standard microtome for staining on 25 x 75 x 1.0 mm microscope slides (Fisher#12-550-20). Tissue Microarray (TMA) for ILC and IDC tumors was accessible from clinical samples obtained through the Health Sciences Tumor Bank (HSTB) at Magee-Womens Hospital, previously prepared by our lab (ILC samples from IRB#PRO11110119; IDC samples from an additional IRB, protocol number unavailable at time of dissertation submission). IHC was performed with SNAIL Cell Signaling antibody (Cell Signaling#3895S) with the collaboration of Ms. Kara Burlbaugh.

2.2.15 Transient SNAIL-LSD1 Overexpression Study in HEK293T Cells and Endogenous Co-IP

SNAIL-HA (a gift from Paul Wade, PhD; Addgene#31697) and LSD1-FLAG (collaboration with Yi Huang, PhD; originally purchased by Dr. Huang from GeneCopoeia) were transiently transfected into HEK293T cells using Lipofectamine3000 manufacturer's protocol for 48 hours (ThermoFisher Scientific#L300015). Isolated samples were processed as previously described for IP (using Cell Signaling SNAIL antibody) and IB. Co-IPs were performed with ChIP-Grade antibodies using the ChIP IP protocol.

2.2.16 Soft Agar Anchorage Independent Assays

Soft Agar Anchorage Independent assays were performed in 35 mm culture dishes (Falcon#353001) arranged in 15 cm^2 dishes with a constantly replenished 35 mm culture dish

containing water, as a modified humidifier chamber to prevent drying of agar. Due to length of assays, Enhanced Media (EM) was generated for each respective cell type, containing basal media, 20% serum final concentration, and 2% NEAA. First, lower 0.6% final concentration agar mixtures were generated (Bacto-Agar; BD Biosciences#214050; autoclaved 1.2% stock in sterile water) by microwaving solidified agar and combining with EM for each respective cell type as a diluent. Agar was immediately incubated in a ~42-45°C water bath to prevent need to continue to microwave and compromise use of agar, and to not shock or kill cells in subsequent steps. Once lower layers were solidified at room temperature for approximately 30-45 minutes, upper layers of agar mixtures were generated. Cells were plated at 10,000 cells/dish for IDCs (standard density) or ILCs (low density), or 50,000-100,000 cells/dish for ILCs (high density, denoted in figure legends) gently on top of 0.6% layers. Upper layers contained 0.4% final concentration of agar, 3% final concentration NEAA, and cells. Agar was always added last to the mixture prior to plating, as it solidified quickly and would cause clumps if not done in this fashion. Agar was added slowly enough to dispense evenly across the top layer and not to slip beneath 0.6% layer, but quickly enough to not induce clumps. Triplicate samples were generated for each cell type or plating density. “Blanks” containing no cells and only EM, additional 1% NEAA, and 0.4% final concentration agar were generated for each media type to be used in crystal violet background subtraction at the end of the experiment. Once all plates solidified for an additional 30 minutes at RT, they were placed in the modified humidifier chamber and into the respective incubator setting. Humidifier chambers were replenished as required, and dishes were collected at $D_{14\text{-}28}$, and stained with 1 mL/dish 0.005% crystal violet (Sigma Aldrich#C3886) for 15 minutes at room temperature prior to washing agar gently with 1 mL/dish sterile water, twice. Blank and experimental dishes were then imaged immediately on an SZX16 (Olympus) dissecting microscope with a Nikon DP73

camera under bright field at 0.8X magnification to obtain whole field views. Colonies were counted using cellSens Dimension (Olympus) software on a consistent region of interest (ROI) after subtraction of background crystal violet staining. Colonies were defined as measured objects with a radius of 25 µm or greater. Debris or aberrancies in the agar were manually removed from counts. Representative images of colonies were obtained by bright field imaging at 10X magnification under an inverted IX83 microscope (Olympus).

2.2.17 Protein Micropatterning/Coating Studies

Protein micropatterning was performed in the Adam Feinberg, PhD laboratory located at Carnegie Mellon University (CMU). All materials and equipment except glass coverslips and tissue culture plates/media were provided by his laboratory. Standard polydimethylsiloxane (PDMS) micropatterning stamps with 20 µm linear patterns were generated by Rebecca Duffy, PhD and Rachelle Palchesko, PhD, who also assisted in training of the subsequent procedures. Glass coverslips (Fisher#12-545-86) were sonicated for 1 hour in 95% Ethanol, and were then dried in a sterile environment for 30 minutes prior to spin coating. PDMS was generated by mixing 10 parts Dow Corning Sylgard 184 elastomer base with 1 part Sylgard 184 elastomer curing agent, and degassing for 10-15 minutes in a THINKY Super Mixer. PDMS was used within 2 hours or less after generation. A standard spin coating machine was utilized to evenly coat the surface of each coverslip as follows: 1/3rd area of the coverslip was coated with a drop of PDMS, and then a sequence of Dispense 1, Ramp 5 – RPM 500 – Dwell 5, Ramp 5 – RPM 1000 – Dwell 5, Ramp 10 – RPM 3000 – Dwell 10, Ramp 10 – RPM 4000 – Dwell 60, Ramp 10 – RPM 2000 – Dwell 15, Ramp 10 – RPM 1000 – Dwell 10, and Ramp 5 – RPM 500 – Dwell 5 was performed (approximately 2 minutes and 45 seconds run time per coverslip). Coverslips were cured in a 65°C

oven overnight prior to patterning. The next day, micropatterning stamps were sonicated in a beaker with 50% Ethanol for 30 minutes and coverslips were treated to UV light and ozone gas to sterilize for 15 minutes. Stamps were dried using a nitrogen gun prior to use and after washing in between uses. Fibronectin (50 µg/mL final concentration), Collagen I (200 µg/mL final concentration), Collagen IV (200 µg/mL final concentration), and Laminin I (200 µg/mL final concentration) were prepared in sterile water, and were stored on ice during use. For the first coating process, each protein of interest was coated onto the surface of a stamp (200 – 300 µL mixture) and incubated at room temperature for one hour. The stamps were then rinsed in sterile water to remove extra protein and were applied to respective coverslips with slight pressure to generate diffraction pattern. The stamps were then rinsed with water, dried with a nitrogen gun, coated again (~100 µL/stamp after the first coating) with 10-minute incubation, and repeated stamping process. Upon completion of stamping, coverslips were submerged in 1% (w/v) Pluronic F-127 solution for five minutes to inhibit cell/protein adhesion to the regions between stamped protein lines. Coverslips were stored in 1X DPBS in 6 welled plates at 4°C until being used within 2 weeks of generation. Complete protein coating studies were performed with the same concentrations described in the previous paragraph, but without micropatterning, on PDMS spin-coated coverslips. Uncoated glass coverslips were used as controls for cell adhesion. Batimastat was a gift from Dr. Adam Feinberg.

2.2.18 Statistics

Technical or biological replicates were described in respective sections and detailed in figure legends. Experiments were repeated at minimum 2-3 times, unless otherwise noted, and data were combined when able or displayed as representative of multiple experimental outcomes.

Corrections, error, and normalization were also described in each respective section, and are highlighted in figure legends. Grubb's test for outliers was used for data sets containing three or more values to remove outliers ($\alpha = 0.05$). Graphs were generated in GraphPad Prism 5.0 or using R statistical software. Dose responses were fitted with three variable parameters to assess IC_{50} values. 2D and ULA proliferation curve fitting was previously described with comparisons of rates between best-fit exponential growth curve fits. Two comparisons were performed with Students t-test, and for data sets with more than two groups, One Way ANOVA followed by Tukey's post-test were performed ($\alpha = 0.05$). Kevin Levine, BS and Ahmed Basudan, BS assisted with statistical analyses on clinical sample data (denoted in Figure legends). A collaboration with Li Zhu, MS of the George Tseng, PhD biostatistics laboratory at the University of Pittsburgh was utilized for comprehensive genomic analyses.

2.3 RESULTS

2.3.1 4OHT Acts as a Partial Agonist in Some ERα Positive ILC Cell Lines

We previously identified a role for *de novo* 4OHT resistance in ILC cell line MDA-MB-134-VI; we observed that 4OHT treatment caused an induction of 2D proliferation in MDA-MB-134-VI over vehicle control treated cells[132]. We expanded our ILC panel to test for this partial agonist proliferation phenotype to include all $ER\alpha^+$ ILC cell lines available, and included E2 dose responses. The 4OHT partial agonist induction of 2D proliferation was reproducible in MDA-MB-134-VI (1 μM 4OHT = +1.70 fold change (FC) relative to vehicle), however, it was not apparent in Sum44PE, BCK4, or MDA-MB-330 (Figure 4A). E2 induced proliferation in MDA-MB-134-

VI, Sum44PE, and BCK4, and only mildly in MDA-MB-330. This was not surprising, as the MDA-MB-330 have minimal ERα activity[132, 184]. Our lab has recently observed a preference for ILC cells to grow in ULA conditions (*Nilgun Tasdemir, PhD data unpublished*), so we asked if this 4OHT-inducing growth phenotype was also present in ULA conditions in a ULA proliferation assay with the maximal dose response concentrations from the 2D conditions (1 μM 4OHT or 1 nM E2). Though E2 treatment significantly induced ULA proliferation (***$p < 0.0001$), 4OHT treatment did not induce proliferation in this environment, and instead had a suppressive impact on proliferation as compared to vehicle (**$p = 0.0002$) (Figure 4B). In contrast, the control 2D proliferation assay showed +1.8 FC 4OHT-induced proliferation relative to Vehicle control (**$p = 0.0046$). We thus concluded that 4OHT induced proliferation in MDA-MB-134-VI in the 2D setting, and pursued most of our remaining assays in this environment.

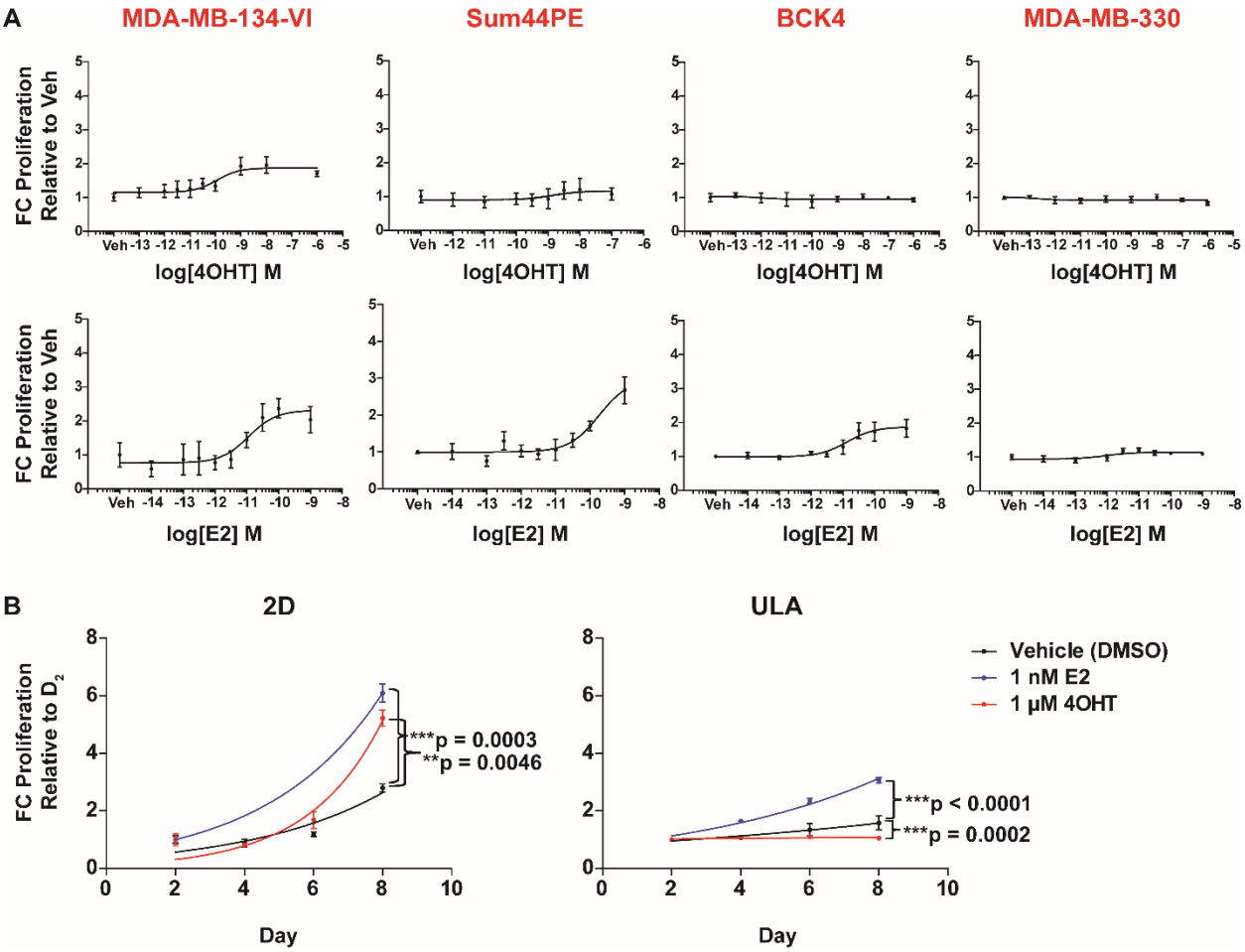

Figure 4: 4OHT Induction of 2D Proliferation in MDA-MB-134-VI

(A) E2 deprivation followed by treatment with increasing doses of 4OHT or E2 for 6-7 days was performed in ERα$^+$ ILC cell lines. Non-linear, three parameter fits were applied to data. Data are representative of a single experiment with six technical replicates ± STDEV, except for MDA-MB-134-VI, which was repeated independently at minimum three times with similar results. (B) 2D and ULA proliferation were measured in MDA-MB-134-VI cells over 8 days with respective top dose response concentrations of 4OHT or E2. Exponential growth curves were fitted to four technical replicates ± STDEV, and rates were compared between vehicle and 4OHT or E2 treated cells (*p < 0.05, **p < 0.005, ***p < 0.0005). Data are representative of two independently performed experiments with similar results in both (2D), or a single experiment (ULA).

2.3.2 SNAIL is Upregulated by 4OHT and E2 Treatments

We next decided to probe the potential mechanism behind this 4OHT-driven induction of 2D proliferation in MDA-MB-134-VI cells. First, we mined previously generated NanoString array

data, which revealed EMT-TF *SNAI1* to be the most potent 4OHT- and second most potent E2-induced gene in MDA-MB-134-VI (+1.389 and +2.012 log2FCs, respectively, relative to time-matched Vehicle control at 24 hours)[132]. To more comprehensively study the effects of E2 on protein regulation in ILC, we performed RPPA in the MDA-MB-134-VI and Sum44PE cells. SNAIL was upregulated by E2 in both cell lines, more potently in MDA-MB-134-VI (+1.491 log2FC) and less robustly in Sum44PE (+0.185 log2FC) (Figure 5). ERα activating phosphorylation at S118 was the only other protein target on this array that was more highly induced than SNAIL in MDA-MB-134-VI cells. Additionally, there were various other targets that were induced or repressed by E2 treatment in these cells, and can be found in Appendix B Figure 65[132, 185].

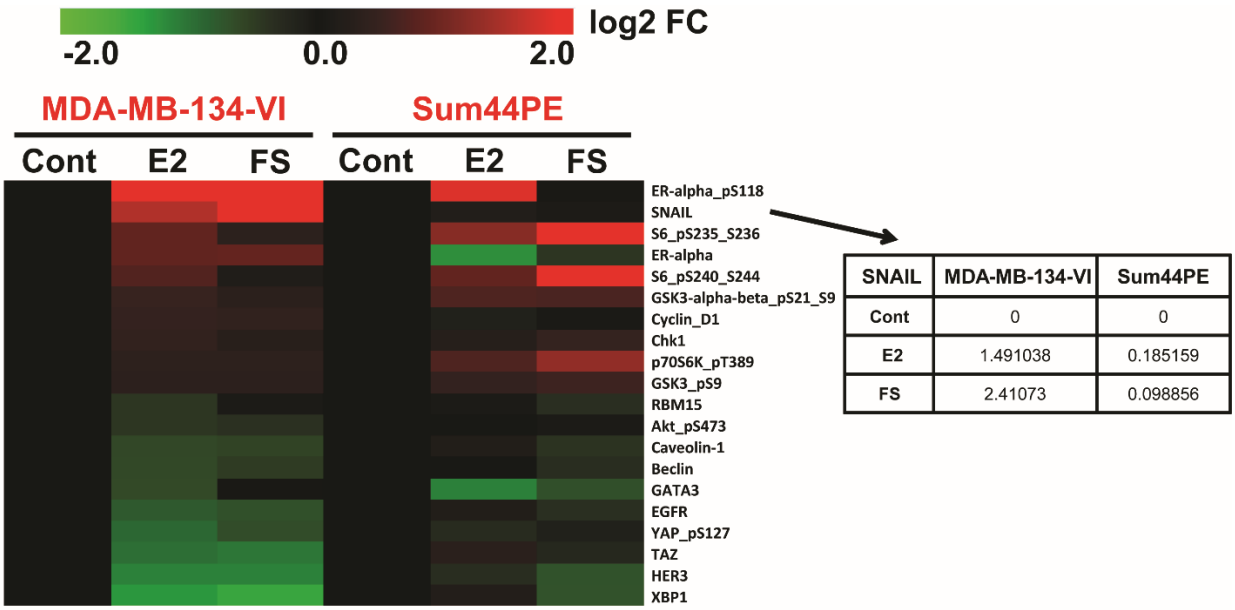

SNAIL	MDA-MB-134-VI	Sum44PE
Cont	0	0
E2	1.491038	0.185159
FS	2.41073	0.098856

Figure 5: RPPA Reveals SNAIL is Induced by E2 in MDA-MB-134-VI and Sum44PE
MDA-MB-134-VI and Sum44PE cells were deprived (Cont) of exogenous E2 for a period of three days followed by treatment with 1 nM E2 for 24 hours. Control, E2-treated, and Full Serum (FS) controls were assessed by RPPA. Single replicate samples were isolated and measured for each cell line and condition. Data were sorted by top ten MDA-MB-134-VI E2-upregulated and top ten E2-downregulated proteins. Extracted data for SNAIL is depicted in the table.

We next validated the E2 and 4OHT mRNA upregulation of *SNAI1* in our panel of ILC ERα$^+$ cell lines, and tested potential upregulation in two IDC ERα$^+$ cell lines, MCF-7 and T47D. Upregulation of *SNAI1* by 4OHT was observed in MDA-MB-134-VI and Sum44PE qRT-PCR, while not present in the other two ILC or two IDC cell lines tested (Figure 6). Instead, E2 upregulated *SNAI1* in most of the cell lines, though most significantly in MDA-MB-134-VI (***p < 0.0005).

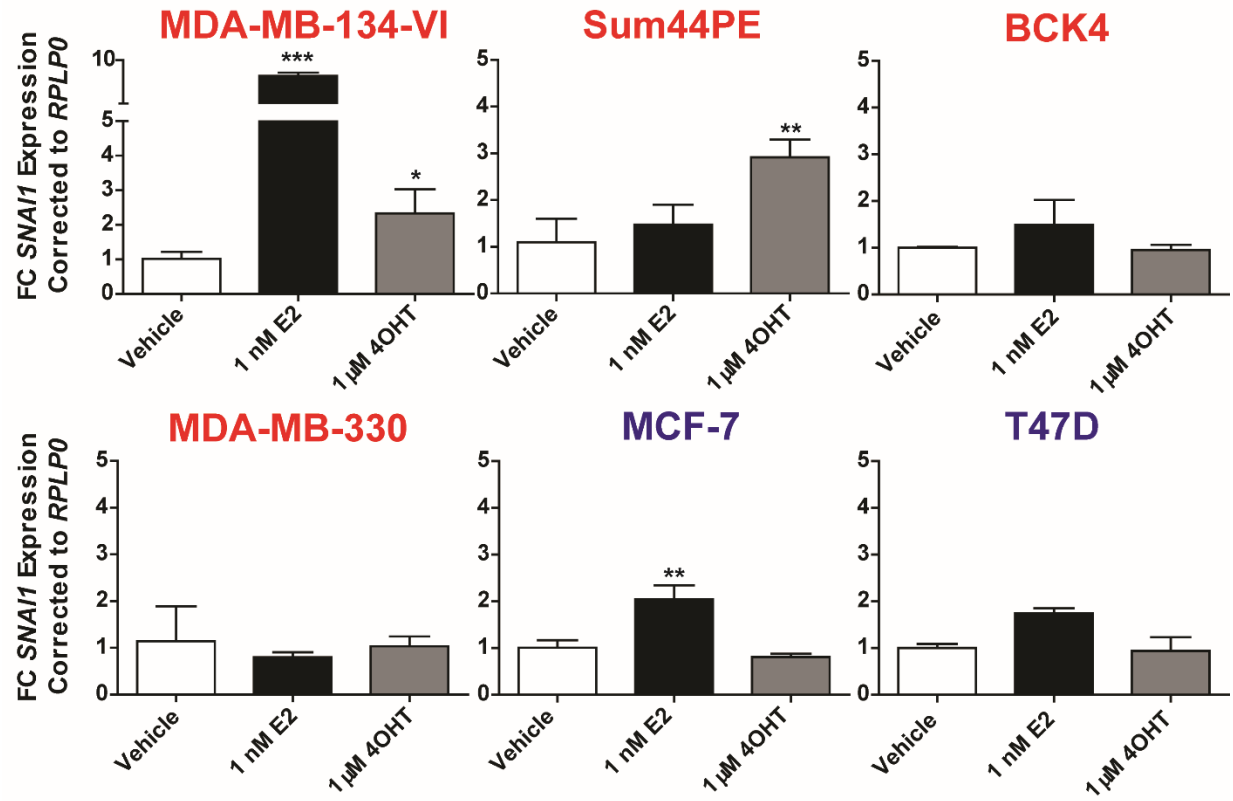

Figure 6: *SNAI1* Expression is Upregulated by 4OHT in Some ILC Cells, But Not IDC Cells
SNAI1 qRT-PCR assessment of ILC (red) and IDC (blue) cells was performed at 24 hours post deprivation/treatments (Vehicle 0.1% DMSO). Quantifications are a representative single experiment ± STDEV of technical triplicates, with similar results in two additional independently performed experiments. Asterisks depict significance compared to Vehicle from One Way ANOVA followed by Tukey's post-test (*p < 0.05, **p < 0.005, ***p < 0.0005).

We also tested if E2 or 4OHT upregulation was restricted to *SNAI1*, or if it could impact expression of other family members such as *SNAI2* or *SNAI3*. *SNAI2* was only expressed in MCF-7 and not significantly regulated by 4OHT or E2 treatments, and *SNAI3* was not significantly regulated by 4OHT or E2 treatments as *SNAI1* was in any cell lines tested (Figure 7).

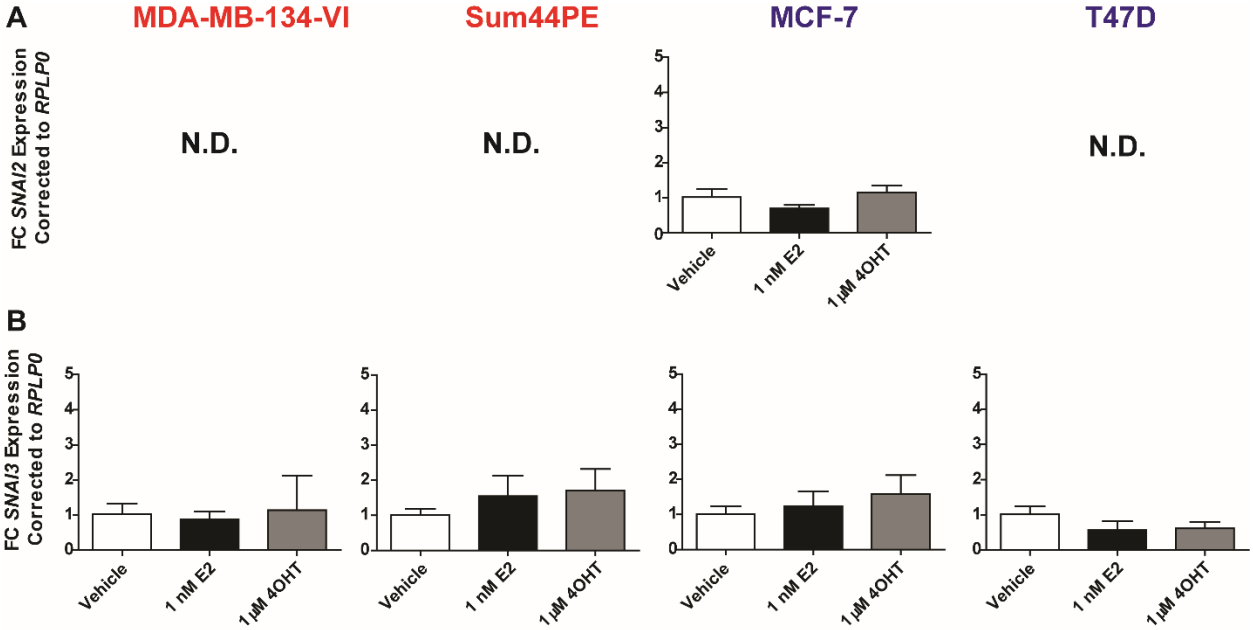

Figure 7: *SNAI2* and *SNAI3* are Not Upregulated by 4OHT or E2 in ILC Cells
qRT-PCR performed for (A) *SNAI2* or (B) *SNAI3* revealed that neither 4OHT or E2 could upregulate the expression of these genes in ILC cells. N.D. indicates "Not Detected." Quantifications are a representative single experiment ± STDEV of technical triplicates (Vehicle 0.1% DMSO). Asterisks depict significance compared to Vehicle from One Way ANOVA followed by Tukey's post-test (*p < 0.05, **p < 0.005, ***p < 0.0005).

In addition, 4OHT or E2 treatments did not impact expression of *TWIST1*, another prominent EMT-TF that has been noted to be expressed in LCIS and ILC (Appendix B Figure 66)[180].

Next, we examined expression of the *SNAI1*/*SNAI2*/*SNAI3* family members by qRT-PCR in Sum44^{TAMR} cells, a cell line model of 4OHT resistance[183]. This model was derived by selecting

for outgrowth of Sum44 cells in increasing concentrations of 4OHT over 18 passages. *SNAI1* baseline expression was decreased in the Sum44^{TAMR} cells relative to parental cells, indicating that *SNAI1* was not causative for 4OHT partial agonist activity in Sum44^{TAMR} cells (Figure 8). *SNAI2* was not expressed in Sum44^{TAMR}, and *SNAI3* expression was not significantly impacted.

Figure 8: SNAIL Family Members are Not Upregulated in Sum44^{TAMR} Cells Relative to Parental Cells
qRT-PCR was performed in parental Sum44 or derived Sum44^{TAMR} cells. Two independent experiments of Sum44^{TAMR} expression are shown. N.D. indicates "Not Detected." Quantifications for each respective bar are a representative experiment ± STDEV of technical triplicates. Asterisks depict significance compared to Parental from One Way ANOVA followed by Tukey's post-test (*$p < 0.05$, **$p < 0.005$, ***$p < 0.0005$).

We then asked if this 4OHT-*SNAI1* induction was ILC-specific, or if loss of E-cadherin was sufficient to induce the 4OHT agonist induction of *SNAI1*. To test this question, we performed E2 deprivation and transiently knocked down *CDH1* in IDC cell line T47D with treatments of 4OHT or E2, as previously performed. *SNAI1* was not induced by 4OHT in this setting, and only E2 induction of *SNAI1* was decreased by loss of *CDH1* expression (Figure 9A). As transient knockdown of *CDH1* is not as complete as sh*RNA* knockdown, we used T47D sh*CDH1* cells generated previously in our lab to test the same question. Stable lentiviral knockdown of *CDH1* was incapable of producing the 4OHT-*SNAI1* induction, although it should be noted that we did

not detect the E2 induction in these cells (Figure 9B). Finally, we chose to use CAMA-1 and ZR-75-30, two E-cadherin mutant cell lines that have been described as "ILC-like" to test the hypothesis that mutational loss of E-cadherin is sufficient to induce 4OHT-agonist induction of *SNAI1*[186]. First, we confirmed ERα positivity and complete loss of E-cadherin protein by IB (Figure 9C). Then, we performed the E2 deprivation and treatment followed by qRT-PCR. Still, mutated E-cadherin cell lines were not capable of producing the 4OHT-driven induction of *SNAI1* (Figure 9D). We thus concluded that loss of E-cadherin expression was not sufficient to allow for 4OHT induction of *SNAI1*.

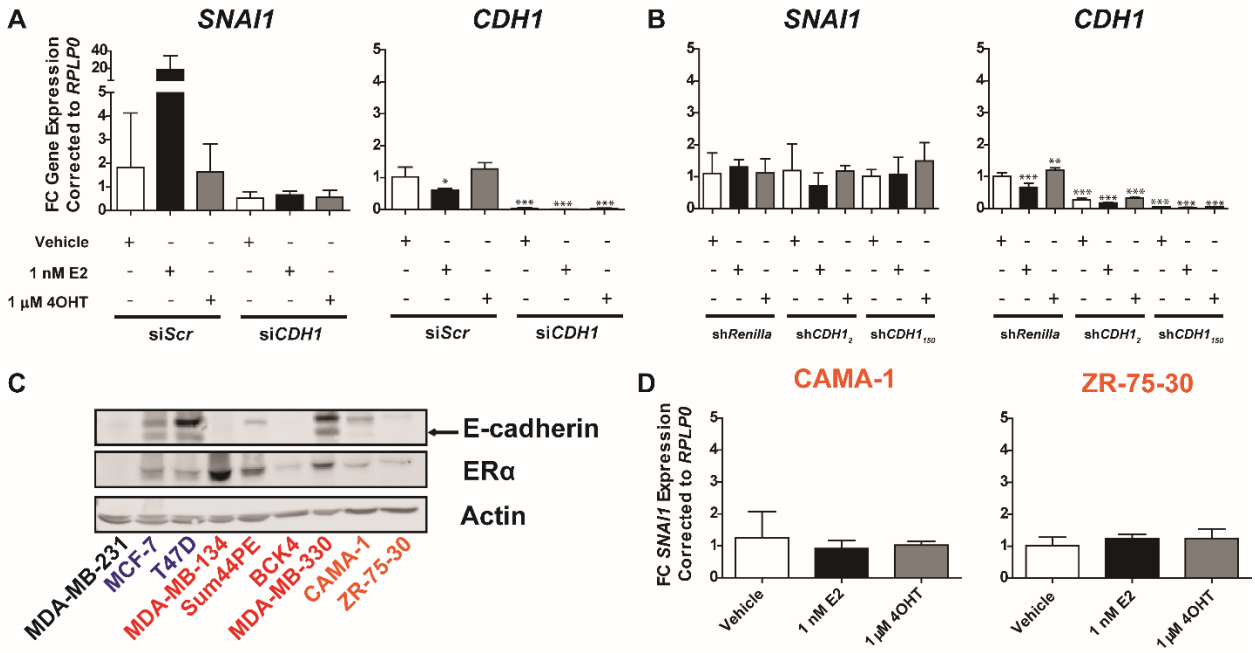

Figure 9: Loss of E-cadherin is Insufficient to Cause 4OHT-Induction of *SNAI1*
(A) T47D cells were transiently reverse transfected with 25 nM si*Scramble* (si*Scr*) or si*CDH1* in an E2 deprivation assay with qRT-PCR for *SNAI1* or *CDH1*. (B) Stable sh*Renilla*, or two of sh*CDH1*$_{2,150}$ were utilized in an additional E2 deprivation/qRT-PCR assay. (C) Protein levels of E-cadherin, ERα, or internal control Actin were measured in a panel of IDC (blue), ILC (red), or ILC-like (orange) cell lines with 50 µg/lane. (D) E2 deprivation assay in two ILC-like cell lines, CAMA-1 and ZR-75-30, with qRT-PCR for *SNAI1* was performed. For qRT-PCRs, quantifications for each respective bar are a representative single experiment ± STDEV of technical triplicates (Vehicle 0.1% DMSO). Asterisks depict significance compared to (A) si*Scr* Vehicle, (B) sh*Renilla* Vehicle, or (D) Vehicle from One Way ANOVA followed by Tukey's post-test (*$p < 0.05$, **$p < 0.005$, ***$p < 0.0005$). Protein is representative of a single experiment.

Finally, we wanted to confirm that this transcriptional regulation lead to modulation of SNAIL protein levels. We performed E2 deprivation in MDA-MB-134-VI and Sum44PE, and found that both 4OHT and E2 treatments induced SNAIL protein expression at the 24-hour time point tested (Figure 10, Appendix B Figure 67). These data confirmed our previous qRT-PCR data that SNAIL is upregulated by 4OHT in a subset of ILC cell lines (MDA-MB-134-VI and Sum44PE), and this upregulation translates to a potentially functional protein product.

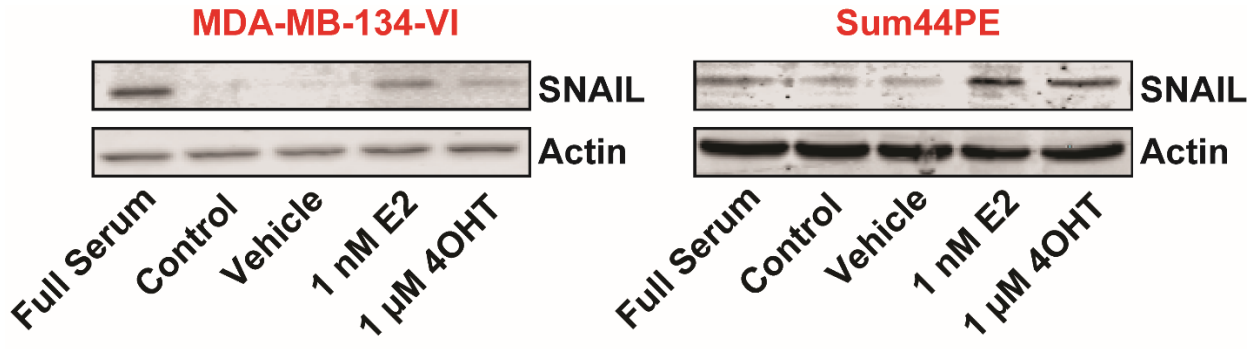

Figure 10: SNAIL Protein is Upregulated by 4OHT, E2 Treatment in ILC cells
IBs were performed in MDA-MB-134-VI and Sum44PE cells for SNAIL or Actin internal control after E2 deprivation assay with 50 μg protein/lane. Images are representative of three independently repeated experiments with single replicates for each condition in each experiment performed.

2.3.3 ERα is Recruited to the Promoter of *SNAI1* After 4OHT, E2 Treatment

To determine if the upregulation of *SNAI1* by 4OHT was through a direct transcriptional mechanism by ERα, we performed ChIP and ChIP qRT-PCR to determine direct binding of ERα at the *SNAI1* promoter. First, we mined the Ross-Inness *et al* ERα ChIP-Seq data and located a conserved estrogen response element (ERE) approximately 1 kb upstream of the *SNAI1* promoter in multiple ERα$^+$ cell lines, primary lesions, and metastases (Figure 11)[187, 188].

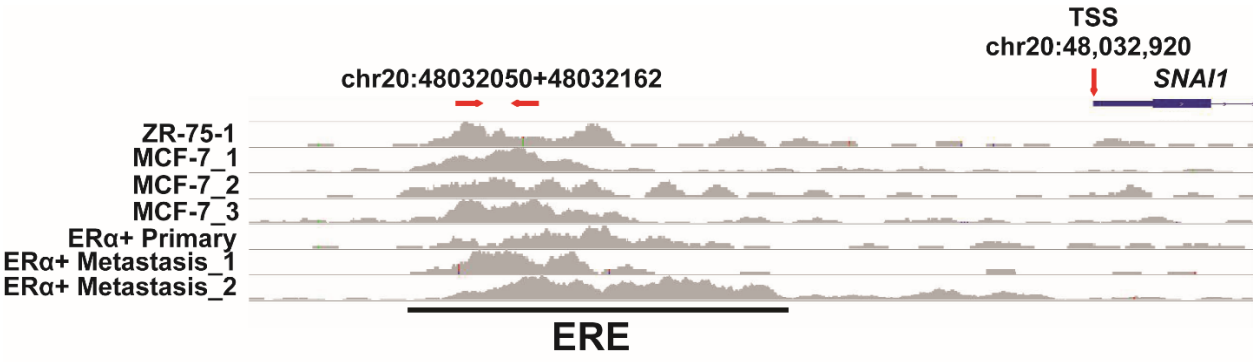

Figure 11: A Conserved ERE is Upstream of the *SNAI1* Promoter
In silico analyses were performed on the Ross-Inness *et al* publicly available ERα ChIP database to search for conserved EREs upstream of the *SNAI1* transcriptional start site (TSS)[187]. Data were aligned in Integrative Genomics Viewer (IGV), a program generated by the Broad Institute[188]. The primer region is denoted by arrows and chromosomal location in hg18.

Next, we performed ERα ChIP in MDA-MB-134-VI after E2 deprivation and treatment with 10-fold molar excess 4OHT or E2 to induce maximal binding at 45 minutes, 3 hours, or 8 hours. Prior to processing samples for ChIP qRT-PCR, we confirmed successful IP of ERα (Appendix B Figure 68). Then, we completed the ChIP qRT-PCR with primers designed around the *SNAI1* promoter region. We observed that 4OHT induced recruitment of ERα to *SNAI1* significantly over IgG and Vehicle controls only at the latest time point tested, 8 hours (Appendix B Figure 69). E2 caused significant recruitment of ERα for all gene regions tested. These data were confirmed at the 8-hour time point, and were consistent with the preliminary results obtained, with successful IP and induction of *SNAI1* at the time point with matched concentrations of 4OHT or E2 (Figure 12A, B). Additionally, we observed recruitment of ERα at *GREB1* with E2, and *IGFBP4* with E2 or 4OHT treatments, respectively (Figure 12C). Therefore, we concluded that both 4OHT and E2 can promote recruitment of ERα directly to the promoter region for *SNAI1*, and treatments can promote recruitment for other classic ERα gene targets in MDA-MB-134-VI.

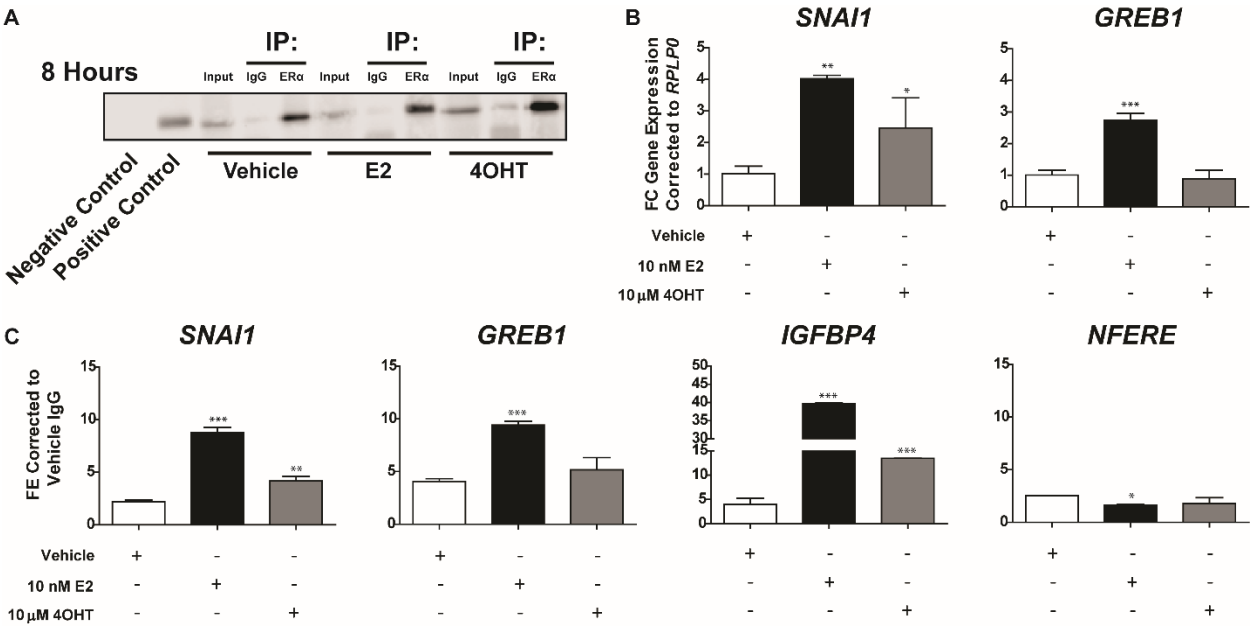

Figure 12: ERα is Recruited to the *SNAI1* Promoter at 8 Hours 4OHT or E2 Treatment
MDA-MB-134-VI cells were treated to E2 deprivation followed by treatments with 4OHT or E2 for 8 hours. Samples were processed for (A) ERα IP confirmation (Negative Control: MDA-MB-231; Positive Control: MCF-7), (B) qRT-PCR for *SNAI1* or *GREB1*, and (C) ChIP qRT-PCR for *SNAI1*, *GREB1*, *IGFBP4*, or negative control *NFERE*. Data represent one experiment with technical triplicates plated during the qRT-PCR ± STDEV. Asterisks depict significance compared to (B) Vehicle (0.1% DMSO) or (C) Fold Enrichment (FE) Vehicle after correction to Vehicle IgG for all samples. Statistics were performed with One Way ANOVA followed by Tukey's post-test with comparisons to Vehicle displayed (*p < 0.05, **p < 0.005, ***p < 0.0005).

2.3.4 *SNAI1* and EMT-TF-Regulated Genes are Basally Upregulated in ILC Cell Lines

Though 4OHT was capable of upregulating SNAIL in ILC cells, we were also curious about basal EMT-TF and EMT-TF-regulated gene expressions in ILC as compared to IDC. Thus, we probed a panel of EMT-TF targets including *SNAI1*, TWIST1 (*TWIST1*), N-cadherin (*CDH2*), Fibronectin (*FN1*), and Vimentin (*VIM*) in ILC and IDC cell lines. qRT-PCR analyses revealed a trend in upregulation for the entire EMT-TF panel tested in ILC cells (Figure 13). Specifically, *SNAI1* was highly upregulated relative to MCF-7 in MDA-MB-134-VI and Sum44PE (+18.00 FC, +6.12 FC, respectively).

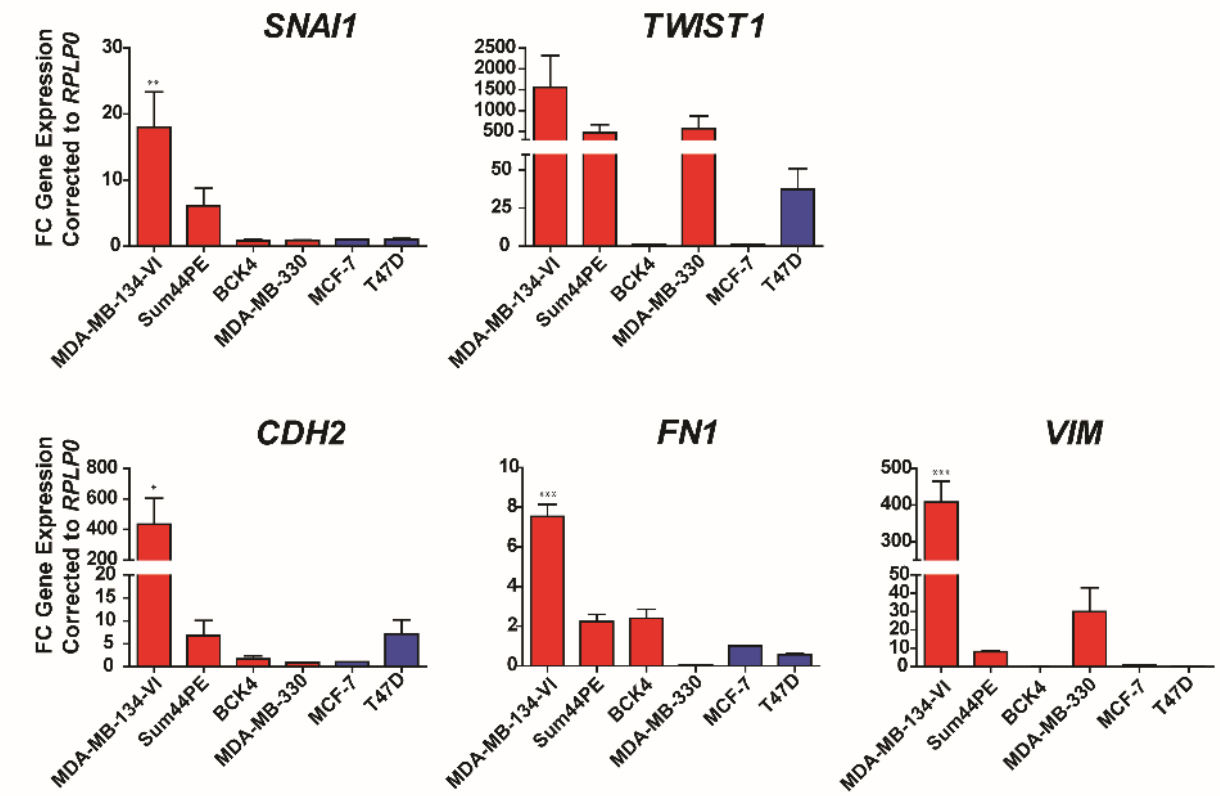

Figure 13: EMT-TFs and EMT-TF-Regulated Genes are Upregulated in ILC
qRT-PCR was performed for *SNAI1*, *TWIST1*, and a panel of downstream EMT-TF-regulated genes (*CDH2*, *FN1*, *VIM*). Quantifications are three independent experiments ± SEM, with technical triplicates in each experiment. One Way ANOVA followed by Tukey's post-test results are displayed with asterisks comparing cells to MCF-7 expression for each gene of interest (*$p < 0.05$, **$p < 0.005$, ***$p < 0.0005$).

Further, *TWIST1*, a potential upstream regulator of *SNAI1*, was upregulated in three out of four of the ILC cell lines (MDA-MB-134-VI, Sum44PE, MDA-MB-330). *CDH2*, *FN1*, and *VIM* were most highly induced in MDA-MB-134-VI relative to IDC cells, but were also induced in 1-2 additional ILC cell lines, for each gene (*CDH2*: Sum44PE; *FN1*: Sum44PE, BCK4; *VIM*: Sum44PE, MDA-MB-330). We next confirmed ERα and E-cadherin protein statuses in the cell line panel prior to probing the levels of the major transcription factors SNAIL and TWIST1. All cell lines were ERα^+, and MCF-7, T47D, and MDA-MB-330 expressed E-cadherin, as expected

(Appendix B Figure 70). Then, we assessed levels of SNAIL and TWIST1 in our cell lines. As both SNAIL and TWIST1 are incredibly labile proteins with short half-lives circa 15 minutes, we chose to include proteasomal degradation inhibitor MG132 in our study[189]. SNAIL and TWIST1 were both consistently expressed in MDA-MB-134-VI cells, and usually observed in Sum44PE cells, with very low levels observed in all other cell lines tested (Figure 14). These data suggested that EMT-TFs and downstream gene targets (*FN1*, *VIM*, *CDH2*) were already expressed in our ILC cells, most significantly in MDA-MB-134-VI, and could contribute to the EMT-like phenotypes of ILC or to the 4OHT-driven 2D proliferation phenotype.

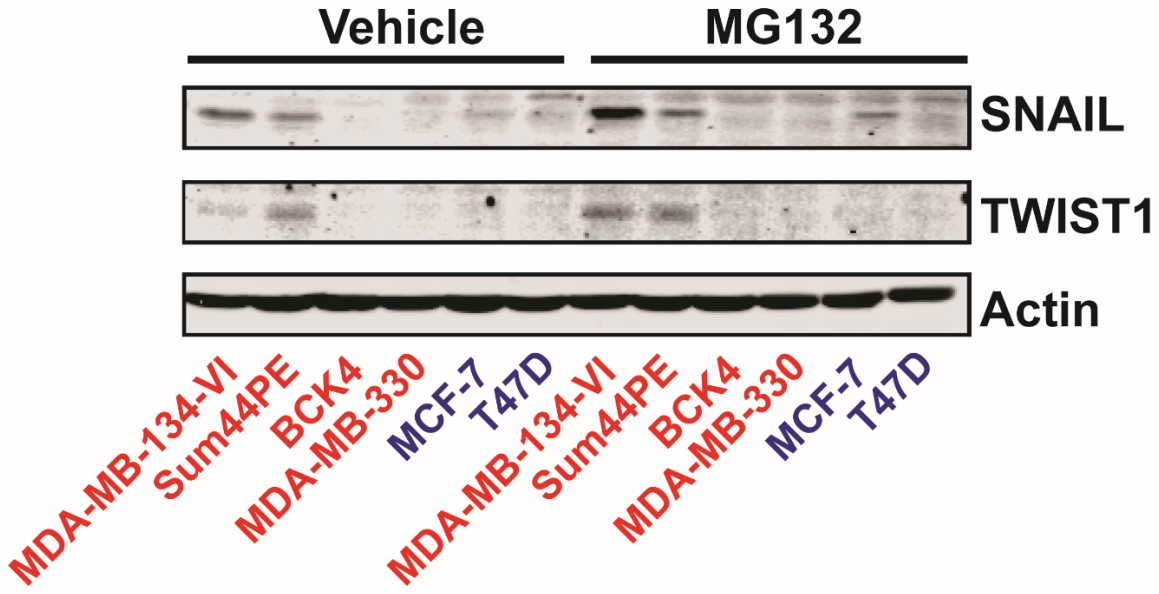

Figure 14: SNAIL and TWIST1 are Relatively Highly Expressed in MDA-MB-134-VI and Sum44PE, and Can Be Further Induced by Inhibition of the Proteasome
IB was performed with 50 µg protein/lane for SNAIL, TWIST1, and Actin (internal control) after treatment ± 5 µM MG132 for two hours. Data are representative of a set of three independently performed experiments with single replicates for each cell line/condition performed in each experiment.

2.3.5 Transient Knockdown of *SNAI1* in ILC Cells Leads to Minimal Impacts on EMT-TF-Regulated Gene Expressions, Opposing 2D/ULA Proliferation Phenotypes in Full Serum

Due to the relatively higher expression of EMT-TF *SNAI1* in MDA-MB-134-VI and Sum44PE cells, and the 4OHT agonist phenotype, we decided to first transiently knock down *SNAI1* to assess changes in the EMT-TF-regulated genes. We attempted to perform a dose response for *SNAI1* transient knockdown in MDA-MB-134-VI and Sum44PE, but only had consistent knockdown in MDA-MB-134-VI, the model with the more robust 4OHT-driven phenotype (Appendix B Figure 71). Thus, we first pursued knockdown of *SNAI1* in MDA-MB-134-VI. We noted that of the previous genes assessed, only *FN1* was significantly and consistently altered in expression in conjunction with knockdown of *SNAI1* (-45%), suggesting that abrogation of *SNAI1* expression could decrease limited EMT-TF target gene expressions in our panel (Figure 15).

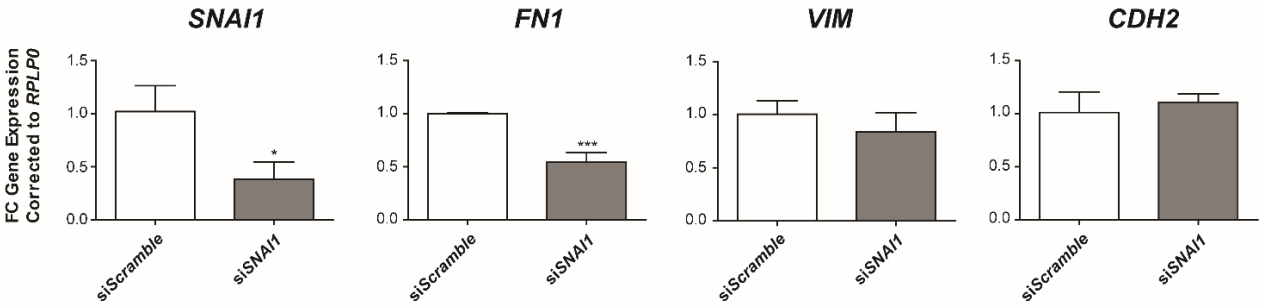

Figure 15: Knockdown of *SNAI1* Significantly Decreases *FN1*, But Not *VIM* or *CDH2* Expressions
Transient knockdown of *SNAI1* was performed in MDA-MB-134-VI and qRT-PCR was performed for EMT-TF panel genes. Quantification represents technical triplicates ± STDEV. Students t-test was performed with asterisks denoting significance (*$p < 0.05$, **$p < 0.005$, ***$p < 0.0005$). Data are representative of two independent experiments with similar results.

Next, we pursued alteration of the 2D and ULA proliferation phenotypes in full serum for the MDA-MB-134-VI cells. We hypothesized that loss of *SNAI1* would lead to decreased proliferation. Intriguingly, opposite phenotypes were observed in the two settings; knockdown of *SNAI1* in MDA-MB-134-VI led to *increased* 2D proliferation and *decreased* ULA proliferation (Figure 16). These results suggest that the context of *SNAI1* knockdown can influence phenotypes in different manners and must be carefully considered when interpreting results.

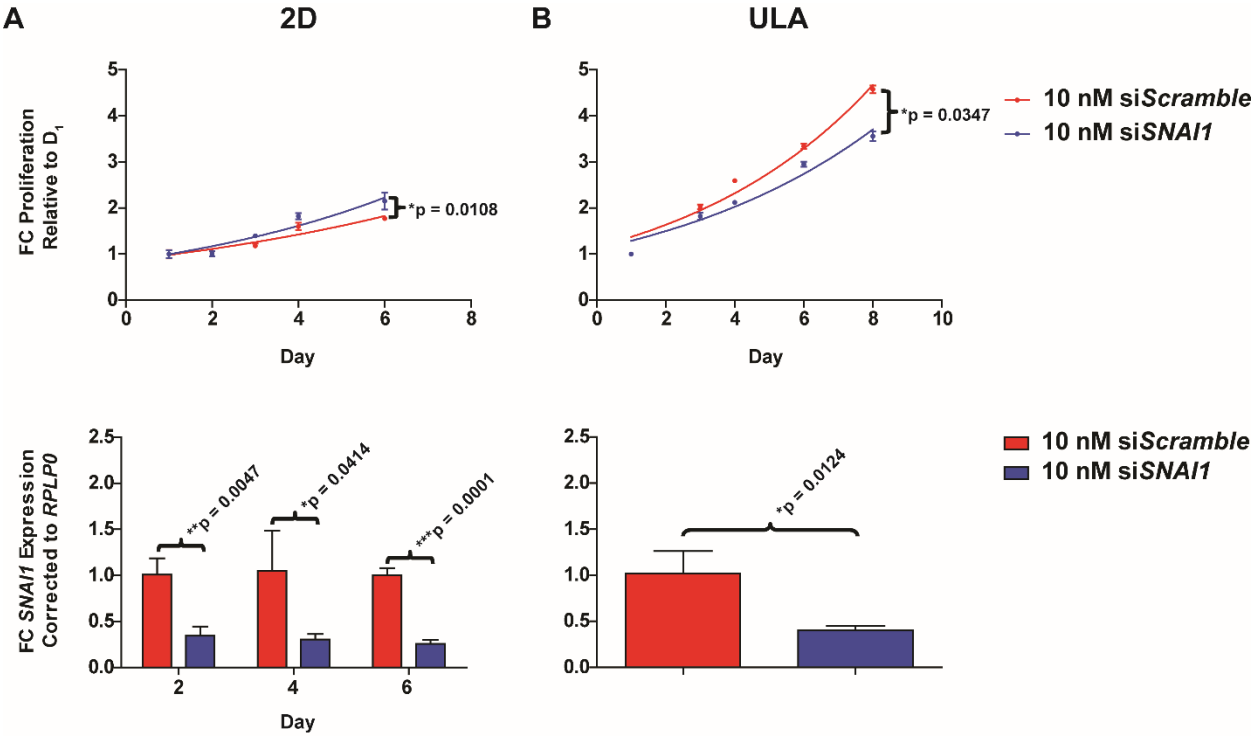

Figure 16: Loss of *SNAI1* Causes Opposite 2D, ULA Proliferation Phenotypes in MDA-MB-134-VI

MDA-MB-134-VI cells were exposed to transient *SNAI1* knockdown for a period of 6-8 days. (A) 2D proliferation was measured with six technical replicates per treatment group ± STDEV, and data were quantified with normalization to D_1 values with non-linear regressions applied to test differences between slopes (*p < 0.05, **p < 0.005, ***p < 0.0005). qRT-PCR for *SNAI1* was performed at $D_{2,4,6}$ with technical triplicates ± STDEV and Students t-test for each si*Scramble* versus si*SNAI1* comparison shown (*p < 0.05, **p < 0.005, ***p < 0.0005). (B) ULA experiments were performed with the same technical replicate numbers and statistical considerations as in 2D experiments. However, qRT-PCR was only performed at $D_{2\text{-}3}$ to assess knockdown relative to si*Scramble* controls. Data are representative of three independently performed experiments.

As we did not anticipate the increased 2D proliferation phenotype that was observed with transient *SNAI1* knockdown, we decided to perform the transient *SNAI1* knockdown assay in MDA-MB-134-VI cells out to 8 days to ensure stability of the increased proliferation. We confirmed this increased 2D proliferation at later time points, along with knockdown of mRNA and protein throughout experiments (Appendix B Figure 72). We then asked if transient *SNAI1* knockdown led to increased 2D proliferation in another ILC cell line, Sum44PE, or in IDC cell lines MCF-7 and T47D. The phenotypes observed in the additional ILC and IDC cell lines tested were inconsistent or not significant, and *SNAI1* expression rebounded in all cell types typically by day 4 of the assay (Appendix B Figure 73). Overall, our data suggested a role for increased 2D and decreased ULA proliferation in MDA-MB-134-VI when *SNAI1* expression was repressed.

2.3.6 *SNAI1* Knockdown is Difficult to Achieve in Deprivation Settings with si*RNA*

Though our full serum 2D proliferation data suggested an alternative role for *SNAI1* than what we had originally hypothesized, we decided to pursue transient knockdown of *SNAI1* in the E2 deprived setting to assess the hypothesis that loss of *SNAI1* would inhibit or decrease the 4OHT 2D partial agonist proliferation previously observed (see Figure 4). We performed this experiment in MDA-MB-134-VI cells multiple times, but were unable to alter the 4OHT-driven 2D proliferation or *SNAI1* gene expression inductions when combining the deprivation and transient knockdown experiments (Figure 17). Often, the si*Scramble* cells did not proliferate differently than Vehicle control in the CSS control treatment group, suggesting the cells were highly stressed after the deprivation, trypsinization, and knockdown process (Appendix B Figure 74). These observations did not allow for conclusions to be made regarding proliferation alterations in si*SNAI1*-treated cells. Additionally, *SNAI1* expression between si*Scramble* and si*SNAI1* Vehicle-

treated cells was not significant, never exceeding 20-40% knockdown. These observations were not surprising, considering the depletion of SNAIL protein levels that was observed during the deprivation process (see Figure 10). In addition, 4OHT induction of *SNAI1* expression was consistently not significantly altered between si*Scramble* and si*SNAI1* treated cells (see Figure 17B). However, transient knockdown of *SNAI1* led to decreased E2 agonist induction of *SNAI1* expression in higher concentration 25 nM si*SNAI1* experiments (Figure 17B, right panel). This outcome suggested that the E2 agonist induction of *SNAI1* was more feasibly abrogated than the 4OHT induction of *SNAI1* in this experimental design. A summary of the full serum and deprivation setting phenotypes with *SNAI1* transient si*RNA* knockdown can be found in Table 3.

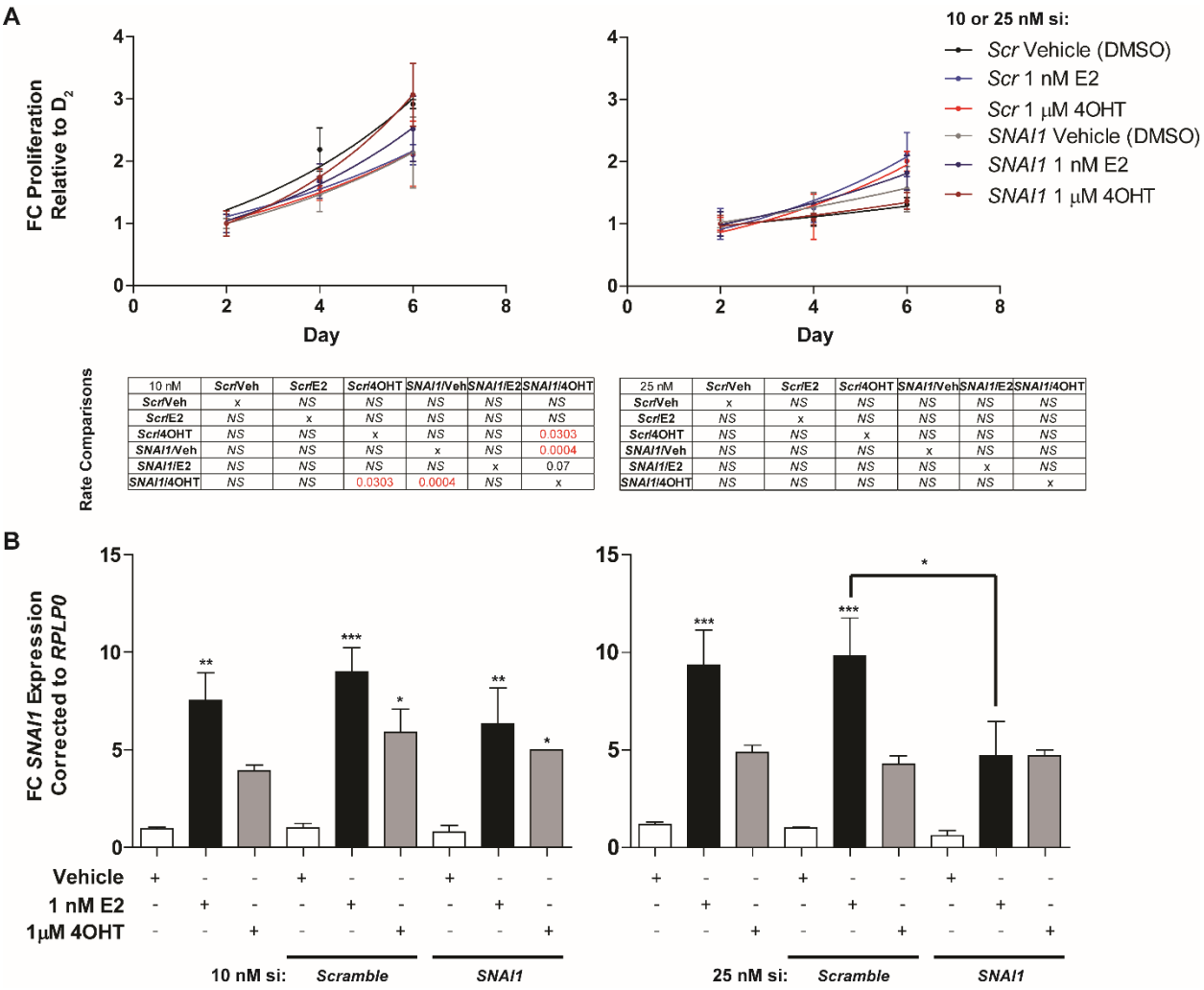

Figure 17: Knockdown of *SNAI* is Inconsistent in the E2 Deprivation Setting

Multiple attempts were performed to combine the transient *SNAI1* knockdown/E2 deprivation assay with Vehicle (0.1% DMSO), 1 nM E2, or 1 μM 4OHT treatments. One attempt of four is shown above. (A) 2D proliferation with (left panel) 10 nM or (right panel) 25 nM si*Scramble* versus si*SNAI1* treatments are shown with five technical replicates per condition/time point ± STDEV, normalized to each respective day 2-time point plate and fitted with non-linear exponential regressions with comparisons of rates displayed beneath each graph in a matrix (*p < 0.05, **p < 0.005, ***p < 0.0005; any significant changes are shown in red font). (B) qRT-PCR was performed for *SNAI1* in simultaneously treated samples with technical duplicate samples ± STDEV, normalized to the si*Scramble* Vehicle control. Statistics are One Way ANOVA followed by Tukey's post-test with assessments between si*Scramble* Vehicle and respective treatments shown (*p < 0.05, **p < 0.005, p < 0.0005). Only one other comparison is displayed that was significant between si*Scramble* and si*SNAI1* treatment groups in the right panel.

Table 3: Summary of *SNAI1* Transient Knockdown Phenotypes

	Full Serum				E2 Deprived	
	2D		**ULA**		**2D**	
	Growth	Knockdown	Growth	Knockdown	Growth	Knockdown
MDA-MB-134-VI	Significant ↑ n = 3	Significant, Consistent Knockdown n = 3	Significant ↓ n = 3	Significant n = 3	*NS* n = 4 attempts; 2 with similar outcomes	*NS* for si*Scr* Veh v si*SNAI1* Veh; Decrease between si*Scr* E2 v si*SNAI1* E2 for 25 nM
Sum44PE	*NS* Unaltered n = 2	Knockdown Rebound by D_{4-6} n = 2	Significant ↓ n = 1	*NS* n = 1	--	--
MCF-7	*NS* ↓ n = 3	Knockdown Rebound by D_4 n = 3	--	--	--	--
T47D	*NS* ↓ n = 2	Knockdown Rebound by D_4 n = 2	--	--	--	--

Comparisons displayed by arrows are indicated relative to si*Scramble* controls for full serum and relative to si*Scramble* Vehicle in the E2 deprived setting. Dashes indicate experiments were not performed.

The following were concluded from the deprivation/si*RNA* studies performed: (1) the process of combined E2 deprivation and transient knockdown with treatments was a stressful process for the cells to go through (observed in the decreased 4OHT-driven phenotype in Scramble controls relative to CSS (see Appendix B Figure 74)), (2) 4OHT induction of 2D proliferation agonist phenotype was modest, showing a ~1.5-FC in 2D proliferation relative to Vehicle control over a period of one week (see Figure 4), (3) 4OHT agonist induction of *SNAI1* was also not consistently observed, (4) the more significant E2 induction of *SNAI1* was altered by knockdown of *SNAI1* (see Figure 17B, right panel), (5) *SNAI1* levels were already depleted after deprivation, and thus, difficult to knock down further, and (6) changing of CSS lots (Gibco, homemade, Gemini) made apparent that residual estrogens and inconsistent removal of other lipophilic factors contributed to the 4OHT-driven phenotypic outcomes (Appendix B Figure 75). Though these

issues remained, we decided to pursue generation of stable knockdown and overexpressing SNAIL cell lines to see if observation (1) could be the rationale for not observing an alteration in phenotype.

2.3.7 Stable SNAIL Knockdown is Difficult to Maintain in MDA-MB-134-VI Cells and Transient Virus Knockdown Produces Conflicting Results

Due to difficulties in decreasing partial agonist 4OHT induction of 2D proliferation with si*SNAI1* experiments, we sought to generate stable constitutive SNAIL knockdown MDA-MB-134-VI cells. Lentiviral shRNA constructs obtained from Timothy Burns, MD, PhD were first utilized (sh*SNAI1*18, 19, 20, 21, 22), and preliminarily provided successful protein knockdown of SNAIL in two cell lines generated (sh*SNAI1*18 and sh*SNAI1*20) (Figure 18A). Interestingly, sh*SNAI1*21 cells never survived selection, and were not able to be tested in this setting. No major morphological changes were noted in the knockdown cells as compared to sh*Scramble* control cells (Figure 18B). We tested 2D proliferation with all these cells in the presence of full serum. We found that knockdown of SNAIL led to decreased 2D proliferation in cell line sh*SNAI1*18; however, this was *not significantly* decreased relative to sh*Scramble* control cells ($p = 0.0980$) (Figure 18C). We attempted to repeat this experiment, but found that *SNAI1* expression was similar between sh*Scramble* and knockdown cells, strongly suggesting rapid outgrowth of cells without *SNAI1* knockdown (Appendix B Figure 76).

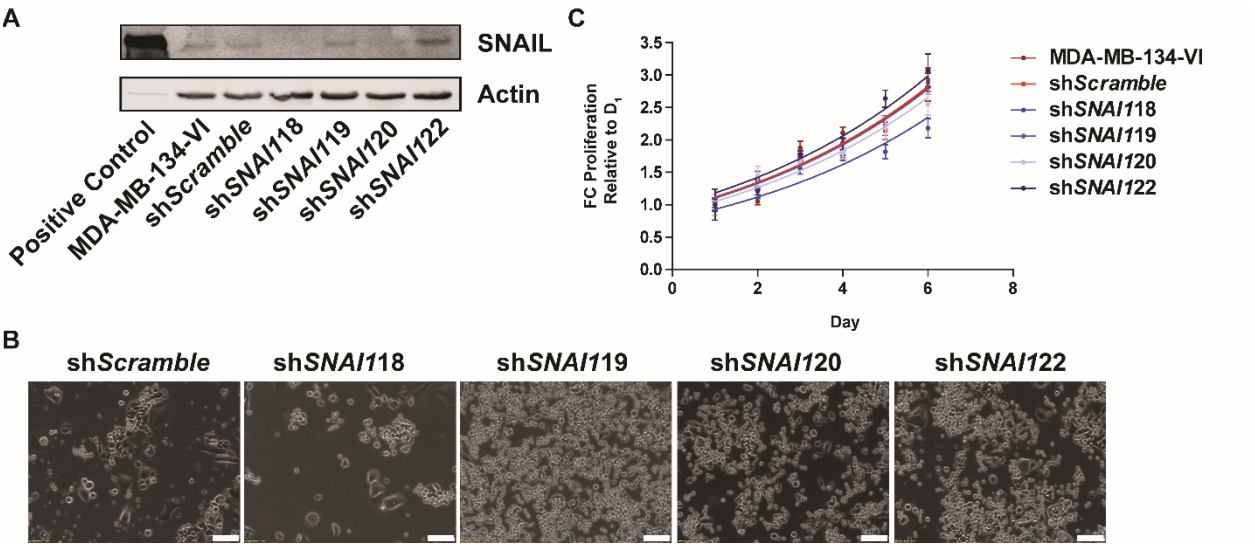

Figure 18: Lentiviral Stable Knockdown of SNAIL Did Not Reveal Significant Effect on 2D Proliferation

MDA-MB-134-VI cells were stably infected with lentiviral sh*SNAI1* constructs, or sh*Scramble* control. (A) Preliminary IB was performed immediately upon sufficient cell density. (B) Phase contrast microscopy was performed on cells (10X magnification; scale bars represent 100 µm). (C) Simultaneous to (A) and (B), 2D proliferation in full serum was assessed for all sh*Scramble*/sh*SNAI1* cells with six technical replicates per cell line ± STDEV, data normalized to respective D_1 values, and rate comparisons performed with non-linear exponential regression fits (*p < 0.05, **p < 0.005, ***p < 0.0005). Uninfected MDA-MB-134-VI cells of similar passage were used as an additional control in experiments from (A) and (C).

We next attempted to utilize the same constructs that had worked effectively in generating stable constitutive knockdown SNAIL cell lines in a transient virus assay. Though we could see a decrease in 2D proliferation with application of virus generated from sh*SNAI1*18 (*p = 0.0228) and sh*SNAI1*20 (*NS* p = 0.2307) relative to sh*Scramble*, we were unable to show knockdown by qRT-PCR or IB for sh*SNAI1*18 virus-treated cells (Figure 19). In fact, sh*SNAI1*20 virus-treated cells showed no significant phenotype, but showed more robust *SNAI1*/SNAIL knockdown. A further attempt to utilize this system with these two constructs and the original panel of all sh*SNAI1* constructs (sh*SNAI1*18, 19, 20, 21, 22), was also unsuccessful (Appendix B Figure 77). The

inconsistencies observed with use of these constructs led us to not pursue their use in further assays.

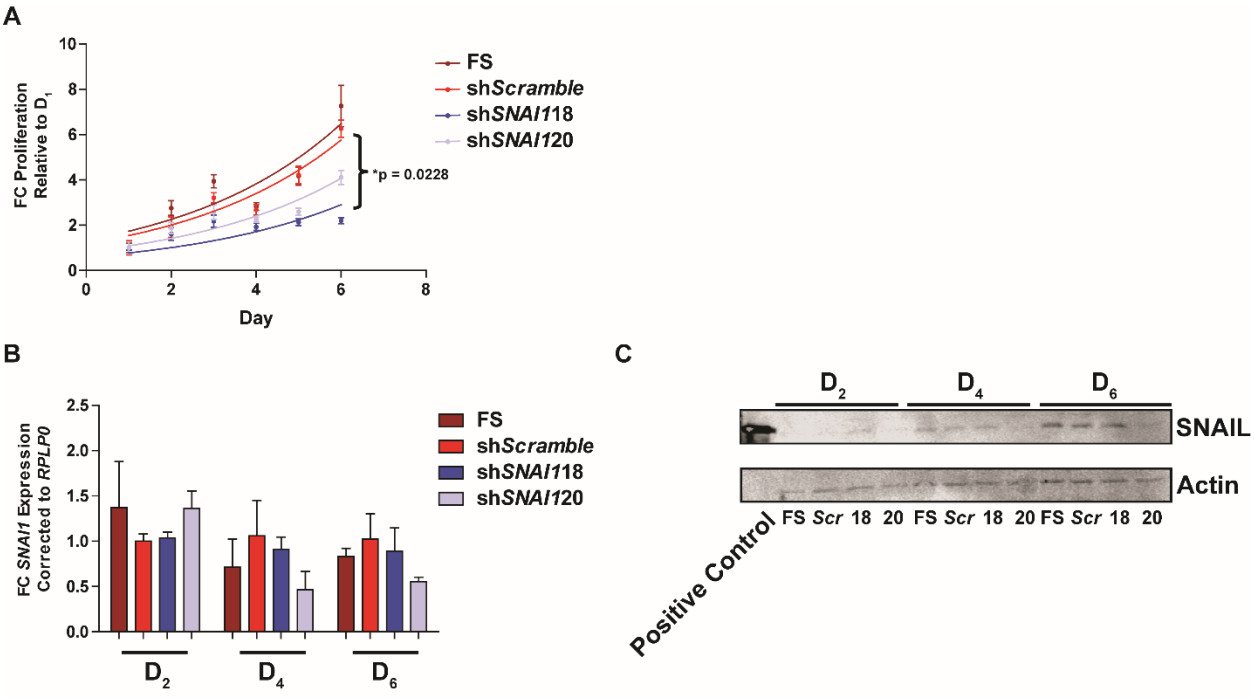

Figure 19: Transient Viral Knockdown of SNAIL Yielded Conflicting Results
Successfully used sh*SNAI1* constructs for sh*SNAI1*18 and sh*SNAI1*20 were used (along with sh*Scramble* control) in a transient virus assay to knock down SNAIL for a short-term assay. (A) 2D proliferation in full serum (FS) with quantification data as previously, was performed; six technical replicates ± STDEV are shown with non-linear regression fits applied and comparison of rates to sh*Scramble* treated cells (*p < 0.05, **p < 0.005, ***p < 0.0005). (B) qRT-PCR for *SNAI1* or (C) IB for SNAIL was performed on $D_{2,4,6}$. qRT-PCR data consisted of technical triplicates ± STDEV for each time point and treatment, normalized to sh*Scramble* treated cells, with One Way ANOVA followed by Tukey's post-test performed (*p < 0.05, **p < 0.005, ***p < 0.0005). Data represent a single experiment, with subsequent attempts producing inconsistent results. FS cells were MDA-MB-134-VI cells that were not subjected to virus treatment.

Thus, we generated new sh*RNA* sequences to target *SNAI1*, and cloned these new constructs into a retroviral system containing GFP, such that we could track the cells that were or were not expressing sh*RNA*. miRE-LEPG sh*SNAI1* sequences were developed as described in the

methods section for regions called sh*SNAI1*150, sh*SNAI1*544, sh*SNAI1*763, sh*SNAI1*1019, sh*SNAI1*1307, and sh*SNAI1*1666. The sh*Renilla*713 construct was utilized as a control vector. sh*SNAI1*1307 was not effectively cloned and was not utilized in these studies. Preliminary GFP assessment in the infected MDA-MB-134-VI cells revealed ~80% or greater of the cells were expressing GFP, and four out of five of the cell lines generated had decreased protein expression of SNAIL (all except sh*SNAI1*1666) (Figure 20). However, there was a notable decrease of SNAIL protein in sh*Renilla*713 relative to control MDA-MB-134-VI cells.

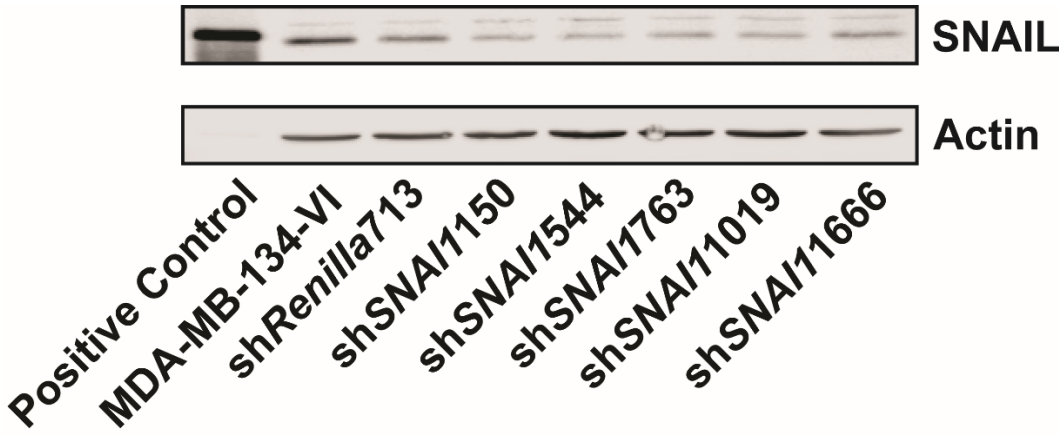

Figure 20: Initial Retroviral Stable SNAIL Knockdown Showed Potential for Most Constructs
Immediately after generation of retroviral stable SNAIL knockdown cell lines, lysates were measured by SNAIL IB relative to Actin internal control with 50 µg/lane. Data represent a single experiment at passage (P) 1.

Immediately after this preliminary expression check, we assessed alteration in 2D or ULA phenotypes of these MDA-MB-134-VI miRE-LEPG sh*SNAI1* cells. There were no significant effects on 2D (Figure 21A) or ULA growth (Figure 21B). It was additionally concerning that the sh*Renilla*713 cells grew significantly worse in 2D than the MDA-MB-134-VI control cells (**p = 0.0021). An IB revealed by this second passage only sh*SNAI1*544 cells had protein knockdown

relative to control cells for this experiment (Figure 21C). This trend in increase of SNAIL expression continued by the next passage, with levels of sh*SNAI1*150, 1019, and 1016 infected cell lines showing no SNAIL knockdown, and sh*SNAI1*763 superseding sh*Renilla*713. Due to these observations, it was concluded that overall, constitutive knockdown of SNAIL was difficult to achieve in these cells, as was transient viral knockdown; both stable knockdown attempts resulted in SNAIL expression rebound, and phenotypes obtained were inconsistent in both settings. While these results suggested that even partial loss of SNAIL resulted in cell death, we concluded that we would have to use inducible knockdown strategies.

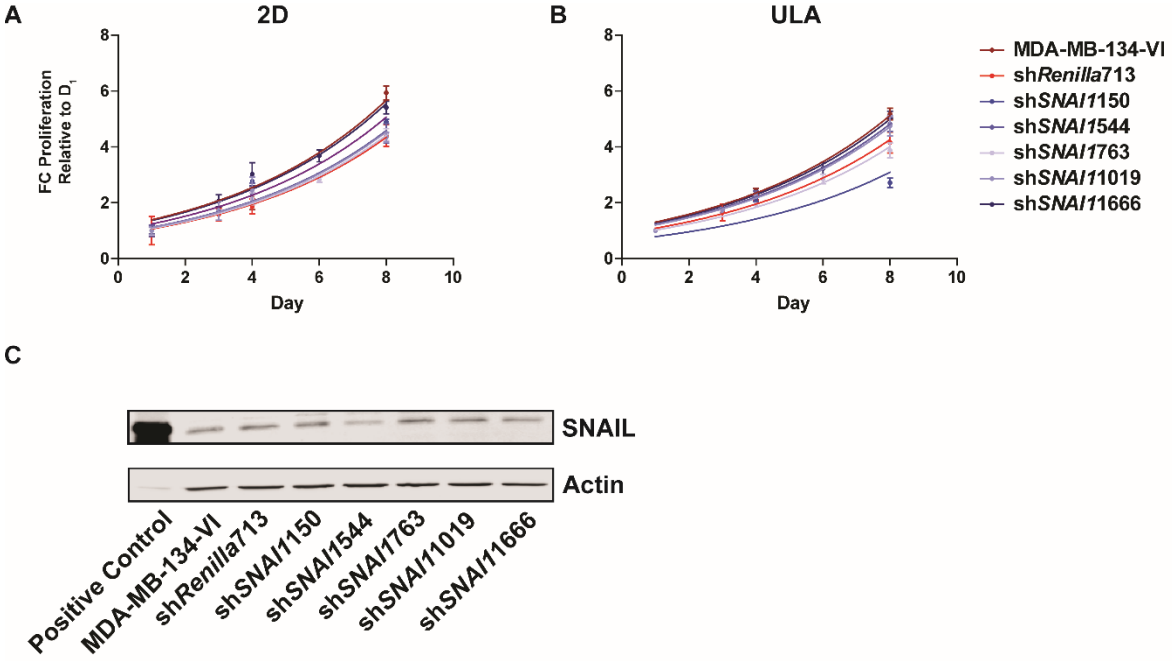

Figure 21: Retroviral Stable SNAIL Knockdown Cells Regained SNAIL Expression in All But sh*SNAI1*544 After Two Passages

Stable retroviral SNAIL knockdown cells were processed for (A) 2D and (B) ULA proliferation assays in full serum one passage after confirmation of SNAIL knockdown. Data were processed as previously with six technical replicates per group ± STDEV, and comparisons performed using non-linear regression comparison of rates (*$p < 0.05$, **$p < 0.005$, ***$p < 0.0005$). (C) IB for SNAIL was simultaneously performed with this experiment to show loss of SNAIL knockdown in most infected cell lines. Data represent a single experiment of the second passage of cells after generation.

2.3.8 Inducible Knockdown of *SNAI1* was Also Unsuccessful

As SNAIL was clearly very tightly regulated in the MDA-MB-134-VI cells, we next attempted to generate an inducible *SNAI1* knockdown system, in which knockdown could be controlled by treatment with Dox in a transient manner[190]. We subcloned the miRE-LEPG retroviral sh*SNAI1* constructs (sh*SNAI1*150, etc.) into an LT3GEPIR sh*RNA* backbone containing GFP. To utilize this system, we used previously generated MDA-MB-134-VI reverse tetracycline (rtTA) cells, which were infected with a construct to produce rtTA protein required to drive the Dox-inducible system[191]. Also, due to the concerning alterations in *SNAI1* expression observed in the miRE-LEPG sh*Renilla*713 MDA-MB-134-VI cells, we included an additional sh*Renilla*826 construct in our cloning efforts.

We tested phenotypes, SNAIL expression, and GFP production with Dox treatment in the first cell lines that grew out during selection, sh*Renilla*826 and sh*SNAI1*763. Though GFP was observed in Dox-only treated cells, protein knockdown was not apparent in the sh*SNAI1*763 cells tested, and altered phenotypes were not observed (Appendix B Figure 78). When sufficient cells were available from most of the panel (sh*Renilla713*, sh*Renilla*826, sh*SNAI1*544, sh*SNAI1*763), we tested mRNA expressions of *SNAI1*, and observed that Dox treatment significantly reduced expression of *SNAI1* in sh*SNAI1*763; however, *SNAI1* expression was already decreased *without* Dox treatment in these cells (Figure 22). This unanticipated outcome led us to consider alternative reasons for this difficulty in achieving *SNAI1* knockdown.

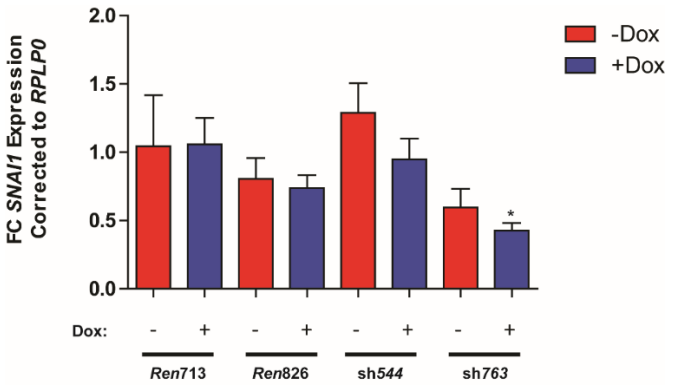

Figure 22: Dox Inducible *SNAI1* Knockdown is Minimally Effective
A 24-hour treatment of ± 0.5 µg/mL Dox was given to the inducible retroviral knockdown *SNAI1* cells and associated controls. qRT-PCR was performed with technical triplicate samples, data displayed ± STDEV, with comparisons to sh*Renilla*713 -Dox after One Way ANOVA followed by Tukey's post-test (*$p < 0.05$, **$p < 0.005$, ***$p < 0.0005$).

Tet-contaminants that resemble Tetracycline or Doxycycline are commonly found at low levels in FBS. This is largely due to the addition of antibiotics to the feed of cows from which FBS is obtained. Low concentrations of these could be sufficient to induce expressions of Tet-driven constructs (*Timothy Burns, MD, PhD unpublished observations*). We therefore hypothesized that low level contaminants of Tet could be in our FBS containing media that we used to generate our inducible sh*SNAI1* cell lines; if knockdown of *SNAI1* was potentially lethal to cells, these cells were dying off during selection and during use in experiments, leaving the most highly expressing *SNAI1* cells in the population. We confirmed with our serum provider that there were low 19 ng/mL levels of Tet in our serum. So, we decided to regenerate the LT3GEPIR sh*SNAI1* cell lines in Tet-free competent serum.

Regeneration of these MDA-MB-134-VI rtTA Tet-free (TF) LT3GEPIR sh*RNA* cells produced similar results to what was observed in the previous attempt in non-TF serum supplemented media. Once sufficient cells were available, a Dox dose and time course was performed. sh*SNAI1*763 cells showed the most trending response to Dox in time and dose

dependent manners, but the trends of increased growth were insignificant (Figure 23A). Interestingly, 1 µg/mL Dox was very toxic to the sh*Renilla*826 cells, as they did not proliferate (*p = 0.0452). It should also be noted that none of the -Dox treatment groups were significantly different than the sh*Renilla*826 -Dox control, except for sh*SNAI1*1019 -Dox (*p = 0.0279). While all cells could induce GFP expression with Dox treatment relative to controls, mRNA knockdown was only present in the sh*SNAI1*763 from 0.5-1 µg/mL (~55%) (Figure 23B). Due to the low basal expression of SNAIL in MDA-MB-134-VI, even though relatively higher than in other cell lines quantified in this chapter, we found great difficulty in manipulating its levels to influence phenotypes. Any future experiments attempting to manipulate this protein in these cells should be attempted either transiently, as previously described, or with a more stringent method, such as CRISPR[192].

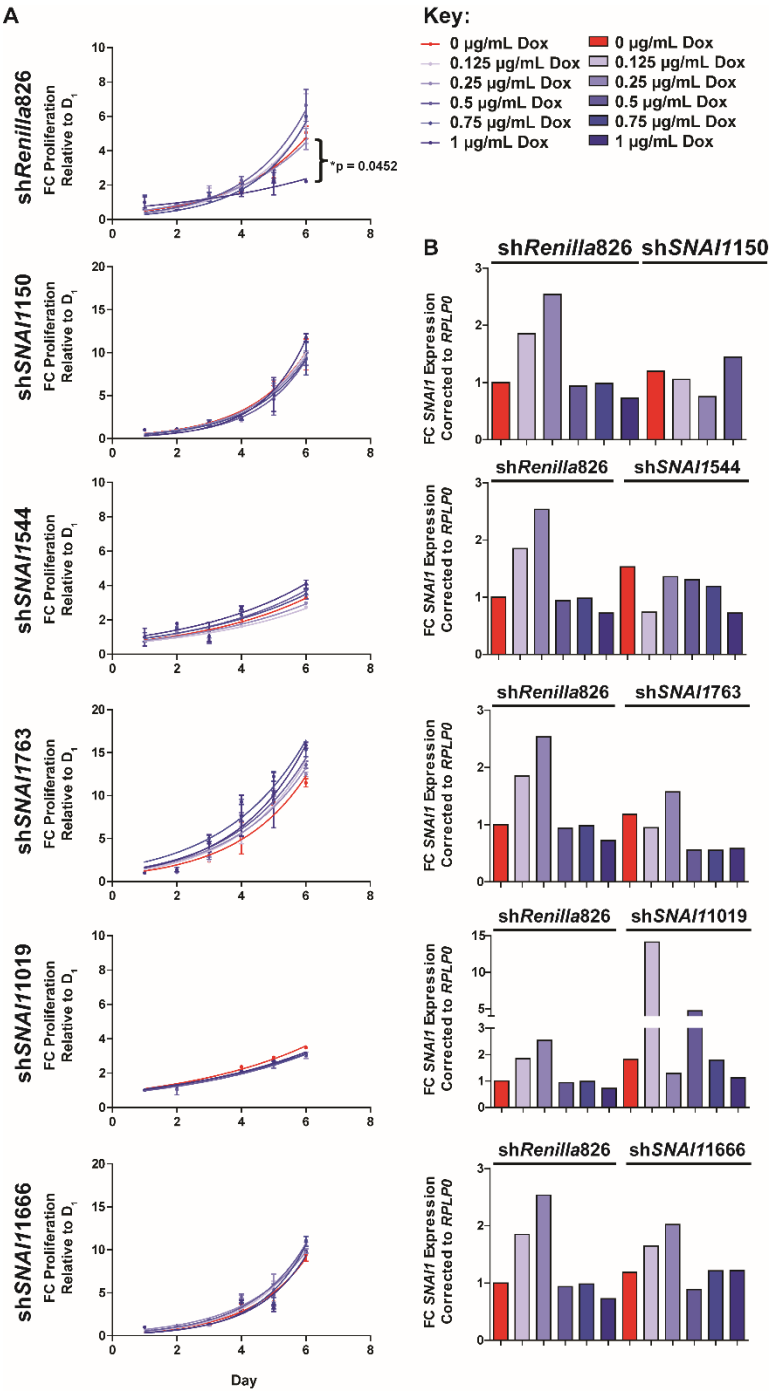

Figure 23: Tet-Free Inducible *SNAI1* Retroviral System Reveals Similar Phenotype to Transient *SNAI1* siRNA in sh*SNAI1*763 Cells, Only

Retroviral Inducible *SNAI1* Knockdown cells were generated in TF competent serum/media. (A) Dox dose/2D proliferation responses were performed for all cells generated with technical triplicates ± STDEV, normalized to day 1 values, and non-linear regressions fitted with comparisons of rates (*p < 0.05, **p < 0.005, ***p < 0.0005). (B) qRT-PCR for *SNAI1* was simultaneously performed on single replicates for each dose at the 24-hour time point. Data are shown in comparison to sh*Renilla*826 -Dox for *SNAI1* expression.

2.3.9 Stable Inducible SNAIL Overexpression Leads to Decreased Proliferation, Invasive, and Stem Cell Phenotypes

As we faced great technical difficulty in knockdown of SNAIL, we decided to attempt the opposite approach by overexpressing SNAIL in lower SNAIL expressing ILC cell lines BCK4, MDA-MB-330, and Sum44PE (refer to Figure 13, 14). We first attempted to generate constitutive stable overexpressing SNAIL cells with Empty Vector (*EV*) or *SNAI1* containing lentiviral constructs in BCK4 cells. The cloned construct was first tested in HEK293T cells to ensure it worked as a viral backbone to produce SNAIL protein and mRNA products (Appendix B Figure 79). Once this was confirmed, the same constructs were utilized on the BCK4 and Sum44PE cells. As soon as sufficient cells to test protein induction became available from BCK4 cells, an IB was run and confirmed protein upregulation of SNAIL in overexpressing cells (Appendix B Figure 79). However, in subsequent passages, this protein overexpression was lost, much like what was observed in the stable constitutive knockdown studies (Appendix B Figure 79, refer to Figure 21, see Appendix B Figure 76). We therefore resolved to attempt to generate a Dox inducible *SNAI1* overexpression system for BCK4, MDA-MB-330 and Sum44PE using inducible construct pINDUCER20-*SNAI1*.

Lentiviral infection of pINDUCER20-*SNAI1* constructs in BCK4, MDA-MB-330, and Sum44PE produced successful protein overexpression of SNAIL in all three cell types relative to no Dox controls (Figure 24A). This was consistent, and did not change with passage or repetition. Dox treatment at 0.5 µg/mL was performed in these cells and we quantified protein expression, 2D, and ULA proliferation phenotypes in all three cell line derivatives. SNAIL overexpression produced an opposite phenotype to transient si*SNAI1* knockdown 2D studies; transient overexpression of SNAIL in all three cell lines led to a decreased proliferative phenotype in *both*

2D and ULA settings (Figure 24B, C). This phenotype was visible in a dose response in both 2D and ULA environments, and simultaneously given doses of Dox did not impact growth of control cells (Appendix B Figure 80, 81, Table 14, 15).

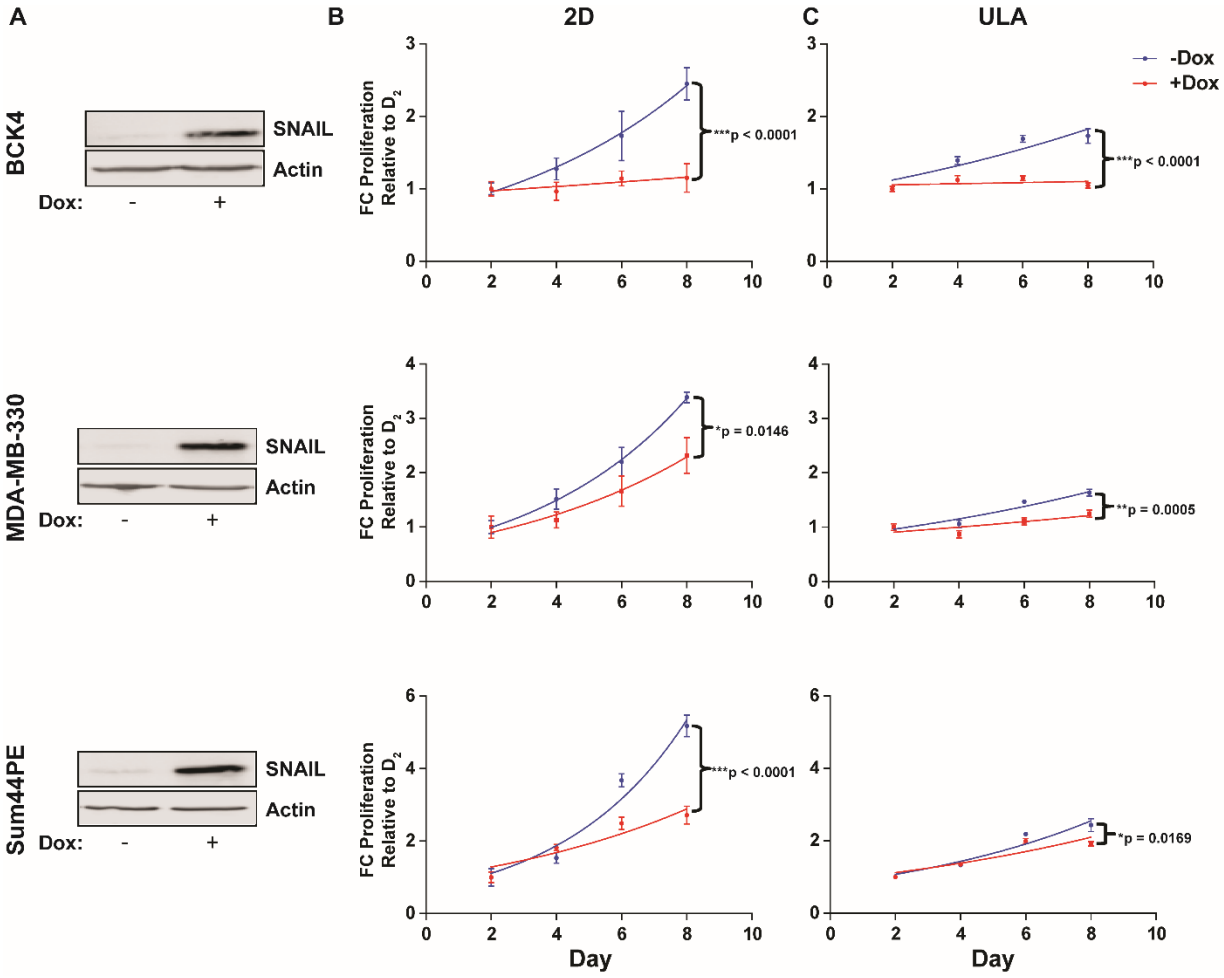

Figure 24: Transient SNAIL Overexpression Leads to Decreased 2D, ULA Proliferation in ILC Cells

Three ILC cell derivatives were generated using pINDUCER20-*SNAI1* lentiviral infection. (A) After treatment ± 0.5 µg/mL Dox for 24-48 hours, IBs were performed for SNAIL with internal control Actin with 25 µg/lane. (B) 2D or (C) ULA proliferation were measured on $D_{2,4,6,8}$ for all three cell line derivatives with six technical replicates per treatment/time point observed, displayed as ± STDEV. Data were fitted with non-linear regressions with comparisons of rates (*p < 0.05, **p < 0.005, ***p < 0.0005). Data are representative of three independently performed experiments.

Increased expression of SNAIL has been previously described to contribute to decreased proliferative phenotypes to allow for cell cycle arrest and invasion phenotypes[193]. We first measured cell cycle profiles in BCK4 pINDUCER20-*SNAI1* ± Dox treated cells at the D_4 time point, a middle point of our previous assays that had dictated the presence of the decreased proliferation phenotypes. We observed cell cycle arrest in G_0/G_1, with concurrent decreases of fraction of cells in G_2/M and S phases (Figure 25A). No phenotypic or cell cycle alterations were noted in Dox treated control BCK4 cells (Figure 25B).

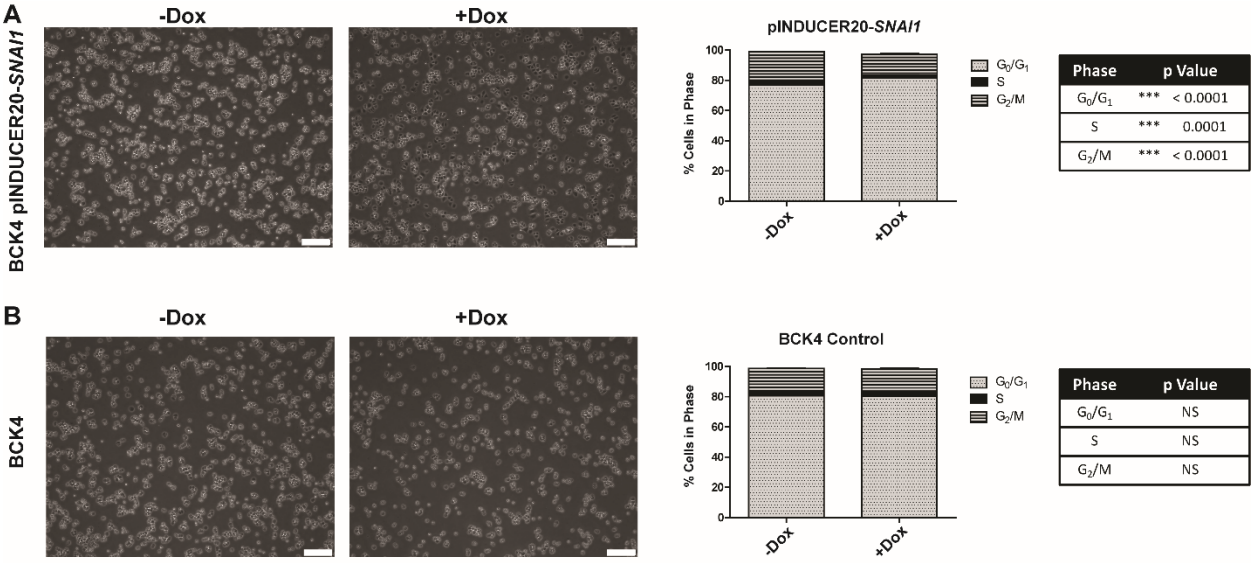

Figure 25: Overexpression of SNAIL Causes Arrest in G_0/G_1
BCK4 pINDUCER20-*SNAI1* and BCK4 control cells were simultaneously subjected to triplicate plating for cell cycle analyses, with treatment of ± 0.5 µg/mL Dox for four days. (A) Phase contrast images were taken and cell cycle profile was measured (10X magnification; scale bars represent 100 µm). (B) Simultaneous experiments were performed in control cells to ensure that Dox was not the cause of any alterations observed. Data are representative of two independently performed experiments with similar outcomes. Students t-test (*$p < 0.05$, **$p < 0.005$, ***$p < 0.0005$) was utilized to compare ± Dox groups for each given phase of the cell cycle.

We next pursued testing of invasive phenotypes in our models by plating cells on top of Matrigel, or embedding cells in Matrigel or Collagen I[194]. MCF-7 and MDA-MB-231 cells served as controls in these experiments. Robust colony formation and invasion were not seen in the BCK4 or MDA-MB-330 pINDUCER20-*SNAI1* cell lines, but were present in control cell lines and in Sum44PE pINDUCER20-*SNAI1* –Dox cells (Figure 26). Intriguingly, this invasive/colony formation phenotype was decreased with induction of SNAIL, an unanticipated outcome. We concluded that overexpression of SNAIL leads to decreased 2D and ULA growth, concurrent with arrest in G_0/G_1 cell cycle, as well as decreased invasive growth.

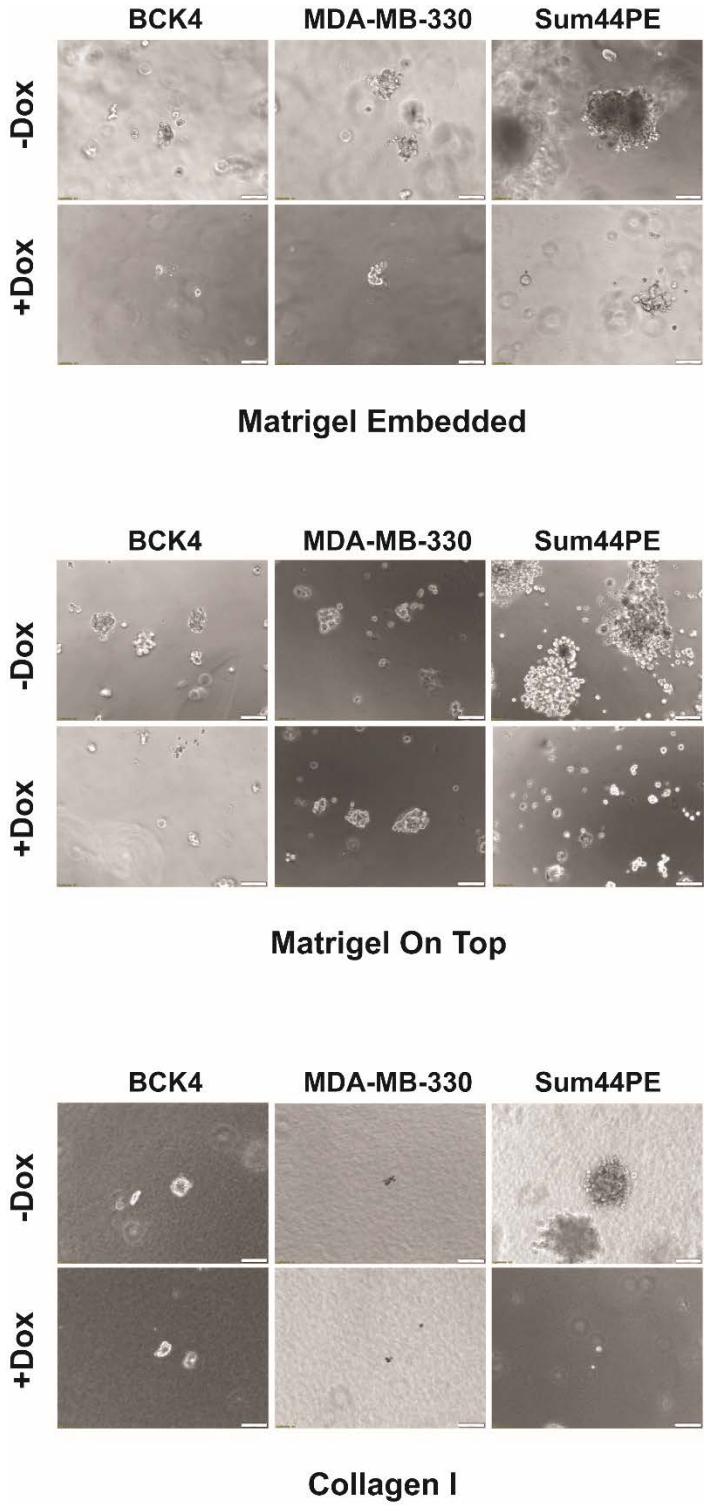

Figure 26: Increased Levels of SNAIL in ILC Reduce Colony Formation in Matrigel, Collagen Environments

ILC inducible overexpression cell lines were seeded into (Matrigel, Collagen I), or on top of (Matrigel) 3D environments to test colony formation in response to SNAIL overexpression by Dox treatment (± 0.5 µg/mL; replenished ~3-4 days) over a period of 24 days. Colonies were imaged as under phase contrast microscopy (10X magnification; scale bars represent 100 µm).

Induction of SNAIL has also been shown to contribute to stem cell behaviors[195, 196]. These phenotypes have been shown to contribute to therapeutic resistance, and might contribute to the observed 4OHT induction of 2D proliferation phenotype in MDA-MB-134-VI. To directly test this, we determined expression of stem cell markers, and performed functional stem cell assays. We first measured ALDH expression in our BCK4 pINDUCER20-*SNAI1* ± Dox cells, a commonly noted feature of stem cell populations[197]. However, we did not detect an ALDH population of stem cells in the inducible overexpressing SNAIL population, unlike our positive control cell line SKBR3 (Appendix B Figure 82). Still, ALDH expression is not a definitive indicator of stem cells[198]. Current data in our lab also showed that alternative stem cell markers $CD24^{low}/CD44^{high}$ are not expressed in our highest SNAIL expressing cell line, MDA-MB-134-VI (*Nilgun Tasdemir, PhD unpublished data*).

We next conducted a functional mammosphere assay to further test this stem cell hypothesis, and used MCF-7 and MCF-10A cell lines as controls in this experiment. BCK4 and MDA-MB-330 cells did not form proper architecture expected of mammospheres, instead forming lattices of cells that were loosely connected into one mass in each well (Appendix B Figure 83)[199]. Sum44PE cells also did not form proper mammospheres, but did form clusters of loosely aggregated cells that decreased with induction of SNAIL expression, and were consistently downregulated from primary to tertiary sphere formation assays (Figure 27). In conclusion, overexpression of SNAIL performed in ILC cell lines BCK4, MDA-MB-330, and Sum44PE led to decreased proliferative, invasive, and stem cell-like phenotypes.

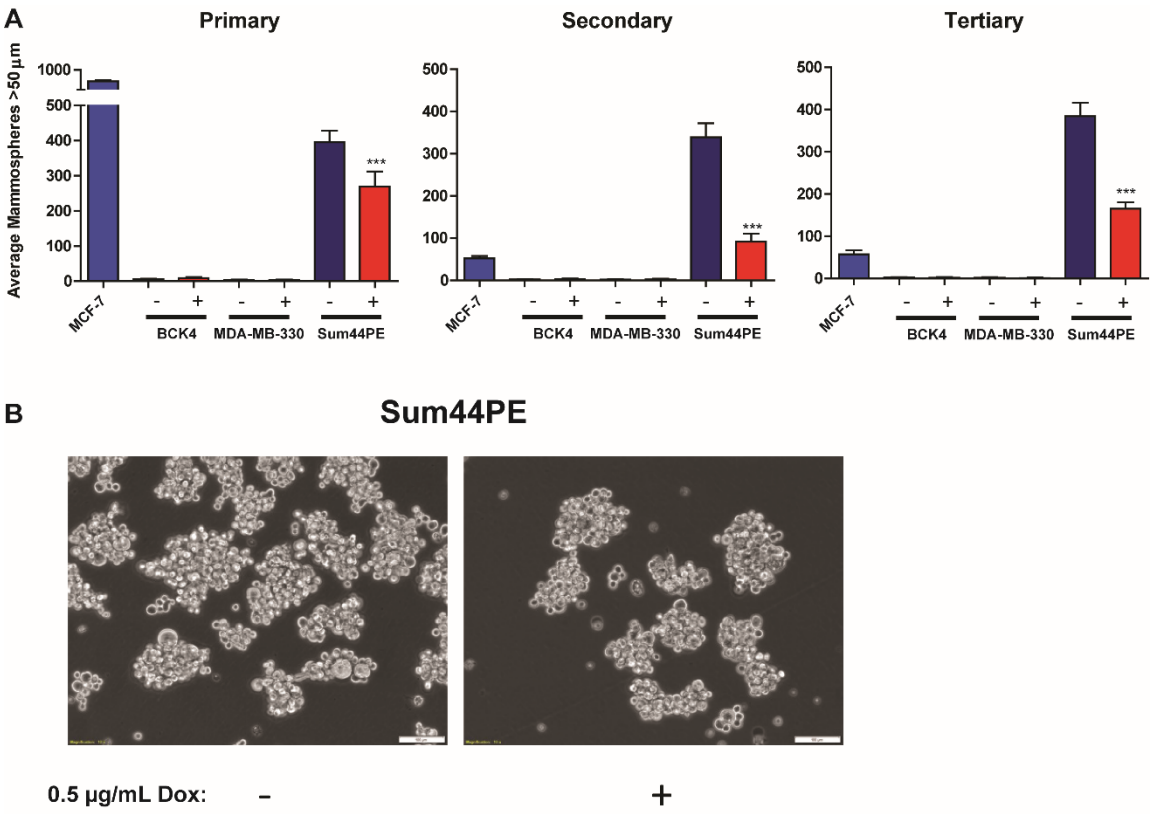

Figure 27: SNAIL Overexpression Causes a Loss of Stem-Like Phenotypes in Sum44PE Cells Inducible overexpression SNAIL cells or control MCF-7 cells were seeded into a mammosphere assay. (A) Quantifications of mammospheres formed were generated for each technical triplicate sample ± STDEV for primary, secondary, or tertiary assays. Comparisons were performed by One Way ANOVA followed by Tukey's post-test with comparisons against -Dox displayed (*$p < 0.05$, **$p < 0.005$, ***$p < 0.0005$). (B) Representative phase contrast images are shown from D_{17} of the assay (20X magnification; scale bars represent 50 µm).

2.3.10 SNAIL Overexpression is Not Sufficient to Induce 4OHT-Driven 2D Proliferation Phenotype in ILC Cells

We finally asked if induction of SNAIL would lead to induction of 4OHT-driven 2D proliferation in ILC cells other than MDA-MB-134-VI. We performed E2 deprivation of our inducible SNAIL ILC cell lines and downstream 4OHT dose response assays, as previously performed (see Figure 4), with or without the addition of Dox. We observed no 4OHT-induced phenotype in these 2D

proliferation assays relative to -Dox controls, in any of our ILC cell lines (Figure 28). These data further supported our findings that SNAIL was not directly contributing to the 4OHT-driven phenotype in ILC that was previously observed (see Figure 4), but suggests that it may instead play other roles that remain undefined (dormancy, marker expressed in response to 4OHT treatment).

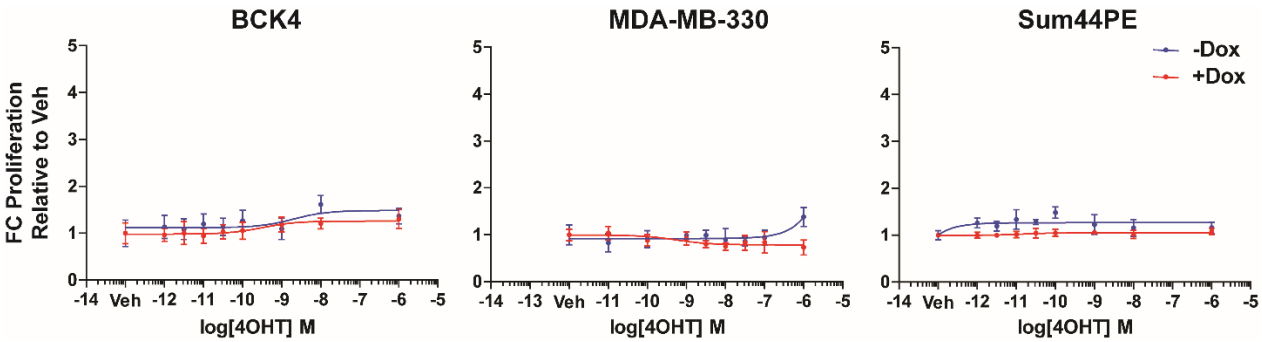

Figure 28: 4OHT-Driven 2D Proliferation is Not Caused by Induction of SNAIL in ILC Cells
BCK4, MDA-MB-330, and Sum44PE pINDUCER20-*SNAI1* cells were plated in six technical replicates per dose of 4OHT/Dox given and quantified for dose response at D_7 post treatment. Dox was given at 0.25 µg/mL final concentration. Data were quantified ± STDEV with normalization to Vehicle (0.1% DMSO) control, representing one experiment.

2.3.11 Minimal Clinical Evidence Currently Supports a Role for SNAIL in ILC

Current literature supports a role for increased SNAIL expression in malignancies, but these data are not clear with respect to ILC[64, 174]. We decided to probe *SNAI1* expression in ERα$^+$ n = 184 ILC versus n = 534 IDC primary tumors from TCGA, but found that there was no significant difference in expression of *SNAI1* between these two groups (Figure 29A). Additionally, *SNAI2* and *SNAI3* were decreased significantly in ILC primary tumors (*p = 0.019, ***p = 2.7e-15) (Figure 29B, C). Only SNAIL was available from TCGA RPPA analyses, and was also not

significantly differentially expressed between ILC and IDC (Appendix B Figure 84). It should be noted that these conclusions were drawn from expressions of *SNAI1*/*SNAI2*/*SNAI3* in primary lesions, not metastatic lesions.

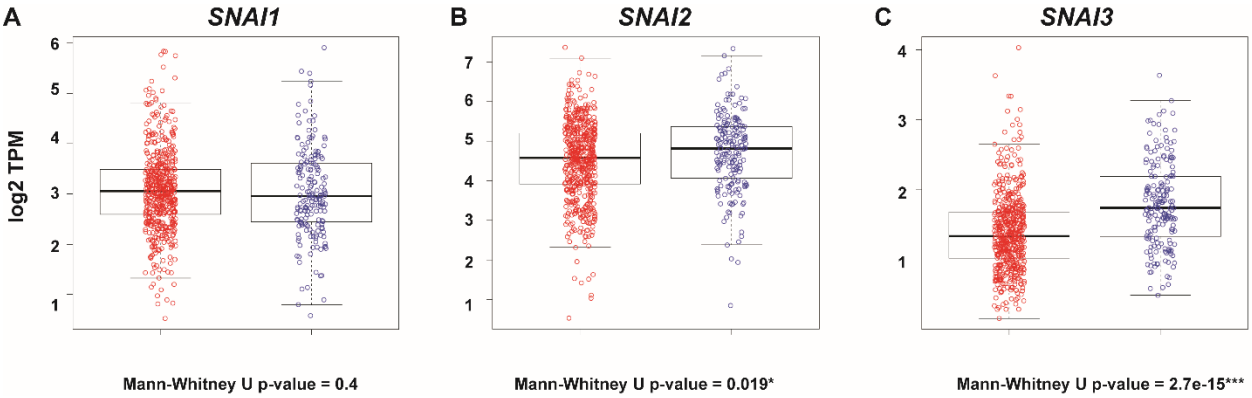

Figure 29: *SNAI2* and *SNAI3*, But Not *SNAI1* Are Significantly Different Between ILC and IDC Primary TCGA Lesions
TCGA ERα^{+} ILC (red) versus IDC (blue) lesions were probed for mRNA expressions of (A) *SNAI1*, (B) *SNAI2*, or (C) *SNAI3*. Mann-Whitney U p-values were applied to each data set. Analyses were performed in collaboration with Kevin Levine, BS.

We then probed survival data in the METABRIC cohort of ILC tumors and asked if high *SNAI1* expression delineated patients into a poorer outcome group as opposed to low *SNAI1* expressing tumors. This was not true, regardless of expression of ERα (Figure 30).

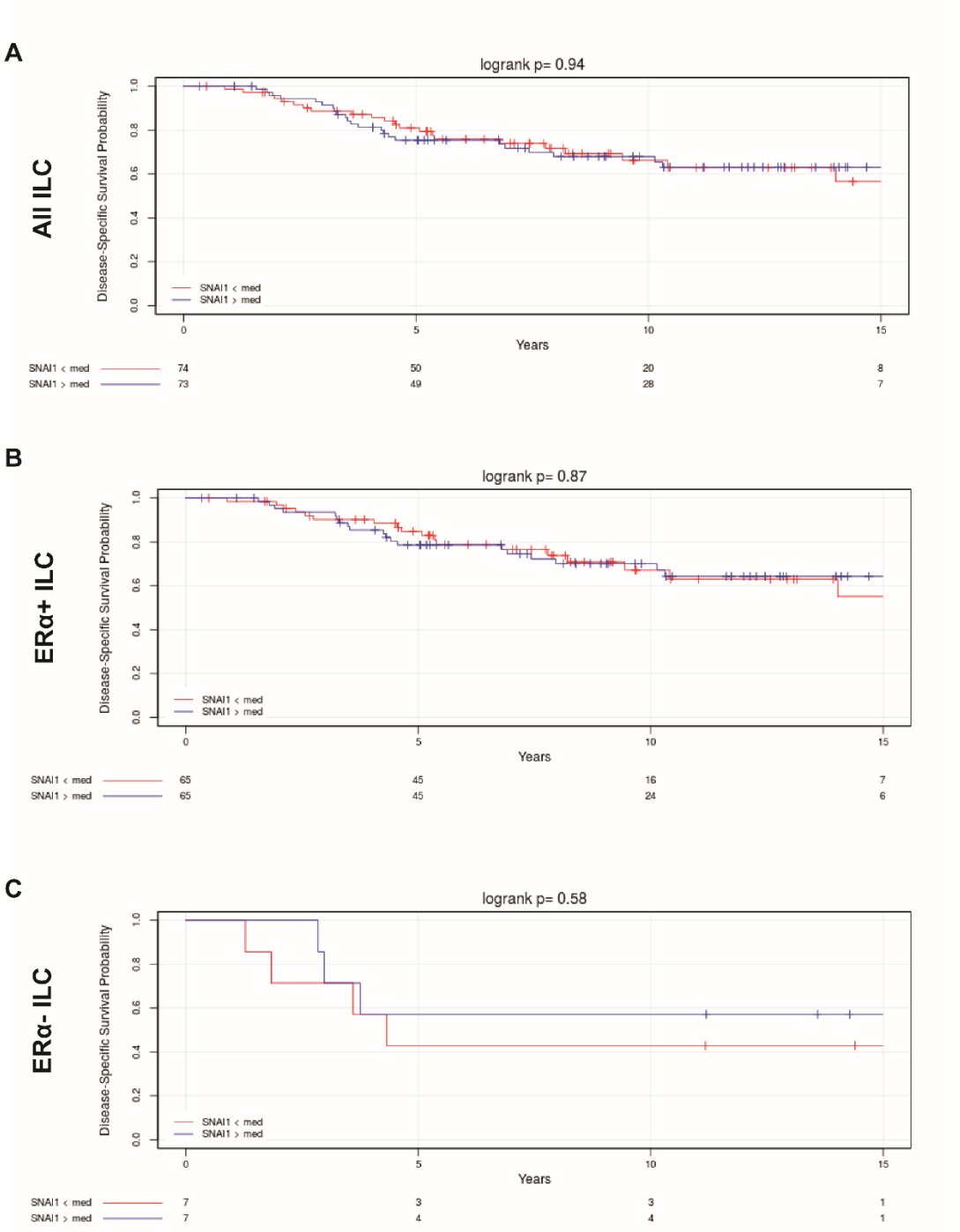

Figure 30: Differential *SNAI1* Expression is Not Associated with Survival in ILC Patients from METABRIC

Data from the METABRIC consortium were accrued and analyzed through collaboration with Kevin Levine, BS. (A) All ILC patients, (B) ERα^{+}, and (C) ERα^{-} ILC patients were separated by Kaplan-Meier curves based on high or low *SNAI1* expression. Log ranks were utilized to test differences in survival.

Though we did not see a significant difference in protein expression for SNAIL from the TCGA RPPA data, we were interested in answering whether protein was differentially expressed in ILC compared to IDC samples in an independent cohort. We first optimized use of the SNAIL antibody on our positive (BCK4 pINDUCER20-*SNAI1* +Dox, MDA-MB-134-VI) and negative (BCK4 pINDUCER20-*SNAI1 –Dox*) control FFPE sections, and determined that the antibody was effective for use at 1:100 dilution. We then stained a TMA containing ILC and IDC cores simultaneously with the BCK4 controls. 5/5 ILC ERα$^+$ and 12/12 IDC ERα$^+$ tumors displayed SNAIL staining, but most staining appeared present in the stroma (e.g.: ILC_1) or cytoplasmic ($ILC_{2\text{-}5}$, $IDC_{1\text{-}5}$) (Figure 31A). Cytoplasmic SNAIL is indicative of an inactive form of the protein, and is usually not considered positive in IHC practices[200]. The ILC samples that were stained on this TMA were also recently assessed in a panel of n = 131 primary ILCs curated, collected, isolated, and assessed by NanoString for a panel of genes of interest in our laboratory (*Matthew Sikora, PhD unpublished results*). $ILC_{1\text{-}5}$ were included on this panel, as was a *SNAI1* probe for gene expression. Interestingly, the NanoString data was consistent with the visual TMA outcomes ($ILC_1 > ILC_2 \geq ILC_3 \geq ILC_4 > ILC_5$ for *SNAI1* expression). Further validation of additional samples and appropriate histological review will be required of these samples to generate further conclusions. Additionally, as samples were treatment naïve at time of excision, it would be difficult to interpret the meaning of lack of or presence of SNAIL/*SNAI1* expression without additional samples from the same patients post treatment regimens.

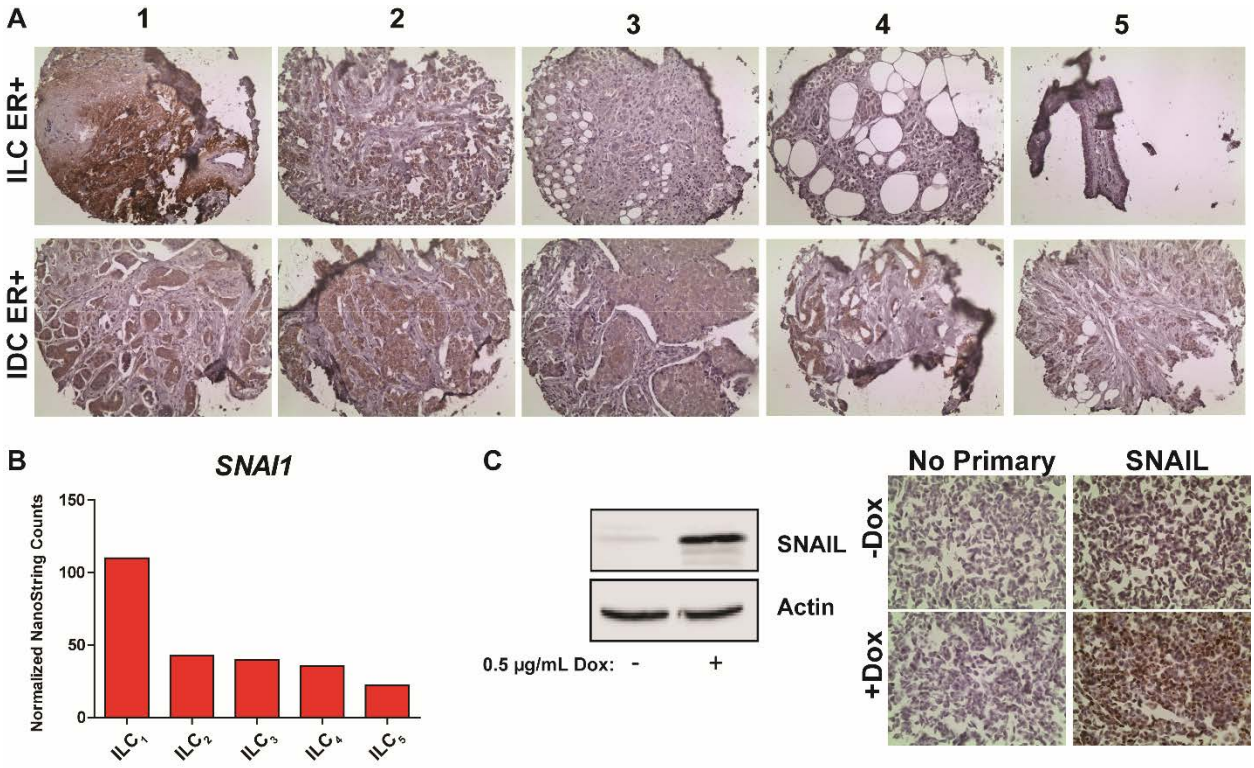

Figure 31: SNAIL is Localized to Cytoplasm in the Majority of TMA IHC Staining
(A) SNAIL protein was stained by IHC in ILC and IDC primary samples from the described TMA. All 5/5 ERα$^+$ ILCs and 5/12 ERα$^+$ IDCs with similar staining patterns are displayed above from bright field microscopic imaging (20X magnification). (B) NanoString data from the five ILC samples was mined from the larger data set. (C) Dox inducible SNAIL BCK4 cells were utilized to generate positive control FFPE pellets for SNAIL antibody optimization and validation. An IB confirmed overexpression of SNAIL on samples that were simultaneously treated to those that were used to generate the FFPE control pellets. A 1:100 dilution of antibody was assessed for use in (A).

We then hypothesized that *SNAI1* expression may be upregulated during progression, and more easily observed in metastatic events. To this end, we mined paired primary-metastatic lesion data that we have generated in-house from ILC patient samples. These RNA sequencing data spanned brain, bone, gastrointestinal (GI) tract, and ovarian metastases, and 3/11 primary-metastatic pairs showed increased *SNAI1* expression from primary to metastatic lesion (Figure 32). It should be noted, however, that the expressions observed in most of these samples were very low

with reads below "1." Interestingly, one of the increased *SNAI1* expressions from primary to metastasis was observed in a SERM-treated patient ($Ovary_2$).

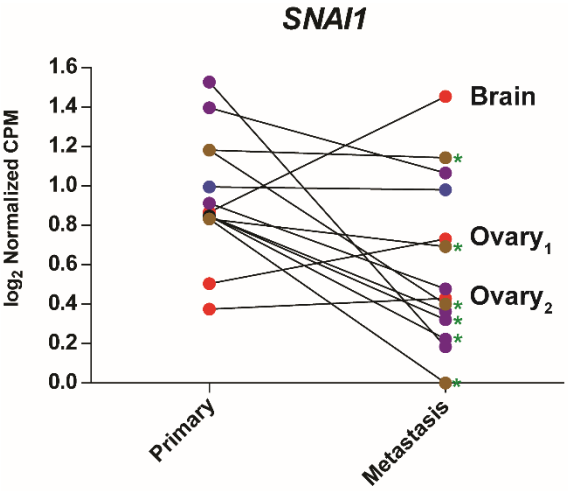

Metastatic Site	Receptor Status of Primary	Therapeutic
Brain	$ER^+/PR^+/HER2^-$	AI
$Ovary_1$	$ER^+/PR^+/HER2^-$	AI
$Ovary_2$	$ER^+/PR^+/HER2^?$	SERM

Figure 32: *SNAI1* Expression is Increased from Primary to Metastasis in Three ILC Pairs
Mined data was generated from samples collected by Nolan Priedigkeit (NP), PhD, Ahmed Basudan (AB), MS, and Rebecca Watters (RW), PhD for n = 11 matched primary/metastatic ILC pairs from brain (NP), ovary (AB), GI tract (AB), and bone (RW) metastases-afflicted patients. Samples with increased *SNAI1* expression were denoted in red for ease of visualization. Three out of eleven of the primary-metastatic pairs had a second metastatic lesion from the same patient, and are denoted with green asterisks. Metastatic sites for each respective pair with increased *SNAI1* expression, receptor status, and therapeutics received are detailed to the right of the main figure.

To conclude, the clinical data we currently possess do not indicate a role for (1) increased expression of *SNAI1* in TCGA primary $ER\alpha^+$ ILC versus IDC tumors (see Figure 29), (2) preliminarily suggest expression of SNAIL/*SNAI1* in some ILCs in an independently tested cohort (see Figure 31), (3) no role for increased *SNAI1* expression correlating with decreased survival for ILC patients regardless of ERα status (see Figure 30), and (4) limited evidence of increased *SNAI1* expression from primary to metastatic ILC lesions in 3/11 total primary-metastatic ILC pairs (see

Figure 32). Overall, this clinical data is not robust, and requires further elaboration and testing in additional ILC samples to confirm the few observations made.

2.3.12 A SNAIL/LSD1 Axis May Play a Role in ILC Phenotypes

While SNAIL was an interesting entity to study in the disease subtype of ILC, we understand that it does not function on its own. An interaction between SNAIL and epigenetic modifier lysine demethylase 1 (LSD1/*KDM1A*) has recently been shown to drive EMT phenotypes in cancer[178]. SNAIL acts as a molecular hook for LSD1, by interacting via the highly conserved SNAG domain of SNAIL. Together, these proteins are capable of being recruited to the promoter region of genes such as *CDH1* to repress expression and drive EMT phenotypes[201].

We decided to probe the potential interaction of SNAIL and LSD1 in our ILC cells. First, we measured expression of *KDM1A* by qRT-PCR and found that MDA-MB-134-VI most significantly expressed this entity as compared to MCF-7 cells (+2.87 FC relative to MCF-7) (Figure 33A). Then, we measured LSD1 protein levels by IB and observed LSD1 expression in all samples (Figure 33B). We also noted that *KDM1A* expression was upregulated significantly in ILC primary tumors as compared to IDCs from TCGA data; this was one of the few EMT-TF panel genes upregulated significantly in ILCs relative to IDCs (Figure 33C, Appendix B Figure 85). *KDM1A* was not regulated by E2 or 4OHT in MDA-MB-134-VI cells (Appendix B Figure 86).

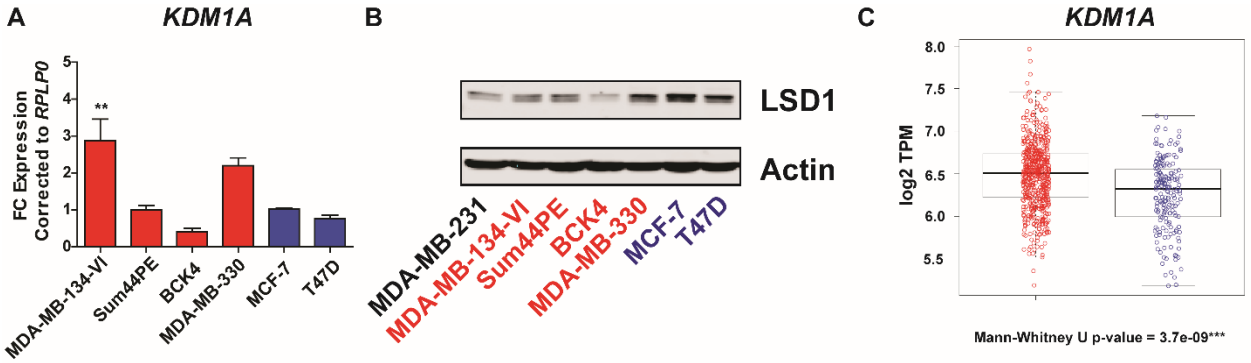

Figure 33: ILC and IDC Cells Express LSD1, But LSD1 is More Highly Expressed in TCGA Primary ERα⁺ ILC Tumors

The panel of ILC and IDC cells were assessed for basal expression of (A) *KDM1A* mRNA or (B) LSD1 protein. MDA-MB-21 served as a positive control for LSD1 expression in (B). Quantifications in (A) represent the combination of three independently performed experiments ± SEM with One Way ANOVA followed by Tukey's post-test with comparisons against MCF-7 displayed (*p < 0.05, **p < 0.005, ***p < 0.0005). IB is representative of three independently performed experiments. (C) Primary ERα⁺ ILC (n = 184) and IDC (n = 534) RNASeq *KDM1A* expressions were compared by Mann-Whitney U p-value through collaboration with Kevin Levine, BS.

With the expression of LSD1 confirmed in our cells and observed overexpression in ILC primary tumors, we next attempted to detect co-IP of this interaction in our highest expressing SNAIL and LSD1 cells, MDA-MB-134-VI. Endogenous co-IP of LSD1 and SNAIL has not currently been performed, to our knowledge. We first confirmed SNAIL-LSD1 interaction existence in a manipulated system by transfecting HEK293T cells with SNAIL or LSD1, with subsequent co-IP performed (Figure 34A). Then, we performed endogenous co-IP in MDA-MB-134-VI cells to detect the SNAIL-LSD1 interaction; this interaction was most easily detected by first performing IP for LSD1, and then detecting SNAIL (Figure 34B). The reverse process to first IP SNAIL and then detect LSD1 did not easily yield co-IP, but this was not surprising as the levels of LSD1 are in excess compared to the relatively lower expressed SNAIL protein. We therefore detected expression of both SNAIL and LSD1 in MDA-MB-134-VI, as well as interaction of these two proteins.

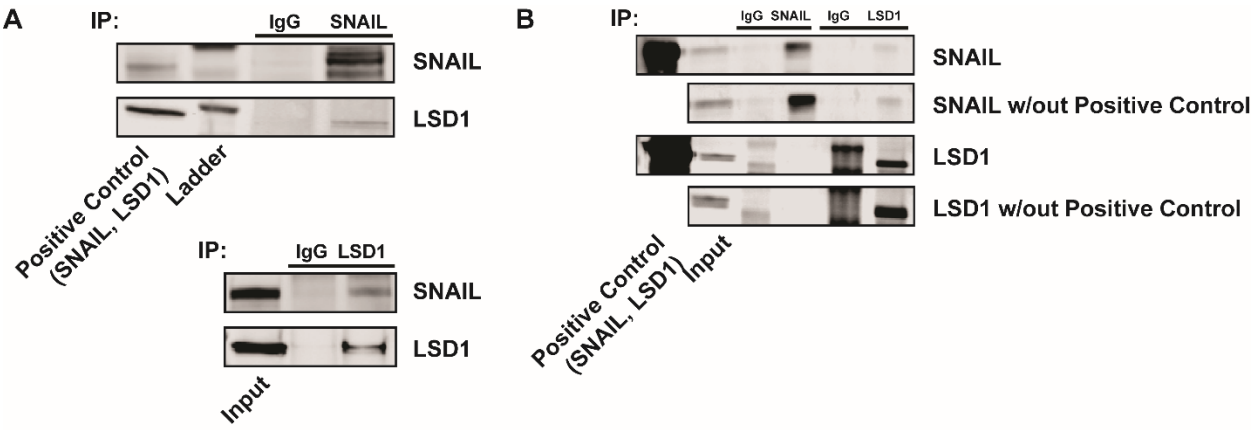

Figure 34: SNAIL and LSD1 Co-IP in a Transient Overexpression HEK293T System, and Endogenously in MDA-MB-134-VI Cells
(A) HEK293T cells were transiently transfected with SNAIL-HA or LSD1-FLAG overexpression plasmids for 48 hours, and lysates were subjected to Co-IP for SNAIL or LSD1. Insufficient input was available for the SNAIL IP, so a positive control was included on each IB. Data represent a single experimental attempt to confirm literature claims of SNAIL-LSD1 interaction. (B) Co-IP was performed in MDA-MB-134-VI cells for IgG controls, SNAIL, or LSD1. IBs were then assessed for interaction of proteins. Data represent two independently performed experiments with similar results obtained in both attempts.

We next asked if transient knockdown of *KDM1A* could influence the EMT-TF panel genes that are upregulated in ILC cells. We performed transient knockdown of *KDM1A* in MDA-MB-134-VI cells and discovered that this loss contributed to decreases in EMT-TF panel gene expressions including *SNAI1*, *FN1*, and *VIM* expressions (Figure 35). Though we did not explore this interaction further prior to the defense, the current evidence suggests the potential role for LSD1 in driving EMT-TF-regulated gene expressions, potentially upstream or in collaboration with SNAIL in ILC cells.

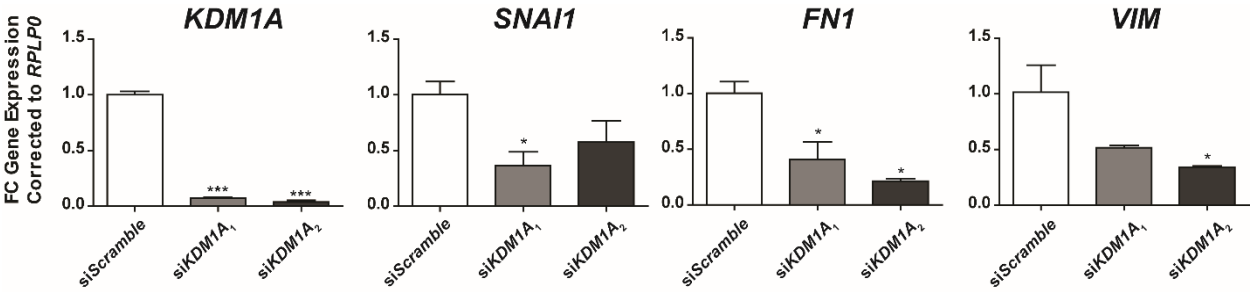

Figure 35: Knockdown of *KDM1A* Contributes to Downregulation of EMT-TF Panel Gene Expressions

MDA-MB-134-VI cells were transiently transfected with 10 nM si*Scramble* or si*KDM1A*$_{1,2}$ (two unique siRNAs targeting *KDM1A*) in technical triplicates, and were subjected to qRT-PCR for EMT-TF panel members. Data are displayed relative to si*Scramble* control ± STDEV with One Way ANOVA followed by Tukey's post-test (*$p < 0.05$, **$p < 0.005$, ***$p < 0.0005$) comparing si*Scramble* to knockdowns. Data represent a single experiment.

Though we did not pursue the SNAIL/LSD1 axis further, we conclude the following from these data: (1) LSD1 is expressed in both ILC and IDC cells, while SNAIL is only most highly expressed in the MDA-MB-134-VI ILC cells relative to other ILC/IDC cells tested (see Figure 13, 14, 33), (2) LSD1 is not altered in expression by E2 or 4OHT treatments (see Appendix B, Figure 86), (3) LSD1 and SNAIL interact endogenously in MDA-MB-134-VI ILC cells (see Figure 34B), and (4) loss of *KDM1A* contributes to a downregulation in expression of EMT-TF panel members (see Figure 35). As stated, the expression of *KDM1A* is also significantly higher in ILC primary TCGA samples as compared to IDCs (see Figure 33C). These data, though preliminary, warrant further investigation.

2.3.13 Faithfully Recapitulating the EMT-like Phenotypes of ILC in *In Vitro* Studies

ILCs have a unique growth pattern in breast tissue that is likely governed by the loss of E-cadherin (refer to Figure 2)[28, 59-63]. However, many of our tissue culture studies were performed in standard 2D proliferation environments, which do not faithfully recapitulate the clinical growth

environment of these cells. We included use of the ULA environment in some of our studies, as members of our lab have observed an increased preference for ILC cells over IDC cells to grow in this environment (*Nilgun Tasdemir, PhD unpublished results*). Further, additional observations have revealed that ILC cells overall do not migrate (scratch assay), invade (coated transmembrane insert assays), or form proper mammospheres (see Figure 27, *Nilgun Tasdemir, PhD unpublished results*). With few easily observable phenotypes for ILC cells, and the understanding that these environments may not recapitulate appropriate growth environments, we decided to observe the phenotypes of our ILC cells in two additional environments that more closely resemble the clinical setting: soft agar anchorage independent growth environment and linear protein micropatterned 2D proliferation.

Soft agar assays involve use of a 3D environment to suspend the cells without any contact to an extracellular matrix[202]. Cells that form colonies in soft agar are considered transformed and carcinogenic. Suppression of E-cadherin can promote soft agar anchorage independent growth for some cell lines, which was an additional rationale for testing this environment[203]. Soft agar assays were performed with MDA-MB-134-VI and MCF-7 cells for 14 days to observe the outgrowth of anchorage independent colonies (Figure 36A). We observed classic colony formation from MCF-7 cells; MCF-7 colonies were dense in the center of each respective colony, and distinctive in their morphologies. However, MDA-MB-134-VI cells did not form the same kinds of cohesive colonies. Instead, colonies were loosely tethered together as clusters of cells. Additionally, significantly fewer colonies formed that were of similar size when equal densities of cells were plated for both MDA-MB-134-VI and MCF-7 (Figure 36B). An additional experiment was performed using the complete ILC (MDA-MB-134-VI, Sum44PE, BCK4, MDA-MB-330) and IDC (MCF-7, T47D) cell line panel, but insufficient colonies were present for counting purposes.

We have provided images of the morphologies of these colonies in Appendix B Figure 87. Overall, ILC cells did not form many colonies, or formed loosely clustered cell aggregates within the agar. From these preliminary data, we concluded that ILC cells do not form classic soft agar colonies and require longer time periods to form colonies or increased plating densities to observe colony formation.

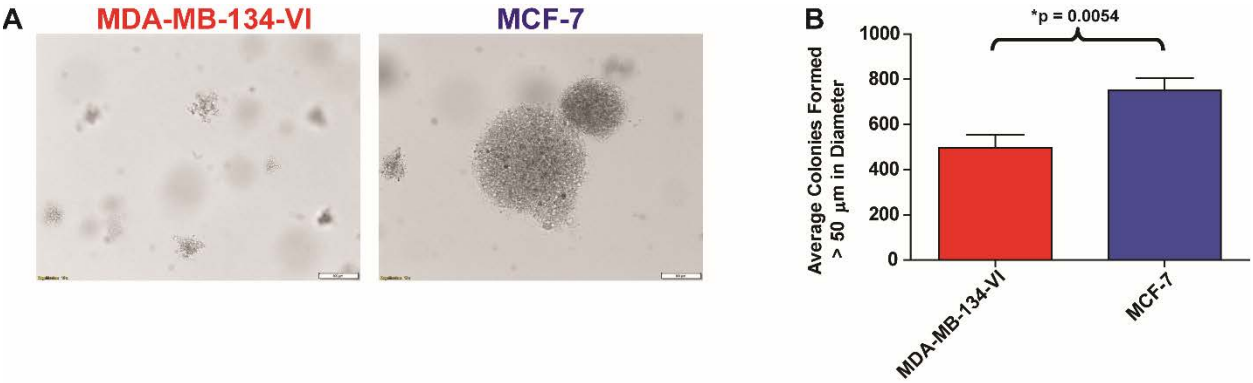

Figure 36: MDA-MB-134-VI Cells Form Fewer, Smaller, and Discohesive Soft Agar Colonies Compared to MCF-7 Cells
MDA-MB-134-VI and MCF-7 cells were plated at the same density (10,000 cells/dish) in triplicate dishes for 14 days to monitor soft agar colony formation. (A) Representative images were taken of colonies that were counted in each dish (10X magnification; bars represent 100 µm). (B) Colonies were defined as clusters of cells with a diameter of 50 µm or greater. Technical triplicate dishes were counted for colonies using cellSens Dimension software, and are displayed ± STDEV. Students t-test was used to compare the two groups (*$p < 0.05$, **$p < 0.005$, ***$p < 0.0005$). Data represent a single experiment.

The second environment in which we tested ILC growth was a linear protein micropatterned 2D proliferation environment. We hypothesized that ILC cells would more preferentially adhere to and proliferate in an environment that would mimic the clinically observed linear growth patterns of ILCs[59-61]. We first generated Fibronectin (FN1) 20 µm micropatterned coverslips and seeded MDA-MB-134-VI or MCF-7 cells onto these environments. Initial

observations at the 24 hour-time point post plating were promising, with both cell types adhering to the micropatterns (Appendix B Figure 88). We next expanded the panel of micropatterned proteins tested to include FN1, Collagen I (COLI), Collagen IV (COLIV), and Laminin I (LAM). The MDA-MB-134-VI cells adhered only somewhat to the FN1 in this attempt, and did not adhere well to the COLI, COLIV, or LAM micropatterns (Figure 37A). Instead of adhering, the cells would cluster together and float over the surface of the micropattern. In contrast, MCF-7 adhered to the FN1, COLI, and COLIV environments, but also did not adhere to the LAM micropattern. We decide to then attempt the experiment again, but with solid coatings of the FN1/COLI/COLIV/LAM proteins as opposed to micropatterns. We also included treatment with 4 nM Batimastat in each third replicate well to attempt to inhibit any matrix metalloproteinases (MMPs) that could be inhibiting the proper adherence of MDA-MB-134-VI to the protein environments. MDA-MB-134-VI cells did not adhere well to the solid protein micropatterns, with or without the addition of Batimastat (Figure 37B), and MCF-7 adhered much like in the previously performed micropatterning experiment (see Figure 37A). Due to lack of adherence of MDA-MB-134-VI to proteins in these repeated experimental attempts, additional attempts of these experiments were not performed. Further, ongoing analyses in our lab have shown that MDA-MB-134-VI cells do not adhere well to all proteins tested in the micropatterning experiments (FN1/COLI/COLIV/LAM) relative to uncoated protein wells in an ECM adhesion assay (*Nilgun Tasdemir, PhD unpublished results*).

These preliminary experiments in soft agar and protein micropatterned growth environments suggested the following: (1) ILC cells do not form classic soft agar colonies, and take longer periods of time to form (see Figure 36, see Appendix B Figure 87), and (2) MDA-MB-134-VI cells do not preferentially adhere to protein micropatterned environments as compared to

MCF-7 cells (see Figure 37, *Nilgun Tasdemir, PhD unpublished results*). Further phenotypic analyses are ongoing in our lab to determine appropriate growth environments for ILC cells.

A

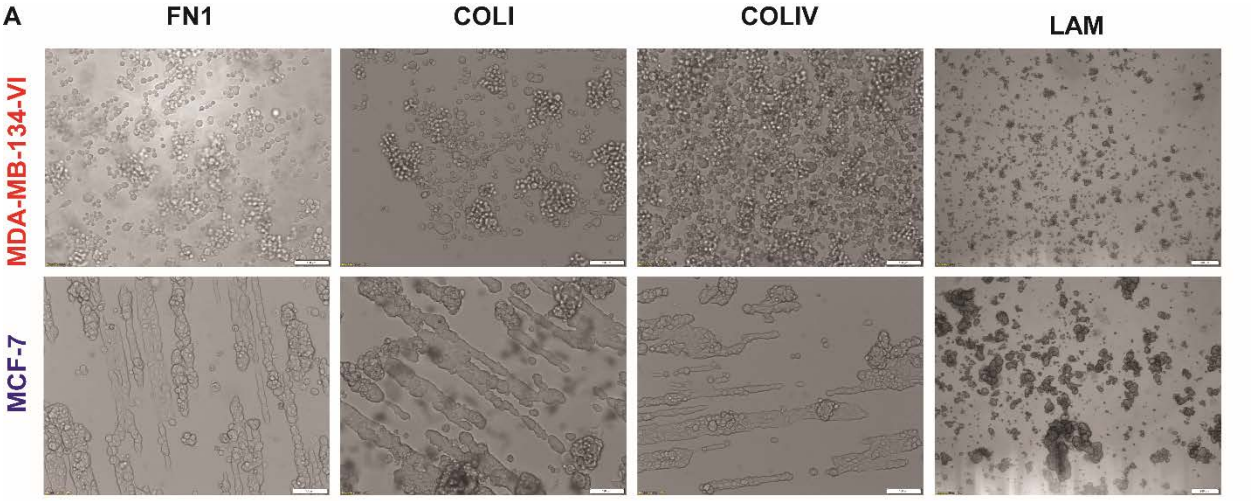

B

Cell Type	Replicate	GLASS	FN1	COLI	COLIV	LAM
MDA-MB-134-VI	1	+	much clumping, little adherence	much clumping, little adherence	much clumping, little adherence	+
MDA-MB-134-VI	2	+	much clumping, little adherence	much clumping, little adherence	some adherence, clumping visible	+
MDA-MB-134-VI	3	+	much clumping, little adherence	much clumping, little adherence	some adherence, clumping visible	+
MCF-7	1	+	+	+	overall good with some clumping	much clumping, little adherence
MCF-7	2	+	+	+	overall good with some clumping	much clumping, little adherence
MCF-7	3	+	+	+	overall good with some clumping	much clumping, little adherence

Figure 37: MDA-MB-134-VI Cells Showed Lower Adherence to Protein Micropatterns or Protein Coatings Compared to MCF-7 Cells

(A) MDA-MB-134-VI and MCF-7 cells were plated on 20 µm linear protein micropatterned, PDMS spin-coated coverslips at 200,000 cells/well in technical triplicate wells. Images were taken 2-3 days post plating under phase contrast microscopy (FN1, COLI, COLIV at 10X magnification; bars represent 100 µm) (LAM at 4X magnification; bars represent 200 µm). (B) MDA-MB-134-VI and MCF-7 cells were plated on glass coverslips, or coverslips completely coated with the same concentrations of FN1 (50 µg/mL), COLI (200 µg/mL), COLIV (200 µg/mL), or LAM (200 µg/mL) as utilized in micropattern assays. Each third replicate well received 4 nM Batimastat, a broad spectrum MMPi, denoted by red text. Observations are detailed in the above table after 2-3 days post plating/treatment.

2.4 DISCUSSION

Recent clinical trial data and observations made in our laboratory suggest a role for endocrine therapy resistance in ILC, particularly from Tamoxifen treatment[116-120, 132]. Understanding the molecular mechanisms for Tamoxifen resistance will be paramount to informing clinical decisions for patients afflicted with ILC. Thus, we decided to pursue the upregulation of SNAIL, an EMT-TF known to contribute to Tamoxifen resistance in alternate major histological subtype IDC, as a key candidate from our ILC 4OHT treatment screen.

We first confirmed upregulation of *SNAI1*/SNAIL in MDA-MB-134-VI and Sum44PE, two commonly utilized ILC cell line models, by qRT-PCR and IB methodologies (see Figure 5, 6, 10). This was first observed in the context of 4OHT and E2 treatments, and was not apparent in IDC cell lines tested. However, we did not observe 4OHT partial agonist activity in BCK4 or MDA-MB-330 ILC cells. BCK4 cells were generated from the murine outgrowth of a human mucinous breast cancer with growth patterns and mutations that mimicked ILC, but is not representative of classical ILC[181, 204]. Additionally, BCK4 cells maintained lower overall ERα expression and response to E2 in our experiments (see Figure 4A, Appendix B Figure 70). MDA-MB-330 cells are often reported as ERα$^-$ cells, though they express ERα (see Appendix B Figure 70). This characterization was likely based upon lack of response to E2 in classic assays, though we see a minor E2 dose response for MDA-MB-330 in our hands (Figure 4A). Still, the lack of robust response by ERα in MDA-MB-330 may contribute to the lack of 4OHT agonist activity in these cells. We will pursue additional time point analyses of these treatments in the complete panel of ILC cell lines in the future, as our studies were limited to 24-hour time points. We could also employ the use of additional ER ligands (E1, E3) in our assays to assess the importance of generic ER activation in ILC cells to promote *SNAI1* expression increases as well as phenotypes. We will

also look for changes in SNAIL localization *in vitro* after 4OHT treatment in our cell lines. Overall, these data suggest a unique agonist behavior of 4OHT in some but not all ILC cell lines that we hypothesized to be mediated, at least in part, by SNAIL.

We confirmed direct interaction of ERα with the promoter region of *SNAI1* by ChIP after 4OHT and E2 treatments (see Figure 11, 12, Appendix B Figure 68, 69). This direct interaction confirms that 4OHT is directing ERα to upregulate alternative targets in ILC that are known to contribute to 4OHT resistance. We noted that this was not restricted to *SNAI1*, but was also apparent in other classic ERα target gene regions (*IGFBP4*, *GREB1*). These data suggest that 4OHT can generically direct ERα to promoters of classic gene targets in MDA-MB-134-VI. This partial agonist activity of 4OHT should be further explored to include additional data such as altered ERα/coactivator/corepressor interactions and binding affinities of 4OHT to ERα in ILC versus IDC cells.

The observed upregulation of *SNAI1* by 4OHT cannot be easily explained simply by the loss of epithelial marker E-cadherin. We addressed this question in three ways: we transiently knocked down *CDH1* in IDC cells (see Figure 9A), utilized a stable *CDH1* knockdown IDC system (Figure 9B), and we used two ILC-like cell lines that harbor mutations in *CDH1* (see Figure 9C, 9D). However, the loss of E-cadherin either by manipulation of transcript levels or by mutation of E-cadherin were insufficient to recapitulate the 4OHT/*SNAI1* phenotypes observed in ILC cells. These data suggest that there is something else other than E-cadherin loss contributing to the observed 4OHT induction of *SNAI1* in some ILC cell lines. Additionally, we observed no alterations to other EMT-TF panel members in our small panel tested (see Figure 7, Appendix B Figure 66), leading us to believe that SNAIL is differentially targeted for upregulation after treatment with 4OHT. This upregulation was only formally tested in the 2D environment, and not

in the ULA environment; as we only observed the induced proliferation phenotype after 4OHT treatment in 2D in conjunction with *SNAI1* induction, we will pursue expression analyses in the ULA environment to assess the hypothesis that *SNAI1* is *not* upregulated by 4OHT in this environment, due to lack of observed phenotype in ULA. We will also probe the expression of other EMT-TF panel members that we studied in this environment.

Interestingly, Sum44^{TAMR} cells, a Tamoxifen resistant derivative of ILC cells, do not show upregulation of *SNAI1*, opposite our original hypothesis (see Figure 8). Instead, expression was decreased relative to parental cells. These data were obtained from a manipulated cell line model system that was outgrown in a tissue culture incubator, as opposed to in a patient, and may not be a true representation of the physiological reaction to ongoing Tamoxifen treatment in an ILC patient. We also did not test an acute treatment of 4OHT on the Sum44^{TAMR} cells in a 24-hour time point as we performed on our other ILC cell lines. It is possible that these cells do not show a transient upregulation of *SNAI1* as parental Sum44 cells do. *SNAI1* may only have implications as a transiently upregulated entity in ILC, either to contribute to short-term manipulations of gene expression programs that we were not able to manipulate in our cells, or it may just be upregulated in response to 4OHT as a marker. Further, we did not test the basal expression of additional EMT-TF panel members studied in the Sum44^{TAMR} cells due to limited mRNA available. We will pursue expression studies of these additional genes in the future.

Manipulations of SNAIL were difficult to maintain unless performed in transient si*RNA* assays (see Figure 18-21). This tight regulation of SNAIL in ILC, and in transient experiments performed in IDC cells (see Appendix B Figure 73), suggest that alternative methods (CRISPR/Cas9) will need to be taken to observe complete loss of SNAIL or that inducible or transient experiments will have to be performed to manipulate this protein[205]. If viral methods of

infection are attempted again using GFP constructs, we will track the quantity of GFP^+ cells present in our cell lines over time to assess outgrowth of uninfected cells. Complete loss of gene function may lead to alternative phenotypic observations, such as lethality, as presence of low levels of SNAIL may be sufficient to override the knockdown cells. However, the manipulation of SNAIL leading to increased proliferative phenotypes in the ILC knockdown setting complemented the decreased proliferative and invasive phenotypes observed in overexpression settings (see Figure 16, 24-27). The intriguing portion of our data was the undescribed role of SNAIL induction in reducing stem-like phenotypes in our ILC cells (see Figure 33). While SNAIL has been well-published to induce these phenotypes, it is possible that the unique background of ILC, including mutation/loss of E-cadherin, may lead to under described roles for the protein. Context is imperative to consider, and SNAIL has not been studied thoroughly in the context of ILC until now. Additionally, though we do not currently understand the mechanism behind these phenotypes, we will pursue this in future studies. We will also pursue additional phenotypic assessments including colony formation in low density growth environments.

The presence of an EMT-TF and EMT-TF target gene upregulation in ILC as compared to IDC cells was apparent in our cell line panel, but not as clear in clinical samples obtained from primary lesions of patients (Figure 13, 14, 29-31, Appendix B Figure 84, 85). Our cell lines were derived from metastatic outgrowths of breast primary lesions, and may recapitulate what is observed in the metastatic as opposed to primary settings[200]. Though not robust, we did observe an increase of *SNAI1* expression from primary to metastatic lesion in 3/11 ILC pairs (see Figure 32). Alternatively, as described previously, *SNAI1* may be upregulated only transiently in ILC to contribute to resistance phenotypes, or as a marker. Future studies could pursue regulation of

SNAI1 in tumor explants obtained from ILC patient tissue. These data may assist in concluding the transient upregulation of *SNAI1* between these systems post 4OHT treatment.

The intriguing interaction between SNAIL and LSD1 was confirmed for the first time, endogenously, in our ILC cells MDA-MB-134-VI (see Figure 34)[206]. LSD1 is also upregulated in both ILC and IDC cells, and its knockdown in MDA-MB-134-VI led to significant decreases in EMT-TF programs (see Figure 33, 35). Additionally, promising increased expression of *KDM1A* in primary ILCs as compared to IDCs was observed (see Figure 33C). Manipulation of this SNAIL/LSD1 axis may be achieved by treatment with LSD1-specific inhibitors that are currently under clinical development for use in cancer[207]. LSD1 belongs to the overarching protein family of Monoamine Oxidases. Interestingly, the class of Monoamine Oxidase inhibitors (MAOis), have been in use clinically for decades for the indication of depression[208]. The role of LSD1 in controlling EMT programs has now been well-described[178, 209]. Further, the interaction between LSD1 and ERα in MDA-MB-134-VI was detailed recently, and may provide an interesting strategy for alleviation of 4OHT-driven phenotypes as compared to targeting *SNAI1*[210]. Altogether, these data suggest that repurposing of MAOi therapeutics, or use of these more targeted inhibitors should be thoroughly explored in the context of ILC.

Finally, we observed the general growth phenotypes of ILC cells in two additional environments that may more faithfully recapitulate the clinical setting for ILC cells: soft agar and protein micropatterned growth environments. The loss of E-cadherin in ILC cells likely contributes to their decreased soft agar colony formation and generally discohesive growth pattern (see Figure 36, Appendix B Figure 87). Our difficulties with adherence of MDA-MB-134-VI cells in the micropatterning experiments were an interesting observation (see Figure 37). These data have been recapitulated in an ECM adhesion assay with the same proteins and the same cells, performed by

a colleague (*Nilgun Tasdemir, PhD unpublished results*). However, the lower attachment in all protein environments was most apparent in MDA-MB-134-VI cells compared to the other ILC cell lines. Further exploration regarding growth of ILC cells in multiple environments will be required in order to understand their basic phenotypes.

In summary, our results indicate that 4OHT-driven phenotypes are present in some ERα$^+$ ILC cells (MDA-MB-134-VI, Sum44PE), and directly causes ERα to promote expression of EMT-TF *SNAI1*. Though manipulation of SNAIL was technically difficult to achieve, its transient overexpression revealed a previously undescribed role for decreased tumorigenic phenotypes as opposed to enhanced EMT. Overall, the EMT panel tested was upregulated in ILC relative to IDC cells, but this does not fully translate to the clinical setting in primary samples studied. Further studies in metastatic lesions are necessary, and will assist in elucidation of the EMT-TF program as a potential target in ILC. LSD1 is an attractive and interesting novel target in ILC that we have identified. Finally, context of ILC proliferation is imperative; cells responded differently to *SNAI1* manipulation in 2D versus ULA, and soft agar growth and protein micropatterning experiments showed that ILC cells do not have the same phenotypes as IDC cells. Overall, our studies provide the first molecular descriptions of SNAIL in ILC, provide evidence for alternative functions for a well-studied protein, suggest a novel therapeutic target for ILC patients that may be confronted with currently FDA-approved inhibitors, and encourage further exploration of the environmental contexts that affect ILC growth.

3.0 ESTABLISHMENT AND CHARACTERIZATION OF NOVEL INVASIVE LOBULAR CARCINOMA CELL LINE WCRC0025-76M (WCRC-25)

3.1 INTRODUCTION

Immortalized and transformed cell line models serve as important tools to understand the etiology, mechanisms, and basic characteristics of diseases[211]. Use of these *in vitro* systems have various benefits including the ability of cells to indefinitely replicate, generally maintain a homogenous population to allow assessment of specific scientific questions in a focused manner, and ease or accessibility for a variety of researchers to obtain and maintain as compared to *in vivo* or clinical models[212, 213]. While highly beneficial to the field of science, cell line models also have limitations. These include the questionable representation of a single cell line for a given subtype of disease, lack of appropriate culture methods to effectively and faithfully recapitulate the clinical setting, and widespread issues with reproducibility due to the existence of variants or unauthenticated cultures[214-216]. To counteract some of these pitfalls, consortiums have been developed to provide guidelines for the proper development and characterization of cell lines, a process that was followed rigorously in the following study[217]. Despite these drawbacks and ongoing rigor and reproducibility concerns, cell line research has successfully contributed to the vast majority of scientific studies that have been undertaken in the last half century.

3.1.1 Brief History of Cell Line Derivation

The first immortal cell line was established by Dr. Gorge Otto Gey of Johns Hopkins University in 1951 from the biopsied cells of a cervical cancer patient, Henrietta Lacks[211-218]. These cells are commonly known by their moniker "HeLa," a nomenclature derived from the first two letters of Lacks' first and last names, respectively. Dr. Gey was a University of Pittsburgh alumnus, having spent his undergraduate years immersed in studying biology, and subsequently moving on to Johns Hopkins to complete his medical degree and initiate a nearly four decades' long tenure as a teacher and researcher[219]. Dr. Gey and his wife, Margaret, are credited with establishing the Tissue Culture Laboratory at Johns Hopkins and attempting to generate immortal cell lines for decades prior to the fortuitous discovery of the special nature of HeLa cells. One of the largest barriers to cell line establishment was identifying a cell population that had lost control of the ability to senesce, or to stop dividing, as most cells do after a few dozen divisions[220-222]. Beyond the lack of these "molecular brakes," it was also known that cells required a highly specialized growth environment with temperature control and complex mixtures of growth factors to support continued proliferation[223-225]. Dr. Gey's highly intuitive roller drum technique allowed him to nurture HeLa cells for use in experiments that have spanned decades of research, covering multitudes of diseases[226]. His pioneering work has become a foundation for cell line establishment, both in the positive aspects described and in the negative, unethical nature by which the original HeLa sample was obtained. This example has spurred ethical considerations regarding informed consent, a process that is now highly respected and upheld within the field of medicine, today[227, 228].

The first breast cancer cell line was established in 1958 in the laboratory of Lasfargues and Ozzello, and is called BT-20[229]. BT-20 was isolated from a primary lesion of a ductal

carcinoma of no special type, and is classified as triple negative ($ER^-/PR^-/HER2^-$)[230-233]. Unlike HeLa, BT-20 was derived using a methodology known as "spilling," where epithelial cells were collected from sliced donor tissue, soaked in culture media in a gentler format devoid of harsh chemical or mechanical dissociation[234]. In a more natural progression, epithelial cells from tumors would leach from tumor tissue along with various other cell types (lymphocytes, fibroblasts, etc.) to generate semi-turbid, heterogeneous cultures. Differential centrifugation or colony picking methodologies such as the "glass ring technique" were utilized to separate precious epithelial tumor cells from the fibroblast compartment, which tended to outgrow all other cell types in a culture dish. Additionally, collagen-coated plates were often employed to mimic a more physiologically relevant growth environment. However, the use of collagen was sometimes unsuccessful, with cells mechanically pulling on the collagen fibers to induce tears, exposing the glass plate, or collagen peeling off plates after media changes. The complexity of media additives also became quickly apparent, as researchers attempted to use umbilical cord sera, add or remove hormones, growth factors, and eventually find the importance of use of standard fetal bovine sera[235]. Further, scientists understood that metastatic lesions, particularly from ascites or pleural effusions, were some of the most successful samples to produce stable cultures[236].

3.1.2 ILC Cell Line Models Overview

Though the isolation and cultivation of BT-20 gave hope to the field of breast cancer research in the late 1950s, and a few cell lines followed, there were many difficulties encountered in the derivation of additional cell lines[237]. Thus, it was not until the 1970s that a series of breast cancer cell lines were established and characterized at MD Anderson in Houston, Texas[236]. This cell line series was indicated with "MDA-MB" in the first portion of their collective names, and include

the first established lobular carcinoma cell line, MDA-MB-134-VI. Initially described in 1974 by Cailleau and colleagues as derived from the pleural effusion of a ductal carcinoma, it was not until 2006 that Reis-Filho and colleagues reclassified MDA-MB-134-VI as a Luminal A ILC through extensive molecular genetics and expression profiling comparisons against classic ILC lesions[238]. Current literature is still filled with conflicts about the origin of this cell line, with many publications citing the original pathology calls given to the patient samples obtained in the early 1970s[204]. This example of reexamination of cell lines by focusing on key genetic aberrations, such as well-established *CDH1* mutations described in ILC clinical samples, may allow for future reclassifications of other cell lines that maintain ILC-like phenotypes and have potentially been misclassified as ductal or adenocarcinomas of the breast (e.g. CAMA-1, ZR-75-30)[186, 239].

The general molecular and physiologic characteristics of MDA-MB-134-VI have been recently described[132, 240]. MDA-MB-134-VI are $ER^+/PR^-/HER2^-$, and have LOH of *CDH1* due to deletion of exon 6, leading to a frameshift mutation and premature stop codon[172]. Additionally, MDA-MB-134-VI have overexpression of FGFR1, attributed to a commonly observed lobular chromosomal gain at 8p11-p12[238, 240]. MDA-MB-134-VI cells are predominantly a rounded morphological cell population, with occasional spindle-shaped cells that seem to become more apparent in higher passage cultures. Doubling times for MDA-MB-134-VI cells are also the fastest among all established ILC cell lines, estimated around two days. Our group is among the first to characterize the limited stable phenotypes of MDA-MB-134-VI. These include generally slower 2D proliferation and enhanced ULA proliferation in comparison to IDC cultures, limited migratory and invasive capacities, and decreased anchorage-independent soft agar growth (see Chapter Two, *Nilgun Tasdemir, PhD unpublished results*). As described in the previous chapter of this dissertation, our group has also recently used this model system to uncover a role for *de novo*

Tamoxifen resistance in lobular carcinoma; 4OHT leads to upregulation of EMT-TF *SNAI1*, and 4OHT partial agonist 2D proliferation induction is abrogated by inhibition of FGFR1[132]. Beyond our group's descriptions of these cells, few studies have utilized MDA-MB-134-VI to describe ILC phenotypes, or ineffectively detailed the capacity of use of the model. For example, only one study previously dictated that injection of MDA-MB-134-VI by tail vein into nude mice did not lead to generation of xenografts[184]. In direct contradiction to this finding, our laboratory has recently discovered the effective use of MDA-MB-134-VI as a xenograft by tail vein injection (nude mice), mammary fat pad injection (NSG mice), and in a **M**ammary Intra**d**uctal Injection (MIND) model (*Nilgun Tasdemir, PhD unpublished results*)[241, 242]. Potential rationales for this discrepancy include the use of subcutaneously implanted slow-release estradiol pellets in our studies to drive the ERα$^+$ tumor growth, and patience in waiting for the cell line xenograft to establish. Future studies will focus on the elucidation of molecular mechanisms that drive the homing of these cells to niches, and establishment of cultures that can be serially transplanted to increase the organ tropism preference of cells. Though these observations will not be detailed in this thesis, they will contribute to our basic understanding of ILC and its general phenotypes. These data challenge the previously stated lack of utility of these cell line model systems in a translational capacity[204].

After MDA-MB-134-VI, MDA-MB-330 was the first cell line pathologically defined to be derived from an ILC pleural effusion in 1974[184]. Conflicting reports dictate that it was devoid of ERα expression, but we have shown that this observation is likely based off its limited response to estradiol as opposed to a lack of mRNA and protein expression[243-245]. Thus, we describe MDA-MB-330 as an ERα$^+$ ILC cell line model. In addition, MDA-MB-330 cells are PR$^-$ and HER2$^+$, with HER2 expression being rare among ILC cell lines and lesions[67]. This expression likely

contributes to its mixed classification as having Luminal-HER2 subtype[233]. E-cadherin is also still expressed at both transcript and protein levels in MDA-MB-330[239, 246]. Instead, these cells harbor a mutation in *CTNNA1*, or α-catenin, which leads to dysfunctional E-cadherin that is incapable of interacting at the adherens junction[63]. The doubling time of MDA-MB-330 is one and a half to two weeks, limiting the use of this culture in many classic phenotypic experiments. The morphology of these cells is more cobblestone-like in appearance, differing greatly from the observed rounded morphology in ILC patient specimens and commonly used MDA-MB-134-VI cell line. Like observations made with cell line xenografts in MDA-MB-134-VI, our group has already assessed that there is potential utility of this cell line in various injection models (*experiments in progress*). MDA-MB-330 was a model of utility in the work of this dissertation, and will likely grow in popularity as a model of ILC as it becomes more well-known in upcoming publications.

Sum44PE is a member of the "SUM" series of cell lines derived by Ethier and colleagues at the University of Michigan in the early 1990s from a malignant pleural effusion[247]. Sum44PE is $ER^+/PR^-/HER2^-$, and classified as Luminal A. A truncation mutant of E-cadherin is produced in Sum44PE by the deletion of a thymidine at position 423 of exon 9. The morphological characterization of Sum44PE is highly heterogeneous, with the existence of three distinct cell populations noted: round, spindle-shaped, and a larger cell type. Careful observation of these populations over time has shown the predominance of the spindle-shaped cell in higher passage cultures. Doubling time has been noted by some groups to be as short as one day, but our group has observed that the doubling time of Sum44PE is closer to five to seven days, with cultures taking the longest period to adhere to culture vessels and often becoming detached easily by premature agitation of a flask[204]. Like MDA-MB-134-VI, Sum44PE is more highly utilized in

ILC research, and maintains amplification of the 8p11-p12 chromosomal locus and FGFR1 overexpression[247]. However, Sum44PE is also maintained in the most complex tissue culture medium, containing many unique growth factors that were deemed necessary during initial epithelial cell selection on collagen-coated plates[248]. Much like previous observations made regarding MDA-MB-134-VI and MDA-MB-330, we find interesting *in vivo* applications for Sum44PE xenografts, and will elucidate on these outcomes in upcoming publications (*Nilgun Tasdemir, PhD unpublished results*).

The next ILC cell line model that was utilized in this dissertation is not a classical ILC cell line. BCK4 cells were derived from a mucinous breast cancer pleural effusion that had been exposed to Tamoxifen, chemotherapy, and radiation treatments, was xenografted into nude mice, and grew out in rounded morphological appearance similar to ILC with a slow doubling time of approximately five to seven days[181, 249]. This ILC-like lesion was established as a tissue culture model by Jacobsen and colleagues, having $ER^+/PR^+/HER2^-$ expressions, and is currently undefined by molecular subtyping. BCK4 cells do not express E-cadherin protein, and the mechanism of loss is currently under investigation in our laboratory. We are also currently establishing the phenotypic and tumorigenic capacity of these cells in *in vitro* and *in vivo* studies (*experiments in progress*). Though this model was utilized throughout this dissertation as a representation of ILC, caution should be taken in interpreting results obtained from BCK4 cells as directly representing ILC. Instead, this model is more "ILC-like," and was used due to limitations in numbers of currently available ILC models.

The final ILC cell line that was obtained for limited use in this dissertation is called IPH-926, and was recently derived by Christgen and colleagues in 2009[182]. The cells were established from metastatic ascites from an originally ER^+ ILC that was refractory to Tamoxifen and

chemotherapies. After establishment, IPH-926 displayed $ER^-/PR^-/HER2^-$ expressions. Despite loss of ER and PR, IPH-926 is still classified as Luminal by molecular subtyping, suggesting that expression of luminal markers is maintained by proteins other than ER[250]. Interestingly, IPH-926 also has the lobular chromosomal gain of 8p11-p12, but does not have concomitant FGFR1 overexpression. Cells maintain a rounded morphology and double at a time of two weeks. Due to this final description, and the lack of ERα expression, these cells were utilized the least in all studies.

A few other ILC or "ILC-like" cell line models exist, and have been described, but were not employed in this dissertation. These include the ILC cell line MA-11 ($ER^-/PR^-/HER2^-$/E-$cadherin^+$), established in the 1990s from a bone marrow metastasis, and HCC-2185 ($ER^-/PR^-/HER2^+$/E-$cadherin^?$) from a pleural effusion of an ILC[251, 252]. Additional cell lines are currently under consideration for being reclassified as ILC and include previously mentioned CAMA-1 and ZR-75-30, as well as HCC-1187, MDA-MB-453, MDA-MB-468, EVSA-T, MPE600, OCUB-F, OCUB-M, SK-BR-3, and SK-BR-5[186, 239]. However, these cell lines are not currently accepted as ILC cell models, and were only recently described as "ILC-like" by Michaut and colleagues in 2016 in a supplemental figure to an ILC proteomic publication[186]. The rationales for not including these additional ILC or "ILC-like" models in the dissertation were inaccessibility (HCC-2185, discontinued by ATCC), lack of use as an $ER\alpha^+$ model (all except CAMA-1 and ZR-75-30), or lack of current acceptance as cell lines as ILC models (all except MA-11 and HCC-2185). Additionally, tissue xenografts have been established and characterized in recent reviews, but were of limited utility in the previous chapter (HCI-013, HCI-013 EI, and WHIM-9 models did not express SNAIL protein)[204, 253]. All described ILC cell lines are detailed in the table below (Table 4).

Table 4: ILC Cell Line Models and Their Basic Characteristics

Cell Line	Source	Doubling Time (Days)	ER	PR	HER2	E-cad
MDA-MB-134-VI[184, 204, 238]	Pleural Effusion	2	+	-	-	$-^{mut}$
MDA-MB-330[204, 243-245]	Pleural Effusion	7-10	+	-	+	$+^{wt}$
Sum44PE[247]	Pleural Effusion	5-7	+	-	-	$-^{mut}$
BCK4[181, 249]	Mucinous Breast Carcinoma	7	+	+	-	$-^{?}$
IPH-926[182]	Ascites	14	-	-	-	$-^{mut}$
MA-11[251]	Bone Metastasis	?	-	-	-	+
HCC2185[252]	Pleural Effusion	?	-	-	+	**?**

Abbreviations: mutant (mut), wildtype (wt), unknown (?); Cell lines in *italics* were used in this dissertation. Note: BCK4 is "ILC-like" and not derived from classical ILC.

3.1.3 Rationale for Establishment of WCRC0025-76M (WCRC-25)

A clear rationale for the subsequent work arose during the progress of this dissertation: few accepted ILC cell line models exist, and additional models of utility and proper characterization are desperately needed to push ILC research in a forward trajectory. Thus, we undertook the task to (1) establish a novel ILC cell line, (2) characterize its general phenotypes and behaviors *in vitro* and *in vivo*, (3) compare and contrast observations with currently available ILC cell lines, (4) describe drug response in targets of interest for ILC as well as became apparent by various DNA/RNA profiles, (5) provide as comprehensive a clinical and computational analyses possible, and (6) set an example for how future cell line models could be established, characterized, utilized, and distributed in a short period of time. While we do not claim to have novel approaches for every aspect of this described work, we do believe that we have combined observations, successes, failures, techniques, and hindsight to tell the story of the generous donation of human tissue samples from an ILC-afflicted patient, whose ultimate demise gave way to a model of utility in an otherwise understudied field of cancer research. The characterization of **W**omen's **C**ancer **R**esearch **C**enter WCRC0025-76M, or WCRC-25, is a culmination of the efforts of a patient,

clinicians, and researchers who all deserve credit for the work described in this chapter. I am humbled to compile these data for the first time, and look forward to the utility of WCRC-25 as a model of ILC in decades to come.

3.2 MATERIALS AND METHODS

3.2.1 Acquisition of Patient Samples

Informed patient consent was performed by trained University of Pittsburgh Cancer Institute (UPCI) staff. The sample utilized to generate the cell line was obtained from the patient "WCRC0025" or "WCRC-25" at Magee Women's Hospital remaining from an aspiration of left pleural fluid (code: 76M). The sample was processed for tissue culture four days after removal from the patient. Remaining samples were obtained and assessed by appropriate immunostaining (see 3.2.5). Staining calls were generated by certified pathologists in respective hospitals from which samples were obtained. Commentary to assist with macrodissection was supplied by certified pathologist Dr. Peter Lucas.

3.2.2 Establishment of Cell Line

Pleural fluid was obtained as previously described. Cells were plated in either standard tissue culture conditions (37°C, 5% CO_2, 21% O_2, 95% Humidity; hereafter referred to as 5% CO_2) or in low oxygen tissue culture conditions (37°C, 5% CO_2, 5% O_2, 95% Humidity; hereafter referred to as 5% O_2) in complete Conditioned Media (hereafter referred to as Conditioned Media, or "CM")

prepared by a modified Schlegel method (Figure 38)[254, 255]. Cells were initially plated in either standard 2D plates or ULA plates, with or without supplementation of Rock inhibitor (±Rocki) (Y-27632, Enzo Life Sciences#ALX-270-33-M005).

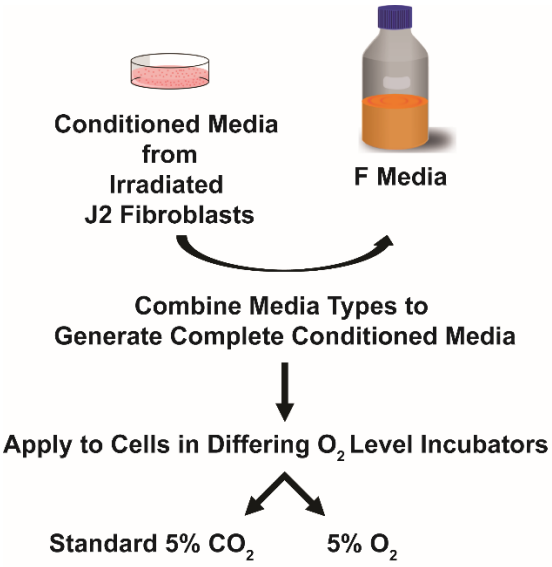

Figure 38: Modified Schlegel Method for Establishment of WCRC-25 Cell Line
Media were prepared in collaboration with Ms. Julie (Arlotti) Scott by the method shown above[254, 255]. J2 fibroblast media were stored in aliquots at -80°C until needed for culturing. Cells were established in both oxygen level environments.

3.2.3 Cell Lines Utilized

ILC cell lines utilized for comparisons to WCRC-25 were previously described in the prior chapter, and include MDA-MB-134-VI, Sum44PE, and IPH-926. IDC cell lines utilized in this chapter include previously described MCF-7, T47D, and MDA-MB-231. The non-tumorigenic human mammary epithelial cell line, MCF-10A, was used as a control for immunofluorescence studies. Also, the triple negative breast cancer cell line, BT-549, was used as a control for immunofluorescence studies (ATCC) (RPMI-1640/10% FBS). Finally, murine (BALB/c) stromal associated fibroblasts (SAFs) stably infected with sh*Scramble* or sh*PRDX1* were graciously

provided by Carola Neumann, MD, and were maintained in DMEM supplemented with 10% FBS, 5% O_2. Both cell types were used, but only sh*PRDX1* SAFs were shown imaged in the immunofluorescence, as the loss of PRDX1 has been published to lead to a cancer associated fibroblast (CAF) phenotype, with expression changes in stromal markers such as α-Smooth Muscle Actin (αSMA)[256-258]. For *in vivo* studies, WCRC-25 cells were stably infected with lentivirus containing red fluorescent protein (RFP) and luciferase, and sorted for the top 5% of highly expressing cells by Flow Cytometry by Nilgun Tasdemir, PhD. As a control for the MIND study, DCIS Sum225 cells were graciously provided by Priscilla McAuliffe, MD, PhD.

3.2.4 Immunofluorescence (IF)

IDC, SAF, or MCF-10A control cells were plated at 100,000 cells/well on autoclaved glass coverslips (Fisher#12-545-84) in 12-welled plates, and ILC cells at 300,000 cells/well. Cells were allowed to adhere for 1.5 days in respective media and incubator conditions, then media was removed, and cells were fixed in 4% final concentration paraformaldehyde (Electron Microscopy Services#15710-S) diluted in 1X DPBS for 30 minutes at room temperature. Coverslips were then stored in 1X DPBS at 4°C until use, not to exceed 1.5 weeks of storage. Coverslips were transferred to 1X DPBS moistened parafilm in large opaque boxes, and were kept moist and unexposed to light throughout the staining process. Samples were blocked in blocking buffer (0.3% Triton X-100 (Sigma#T8785-50ML), 5% BSA (Sigma-Aldrich#A9647-500G), 1X DPBS) for 30 minutes at room temperature. Blocking buffer was removed from all but the "No Primary Control" coverslips, and samples were incubated in primary antibodies at ~100-200 µL/slip for one hour at room temperature (Appendix A Table 11). Coverslips were then washed in 1X DPBS three times, and then were all incubated in respective secondary antibodies at ~100-200 µL/slip for 45 minutes at

room temperature (Appendix A Table 11). Samples were again washed in 1X DPBS three times, and then remaining liquid were carefully wicked with a KimWipe prior to application to ~15 µL DAPI Prolong Diamond (Thermo Fisher#P36962) on glass slides. Slides were stored at room temperature in a dark drawer, overnight, and then stored long-term at 4°C in a light-resistant folder. Preliminary images were obtained on the Inverted IX83 Olympus Microscope/Nikon Camera and final images were taken on a Confocal Microscope at 40X with assessment of No Primary Controls and adjustments made to the most/least expressing entities prior to taking images at the same exposure settings.

3.2.5 Clinical Sample IHC

Hematoxylin and Eosin (H&E), E-cadherin/p120, and ERα staining was performed within the University of Pittsburgh Medical Center hospital system. Slides were deparaffinized at 72^0C and conditioned by ULTRA cell conditioner process. Then, slides were incubated with E-cadherin antibody, ultra-blocked, and denatured at 80^0C. Dual staining was performed by incubating slides with p120 antibody, then counterstaining with hematoxylin, and completing by addition of a coverslip. A similar process was performed for ERα, but without dual staining. Antibodies used can be found in Appendix A Table 12.

3.2.6 IB

Immunoblotting was performed as previously described in the prior chapter by the RIPA/SDS Protocol. Antibodies and concentrations used can be found in Appendix A Table 6.

3.2.7 FFPE Generation and E-cadherin/p120 IHC

WCRC-25 cells were cultured in CM-Rocki or DMEM/10% FBS, 5% O_2 until P17. Cells were grown to ~90% confluence in 15 cm^2 dishes, and samples were processed as previously described (see 2.2.15). The Magee-Womens Research Institute Histology and Microimaging Core facility embedded, cut, and stained samples for E-cadherin/p120 (see 3.2.5). Images were obtained on a bright field microscope at 20X magnification. Unstained sections were used for isolation of mRNA/DNA to control for FFPE degradation of nucleic acids.

3.2.8 E2/SERM/SERD Response Assays

Estrogen deprivation assays were performed as previously described (see 2.2.2). mRNA studies utilized 1 nM E2, 1 µM 4OHT, or 1 µM ICI. Vehicle conditions were matched when required in experiments performed. Downstream assessment of mRNA expression was performed after 24 hours of treatment, as previously described, with 500 ng of converted mRNA per triplicate sample. qRT-PCR primers used can be found in Appendix A Table 5. Dose responses were performed with 5,000, 10,000, or 15,000 cells/well in CM-Rocki, 5% O_2 in 2D 96 welled plates containing 6 technical replicates per dose E_2 given. One plate was also assessed with 15,000 cells/well in CM-Rocki, 5% CO_2. Plates were collected at D_7 and measured by Hoechst Fluorescence with correction and normalization as previously described (see 2.2.3).

3.2.9 Sequencing for *CDH1*/CDH1 Mutation

mRNA was converted into cDNA using standard protocol previously described, and then *CDH1* primers were supplemented to products and sent to Genewiz for Sanger Sequencing (primers are listed in Appendix A). Genomic DNA (gDNA) were isolated from WCRC-25 cells using the DNeasy Blood & Tissue Kit manufacturer's protocol (Qiagen#69506). gDNA were amplified by PCR using the primer set surrounding Exon 13, listed in Appendix A Table 13. Amplified products were run on a 1% agarose gel by standard gel electrophoresis, and the band of interest was excised and purified using the QIAquick Gel Extraction Kit manufacturer's protocol (Qiagen#28706), followed by concentration of product using the DNA Clean & Concentrator™-5 Kit manufacturer's protocol (Zymo Research#D4014). Samples were sent to Genewiz for Sanger Sequencing (WCRC-25 Mutant Forward Primer: GAAGCCAAAGATGGCCTTAGA; WCRC-25 Mutant Reverse Primer: GGCATAACTTGGGAGTCTCTTT).

3.2.10 Circulating Free DNA (cfDNA) Isolation and Droplet Digital Polymerase Chain Reaction (ddPCR)

cfDNA were isolated in collaboration with Ahmed Basudan, BS and Karthik Kota, MD. The ddPCR probe was custom-generated through Thermo Fisher Scientific. Blood samples were obtained through patient consent at Magee Women's Hospital. Sterile isolation was performed in a circulation-free environment with Qiagen QIAamp Circulating Nucleic Acid Kit (Qiagen#55114) using LoBind/PCR clean Eppendorf Tubes and Filter Tips, only (Eppendorf). Plasma samples were first centrifuged at 1,500 rpm for 5 minutes to pellet any potential debris, and clear supernatant were kept for cfDNA isolation. Supernatant were combined with 10% (of original

plasma volume) volume Qiagen Proteinase K (Qiagen#19131), followed by 80% (of original plasma volume) volume Buffer ACL. Samples were pulse-vortexed for 30 seconds, or until a homogenous solution formed. Samples were then incubated at 60°C in a water bath for 30 minutes. After incubation, 180% (of original plasma volume) volume Buffer ACB were combined with the samples, followed by pulse-vortexing for 30 seconds, and incubation on ice for 5 minutes. Samples were then applied to a QIAamp Mini column vacuum system. Buffer ACW1 (600 µL), Buffer ACW2 (750 µL), and 100% Ethanol (750 µL) were then passed through the vacuum in sequential order. The columns were then centrifuged at 14,000 rpm at room temperature for 3 minutes in collection tubes to remove residual Ethanol. The columns were then transferred to new collection tubes with incubation at 56°C for 10 minutes to dry the membrane completely. Columns were finally transferred to final collection tubes and cfDNA were eluted in 25 µL volumes of Buffer TE after incubation at room temperature for 3 minute and centrifugation at 14,000 rpm for 1 minute. Samples were always eluted this way, twice, with the same 25 µL of original flow through to maximize yield. cfDNA were quantified by Qubit High Sensitivity dsDNA measurement (Qubit#Q32871) with 1 µL sample volume. cfDNA were measured by ddPCR using a probe for the *CDH1* Q706* mutation, ordered through Life Technologies (see Appendix C) on the BioRaad QX100 ddPCR System. 4 to 10 ng of unamplified or target amplified cfDNA, WCRC-25 DNA, or non-template control (NTC; quality control) were mixed with 1X final concentration ddPCR Supermix (BioRad#1863024) and 1X final concentration probe with remaining volume in Nuclease Free Water to 26 µL total volume. Droplets were generated using 20 µL of reaction mixture and 70 µL droplet generation oil. The cell line served as a positive control for the mutation, and the Buffy Coat from the patient samples served as the negative control. Samples were assayed in single replicates, with minimum 10,000 genome equivalents measured.

3.2.11 Population Doubling Assessment

Immediately after sufficient WCRC-25 cells were available for use from the established CM-Rocki, 5% O_2 environment, cells were split into four conditions for assessment of population doubling (5% O_2 or 5% CO_2; CM-Rocki or DMEM/10% FBS). After minimum two passages in these environments, population doubling was measured by plating cells at three differing densities (5,000, 10,000, or 15,000 cells/well) in six replicate wells of 2D 96 welled plates. This was performed at passages (P) P3, P5, and P7. For the first doubling assessment at P3, multiple plates were collected from D_0, D_3, D_7, D_{10}, and D_{14} time points, but subsequent data only included D_0 and D_7.

Calculations for population doubling were performed as follows:

$$Doubling\ Time\ in\ days = \frac{duration\ of\ assay\ in\ days * \log(2)}{\log(Final\ Timepoint\ Value) - \log(Initial\ Timepoint\ Value)}$$

3.2.12 Proliferation and Soft Agar Anchorage Independent Assays

2D and Soft Agar Anchorage Independent Assays were performed as described in the prior chapter (see 2.2.9 and 2.2.16, respectively). Both incubator settings (5% O_2 and 5% CO_2) were used as described in the appropriate figure legend.

3.2.13 RNA Sequencing

Samples were prepared and analyzed in collaboration with Ahmed Basudan, BS. FFPE samples with pathologist-directed marodissection notes were isolated for RNA and DNA simultaneously using manufacturer's protocol of the AllPrep DNA/RNA FFPE Kit (Qiagen$^{\#}$80234). RNA

concentration was determined with the Qubit. DV_{200} metrics were performed using the Agilent 4200 TapeStation. Exome-capture RNA-sequencing was performed at the Health Sciences Sequencing Core at Children's Hospital (Pittsburgh, PA) using 25 ng or more RNA in Illumina's TruSeq RNA Access Library with sequencing 40-50 million reads per sample on the Illumina NextSeq 500 platform with High Output flow cell (2 x 75, stranded, paired-end reads). FASTQ files were mapped and quantified with k-mer based lightweight-alignment with seqBias and gcBias corrections (Salmon v0.8, quasimapping mode, 31-kmer index built from GRCh38 Ensembl v82 transcriptome annotations). Tximport255 was used to collapse gene-level estimates from transcript-level abundance, and log2 transformed TMM-normalized CPM (log2normCPM) values were utilized for outputs.

3.2.14 Dose Responses for Chemotherapeutics of Interest

Dose responses were performed as previously described (see 2.2.3) in 2D or ULA 96 welled plates with a control breast cancer cell line with known response (from nM to mM potency) or WCRC-25. Cells were plated at 5,000 cells/well if IDC, 15,000 cells/well if ILC other than WCRC-25, and 10,000 cells/well if WCRC-25. Doxorubicin Hydrochloride (Fisher#D1515), Cisplatin (Selleckchem#S1166), and Paclitaxel (Sigma-Aldrich#T7402-5MG) were dissolved in DMSO. NVP-BEZ235 (BEZ235; Selleckchem#S1009) was dissolved in Dimethylformamide (DMF; Fisher). Plates were collected at D_5 and measured by Hoechst Fluorescence or CellTiter-Glo, as previously described, with corrections and normalization as previously performed (see 2.2.9).

3.2.15 *In Vivo* Studies

All mice used were female. Collaborative efforts were undertaken to perform initial injections of cells: WCRC-25 RFP cells were injected by Mr. Weizhou Hou into the tail veins (TVs) of n = 6 NU/J (nude), 6-week old mice (Jackson Laboratories, Stock#002019), by Ms. Julie (Arlotti) Scott into the mammary fat pads (MFPs) of n = 8 NOD.Cg-Prkdc^{scid} Il2rg$^{tm1Wjl/SzJ}$ (NSG), 6-week old mice (Jackson Laboratories, Stock#005557), or by Daniel Brown, PhD by MIND injection into the fourth and fifth, left and right inguinal nipples of n = 8 NSG, 12-week old mice (Jackson Laboratories, Stock#005557). One control NSG mouse was simultaneously injected with DCIS control cell line Sum225. Due to lack of ERα expression and response, animals were not initially given E2 pellets. TV and MFP mice were housed at the Hillman Cancer Center Animal Facility, and MIND mice were housed at the MWRI Animal Facility. TV and MFP animals were imaged by luciferin injection (Gold Bio#LUCK-1G) of 100 µL/mouse with imaging performed on an IVIS 200 (Xenogen) after 5 minutes of anesthetization and circulation of luciferin. Imaging was performed immediately after respective injections on auto exposure, the subsequent week at 60 seconds exposure, and then on a biweekly basis until palpable tumors formed. Imaging was quantified by measuring luciferase intensity in regions of interest (ROIs). Animal studies are currently ongoing, and will be completed after the publication of this dissertation. Preliminary outcomes and experimental descriptions are provided within this chapter for discussion purposes.

3.2.16 Statistics

Statistics were performed as described in the previous chapter, and are described beneath respective experiments for clarification (see 2.2.18).

3.3 RESULTS

WCRC-25 cells were established from the ERα$^-$ pleural effusion of a 76-year old Caucasian woman afflicted with ER$^+$ ILC.

3.3.1 Patient WCRC-25 Had a Complex Clinical History

Patient WCRC-25 was a postmenopausal, Caucasian woman, admitted to the hospital with complaints of gastric discomfort. Initial biopsies were taken from the stomach and duodenum, revealing poorly-differentiated adenocarcinoma with signet ring features. Routine mammography had been performed merely weeks prior to this visit, with notations of the presence of dense breast and some scattered calcifications, assessed to be benign. The patient returned to the hospital for an additional biopsy of the gastroesophageal junction, which revealed the same pattern of carcinoma. A short period later, the patient was readmitted to have an aspirate of pleural fluid and biopsy of falciform ligament obtained. The diagnoses for these lesions were all stated to be gastric carcinoma, and the patient was subsequently treated with Folinic Acid, Fluorouracil, and Oxaliplatin (FOLFOX), a common chemotherapeutic for gastric cancers[259]. WCRC-25 continued FOLFOX for approximately 5 months until the appearance of peritoneal lesions, which were diagnosed to be consistent with the gastric carcinoma. The chemotherapy regimen was thus altered to a combination of Carboplatin and Paclitaxel, additional accepted therapies for advanced, pre-treated gastric carcinoma[260].

Approximately two weeks into the combined treatment regimen, the patient noted concern over changes in her right breast. A routine breast exam performed revealed central retraction, nipple and areola distortion with crusting, and a large palpable mass. No obvious abnormalities or

palpable masses were noted in the left breast, and no palpable lymph nodes were felt on either side. A bilateral mammogram and ultrasound were performed shortly thereafter.

Upon examination, the bilateral mammogram revealed a large mass in the central portion of the right breast and associated calcifications. In addition, the left breast had a heterogeneous breast tissue appearance with scattered calcifications, again assessed to be benign. The ultrasound that was performed next confirmed the presence of the large right mass, and did not reveal any additional lesions on this side or in the axilla. However, the left breast had hyperechoic regions in two portions, and no associated adenopathy. A final bilateral tomosynthesis was utilized to confirm the findings of the initial mammogram and ultrasound. Thus, WCRC-25 was subjected to core needle biopsies; one in the right breast, and one of the two regions in the left breast. Staining of these core biopsies confirmed $ER^{+}/PR^{-}/HER2^{-}/Ki67^{moderate}/E\text{-}cadherin^{-}$ status. It was at this point that the patient was diagnosed with ILC in both breasts. Retrospective immunohistochemistry was performed on the available original lesions, and these were diagnosed as metastatic ILC lesions showing ER expression.

As WCRC-25 had ER^{+} ILC, and was postmenopausal, the treatment course was altered to Anastrazole in combination with Fulvestrant. An addition of Denosumab was given shortly into this endocrine regimen, to offset the negative impacts of bone loss and osteoporosis that afflict patients undergoing AI therapy, and to prevent or control potential bone metastases[261, 262]. Amidst this treatment course, the region that had not been biopsied originally in the left breast was then checked by core biopsy for presence of carcinoma. Staining of this potential unique primary or local recurrence revealed the presence of $ER^{-}/PR^{-}/HER2^{-}$ ILC cells. This observation prompted the examination of left sentinel nodes, which were positive for metastatic carcinoma. This informed the decision to perform bilateral mastectomies. The right breast lesion and both left breast lesions

were confirmed to be of the same receptor status and diagnoses given to prior core biopsies. WCRC-25 remained on endocrine treatments, and stopped Fulvestrant treatment abruptly (16.3 months total treatment time) prior to the removal of left pleural fluid aspirate. This sample was confirmed to be metastatic ILC, $ER^-/PR^-/HER2^-/Ki67^{high}$, and remaining sample was given to our laboratory for generation of the subsequently described cell line.

Treatment was again altered for the patient to include Pegylated Liposomal Doxorubicin in combination with Anastrazole and Denosumab. Two additional pleural fluid aspirates were taken, one of which was confirmed by pathology records to be $ER^-/PR^-/E\text{-cadherin}^-$. Doxorubicin was stopped, and small biopsies from the stomach and gastroesophageal junction revealed the presence of minimal carcinoma with ER expression. The patient then stopped Anastrazole treatment and was immediately put on Exemestane. Shortly after, more pleural fluid ($ER^-/PR^-/HER2^-$) was aspirated, prompting the addition of Gemcitabine to the treatment. Skin biopsies, further pleural fluid aspirates, and pericardial fluid aspirates taken during this time period were also determined to be ER^- breast cancer metastases. Gemcitabine was then switched to Eribulin, still in conjunction with the Exemestane and Denosumab. During the Gemcitabine and Eribulin treatments, four blood draws were taken over a 4-month period; three were from the Gemcitabine treatment and one during the Eribulin. These were promptly processed for isolation of cfDNA in our laboratory, and will be described in a later section of this chapter. Pleural fluid aspirates and peritoneal fluid aspirates continued to persist until the patient's death. This complex clinical course and clinical sample collection is detailed in Figure 39 (sample numbers included in similar version in Appendix C Figure 89), with sample images and associated IHC in Figure 40-44, and an overview of staining in Appendix C Table 16.

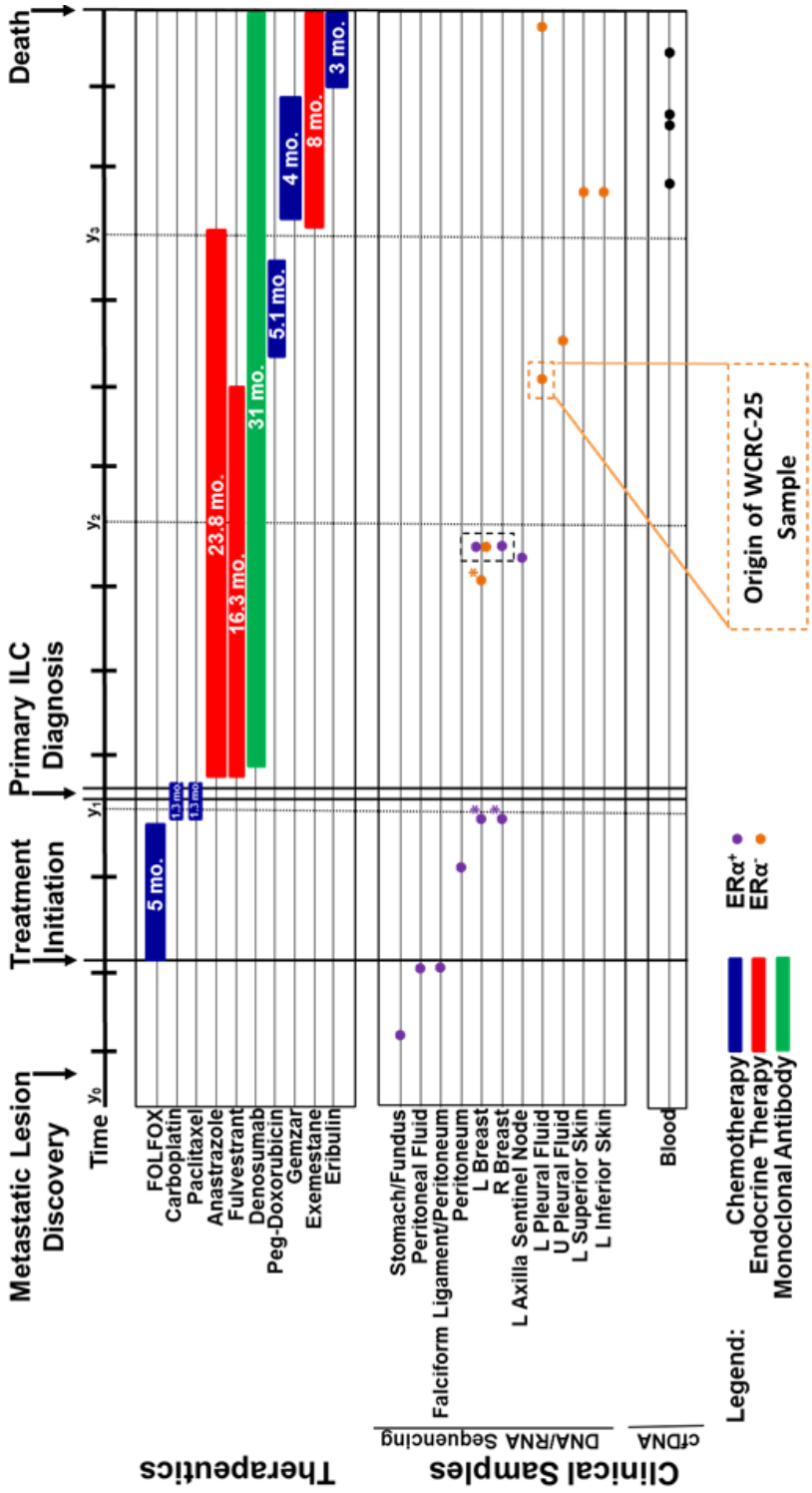

Figure 39: WCRC-25 Patient Clinical and Sample Acquisition Timeline
A compressed timeline (not to scale) of the WCRC-25 patient's clinical course is detailed above. De-identified clinical information was provided by Karthik Kota, MD. Samples pertinent to this project were listed. Asterisks (*) denote samples taken during biopsy. Dashed boxes around the breast samples indicate the time of double mastectomy. The figure was rotated for ease of visualization.

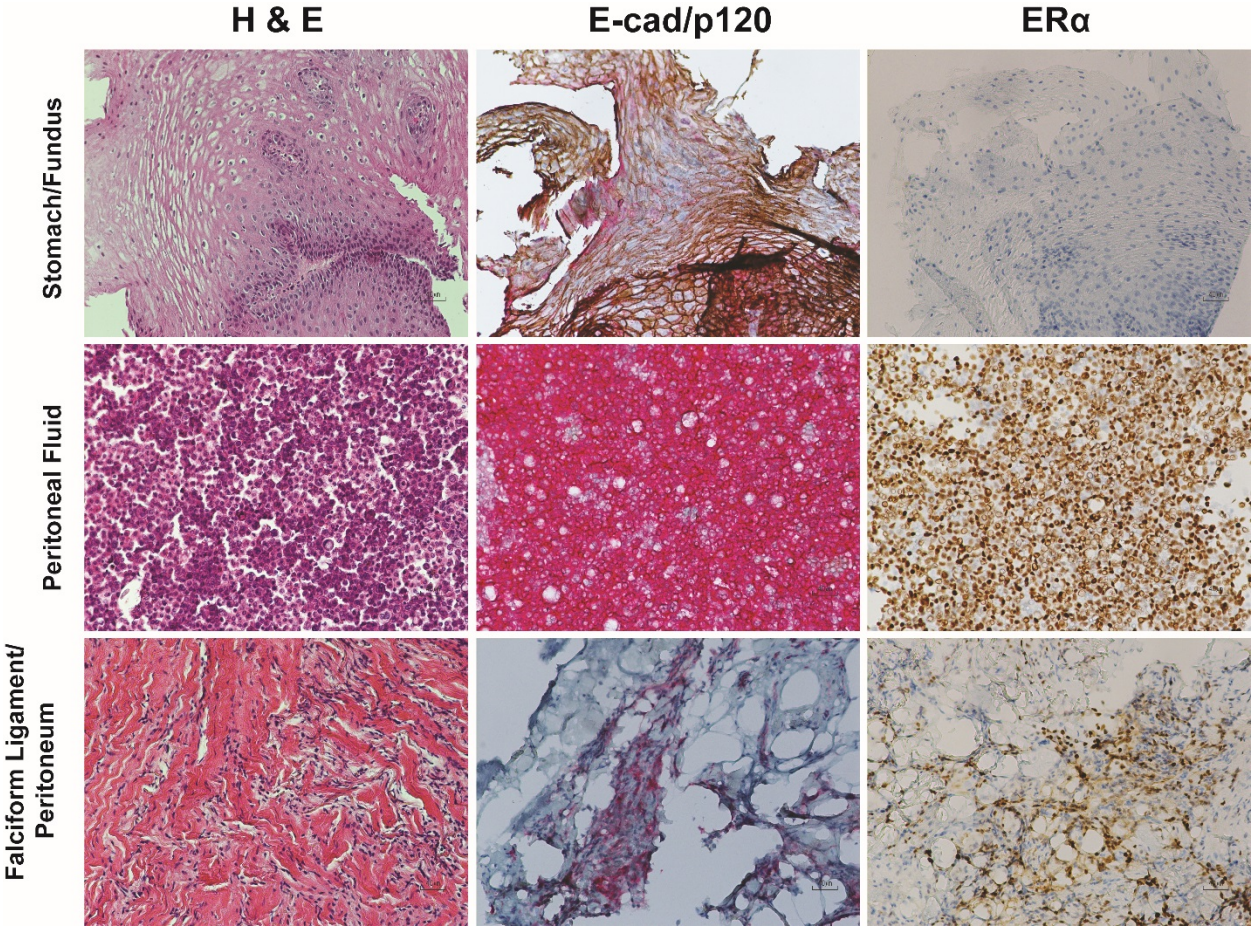

Figure 40: IHC from Therapy Naïve Samples from WCRC-25 Patient
IHC including H & E, E-cadherin/p120, and ERα staining was performed on WCRC-25 patient samples. Above are 20X magnification, bright field images from the therapy naïve samples taken when the patient was diagnosed with gastric carcinoma.

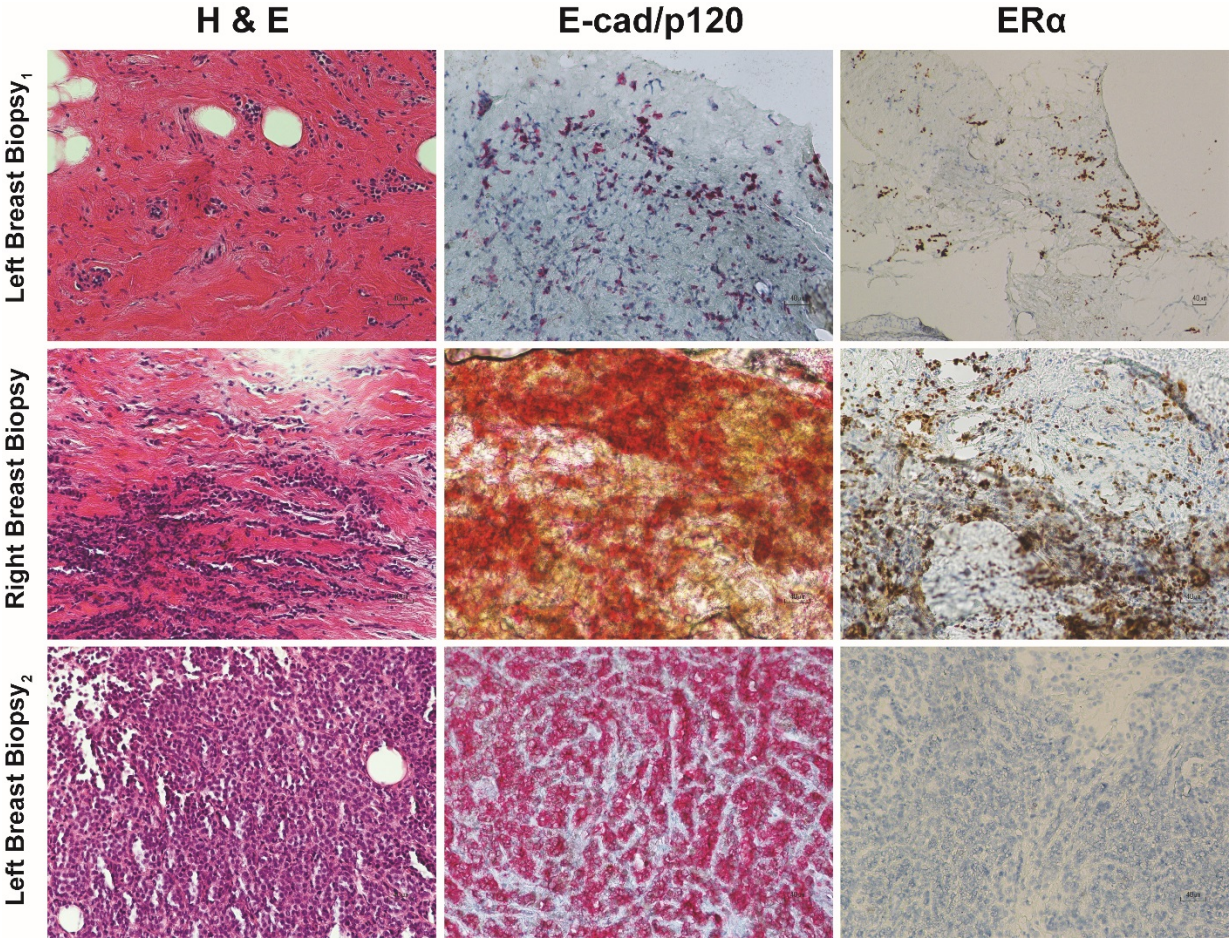

Figure 41: IHC from Breast Biopsy Samples from WCRC-25 Patient
IHC including H & E, E-cadherin/p120, and ERα staining was performed on WCRC-25 patient samples. Above are 20X magnification, bright field images from the chemotherapy treated (Left $Biopsy_1$, Right) and endocrine therapy treated (Left $Biopsy_2$) samples. It should be noted the E-cad/p120 staining for Right Biopsy was of poor quality.

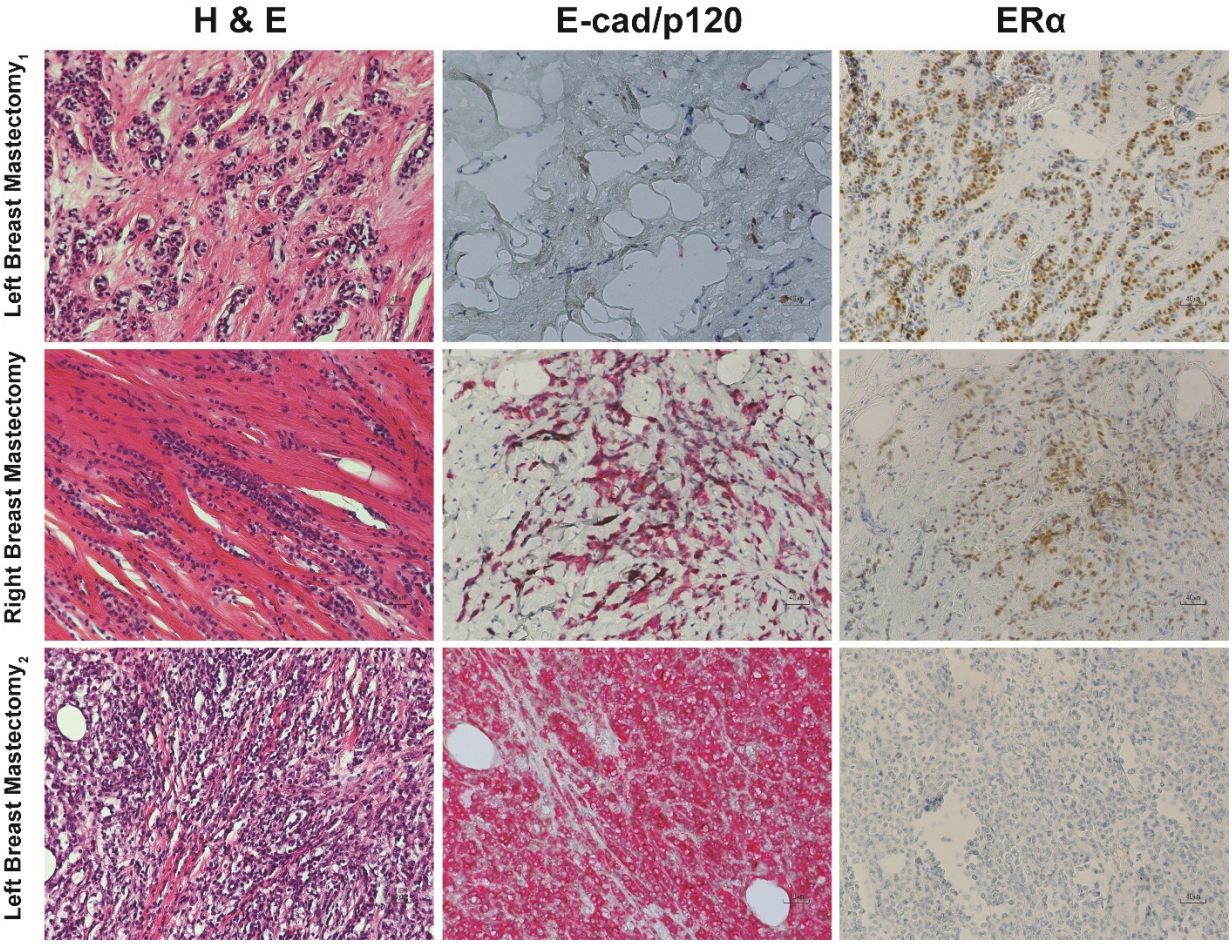

Figure 42: Double Breast Mastectomy IHC for WCRC-25 Patient
IHC including H & E, E-cadherin/p120, and ERα staining was performed on WCRC-25 patient samples. Above are 20X magnification, bright field images from the chemotherapy and endocrine therapy treated left and right double mastectomy samples. The Left $Mastectomy_1$ and Left $Mastectomy_2$ coordinate with the positions of appropriately numbered biopsies. Left $Mastectomy_1$ had few tumor cells in the slide stained.

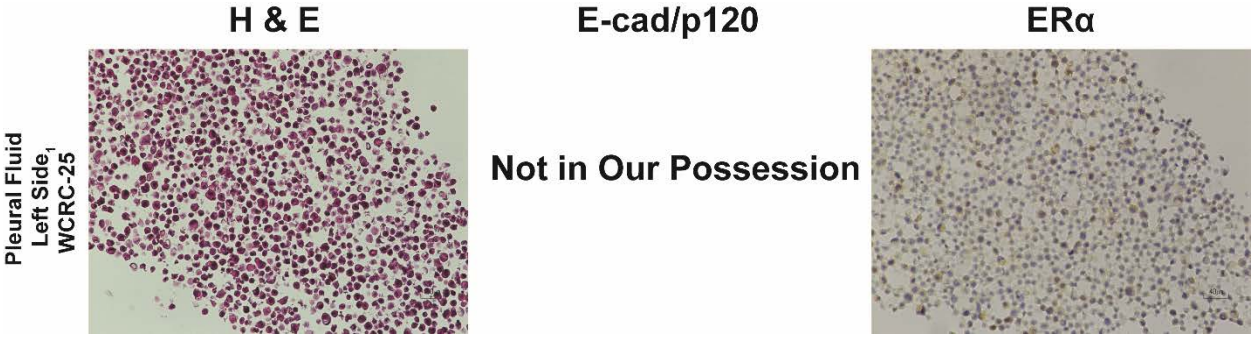

Figure 43: IHC from WCRC-25 Cell Line Sample of Origin

IHC including H & E and ERα staining was performed on WCRC-25 patient samples. E-cad/p120 was not performed for this sample. Above are 20X magnification, bright field images from the chemotherapy and endocrine therapy treated Pleural Fluid Left $Side_1$ sample, the same sample that was used to establish the WCRC-25 cell line.

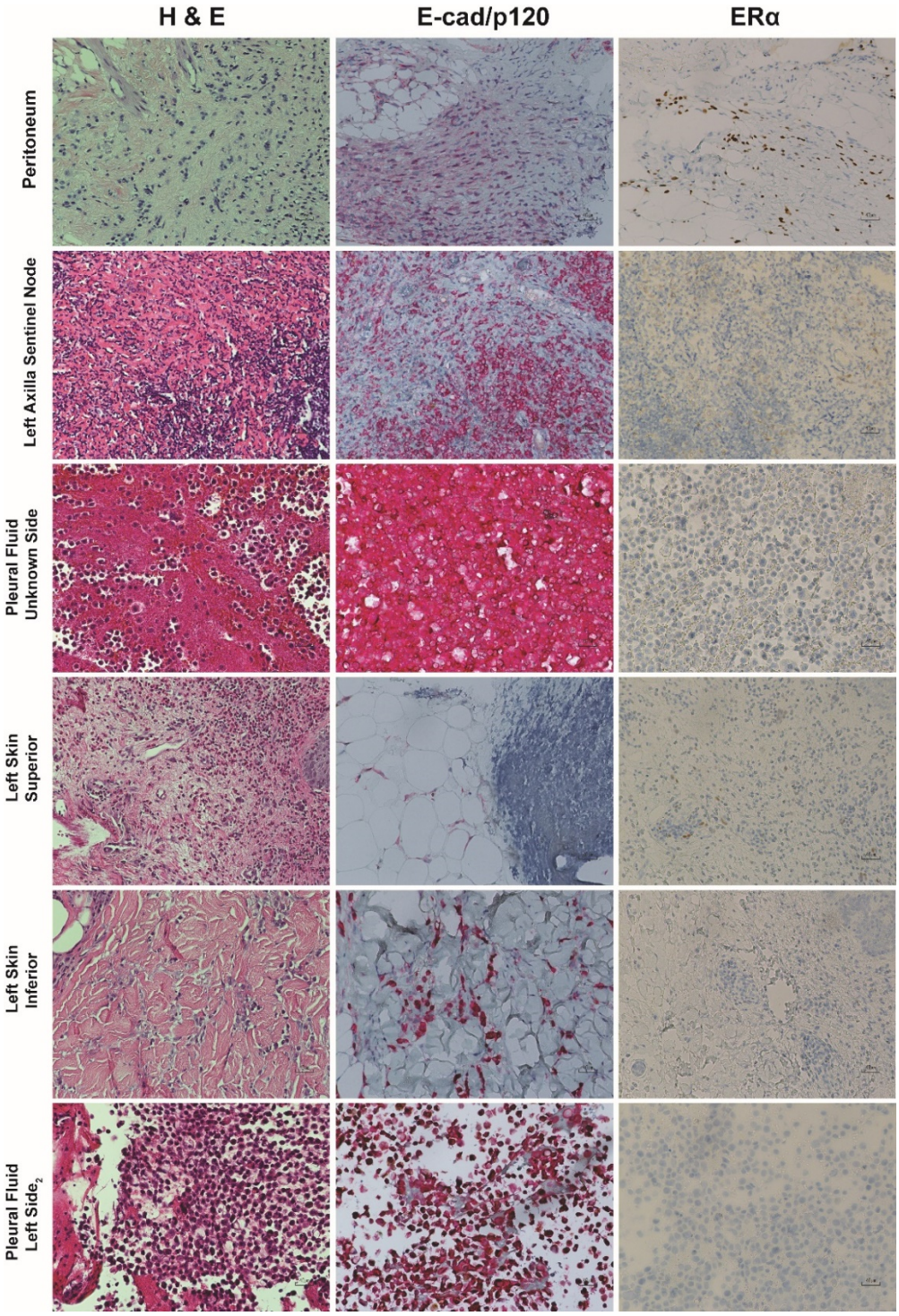

Figure 44: IHC from All Chemotherapy or Endocrine Therapy Treated Metastatic Lesions, Except WCRC-25 Cell Line Origin Sample

IHC including H & E, E-cadherin/p120, and ERα staining was performed on WCRC-25 patient samples. Above are 20X magnification, bright field images from the chemotherapy (Peritoneum) and endocrine therapy treated (all other) samples. Samples are in chronological order of resection from the patient. The Pleural Fluid Left $Side_2$ was the last sample acquired from the patient prior to death that is in our possession.

3.3.2 Establishment of WCRC-25 Cell Line from Patient Sample

As described in the methods section, a left pleural effusion sample aspirate was obtained in our laboratory and processed for tissue culture establishment. Evaluation of FFPE sample was immediately performed, and revealed ERα$^-$ status, as previously described (see Figure 43). Cells plated in the ULA plates in CM±Rocki at 5% CO_2 had zero viability, but those in the 5% O_2 incubator had some viability. A later attempt to resuscitate the ULA CM-Rocki 5% O_2 cells was performed, and though cells were kept in culture for a few months, viability was determined to be very low by Trypan Blue exclusion, and cells were frozen down for liquid nitrogen storage. Unfortunately, due to a malfunction in the liquid nitrogen tank where these ULA CM-Rocki 5% O_2 cells were being stored, the cells were lost, and cannot be replaced. However, the vial of ULA CM+Rocki 5% O_2 remains in an alternative storage location, and may be used in the future should an attempt to expand these cells be deemed necessary.

Attempts to establish the WCRC-25 cell line in the 2D plates was successful. Cells adhered to plates in all conditions, and showed the most viability in the 5% O_2 CM-Rocki condition. Cells were partitioned from the 5% O_2 CM-Rocki condition into an additional media condition of DMEM supplemented with 10% FBS, in either incubator setting, and were cultured for all downstream studies from P3. Phase contrast images revealed a similar morphology for these cells in all conditions, with less viability noted in the CM-Rocki 5% CO_2 environment (Figure 45). In addition, these cells appear larger than other ILC cells, such as MDA-MB-134-VI, BCK4, or IPH-926, and have a less rounded morphology with faster adherence to 2D plates compared to MDA-MB-134-VI or Sum44PE.

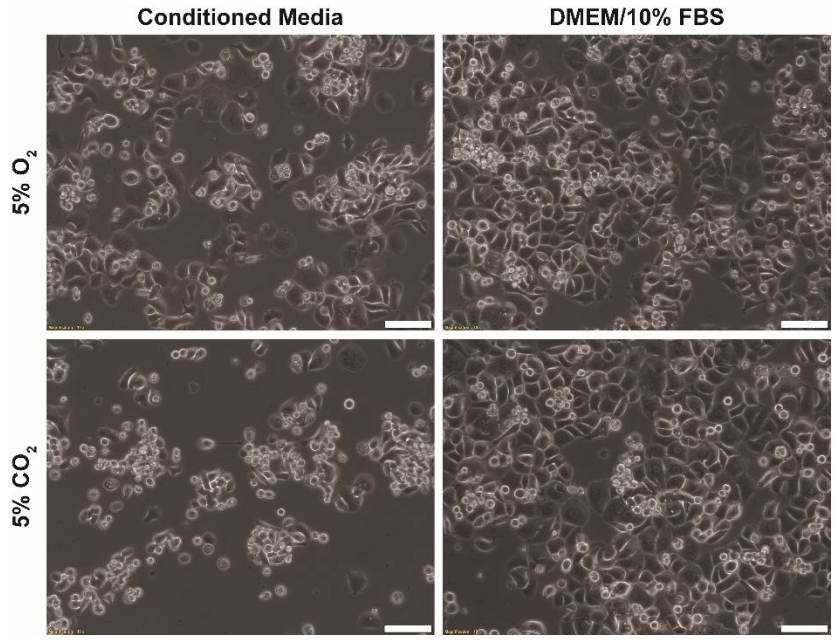

Figure 45: Established WCRC-25 Cell Line in Differing Culture Conditions
WCRC-25 cells were established in the Conditioned Media (CM)-Rocki media, 5% O_2 incubator (top left). Cells were then distributed four ways: CM-Rocki versus DMEM/10% FBS, and 5% O_2 versus 5% CO_2. Cells were imaged under phase contrast at P11 (10X magnification; bars represent 100 μm).

3.3.3 Expression of Epithelial/Stromal Markers in WCRC-25

WCRC-25 cells cultured in CM-Rocki 5% O_2 were assessed for expression of a panel of epithelial and stromal markers to characterize basic luminal/basal marker expression and to exclude these cells from the stromal compartment. WCRC-25 cells expressed high levels of epithelial luminal markers CK8/18 and epithelial marker EpCAM, as did IDC cell line MCF-7 and ILC cell line MDA-MB-134-VI (Figure 46). EpCAM was noted to be "patchy positive" upon examination of the original pleural effusion sample tested in clinic, per retrospective pathology report analyses. The cell line staining suggests a potential enhancement for this expression through the short-term culturing that had occurred, perhaps by outgrowth of the epithelial cells as opposed to any contaminating stromal or immune cells[263]. Further, lack of expression of the most commonly cited fibroblast marker αSMA in WCRC-25 confirmed the presence of epithelial as opposed to

stromal cells in the continued cultures. Lack of αSMA expression in WCRC-25 was also confirmed by IB (Appendix C Figure 90).

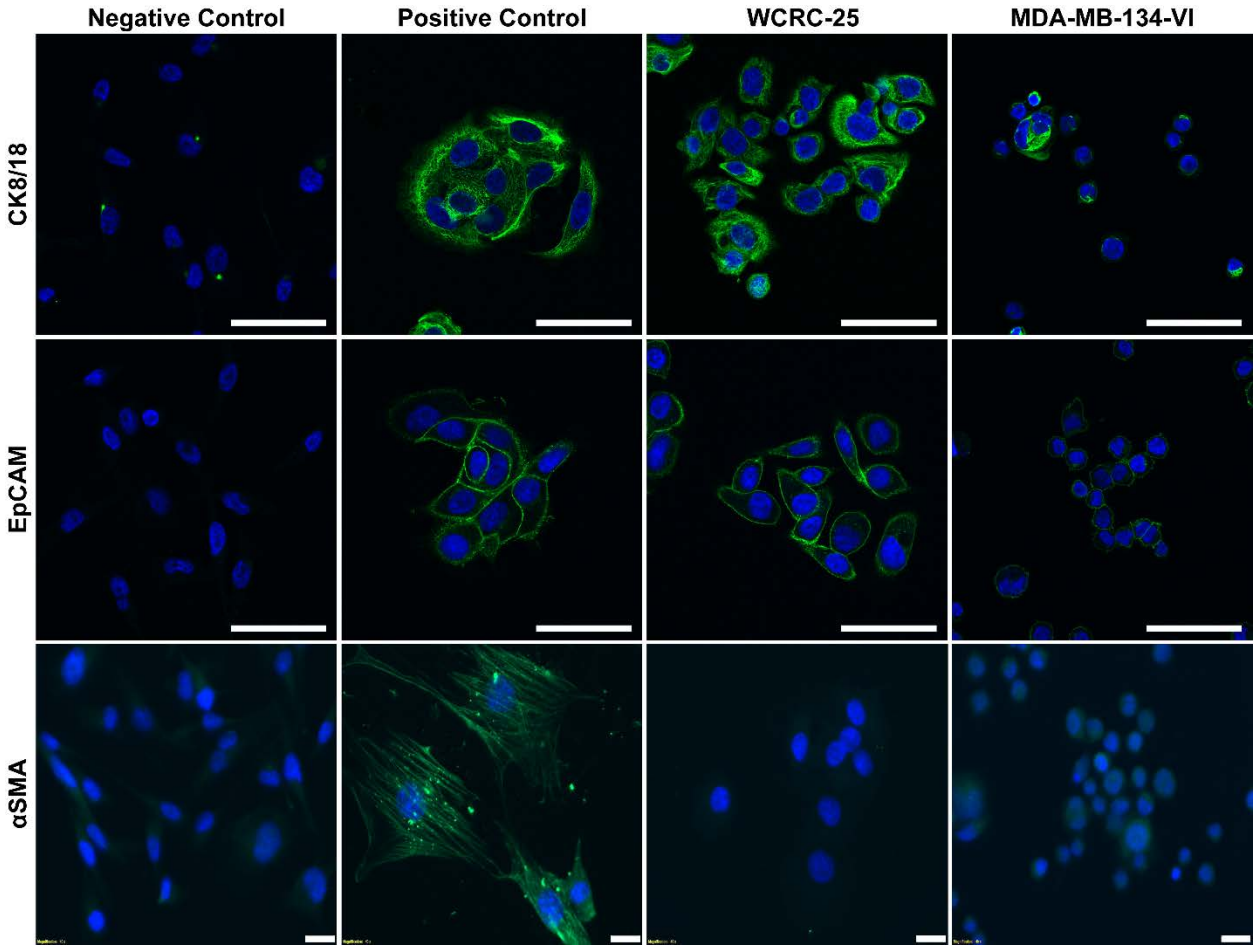

Figure 46: WCRC-25 Cells Express Epithelial, Not Stromal Markers
WCRC-25 cells and appropriate negative (CK8/18, EpCAM, and αSMA: MDA-MB-231) and positive (CK8/18 and EpCAM: MCF-7; αSMA: sh*PRDX1*) controls were stained for epithelial markers CK8/18, EpCAM, and stromal marker αSMA. Images were taken on a confocal microscope at 40X (CK8/18, EpCAM) or an inverted fluorescent microscope (αSMA) at 40X magnification. Bars in confocal images represent 100 µm and in inverted images represent 20 µm.

IF was then performed for E-cadherin and ERα in WCRC-25. Punctate, cytoplasmic E-cadherin staining was observed in WCRC-25, much like MDA-MB-134-VI, and unlike the cell

membrane localized E-cadherin visualized in MCF-7 cells (Figure 47). Though highly vibrant puncta were observed in the ILC cells, little concern was felt. This is because punctate E-cadherin staining has previously been visualized in ILCs, sometimes called a “beaded” staining pattern by pathologists[75, 173, 264, 265]. ERα expression appeared only as a haze across the entire cell for WCRC-25, as observed in negative control cell line MDA-MB-231. Positive nuclear ERα staining was confirmed in control cell line MCF-7 and ILC cell line MDA-MB-134-VI.

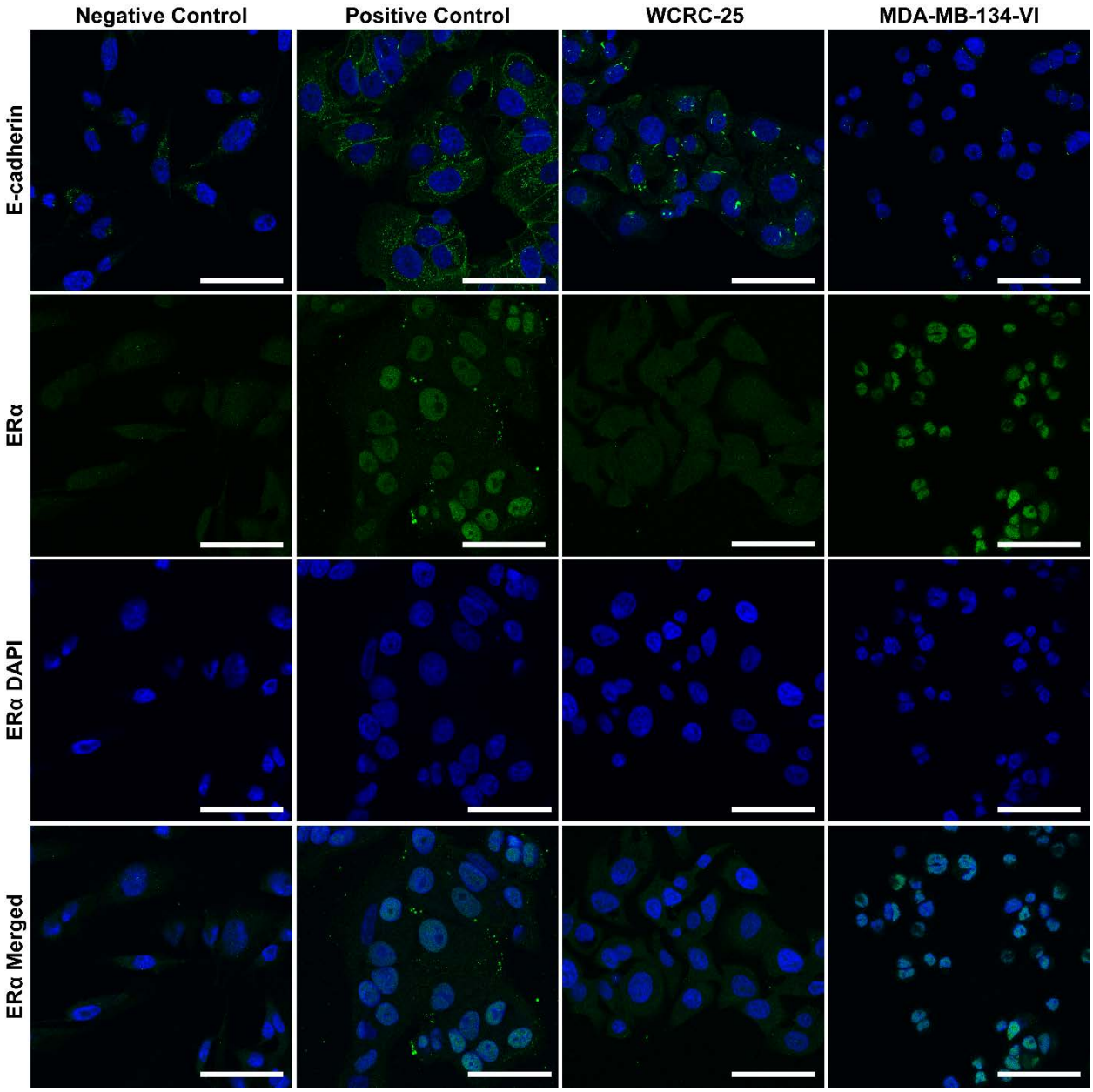

Figure 47: E-cadherin and ERα Are Not Expressed in WCRC-25 Cells
WCRC-25 cells and appropriate negative (E-cadherin and ERα: MDA-MB-231) and positive (E-cadherin and ERα: MCF-7) controls were stained for E-cadherin and ERα. Images were taken on a confocal microscope (40X magnification; bars represent 100 µm).

E-cadherin was confirmed to not be expressed at the protein level in both WCRC-25 and MDA-MB-134-VI by IB and in WCRC-25 by IHC, with characteristic cytoplasmic p120 staining observed in IHC (Figure 48A, B). ERα was also confirmed to not be expressed at the protein level

in WCRC-25 by IB (Figure 48A). Together, these data confirmed the lack of E-cadherin and ERα expression in WCRC-25.

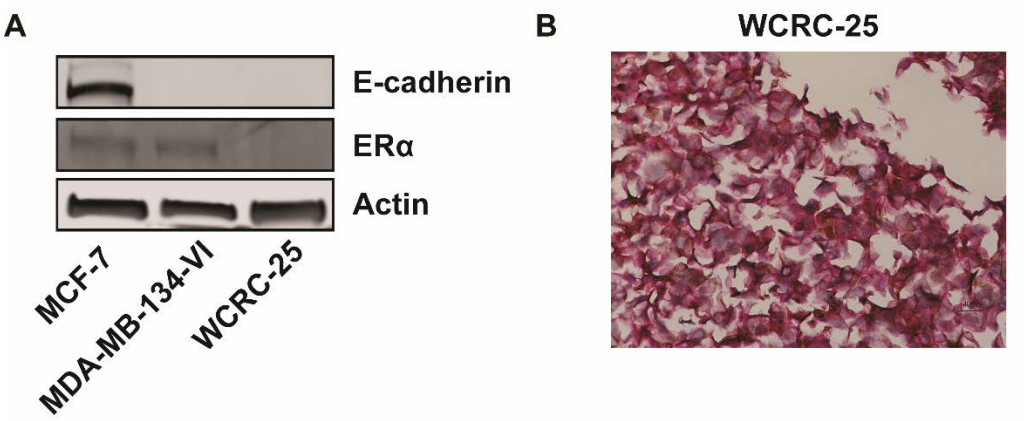

Figure 48: E-cadherin and ERα Are Not Expressed at the Protein Level in WCRC-25
(A) E-cadherin, ERα, and internal control Actin were probed by IB in WCRC-25 cells beside control cell lines MCF-7 (E-cadherin$^+$, ERα$^+$) and MDA-MB-134-VI (E-cadherin$^-$). IB is representative of three independently performed experiments. (B) IHC was performed on FFPE WCRC-25 cell pellet for E-cadherin/p120. Image was taken at 20X magnification under bright field microscopy.

As WCRC-25 appeared to have more basal expression characteristics, two basal markers that have been classically associated with poor prognosis were also assessed by IF: CK5 and CK14[266]. WCRC-25 did not express CK5, but did express CK14 (Figure 49). Interestingly, a recent study has indicated the existence of a basal subtype of ILC tumors that express CK5/6; this study did not measure CK14 in this basal subtype of ILC tumors, so it is possible that CK14 could also be a marker for this subset of ILCs[267, 268]. MDA-MB-134-VI, a noted luminal cell line, expressed CK14. This observation may be explained by identification of a basal marker-expressing (CK5, CK14, EGFR) subset of luminal tumors with ER$^+$/HER2$^-$ status[269]. This unique subtype

has been preliminarily described to have better prognosis than other subtypes, such as TNBC, that express basal markers.

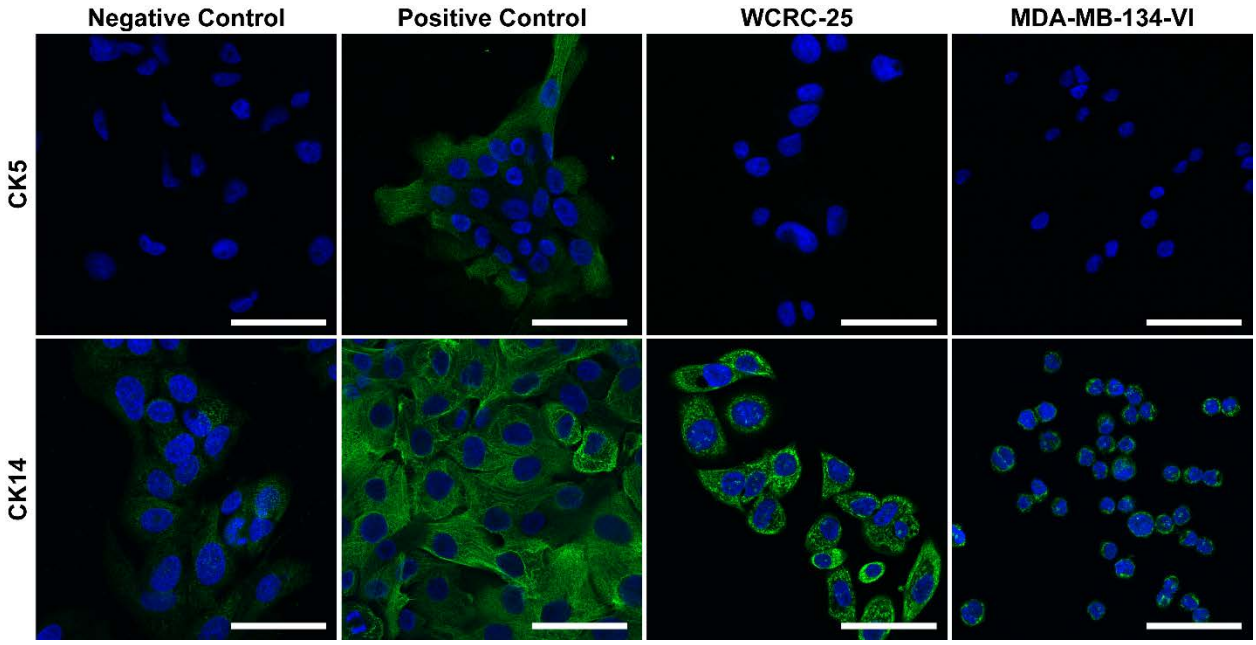

Figure 49: CK14, But Not CK5, Is Expressed in WCRC-25
WCRC-25 cells and appropriate negative (CK5: MDA-MB-231; CK14: MCF-7) and positive (CK5 and CK14: MCF-10A) controls were stained for basal markers CK5 and CK14. Images were taken on a confocal microscope (40X magnification; bars in confocal images represent 100 μm).

Overall, we identified the expression of epithelial markers (CK8/18, EpCAM), a basal marker (CK14), and the lack of ERα, E-cadherin, CK5, or stromal marker αSMA in WCRC-25. We thus concluded from these data that WCRC-25 is an epithelial ILC cell line with loss of expression of characteristically expressed ERα and potential basal characteristics.

3.3.4 A Continued Elaboration on ERα Function in WCRC-25

Though ERα did not appear to be expressed at the protein level by IF or IB, the original pleural effusion FFPE IHC we had in our possession had suggested potential low levels of ERα expression (see Figure 43). To assess if there was still some small residual amount of ERα left in WCRC-25 that was difficult to visualize by IF or IB, we first performed qRT-PCR for *ESR1* with WCRC-25, MDA-MB-231 (negative control), and MCF-7 (positive control) cells. We observed significantly higher *ESR1* expression in MCF-7 as compared to WCRC-25 and MDA-MB-231 cells (***$p < 0.0005$) (Figure 50A). Though not significant, we did observe an increase in *ESR1* expression in WCRC-25 cells relative to MDA-MB-231 cells (WCRC-25: Ct = 35-36; MDA-MB-231: Ct = 38 or N.D.). This observation of *ESR1* mRNA expression in WCRC-25 led us to next test if this low level *ESR1* was producing low level functional protein product. We treated WCRC-25 CM-Rocki 5% O_2 cells with 1 μM ICI for 24 hours to see if any endogenous ERα activity could be decreased through classic target gene *GREB1* expression or *ESR1* expression itself; however, this was not observed (Figure 50B). We also performed E2 deprivation of our CM-Rocki 5% O_2 cells followed by treatment with Vehicle control, 1 nM E2, or 1 μM 4OHT for 24 hours to assess ERα-regulated gene expression, and found only mild and non-significant inductions of *GREB1* and *ESR1* (Figure 50B). A similar mild induction of *SNAI1* was observed in WCRC-25 cells when E2 or 4OHT were applied **(**Appendix C Figure 91).

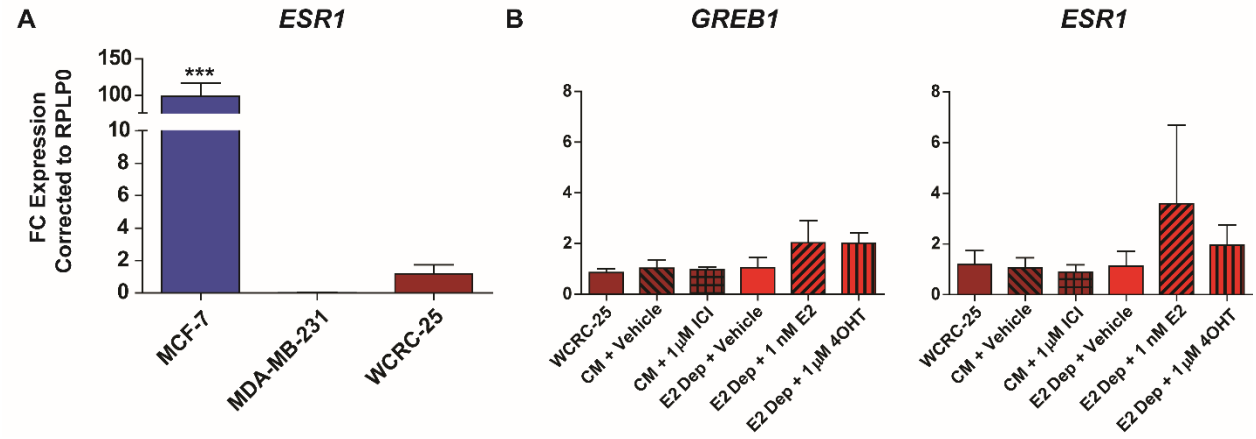

Figure 50: *ESR1* is Expressed at Low Levels in WCRC-25 and ERα-Targets Are Not Regulated by Endocrine Treatments

(A) WCRC-25, positive control (MCF-7) and negative control (MDA-MB-231) cells were first assessed by qRT-PCR for *ESR1* expression. (B) Then, WCRC-25 cells were treated to 1 μM ICI or E2 deprivation followed by 1 nM E2 or 1 μM 4OHT with assessment of *GREB1* or *ESR1* expression alterations by qRT-PCR. Quantifications are a representative single experiment of three independent attempts (A) or of a single experiment with technical triplicates ± STDEV, normalized to WCRC-25 without treatment (B). Statistics were performed with One Way ANOVA followed by Tukey's post-test (*$p < 0.05$, **$p < 0.005$, ***$p < 0.0005$) with comparison to WCRC-25 untreated.

Additionally, endogenous *GREB1* expression patterns matched with each cell line based on measured *ESR1* expression (highest to lowest: MCF-7 > WCRC-25 > MDA-MB-231), even though we were unable to decrease *GREB1* expression by inhibiting ERα activity with ICI treatment (Appendix C Figure 91, see Figure 50B). Interestingly, treatment with E2 and 4OHT did lead to slight inductions of *GREB1*, but these levels were variable and not significant relative to Vehicle control. *PGR* was only expressed in MCF-7 cells with no Cts or occasional Cts around 38 observed in WCRC-25 cells. *SNAI1* expression was higher in WCRC-25 than in both MCF-7 and MDA-MB-231, an endogenous expression pattern observed in other ILC cell lines. However, induction of *SNAI1* by E2 or 4OHT treatment, like *GREB1*, revealed highly variable expression changes that were not significant relative to Vehicle control (Appendix C Figure 91).

We next performed dose response with E2 in the WCRC-25 cells to assess any effect on proliferation for these cells. E2 treatment did not influence the 2D proliferation of WCRC-25 over 6-7 days in the 5% O_2 incubator (Figure 51). Intriguingly, low doses of E2 caused inductions in 2D proliferation for WCRC-25 cells cultured in the 5% CO_2 incubator at high density (5K O_2 v 15K CO_2 **p = 0.0088; 10K O_2 v 15K CO_2 ***p = 0.0005). Overall, we concluded that there was no phenotypic response to E2 for WCRC-25 in these environments tested with a minimal induction in the CO_2 environment that will be further explored in future studies. Altogether, our data indicate that these cells are functionally ERα-. We are currently pursuing obtaining the original stain performed within the hospital that was used to make the pathology call for the patient sample and will describe this outcome in our upcoming publication.

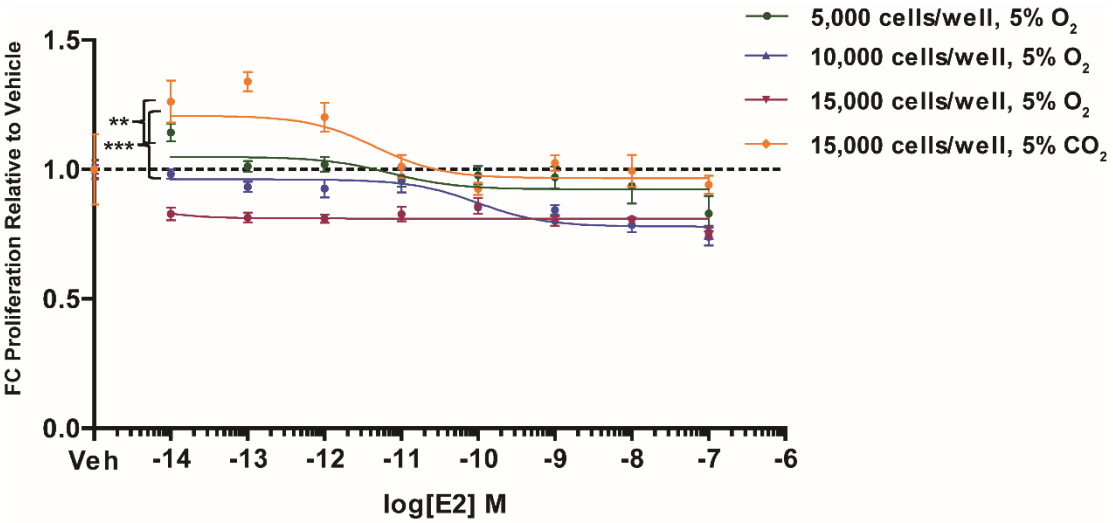

Figure 51: WCRC-25 Cells Do Not Respond to E2 with Increased Proliferation by Dose Response

WCRC-25 cells were E2 deprived and plated at three densities (5-15,000 cells/well) or one density (15,000 cells/well) in the 5% O_2 or 5% CO_2 incubators, respectively. Plates were collected at D_{6-7}. Samples were plated in six technical replicates per dose and data were displayed ± SEM with three parameter non-linear curves fit, as previously. Data represent one experiment. Non-linear comparisons of Top dose responses were performed and comparisons are displayed by asterisks (*p < 0.05, **p < 0.005, ***p < 0.0005).

3.3.5 Discovery of a Novel E-cadherin Mutation in WCRC-25 and LOH

Loss of E-cadherin is the most common molecular feature that differentiates ILC from IDC, and WCRC-25 did not express E-cadherin protein by IF or IB. We next sought to understand the mechanism for this loss of E-cadherin protein expression by sequencing mRNA and DNA products from the cell line. A primer scheme was first developed to cover the entire *CDH1* coding region, as the location of a potential mutation was unknown (Figure 52A). In cDNA samples (converted from mRNA), we observed a nonsense mutation at Q706 of a C>T conversion, leading to the formation of a premature termination codon (PTC) (NM_004360.4:c.2240C>T, p.Q706*) (Figure 52B). This mutation was confirmed with genomic DNA isolated from WCRC-25 (NG008021.1:g21078C>T, p.Q706*) (Figure 52C).

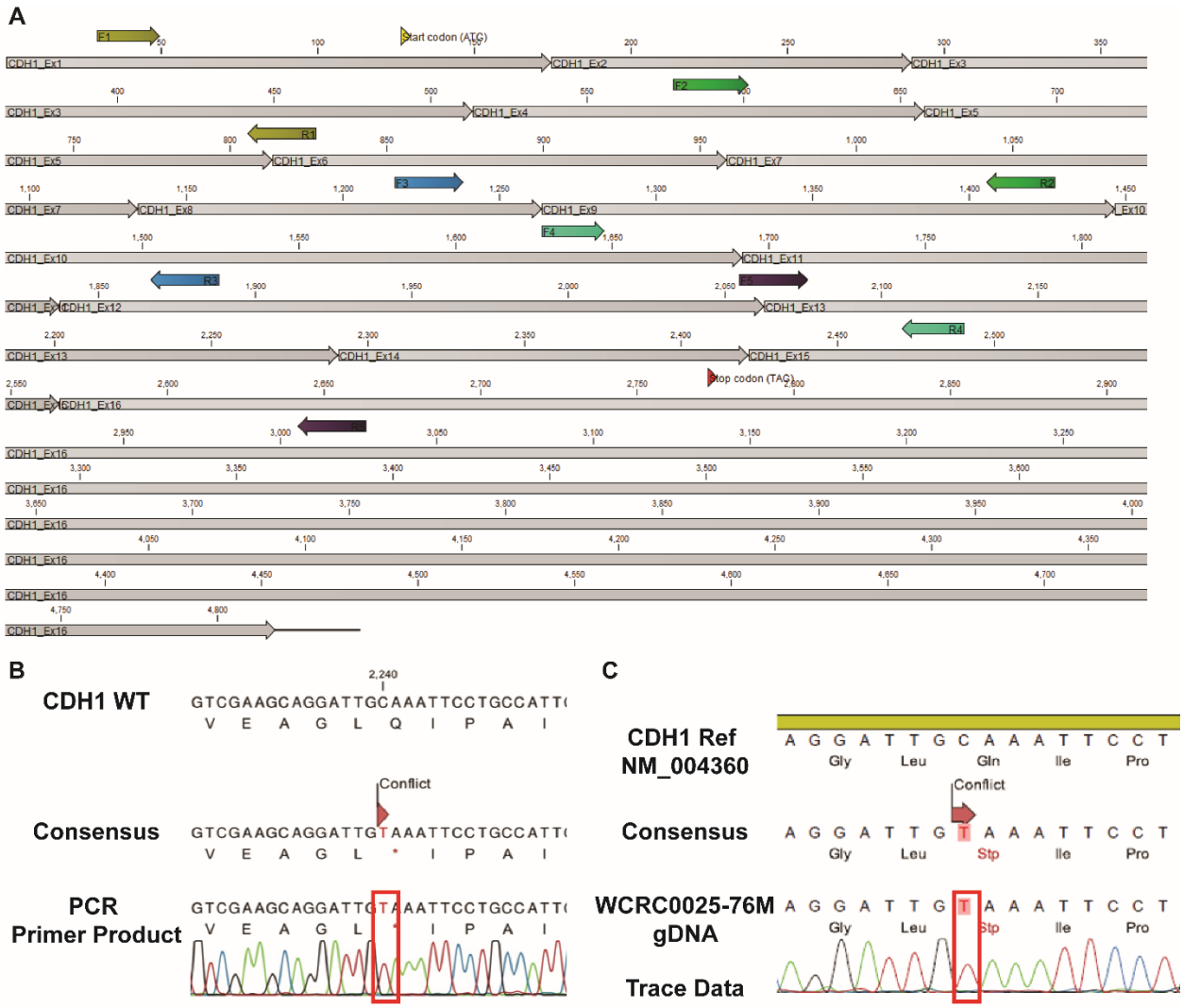

Figure 52: A Novel CDH1 Mutation is Present in WCRC-25 at Q706*
(A) Primer scheme for complete coverage of the coding regions of *CDH1*. (B) Sanger sequencing results from cDNA amplifications after alignment to a wildtype (WT) *CDH1* sequence. (C) Confirmation of cDNA results were performed for gDNA with Sanger sequencing. Mutations are denoted in chromatograms with red boxes.

This mutation was discovered in exon 13 of *CDH1*, which would potentially generate a protein product that would be truncated in the transmembrane domain. However, nonsense mutations should be recognized by the nonsense-mediated RNA decay (NMD) machinery, leading to identification of the PTC, and targeting for degradation[270]. We will discuss the implications of

these statements further in section 3.3.8 and in the overall discussion for this chapter. The mutation of a single nucleotide causing PTC, and the lack of E-cadherin protein expression (see Figure 47, 48) made us ask if the other allele was lost by a common mechanism observed in ILC: LOH.

Therefore, in addition to probing the mechanism of *CDH1* mutation in WCRC-25, we asked if LOH was responsible for the complete loss of E-cadherin protein by assessing copy number status of *CDH1*. We mined Copy Number Alteration (CNA) NanoString data previously performed by our group and revealed that WCRC-25 had only one copy of a *CDH1* allele, much like ILC cell lines MDA-MB-134-VI and Sum44PE, and unlike MCF-7, which had two copies of the allele (Figure 53). We then concluded that one copy of *CDH1* is lost in WCRC-25, and one copy is mutated at Q706*, leading to LOH of *CDH1* in this cell line; these observations are common to other ILC cell lines that have been studied.

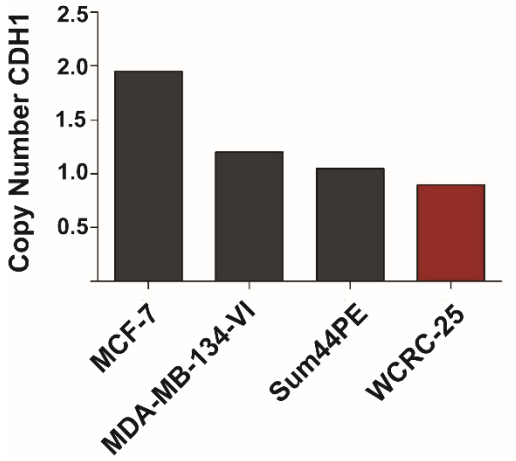

Figure 53: LOH of *CDH1* is the Mechanism of E-cadherin Loss in WCRC-25
IDC and ILC copy number quantifications were mined from NanoString data available in the Oesterreich Lab. MCF-7 cells were used as a control for presence of both alleles, while MDA-MB-134-VI and Sum44PE were used as controls for presence of only one allele, each, due to LOH.

3.3.6 Measurement of Q706* in cfDNA Samples from WCRC-25 Patient

Since we had established the position of the *CDH1* mutation in WCRC-25 cells, we next asked if we could detect this mutation in cfDNA samples obtained from blood obtained from the patient. These samples were taken when the patient had high metastatic burden, so the likelihood of the blood samples containing cfDNA shed from the tumors was increased[271]. We isolated cfDNA from these samples and from our WCRC-25 cells, and used a custom ddPCR probe for our *CDH1* Q706* mutation or a control wildtype *CDH1* probe to assess presence of this mutation in the longitudinal samples.

Buffy coat contained nearly 100% allele frequency (AF) of the wildtype *CDH1* allele, and a 0.6% AF of the *CDH1* Q706* (Figure 54). The low expression of the mutant in the buffy coat confirmed that the mutation was somatic as opposed to germline, which we would hypothesize to be enriched. As expected, the cell line WCRC-25 contained 97.9% AF of *CDH1* Q706*, and 0% AF of the wildtype *CDH1*. In the first and final draws taken from the patient, an increase of *CDH1* Q706* was observed from 0.27% (draw 1, *data not shown*) to 8.3% (draw 4). The higher level of detectable mutant in the buffy coat from draw 4 compared to the cfDNA fraction in draw 1 (Buffy = 0.6% versus Draw 1 cfDNA = 0.27%) was not concerning, as the same buffy coat was utilized in other experiments and showed 0.19% AF of the *CDH1* Q706* (*data from Ahmed Basudan, BS, not shown*). This suggests the potential of minor contamination of the buffy coat during the PCR procedure. The enrichment for the *CDH1* Q706* mutation over time and increased disease burden for the patient confirms that this technique is feasible for clinically tracking disease progression and for research purposes to confirm prevalence of specific mutations for given genes.

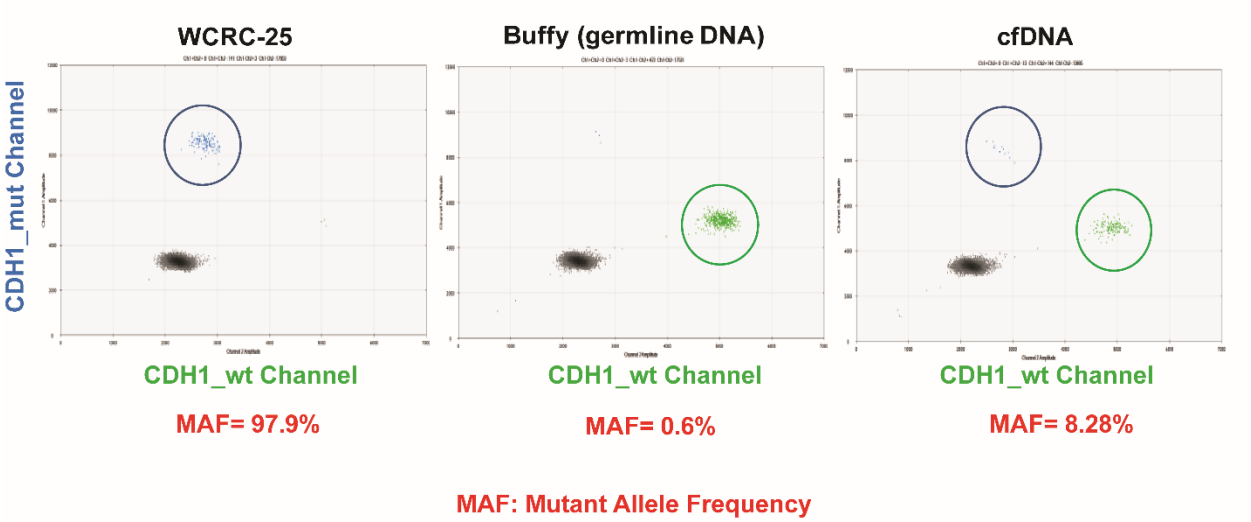

Figure 54: ddPCR Shows Q706* is Detected in cfDNA from WCRC-25 Patient
ddPCR was performed in the WCRC-25 cell line, Buffy Coat, or cfDNA (draw 4 shown) from the WCRC-25 patient. Probes were utilized against either wildtype (wt) CDH1 or the Q706* mutant CDH1 (mut). Blue or green dots represent droplets that contained DNA with each respective genotype (mutant or wt). Black dots indicate droplets that did not contain DNA. Mutant allele frequencies (MAF) are displayed beneath each respective plot.

3.3.7 Phenotypic Characteristics of WCRC-25

We next assessed three basic phenotypes or characteristics of WCRC-25: (1) population doubling, (2) 2D proliferation, and (3) soft agar anchorage independent growth. Population doubling assays were performed in P3, P5, and P7 of the WCRC-25 cells after two, four, or six passages in respective incubator/culture environments, as described. We assessed the average doubling time of WCRC-25 to be approximately 5 days, a comparable time to other ILC cell lines (MDA-MB-134-VI: 2 days, Sum44PE: 5-7 days; Figure 55). Population doubling remained most stable in all conditions, across passages for the middle density of cells tested (10,000 cells/well). It was therefore determined that WCRC-25 cells had a stable population doubling in DMEM/10% FBS 5% O_2 conditions, and cells were continually maintained in this condition for future experiments. To ensure that this alteration in media type did not greatly influence major changes in population

doubling later, a side-by-side comparison of all media growth conditions will be performed once cells reach ~P50, or the Hayflick limit[220]. Additionally, to confirm that this media choice did not overtly influence major changes in gene expression programs, cell pellets were generated in FFPE blocks from P17 CM-Rocki 5% O_2 and P17 DMEM/10% FBS 5% O_2 WCRC-25 cells for use in any sequencing experiments.

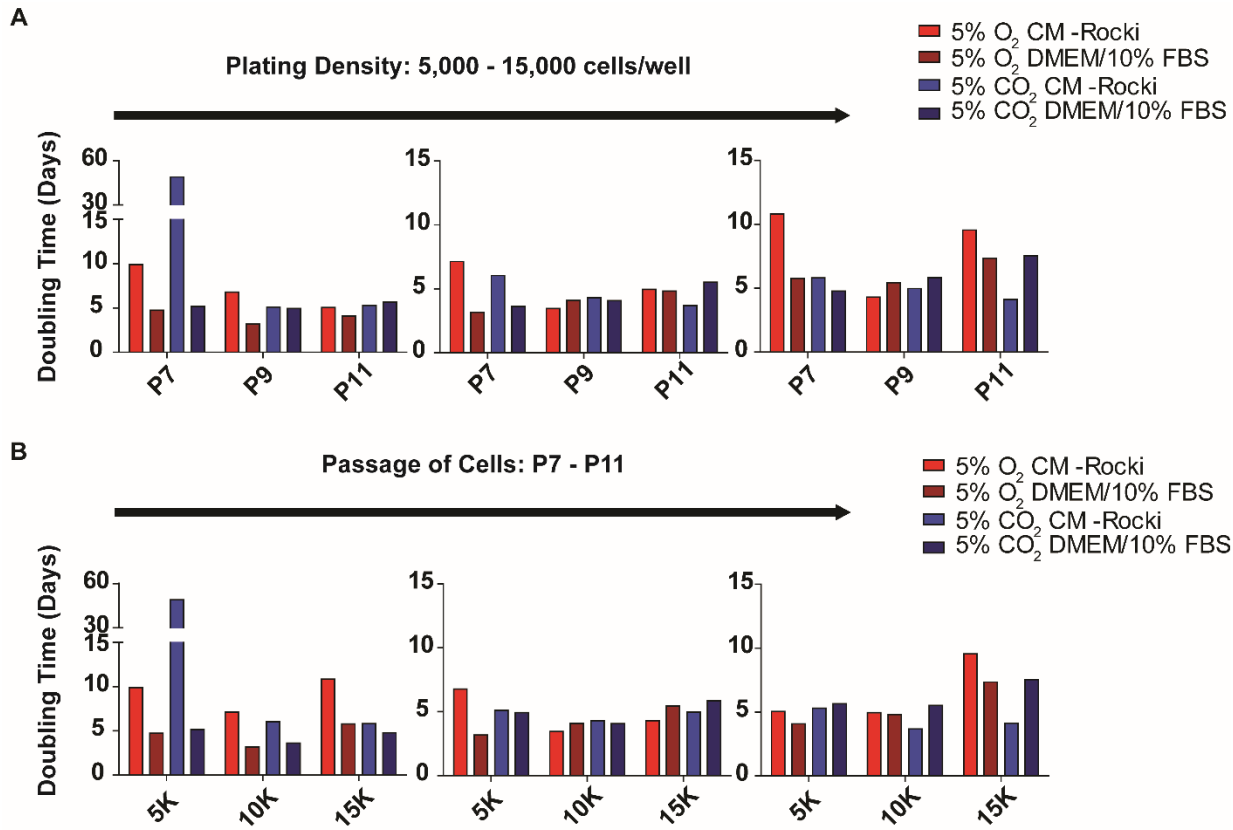

Figure 55: Population Doubling Time for WCRC-25 is Circa 5 Days
Population doubling was assessed in WCRC-25 cells in the four conditions previously mentioned, at three densities (5-15,000 cells/well), and over three different passages (P7, P9, P11). Data were represented either by (A) increased plating density or (B) increased passage.

Our 2D proliferation assays confirmed our population doubling observations. Cells proliferated efficiently in DMEM/10% FBS, 10,000 cells/well, 5% O_2, expanding to approximately 2-3 fold the original cell population over 6 days of growth (Figure 56A). Though increased growth of DMEM/10% FBS, 10,000 cells/well was noted in 5% CO_2, these assays were performed with later passage (~P30) cells than performed with our population doubling assays. Additionally, these cells were in stated media/incubator environments for only two passages prior to using in experiments, and our population doubling assays tested whether cells established long-term in these environments would have set doubling times.

For our final preliminary phenotype assessment, we chose to pursue anchorage independent growth, or soft agar growth, as an environment of interest for WCRC-25. Our preliminary studies have shown that ILC cells do not form cohesive soft agar colonies like control IDC cell line MCF-7, and instead form small, discohesive clusters of cells. This is likely due to their loss of E-cadherin. In addition, these loose colonies take an extended period of time to form that are not conducive to ease in experimental use (MCF-7 ~2 weeks; MDA-MB-134-VI ~4 weeks; IPH-926 ~18 weeks). We tested our WCRC-25 cells in the soft agar assay at either a low density (10,000 cells/well) or high density (50,000 cells/well) for a period of 2 weeks against MCF-7 control cells. As expected, MCF-7 cells formed countable, cohesive colonies in this timeframe, but WCRC-25 formed few colonies at either density, in either incubator setting, with much smaller, discohesive structures (Figure 56B, C). Ongoing assays are probing the length of time to form significant numbers of soft agar colonies.

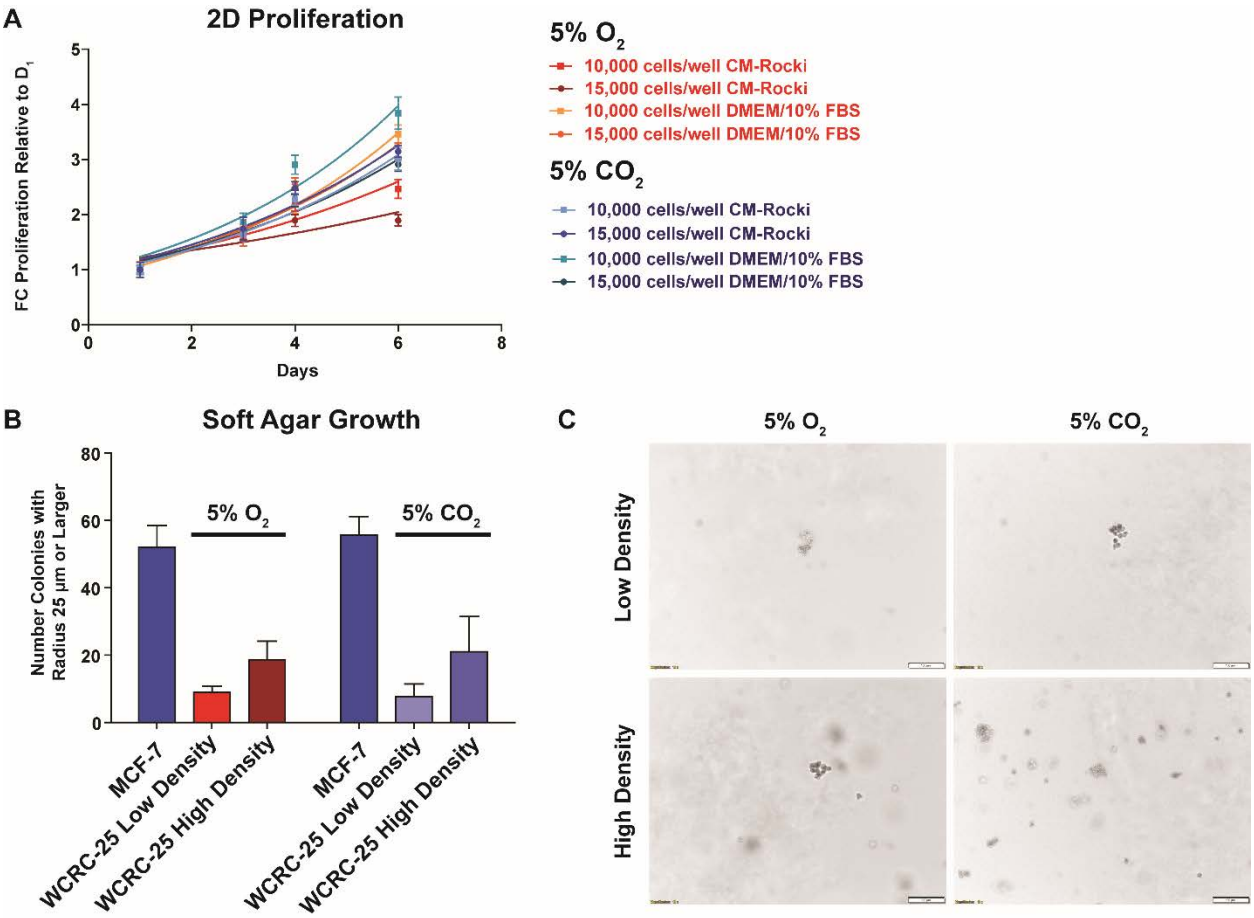

Figure 56: 2D Proliferation and Soft Agar Growth Phenotypes for WCRC-25
WCRC-25 cells were plated for (A) 2D Proliferation assay or (B) Soft Agar Anchorage Independent Growth assay. Both assays were performed in either the 5% O_2 or 5% CO_2 incubators. 2D proliferation was performed in both media conditions with six replicates per condition and data quantified as previously ± STDEV, non-linear exponential regressions fitted to data. Soft agar was performed with either 10,000 cells/dish (low density) or 50,000 cells/dish (high density) in triplicate dishes for each condition, for 2 weeks MCF-7 served as a control. Both assays are single experiments with two similar experimental outcomes observed for (A), only. (C) Representative images of the soft agar colonies formed for WCRC-25 by 2 weeks were taken (10X magnification; bar represents 100 µm).

3.3.8 RNA Sequencing Analyses of Patient Samples and Cell Line

We then asked about the transcriptional programs in WCRC-25 and in all of the patient samples we obtained. We isolated RNA from FFPE cell blocks (WCRC-25) or patient samples and

measured for FFPE RNA quality using Illumina DV_{200} (*in collaboration with Ahmed Basudan, BS*). DV_{200} is a measurement of the percentage of RNA fragments obtained that have more than 200 nucleotides present. This metric is more sensitive than previously used RNA Integrity Number (RIN) assessment, due to its heightened sensitivity for FFPE fragments. A DV_{200} value of 30 or less is highly degraded and of too poor quality for use in RNA Sequencing. For all samples prepared except for the peritoneum sample, DV_{200} values of greater than 30 were achieved. Although the value from the peritoneum sample was quite low (13.45), we proceeded to use this sample in the subsequent RNA Sequencing run. Samples were sequenced (see 3.2.13 for methods) and data were first quality checked for interpretability (Appendix C Figure 92).

We next performed principle component analysis (PCA) for the top 5,000 most variable genes. This measurement transformed the original data to enable better resolution of the variation between samples. PCA showed that most of the ER^+ samples clustered together, except for the peritoneal fluid sample, which clustered closer to the ER^- samples from the left breast (Figure 57). Additionally, the two skin samples clustered together, as anticipated. The cell line samples from either CM-Rocki or DMEM/10% FBS clustered together and also with other pleural fluid samples taken. Finally, and not completely unexpected, the stomach sample did not cluster with any of the samples, further suggesting that this sample was an outlier (see Appendix C Figure 92).

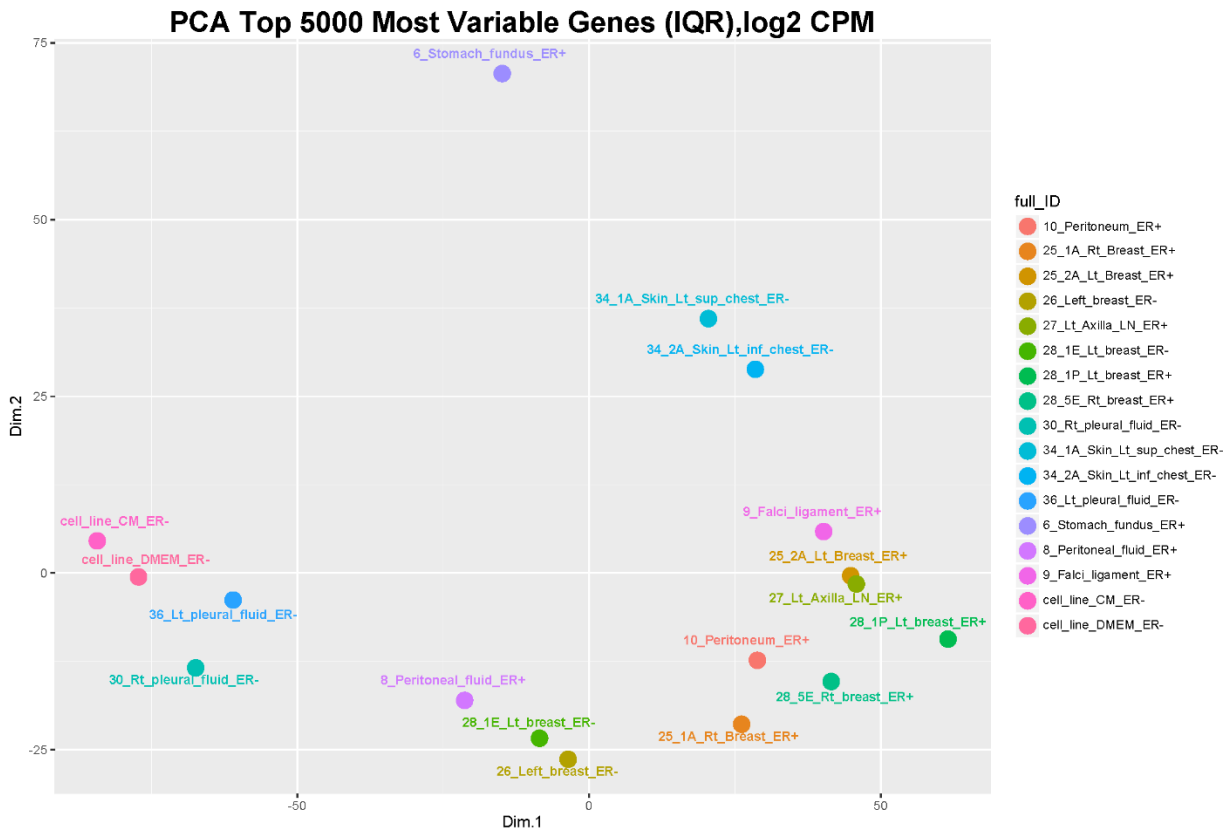

Figure 57: PCA from WCRC-25 RNASeq
PCA was performed for WCRC-25 RNASeq analyses to show clustering of data using the top 5000 most variable genes interquartile range (IQR) log2CPM. Samples are labeled with their location of collection, ER status, and numerical description.

PAM50 calls were then made with the sequencing data for all samples using the *genefu* R package. We noticed that different samples had different calls, comprising all call types (Luminal A, Luminal B, HER2, Basal) (Figure 58). All the ER^+ samples were called as Luminal A, with the exceptions of the peritoneal fluid sample (Luminal B) and the stomach sample (HER2). The stomach sample call may be explained by the aforementioned potentially poor quality of the data from this sample. Interestingly, the left breast ER^- samples and right pleural fluid ER^- samples were also called as Luminal B. All remaining samples, including the cell line samples, were called as HER2, except for the left superior skin ER^- sample, which was called as Basal. Upon close examination of the numerical calls, it appeared that many the samples were a nearly 50:50 ratio

for the Luminal B or HER2 call. Though no bi-call is currently in existence for PAM50 subtypes, it is possible that either by tumor heterogeneity or expression of certain entities (e.g. Ki67) drove the subtype call for given samples[272].

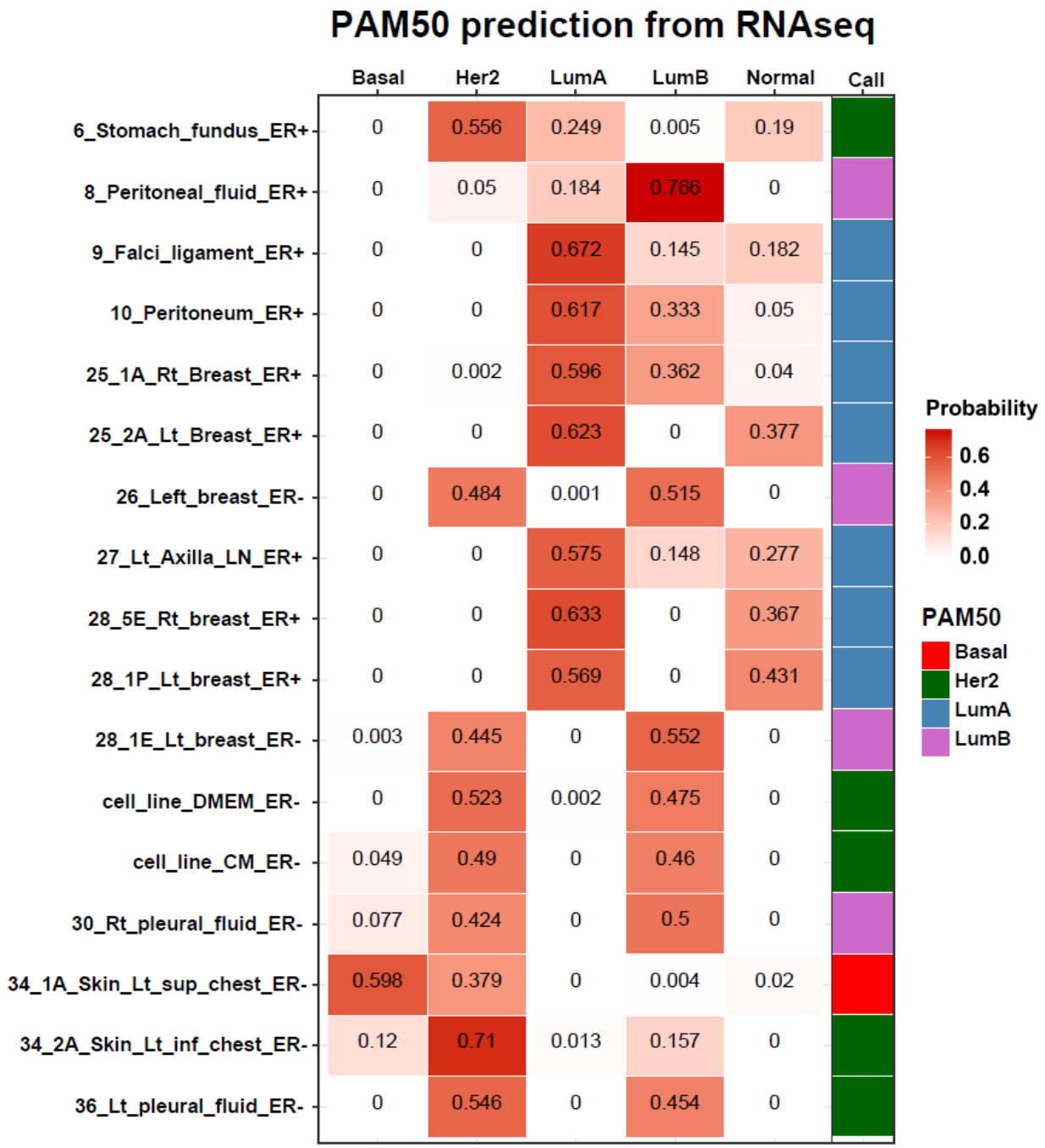

Figure 58: PAM50 Subtypes for WCRC-25 Patient Samples Suggest Heterogeneity in the Disease

PAM50 subtypes were called using *genefu* package and probabilities of calls were displayed for each sample with a definitive PAM50 call listed in the far-right column. Samples are listed from top to bottom in chronological order of acquisition from the patient.

Assessment of expression of genes of interest was performed to confirm pathology interpretations of original samples and to probe expression of genes of interest. *ESR1, PGR, HER2,* and *Ki67* expressions were as anticipated based off pathological interpretations (Figure 59A, B). *ESR1* expression was also low in the stomach sample, which agreed with our observations of the ER IHC (see Figure 40, Appendix C Table 16) even though pathological calls had stated the sample was ER^+. *PGR* was not expressed in the cell line samples, as we observed in our qRT-PCR studies (see 3.3.4). *ERBB2* expression was relatively high, which contradicted clinical observations that samples were HER2- (*data not listed in pathology calls as was not available for every sample*). As anticipated from observations of other ILC cell lines, *CDH1* was still expressed at the RNA level in all samples (Figure 59B, Left Panel). The overall levels of RNA were high (compare to *ESR1*) and suggest that though the ILC maintained mutated *CDH1* at Q706*, the cells still attempted to generate RNA. These observations are being probed in ILC cell lines in our lab, as we have made similar observations of high detection of *CDH1* mRNA by qRT-PCR (*data not shown*). *MKI67* levels were similar in all samples except the Left Breast $Mastectomy_1$ sample (ER^+; Figure 59B, Middle Panel). *TP53* levels were also similar across all samples (Figure 59B, Right Panel). Finally, a brief assessment of PI3K pathway members was performed. We included *PIK3CA*, the gene that encodes for PI3K, and two downstream gene targets related to survival, *CCND1* and *BIRC5*. While *PIK3CA* and *CCND1* levels were similar across all samples, *BIRC5* was slightly more highly expressed in the samples taken toward the end of the patient's life (Figure 59C). These preliminary observations confirm the original pathology calls made for each sample, and give further confidence to the quality of RNA Sequencing data. Additionally, we probed the expression of multiple genes in the PI3K pathway (*PIK3CA*, *CCND1*, *BIRC5*) and cautiously interpret these data as they are mRNA and not functional protein.

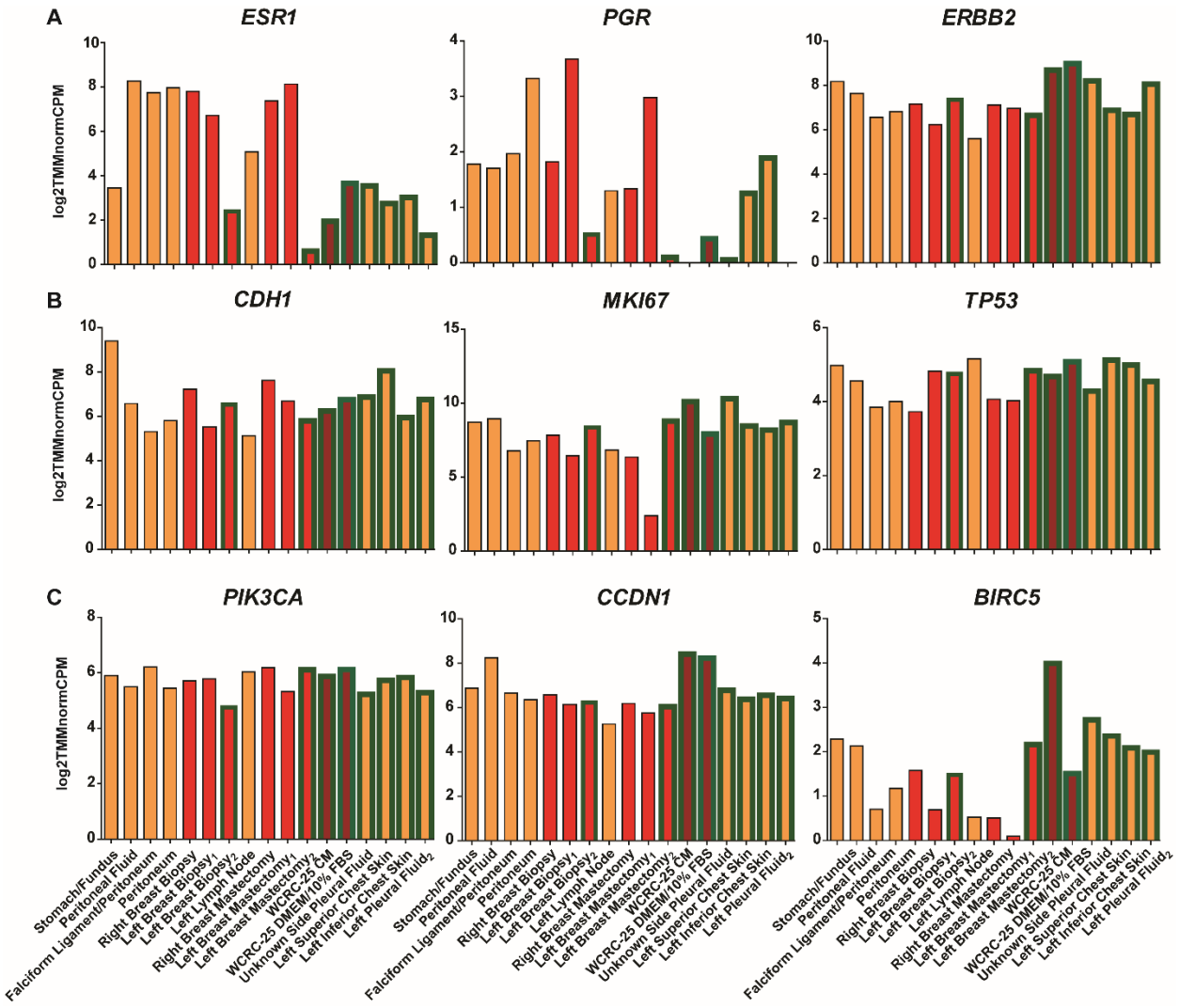

Figure 59: RNASeq Data Confirms Clinical Observations and Allows for Probing of PI3K Signaling

Gene expression for (A) *ESR1*, *PGR*, and *ERBB2*, (B) *CDH1*, *MKI67*, and *TP53*, and PI3K pathway members (C) *PIK3CA*, *CCND1*, and *BIRC5* were called from RNASeq data. ER$^-$ patient samples are highlighted in green, metastases are orange, primary breast samples are in red, and cell line samples are in maroon. Samples are listed in chronological order of collection, from left to right.

As RNA Sequencing data was obtained and processed shortly before the compilation of this dissertation, only the described data were available. A forthcoming publication will detail further analyses including pathway analyses, probing expression of genes of interest related to

ILC, and alterations in genes of interest by targeting aforementioned gene products with siRNA or drugs to alter phenotypes in WCRC-25.

3.3.9 Drug Responses in WCRC-25

Two approaches were taken to assess therapeutic responses in WCRC-25. First, the patient clinical history was examined and therapeutics were selected from the treatment regimen with hypotheses of dose response outcomes designated based upon the original pleural effusion sample of origin in relation to treatments given. For example, we hypothesized that since WCRC-25 cells were already exposed to Carboplatin and Paclitaxel (a platinum-based DNA interfering and taxane-based tubulin inhibitor, respectively), they would thus be more resistant to these therapies. To test this hypothesis, we chose to use Cisplatin, another platinum-based DNA interfering chemotherapeutic with similar mechanism and outcome to Carboplatin, and Paclitaxel to perform 2D proliferation-inhibitory dose responses. Paclitaxel was highly potent compared to Cisplatin; an IC_{50} value of 0.4 nM was obtained for WCRC-25 cells for Paclitaxel compared to 2 mM for Cisplatin (Figure 60A, B). The lack of observed resistance to Paclitaxel was intriguing, as WCRC-25 responded with a similar IC_{50} as compared to cell line MCF-7 (IC_{50} = 0.2 nM). Additionally, it should be noted that the potency of Paclitaxel was higher in WCRC-25 at higher doses, as compared to MCF-7 (WCRC-25 IC_{75} = 1.1 nM; MCF-7 IC_{75} = 6.2 nM). Cisplatin IC_{50} values were quite high for both cell lines tested (WCRC-25 IC_{50} = 2 mM; T47D IC_{50} = 1.5 mM). This is perhaps not surprising, as Cisplatin is often utilized in combination therapies in the clinic to increase its effectiveness as a therapeutic[273]. Thus, future studies will probe the combination of these therapeutics in order to ascertain if the combination of Paclitaxel and Cisplatin are more resistant in WCRC-25 compared to a positive control cell line. It is also important to remember that patient WCRC-25 received

endocrine therapies after the course of Paclitaxel/Carboplatin, which may have led to further alterations in the cells, including loss of resistance to these therapeutics.

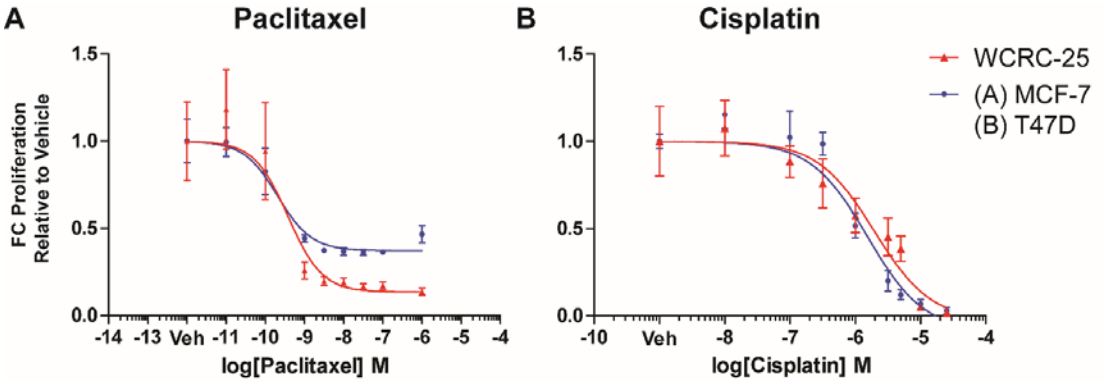

Figure 60: Dose Responses of Paclitaxel and Cisplatin in WCRC-25 Cells
WCRC-25 cells or cells known to produce some kind of dose response to each drug ((A) MCF-7, (B) T47D) were treated to dose responses for (A) Paclitaxel or (B) Cisplatin in 2D proliferation environments for 5 days. Data were fit with three parameter agonist non-linear regression curves after normalization to each respective Vehicle, with six replicate data points per point shown ± STDEV. Data represent a single experiment performed.

We next asked if a therapeutic that the cells had not yet been exposed to prior to the acquisition of the sample would be highly potent in inhibiting 2D proliferation of WCRC-25. We chose to test Doxorubicin dose response in WCRC-25 against positive control cell line MCF-7. The IC_{50} of Doxorubicin in WCRC-25 was 7.3 nM compared to 11.3 nM in MCF-7 (Figure 61). As only a subtle increased sensitivity was noted in WCRC-25 cells, these data suggest that Doxorubicin inhibition of 2D proliferation is similar between WCRC-25 and MCF-7.

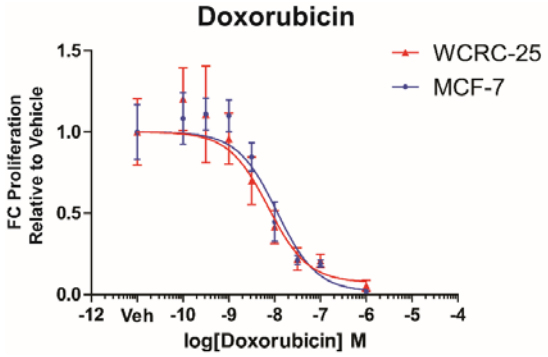

Figure 61: Doxorubicin Dose Response in WCRC-25 Cells
WCRC-25 or MCF-7 cells were treated to dose responses for Doxorubicin in 2D proliferation environments for 5 days. Data were fit with three parameter agonist non-linear regression curves after normalization to each respective Vehicle, with six replicate data points per point shown ± STDEV. Data represent a single experiment performed.

For our second approach, we chose to test response of WCRC-25 to a drug that the patient was not exposed to during treatment. The choice of this drug was based off of prior indication for rationale of use in the literature. First, we tested 2D dose response of the dual PI3K/mTOR inhibitor, Dactolisib (BEZ235). Though BEZ235 is not currently FDA-approved for use in the clinic, mounting scientific evidence for targeting of the PI3K/mTOR axis has led to its use in clinical trials since 2006[274, 275]. As described in the introduction, targeting of the PI3K/mTOR pathway may provide clinical benefit for ILC patients, whose tumors often carry elevated PI3K/AKT signatures or PI3K mutations[67, 94]. 2D proliferation-inhibition dose response revealed that WCRC-25 had a BEZ235 IC_{50} of 1 nM, while positive control cell line MDA-MB-134-VI had an IC_{50} of 3.7 nM (Figure 62A). These inhibitions were very promising, especially when observed at nM potency, and we thus decided to ask if this inhibition was present in other growth environments, such as ULA. BEZ235 ULA IC_{50} for WCRC-25 was right-shifted slightly to 1.7 nM, while MDA-MB-134-VI positive control cell line had an IC_{50} of 3.1 nM (Figure 62B). We then decided to observe the signaling effects of BEZ235 in 2D and ULA.

Using 1 nM BEZ235 treatment for 24 hours in both 2D and ULA environments, we measured alterations in levels of total AKT, pAKT^{S473}, pAKT^{T308}, total S6, and pS6$^{S235/236}$, all major components of the PI3K/AKT/mTOR pathway. pAKT^{S473} levels were low in both cell lines, and only interpretable in WCRC-25 cell lysates (Figure 62C). Interestingly, WCRC-25 had higher pAKT^{S473} levels in ULA than in 2D, while total AKT levels appeared relatively similar between both settings. This increase in pAKT^{S473} in ULA may be explained by the anoikis resistance phenotype exhibited by successful ULA proliferation; it has been shown that upregulation of the PI3K pathway is one of the most common mechanisms for anoikis resistance in breast cancer[276]. In both 2D and ULA settings, BEZ235 showed a minor reduction in pAKT^{S473} levels. A slight decrease in total AKT levels was also detected in the 2D setting for WCRC-25 when BEZ235 treatment was given. pAKT^{308} was difficult to visualize in all samples tested. As a side note, total levels of total AKT were decreased in MDA-MB-134-VI after BEZ235 treatment in 2D, an unexpected outcome. No current explanation is available for this observation, but it is possible that a previously undescribed role for BEZ235 promoting protein degradation mechanisms may be at play[277]. For mTOR pathway, we observed a different pattern of total S6 and pS6$^{S235/236}$ protein expressions and alterations in WCRC-25. Both total and phosphorylation levels of S6 were elevated in WCRC-25 2D compared to ULA environments, and slight decrease in pS6$^{S235/236}$ was evident after BEZ235 treatment in the ULA environment, only. MDA-MB-134-VI were impacted differently, with higher total S6 levels in the 2D environment, decreased total S6 levels observed in 2D with BEZ235 treatment, and pS6$^{S236/237}$ observed in both environments. These data led us to conclude the following: (1) WCRC-25 have higher overall PI3K/AKT/mTOR signaling than MDA-MB-134-VI, (2) WCRC-25 have higher basal PI3K/AKT signaling in ULA than in 2D, and the decrease in pAKT^{S473} was seen more effectively in the 2D setting, and (3) the mTOR pathway

observed was relatively unaffected by treatment with BEZ235, unlike what was observed in the MDA-MB-134-VI cells. The lack of mTOR pathway response observed is interesting, but we only tested one marker of mTOR activity ($pS6^{235/236}$). The PI3K/AKT/mTOR pathway is very complex, and we are pursuing experiments that will assess the impacts of BEZ235 on other parts of mTOR signaling. Overall, these interesting outcomes suggest that environmental context can influence major oncogenic pathway signaling and response to therapeutics, suggesting the rationale to screen dose responses in multiple environments in the future.

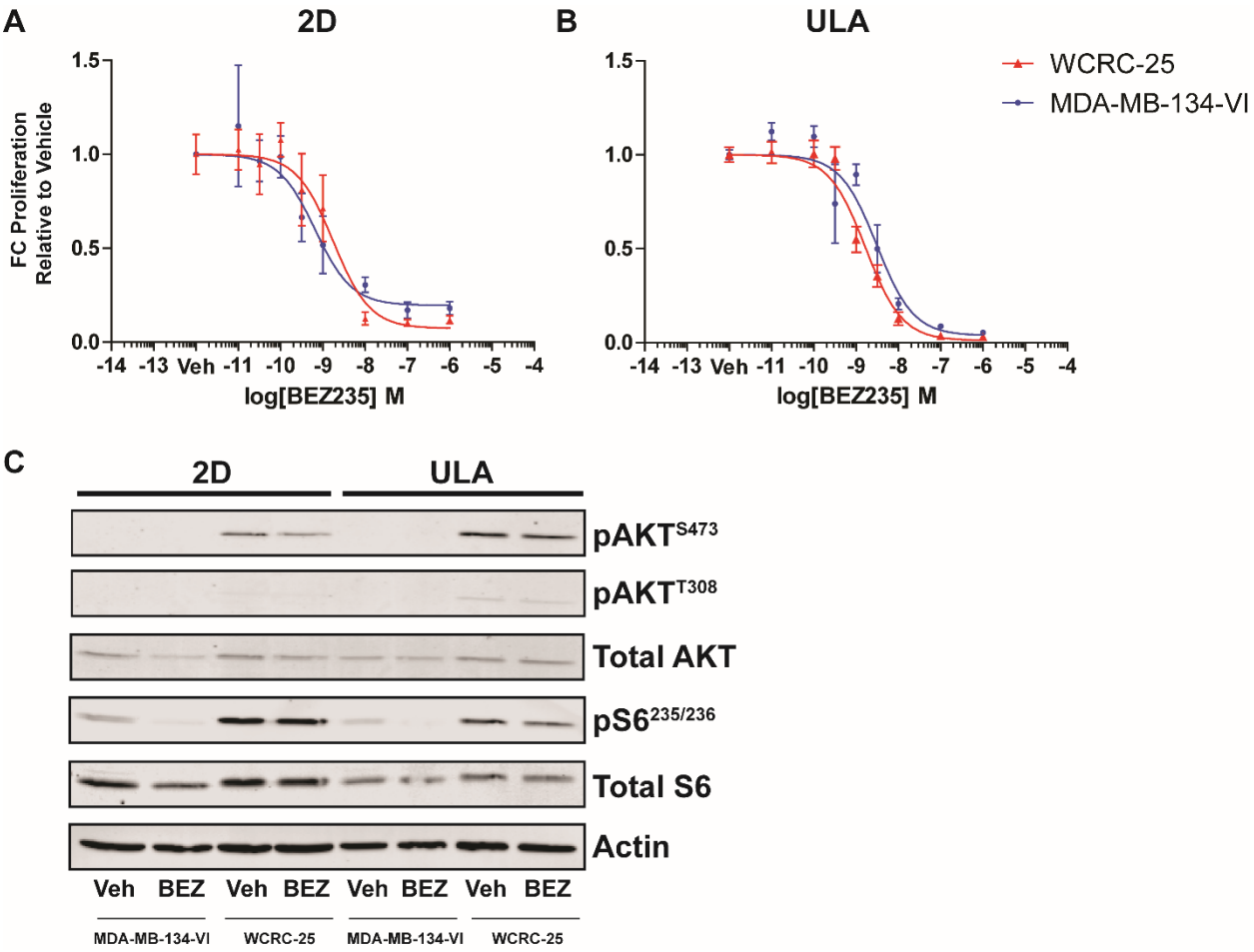

Figure 62: BEZ235 is a Potent Inhibitor of WCRC-25 2D and ULA Proliferation with Impacts on P13K Signaling

WCRC-25 cells were treated to dose responses along with positive control cell line (MDA-MB-134-VI) in (A) 2D or (B) ULA proliferation environments. Data were analyzed as in Figure 61. (C) IC_{50} concentrations of therapeutics were utilized to treat WCRC-25 or MDA-MB-134-VI for 24 hours prior to protein acquisition and IB for markers of the PI3K/AKT/mTOR pathways relative to Actin internal control.

In summary, we designed a series of dose response assays to test various therapeutic responses of WCRC-25. In our clinical treatment approach, we observed little resistance of WCRC-25 to Paclitaxel or Cisplatin treatments relative to positive control cell lines, and indicate that resistance may only be observed when both therapeutics are used in combination. Alternatively, the cells may no longer be resistant to aforementioned therapies, as they were also

exposed to endocrine therapies prior to being established. Also, environmental context is important, as shown in our 2D v ULA BEZ235 assays (see Figure 62); our cells may not respond to therapeutics the same in all environments tested. We observed a potent response of WCRC-25 to Doxorubicin relative to the positive control cell line tested. Then we tested efficacy of a clinically relevant, targeted therapeutic against PI3K/mTOR (BEZ235). BEZ235 showed promise as a slightly more potent therapeutic in WCRC-25 than in positive control ILC cell line MDA-MB-134-VI (2D WCRC-25 IC_{50} = 1 nM v 2D MDA-MB-134-VI IC_{50} = 3.7 nM), with downregulation of $pAKT^{S473}$ noted in WCRC-25. The lack of inhibition of the mTOR pathway in WCRC-25 was interesting, but may suggest that another portion of the PI3K/AKT pathway is being inhibited, or an mTOR specific targeted agent such as Rapamycin may be needed to decrease the $S6/pS6^{S236/237}$ signaling observed[278]. Also, we noted that BEZ235 showed potent inhibition of WCRC-25 cells in ULA, an important note for an ILC cell type that has shown preferential anoikis resistance phenotypes[276].

3.3.10 Ongoing *In Vivo* Studies

A final important question in assessing the utility of WCRC-25 as a model of ILC is to understand if WCRC-25 has tumorigenic properties in an *in vivo* setting. As previously described in the introduction to this chapter, ILC cell line xenograft models appear to be of limited utility due to the length of time required to form palpable tumors[204]. WCRC-25 cells were determined to be $ER\alpha^-$, and thus the animals were not supplemented with E2 pellets at the time this dissertation was completed. Injections performed in the Tail Vein (TV), Mammary Intraductal (MIND), and Mammary Fat Pad (MFP) models have already begun to yield potential development of metastatic lesions in athymic nude (TV) or NSG (MIND, MFP) mice. The TV and MFP mice are currently

bi-weekly analyzed by IVIS imaging, and will continue to be monitored for development of outgrowths. An example of the beginning of potential abdominal or ascites outgrowths can be seen in some of our TV mice that were injected approximately two months prior to the images shown in Figure 63A. In addition, our MFP tumors are growing and will be palpable for measurement at the time of publication of this dissertation (Figure 63B). We look forward to the utility of these systems in understanding the pathology of WCRC-25 in the larger scope of ILC.

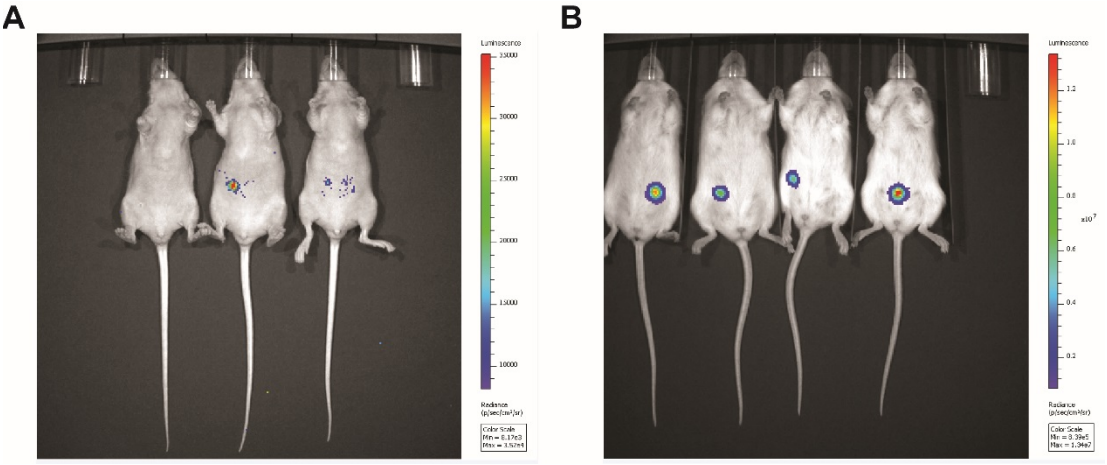

Figure 63: IVIS Imaging Examples from TV or MFP Mice Injected with WCRC-25
Mice were injected by (A) TV or (B) directly into MFPs with WCRC-25 cells labeled with RFP for visualization on the IVIS system. Representative images of mice at 2 months or 3 weeks, respectively, post injections are displayed.

3.4 DISCUSSION

Cell line models are important tools for uncovering the molecular, phenotypic, and basic characteristics of diseases. For ILC, few cell line models exist, and have been minimally explored as appropriate model systems to represent the disease[204, 249-251]. We have therefore provided a detailed account of the establishment and characterization of a novel ILC cell line, WCRC-25,

which we believe represents some of the many characteristics observed in other ILC cell lines and in the clinical setting. Further, we present the WCRC-25 cell line as a potential model of endocrine therapy resistance, a common issue in breast cancer and within ILC[8, 165].

Patient WCRC-25 had a complicated clinical course that initiated with a misdiagnosis of gastric carcinoma (see Figure 39). Gastric carcinoma does maintain some signet ring cell features that mimic the morphology of cells in ILC, and case studies have attempted to inform clinicians of the initial presentation of ILC as gastric metastasis[279, 280]. Further, *CDH1* mutations and loss of expression are also a key feature of Hereditary Diffuse Gastric Carcinoma (HDGC). The similarities between features of the diseases and the indolent nature of ILCs, particularly in reference to their visibility in mammograms, may continue to cause difficulties in diagnosing the disease. Further research is currently required to understand the relationship between the two diseases and to prevent misdiagnoses. Beyond this point, endocrine therapy resistance played a role in the progression of lesions in WCRC-25, as most outgrowths toward the end of the timeline were from the ER^- potential local recurrence in the left breast that had seeded from the ER^+ original left breast primary. The contralateral tumor in the right breast also followed with the known predominance of this to occur in patients afflicted with ILC[60].

We successfully established WCRC-25 using a newer method of cell reprogramming, and then characterized its marker expression, growth characteristics, and mutational profile against original clinical samples from the patient[254]. We determined that WCRC-25 is an epithelial, $ER\alpha^-$ cell line harboring basal characteristics of CK14 expression. While at first this was concerning to us, the literature provided clues that basal marker expression was perhaps not an anomaly for ILCs. In a recent study, Fadare and colleagues measured the expression of another basal marker, CK5/6, in n = 82 ILCs, and noted that 17% of these lesions maintained positive expression[267]. They

concluded from these data that there exists a basal-population of ILC cells. In contrast, Khilko and colleagues published IHC of CK5/6, CK14, and CK17 in a smaller cohort of n = 53 ILC patients, whose tumors were all negative for these markers[268]. Engstrom and colleagues further complicated the data observed in their recent study of a larger Norwegian cohort of n = 1423 ER^+ breast cancers; they revealed that luminal tumors that express basal markers have better survival outcomes compared to those that do not, challenging prior accepted clinical observations[269]. The ILC cohort listed in this study was larger than in the previously described studies, including n = 176 patient samples. Interestingly, 22 of these ILC patient samples *did* express basal markers, though which markers and relationship to survival were not specified. Finally, we note that the previously described studies were performed in primary ILC, whereas our samples were generated from metastatic ILC samples. These points suggest that our data for prevalent CK14 expression in ILC cells is feasible, and that expression of basal markers may influence survival outcomes for ILC patients.

Importantly, our IB and IHC data indicated that E-cadherin was not expressed in WCRC-25, but more highly sensitive IF did reveal the presence of diffuse, punctate E-cadherin staining. Due to the peptide recognition of our antibody for E-cadherin (C-terminus; aa735-883), it does not seem likely that this staining is E-cadherin as this region is not present in WCRC-25 or MDA-MB-134-VI due to PTC locations being upstream of this region and LOH of the alternate allele. As previously stated, this punctate E-cadherin has been seen in other ILC cell lines (MDA-MB-134-VI), which also harbor PTCs upstream of this peptide detection region. Thus, there are two possibilities: (1) there exists cross-reactivity of our antibody with another protein that is detected more easily by IF (possibly another cadherin, such as P-cadherin, that is suggested by the manufacturing company BD Biosciences), or (2) there is a small population of *CDH1* wildtype

allele cells within the overall cell population, insufficient to be detected by IB or IHC, but sufficient to be detected by sensitive IF. Future analyses will be performed by our group to discern the rationale for observation of punctate E-cadherin staining in ILC cells. We will also continue to probe the role of mRNA expression of *CDH1* that is observed in ILC cells, and in the WCRC-25 clinical samples (see Figure 59B, Left Panel).

Using our cells, we established the presence of a novel *CDH1* mutation in Q706*, generated a ddPCR probe for this mutation, and used this tool to detect the mutation in cfDNA obtained from patient sample blood draws. While this practice is not currently utilized in the clinic on a regular basis, our data suggest that sequencing a patient's tumor for genetic aberrations (e.g. *CDH1* mutations in ILC patients) can allow for the development of a feasible, non-invasive test for tracking of disease progression. The increase in WCRC-25 blood draws of the *CDH1* Q706* mutation was striking, and tracked with metastatic burden.

Though the loss of ERα was unfortunate due to the necessity for additional ERα$^+$ ILC cell line models, we could focus on other mechanisms of therapy resistance/response in WCRC-25 without restriction. The therapeutic responses to drugs given to the patient during the treatment course (Doxorubicin, Cisplatin, Paclitaxel), as well as rationally chosen experimental drug BEZ235, were particularly informative considering recent knowledge regarding novel pathways of interest in ILC. *PIK3CA* mutations have been well-described in cancer, and are becoming very intriguing in ILC research[67, 275, 276]. The potency of BEZ235 in WCRC-25 will make it a useful model for the growing field of PI3K/AKT inhibitor work in ILC and in cancer. Also, our unclear observations of the role of BEZ235 in inhibition of PI3K/AKT/mTOR signaling will be further probed considering the increased expression of downstream pathway member *BIRC5*, or Survivin (See Figure 59C, Right Panel). This protein has been shown to inhibit apoptosis, is a newer

therapeutic target in cancer research, and will be among many other interesting targets that we will further explore in this system[281]. These observations were preliminary, and much remains to be discovered in relation to WCRC-25's response to other therapeutics.

For example, an additional therapeutic we will test in WCRC-25 is Palbociclib, a recent FDA-approved inhibitor of CDK4/6[150]. The use of Palbociclib combination therapy has been approved for use in advanced metastatic hormone receptor positive, $HER2^-$ breast cancer, a group of tumors that have essentially become endocrine therapy resistance. If we hypothesize that the loss of ERα expression in our WCRC-25 cells is the result of pressures induced by endocrine therapy resistance, it would be rational to further hypothesize that Palbociclib may show efficacy in this setting. In addition, and as described in the introduction to the dissertation, the ongoing PELOPS trial will evaluate the outcome of combination endocrine therapy and Palbociclib or endocrine therapy alone in ILC and IDC patients. The outcomes of studies like these will be detailed in our upcoming manuscript.

Phenotypically, we observed WCRC-25 behaved similar to other ILC cells. WCRC-25 doubles similarly to MDA-MB-134-VI (~2-3 days) and Sum44PE (5-7 days) ILC cell lines, and faster than comparably sized ILC cell line, MDA-MB-330 (~1.5-2 weeks). The combination of larger size and relatively faster doubling time contribute to faster use of media contents, and enhanced rate of filling the space of a given well. WCRC-25 cells were also able to adapt to their new environments over passage, suggesting that the importance of continuing these cells in their CM-Rocki culture setting was likely unnecessary. CM-Rocki may therefore be important for establishment of a given culture, but once established, other media types may be evaluated for ease of use in future experiments.

Our current phenotypic analyses in ILC have provided little evidence for robust growth behaviors in different environments (2D, soft agar). ILC cells proliferate so slowly compared to other breast cancer cell lines that either insufficient material is available to pursue many assays or to see phenotypes in standard timeframes applied to classic phenotypic assays. For example, we know that our ILC cells do not tend to migrate or invade in classic scratch or Boyden Chamber assays (*Nilgun Tasdemir, PhD unpublished results*). The lack of these phenotypes is likely due to the loss of polarity in these cells induced by loss of E-cadherin; without polarity, the cells are unable to easily follow chemoattractant signals or to collectively invade as IDC cells do[28, 30, 62]. Further, most ILC cells are unable to survive in the highly confluent conditions required of certain experiments (e.g. Scratch assay), and will instead lift off their growth surface to die. This complicates the use of conventional assays and emphasizes the importance of careful tissue culture maintenance and establishment of appropriate plating densities for all experiments. In the future, we will probe the true behaviors of these indolent cell types further, particularly in novel environments of interest for ILC (e.g. ULA). However, the phenotypic assays that will assist in defining the characteristics of these cells will likely need to be modified versions of classically available assays, or novel approaches that test cells that have slower proliferation and loss of polarity.

In conclusion, our novel established ILC cell line, WCRC-25, is a useful tool for ILC research. The comprehensive analyses that we have performed to understand the origin of disease, progression, molecular, phenotypic, and *in vivo* characteristics (ongoing) of this new model would not have been possible without collaborative and trans-disciplinary efforts by a team of investigators. We highly support the use of this novel model as a tool in ILC and cancer research, and look forward to seeing the utility of this system explored further.

4.0 DISCUSSION

Breast cancer is a complex disease comprised of two major histologic subtypes, ILC and IDC. Though nearly 40,000 women are diagnosed annually in the U.S. with ILC, it remains a highly understudied disease[1]. Few studies to date have provided comprehensive analyses of ILC, and of these, we have gained some clinical insight to the progression of disease[67, 115-120]. ILCs are slow growing, difficult to detect, and often recur nearly a decade after the primary diagnosis. These factors all contribute to a unique disease phenotype that necessitates further study in light of the therapeutic interventions that can be provided to patients.

Endocrine therapy resistance is a clinical problem for patients with ILC, and we have observed this phenomenon at a cellular level[132]. Our investigation into the role of 4OHT as an agonist in ILC (Chapter Two) provided evidence that ERα is directed to induce proteins, such as SNAIL, that could potentially contribute to EMT-like phenotypes that are observed in ILC[64]. These data were accompanied by observations of the upregulation of other ERα-regulated targets (*GREB1*, *IGFBP4*) that are known to be E2-induced in IDC cells[132]. However, our observations have suggested that 4OHT can direct the expression of many other proteins (yet to be described) in ILC that are normally repressed or unaffected. Though our manipulation of SNAIL was not successful in suppressing 4OHT partial agonist activity in MDA-MB-134-VI cells, we did uncover a unique limited EMT-TF panel that is upregulated in cell line models (*SNAI1*, *TWIST1*, *FN1*, *VIM*, *CDH2*) and somewhat in ILC clinical samples (*FN1*, *KDM1A*). These data contribute to the ILC research field's understanding of the importance of these EMT profiles in the clinical setting, a debated topic[64, 174]. Additionally, we uncovered an understudied role for SNAIL that was unanticipated based upon prior literature. Induction of SNAIL led to decreased tumorigenic

phenotypes, and suggested that context, both environmentally and of disease subtype, can greatly influence the behaviors of commonly known oncogenes. However, we also noted that manipulation of SNAIL was not well tolerated by ILC cells (MDA-MB-134-VI and Sum44PE knockdown attempts; BCK4 stable inducible overexpression attempt).

Our brief findings regarding the endogenous interaction of SNAIL and LSD1 in ILC, as well as its potential as a therapeutic axis in the disease subtype, should be further explored. The clinical repurposing of FDA-approved agents, when successful, can save decades of development and research, along with billions of dollars. Most importantly, it is a way to fast-track a drug of utility to patients in need. LSD1 inhibitors have been clinically used to treat depression for decades, and are being studied for repurposing as targeted agents in various types of cancer[207, 208]. If this SNAIL/LSD1 axis that we have discovered in ILC is imperative to the phenotypes observed clinically, then LSD1 inhibitors may also have utility in ILC.

Observations such as those made regarding the SNAIL/LSD1 axis in ILC may or may not have direct implications in endocrine therapy resistance. The ongoing window trial by Jankowitz and colleagues will provide the first analyses of ER-regulated gene targets in ILC patients treated with either Tamoxifen, Anastrazole, or Fulvestrant[121]. It would be beneficial to assess *SNAI1* and other EMT-TF related target gene expressions in the Tamoxifen treated group, in particular. For example, *TWIST1* was not modified by 4OHT treatment in our studies, but has been observed to be upregulated in LCIS and ILC clinical samples[64, 180]. Further studies related to the implications of *TWIST1* in ILC would be beneficial, within the scope of endocrine therapy resistance or disease development and progression. Overall, these data will provide additional gene targets in the clinical setting that are altered in relation to endocrine therapy treatments.

The second portion of our work was devoted to the establishment and characterization of a novel ILC cell line. There are 7 (now 8 with the characterization of WCRC-25) ILC cell lines in existence today, and the classification of many of these cell lines as ILC is still debated in the field. We supplied a complete and comprehensive story about WCRC-25, an epithelial, ERα$^-$ cell line derived from the pleural effusion of an ILC patient (Chapter Three). Our clinical observations of the patient were supplemented with genetic and expression analyses that allowed us to reveal a novel *CDH1* mutation in ILC (*CDH1* Q706*).

We continue to probe additional mutations in MammaSeq analyses. MammaSeq is an Ion Torrent sequencing panel comprised of 78 genes, with 688 amplicons targeting 1398 mutations (*Smith et al in preparation*; trademark of UPMC). Preliminary analyses are currently ongoing, but we have already observed an additional unique *CDH1* mutation at Q23* in some of our patient samples, along with mutations in *PIK3CA* and *TP53*. These data will assist in our understanding of the timeline of the patient's disease from the primary lesions to the metastatic lesions.

Importantly, we have contributed a novel model to the field of ILC research, as well as the larger cancer research community. WCRC-25 responds to PI3K/AKT/mTOR inhibitor BEZ235 in two unique phenotypic environments (2D, ULA). This observation makes sense considering the recently defined, common occurrence of PI3K/AKT activation in ILC patients[67]. Interestingly, the signaling alterations observed were restricted to a mild decrease of pAKT^{S473}, and less clear with regard to mTOR signaling (S6$^{235/236}$). Our future analyses will probe other parts of the PI3K/AKT/mTOR pathway to understand the mechanism behind the 2D/ULA proliferation inhibition by BEZ235. Additionally, considering our observations in the WCRC-25 clinical samples from the end of the patient's life, *BIRC5* may be another interesting target to pursue in relation to PI3K/AKT/mTOR downstream signaling[281]. Finally, the low levels of *ESR1*

expression in WCRC-25 relative to negative control MDA-MB-231 suggest a very low level of endogenous expression. This observation will be pursued in future studies by attempting to re-express ERα in WCRC-25 cells to test response to E2 and other endocrine modalities. WCRC-25 will therefore be a key model in future analyses related to understanding PI3K/AKT pathway regulation in ILC, and endocrine therapy resistance. Our ongoing studies with therapeutics, phenotypes, and *in vivo* modeling will culminate in a publication after the completion of this dissertation.

In summary, ILC is a unique disease within breast cancer, and is characterized by late endocrine therapy resistance. Our studies have established the upregulation of an EMT-like program in ILC, as well as have contributed a novel model system to the field of research. These combined data lay a foundation for future work in understanding the clinical impacts of current therapeutic regimens for ILC patients, and offer insight into understanding the complex process of disease progression that has been relatively undefined for this patient subset. This basic knowledge and novel tool will assist in pursuing improved therapeutic options for patients afflicted with ILC.

APPENDIX A

qRT-PCR primers utilized in Chapters Two and Three are provided below.

Table 5: qRT-PCR Primers

Gene	Forward Sequence (5' → 3')	Reverse Sequence (5' → 3')
CDH1	GAACAGCACGTACACAGCCCT	GCAGAAGTGTCCCTGTTCCAG
CDH2	GACGGTTCGCCATCCAGAC	TCGATTGGTTTGACCACGG
ESR1	GAGTATGATCCTACCAGACCCTTC	CCTGATCATGGAGGGTCAAATC
FN1	CCGCCGAATGTAGGACAAGA	TGCCAACAGGATGACATGAAA
GREB1	GGTTCTTGCCAGATGACAATGG	CTTGGGTTGAGTGGTCAGTTTC
KDM1A	CTAATGCCACACCTCTCTCAA	ACACGAGTAGCCATTCCTTAC
PGR	TCGCCTTAGAAAGTGCTGTC	GCTTGGCTTTCATTTGGAACG
RPLP0	TAAACCCTGCGTGGCAATC	TTGTCTGCTCCCACAATGAAA
SNAI1	GGAAGCCTAACTACAGCGAG	CAGAGTCCCAGATGAGCATTG
SNAI2	AGCATTTCAACGCCTCCA	GGATCTCTGGTTGTGGTATGAC
SNAI3	GTGAAAACGCACTCCAGC	AGAGCAGGCACCATTGATT
TWIST1	TGTCCGCGTCCCACTAGC	TGTCCATTTTCTCCTTCTCTGGA
VIM	CAACCTGGCCGAGGACAT	ACGCATTGTCAACATCCTGTCT

Antibodies used in IB experiments from both chapters are listed below.

Table 6: Antibodies Used in IB Experiments

Protein	Company	Catalog Number	Host Species	Dilution
αSMA	Abcam	ab5694	Rabbit	1:1000
Actin	Sigma	A5441	Mouse	1:5000
AKT	Cell Signaling	2920	Mouse	1:1000
$pAKT^{T308}$	Cell Signaling	13038	Rabbit	1:1000
$pAKT^{S473}$	Cell Signaling	4060	Rabbit	1:1000
E-cadherin	BD Biosciences	610182	Mouse	1:1000
ERα	Leica Biosystems	6F11	Mouse	1:200
LSD1	Cell Signaling	2184S	Rabbit	1:1000
S6	Cell Signaling	2217S	Rabbit	1:1000
$pS6^{S235/236}$	Cell Signaling	4858S	Rabbit	1:1000
SNAIL	Cell Signaling	3895S	Mouse	1:500
TWIST1	Abcam	ab50887	Mouse	1:500

Antibodies used in ChIP or IP experiments are provided here.

Table 7: Antibodies Used in ChIP or IP Experiments

Protein	**Company**	**Catalog Number**	**Host Species**	**Concentration**
ERα	Santa Cruz	sc-543	Rabbit	2-4 µg
LSD1	Abcam	ab17721	Rabbit	2-5 µg
SNAIL	Cell Signaling	3895S	Mouse	2 µg
SNAIL	R & D Systems	AF3639	Goat	10 µg
IgG	Santa Cruz	sc-2027	Rabbit	2-4 µg
ChIP Grade IgG	Abcam	ab46540	Rabbit	2-5 µg
IgG	Santa Cruz	sc-2025	Mouse	2 µg
IgG	Santa Cruz	sc-2028	Goat	10 µg

ChIP qRT-PCR primers utilized in Chapter Two are listed below.

Table 8: ChIP qRT-PCR Primers

Gene	**Forward Sequence (5' → 3')**	**Reverse Sequence (5' → 3')**
GREB1	GTGGCAACTGGGTCATTCTGA	CGACCCACAGAAATGAAAAGG
IGFBP4	GGGTTGGGCAAGGAAAAGTT	GGGTTGGGCAAGGAAAAGTT
NFERE	CTGCCTAGGCTGGGATAACA	ATCAGGCATCTGTGCTTCCT
SNAI1	TCCCTTGATAATTCTTCACTTCCT	AAGGGAAGTGTGCTTTGGT

Plasmids utilized in viral studies in Chapter Two are listed below.

Table 9: Plasmids Used in Viral Knockdown Studies

Plasmid	Backbone	Sel	GFP	Virus	Use	Sequence
*sh*PASHA	N/A	N/A	N	Lenti	RNAi	N/A
pLp1	3rd Gen	N/A	N	Lenti	Pack	N/A
pLp2	3rd Gen	N/A	N	Lenti	Pack	N/A
pLp3 VSVG	3rd Gen	N/A	N	Lenti	Pack	N/A
*sh*Scramble	pLKO.1	Puro	N	Lenti	Const	N/A
*sh*SNAI1*18*	pLKO.1	Puro	N	Lenti	Const	CCAATCGGAAGCCTAACTACA
*sh*SNAI1*19*	pLKO.1	Puro	N	Lenti	Const	CCAAGGATCTCCAGGCTCGAA
*sh*SNAI1*20*	pLKO.1	Puro	N	Lenti	Const	GCAGGACTCTAATCCAGAGTT
*sh*SNAI1*21*	pLKO.1	Puro	N	Lenti	Const	CCACTCAGATGTCAAGAAGTA
*sh*SNAI1*22*	pLKO.1	Puro	N	Lenti	Const	CCAGGCTCGAAAGGCCTTCAA
VSVG	2nd Gen	N/A	N	Retro	Pack	N/A
*sh*Renilla*713*	miR-E LEPG (pMSCV)	Puro	Y	Retro	Const	CAGGAATTATAATGCTTATCTAT AGTGAAGCCACAGATGTATAGA TAAGCATTATAATTCCTATGCCT A
*sh*CDH1*2*	miR-E LEPG (pMSCV)	Puro	Y	Retro	Const	CTAGGAGTTCTCTGATGCAGAAT AGTGAAGCCACAGATGTATTCTG CATCAGAGAACTCCTAT
*sh*CDH1*150*	miR-E LEPG (pMSCV)	Puro	Y	Retro	Const	CAAGTGTGTTCATTAATGTTTAT AGTGAAGCCACAGATGTATAAA CATTAATGAACACACTTA
*sh*SNAI1*150*	miR-E LEPG (pMSCV)	Puro	Y	Retro	Const	AAGGACTCTAATCCAGAGTTTAT AGTGAAGCCACAGATGTATAAA CTCTGGATTAGAGTCCTG
*sh*SNAI1*544*	miR-E LEPG (pMSCV)	Puro	Y	Retro	Const	CCAACTGCAAATACTGCAACAA TAGTGAAGCCACAGATGTATTGT TGCAGTATTTGCAGTTGA
*sh*SNAI1*763*	miR-E LEPG (pMSCV)	Puro	Y	Retro	Const	CCCAGACCCACTCAGATGTCAAT AGTGAAGCCACAGATGTATTGA CATCTGAGTGGGTCTGGA
*sh*SNAI1*1019*	miR-E LEPG (pMSCV)	Puro	Y	Retro	Const	CCAGGACTTTGATGAAGACCATT AGTGAAGCCACAGATGTAATGG TCTTCATCAAAGTCC
*sh*SNAI1*1666*	miR-E LEPG (pMSCV)	Puro	Y	Retro	Const	CCAGTTTATTGATATTCAATAAT AGTGAAGCCACAGATGTATTATT GAATATCAATAAAC
pMDL	3rd Gen	N/A	Y	Lenti	Pack	N/A
pREV	3rd Gen	N/A	Y	Lenti	Pack	N/A
pVSVG	3rd Gen	N/A	Y	Lenti	Pack	N/A
*sh*Renilla*713*	miR-E LT3GEPIR (pRRL)	Puro	Y	Lenti	Ind	See Above
*sh*Renilla*826*	miR-E LT3GEPIR (pRRL)	Puro	Y	Lenti	Ind	N/A
*sh*SNAI1*150*	miR-E LT3GEPIR (pRRL)	Puro	Y	Lenti	Ind	Subcloned from above
*sh*SNAI1*544*	miR-E LT3GEPIR (pRRL)	Puro	Y	Lenti	Ind	Subcloned from above
*sh*SNAI1*763*	miR-E LT3GEPIR (pRRL)	Puro	Y	Lenti	Ind	Subcloned from above
*sh*SNAI1*1019*	miR-E LT3GEPIR (pRRL)	Puro	Y	Lenti	Ind	Subcloned from above
*sh*SNAI1*1666*	miR-E LT3GEPIR (pRRL)	Puro	Y	Lenti	Ind	Subcloned from above

Table 10: Plasmids Used in Viral Overexpression SNAIL Studies

Plasmid	Backbone	Sel	GFP	Virus	Use	Sequence
pLp1	3rd Gen	N/A	N	Lenti	Pack	N/A
pLp2	3rd Gen	N/A	N	Lenti	Pack	N/A
pLp3 VSVG	3rd Gen	N/A	N	Lenti	Pack	N/A
SNAI1 *ORF124*	pENTR-221	N/A	N	Lenti	Gateway	Targets NM_005985.2
W118	pLENTI-CMV	G418	N	Lenti	Const	N/A
W118-SNAI1	pLENTI-CMV	G418	N	Lenti	Const	Targets NM_005985.2
pMDL	3rd Gen	N/A	N	Lenti	Pack	N/A
pREV	3rd Gen	N/A	N	Lenti	Pack	N/A
pVSVG	3rd Gen	N/A	N	Lenti	Pack	N/A
pINDUCER20	pINDUCER20	G418	N	Lenti	Ind	N/A
pINDUCER20-SNAI1	pINDUCER20	G418	N	Lenti	Ind	Targets NM_005985.2

Below is a table of antibodies utilized for all IF studies in Chapter Three.

Table 11: IF Antibodies for WCRC-25 Characterization Studies

IF Marker	Company	Catalog Number	Lot Number	Host Species	Dilution
DAPI	Thermo Fisher	P36962	1850967	N/A	~15 µL
Anti-Mouse AlexaFluor488	Invitrogen	A11017	1694699	Mouse	1:200
Anti-Rabbit AlexaFluor488	Invitrogen	A21206	57542A	Rabbit	1:200
Anti-Rat AlexaFluor488	Invitrogen	A11006	1728142	Rat	1:200
CK5	Leica	CK5-L-CE	Unknown	Mouse	1:200
CK8/18	DSHB Troma	Troma-1-c	Unknown	Rat	1:200
CK14	Covance	PRB-155P-100	D14IF01918	Rabbit	1:200
EpCAM	Cell Signaling	2929S	5	Mouse	1:200
α-SMA	Abcam	ab5694	GR87726-1	Rabbit	1:400
FAP	Abcam	ab28244	GR132121-8	Rabbit	1:200
ERα	Leica	NCL-L-ER-6F11	6039612	Mouse	1:50
E-cadherin	BD Biosciences	610182	5113982	Mouse	1:100

Below is a table of antibodies used in the UPMC system for ERα or E-cadherin/p120 IHC in Chapter Three.

Table 12: IHC Markers for Clinical Sample Staining

IHC Marker	Company	Catalog Number	Host Species	Dilution
ERα	Leica	NCL-L-ER-6F11	Mouse	1:50
ERα (SP1)	Ventana	790-4324	Rabbit	*Unknown*
E-cadherin (Clone 36)	Ventana/Roche	790-4497	Mouse	*Unknown*
p120	BD Biosciences	610134	Mouse	1:200

Primers used to cover the entire exon regions of *CDH1* are listed below.

Table 13: Primers for Complete *CDH1* cDNA Sanger Sequencing

Exon Region	**Forward Sequence (5' → 3')**	**Reverse Sequence (5' → 3')**
1-5	TGAGCTTGCGGAAGTCAGTT	GCGTGAGAGAAGAGAGTGTATG
5-9	GACAGAAGAGAGACTGGGTTATTC	CCATCGTTGTTCACTGGATTTG
9-11	CAGTCACTGACACCAACGATAA	CATCAGACAGGATCAGCAGAAG
11-14	TGGGCCAGGAAATCACATCC	TGCAACGTCGTTACGAGTCA
13-16	CGACCCAACCCAAGAATCTATC	TGGACATCACCACCATGTAAAG
Full Length	TGAGCTTGCGGAAGTCAGTT	TGGACATCACCACCATGTAAAG

APPENDIX B

The following section is comprised of all supplemental data for Chapter 2.

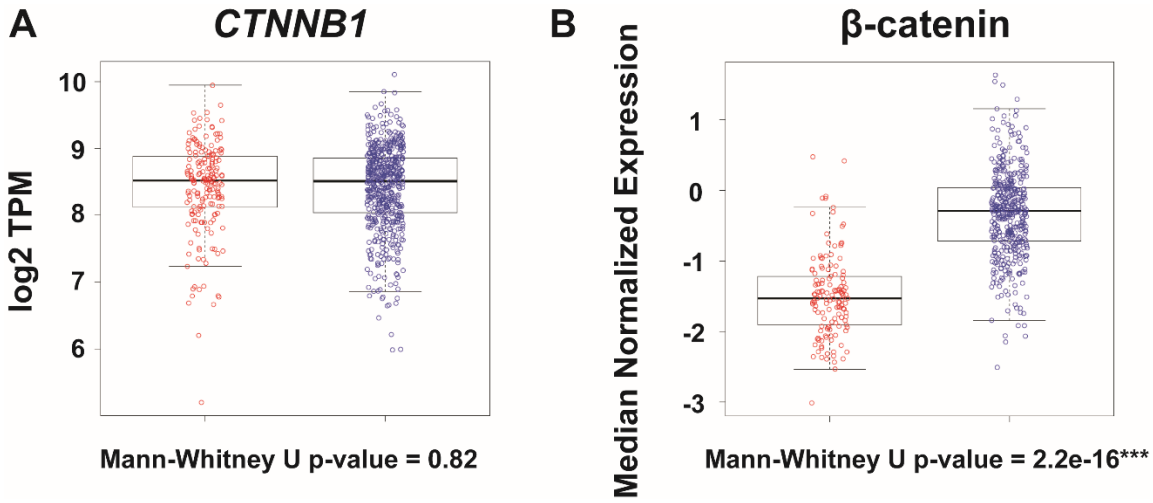

Figure 64: *CTNNB1* is Not Significantly Different Between ILC and IDC Primary Lesions, But Protein is Significantly Reduced in ILC Compared to IDC
(A) RNA Sequencing data from TCGA primary ILC (n = 184, red) and IDC (n = 584, blue) ERα^{+} samples was analyzed for expression of *CTNNB1*. (B) RPPA from TCGA primary ILC (n = 137, red) and IDC (n = 417, blue) samples was analyzed for expression of β-catenin. Mann-Whitney U p-values were applied to each data set. Data were analyzed in collaboration with Kevin Levine, BS.

Figure 65: Complete ILC E2 RPPA

Complete RPPA data was obtained from the previously described experiment (see 2.3.2) performed in MDA-MB-134-VI and Sum44PE for (A) E2-upregulated or (B) E2-downregulated proteins in MDA-MB-134-VI (see Figure 5). Data were sorted by log2 normalized median centered induction relative to deprived controls. EMT proteins are highlighted with red asterisks.

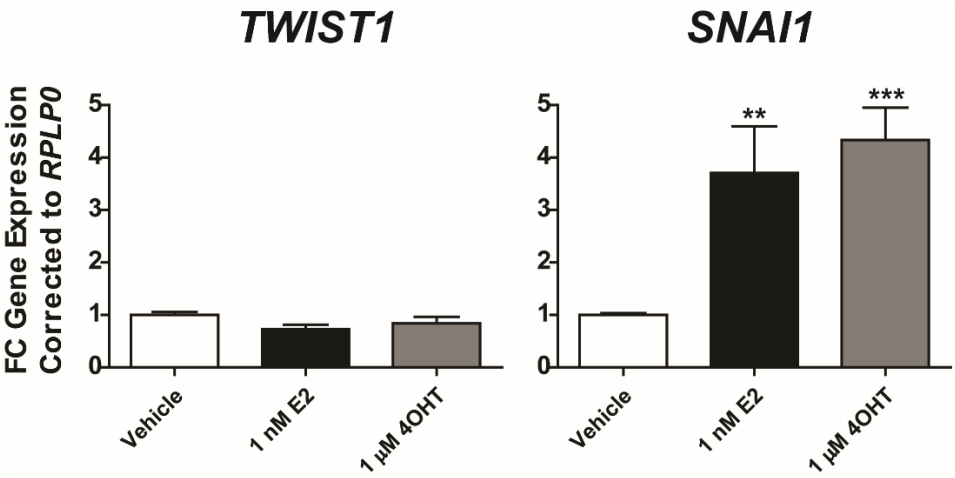

Figure 66: *TWIST1* is Not Regulated by 4OHT or E2 in MDA-MB-134-VI
TWIST1 or *SNAI1* qRT-PCR were performed in MDA-MB-134-VI at the 8-hour treatment time point after E2 deprivation and treatment with Vehicle (0.1% DMSO), 1 nM E2, or 1 µM 4OHT. Quantifications are a representative single experiment ± STDEV of technical triplicates. Asterisks depict significance compared to Vehicle from One Way ANOVA followed by Tukey's post-test (*p < 0.05, **p < 0.005, ***p < 0.0005).

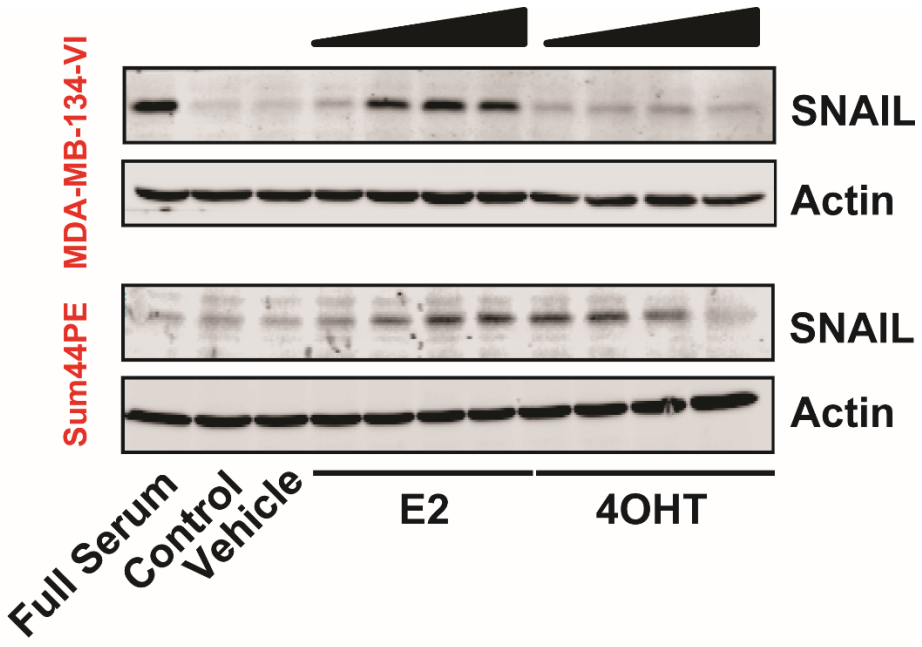

Figure 67: Dose Responses of 4OHT, E2 Show SNAIL Protein Induction in MDA-MB-134-VI and Sum44PE ILC Cells
MDA-MB-134-VI and Sum44PE cells were treated to E2 deprivation assay with increasing doses of E2 (0.01, 0.1, 1, 10 nM) or 4OHT (0.01, 0.1, 1, 10 µM) administered for 24 hours. IB is representative of a single experiment with single replicates per treatment condition at 50 µg/lane.

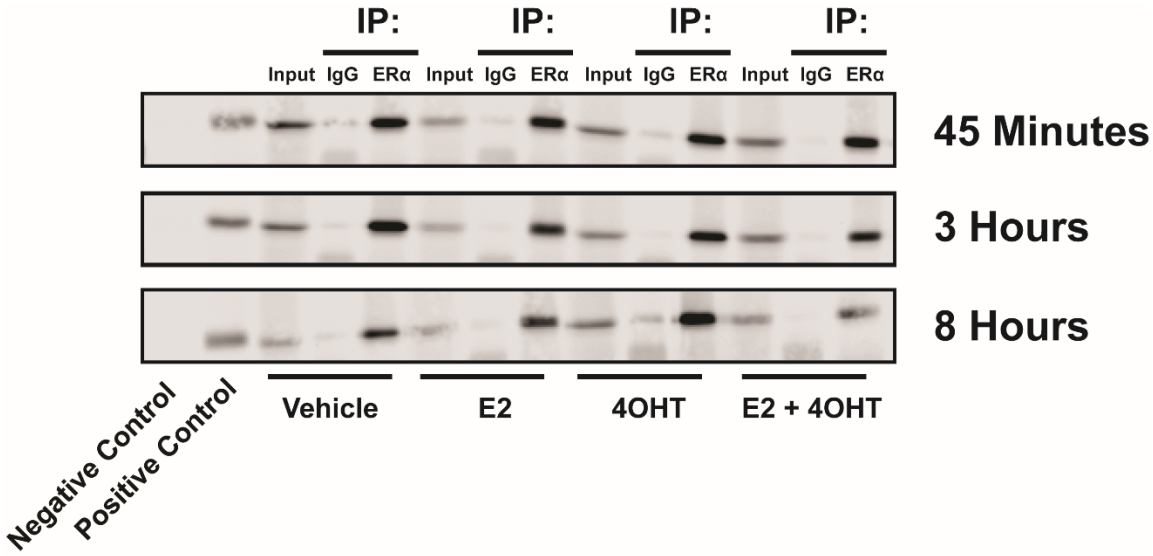

Figure 68: ERα ChIP Time Course IP Confirmation
MDA-MB-134-VI cells were treated to E2 deprivation followed by Vehicle (0.1% DMSO), 10 nM E_2, 10 µM 4OHT, or combination treatments for 45 minutes, 3 hours, or 8 hours. After initial ChIP processing, ERα IP was performed to validate use of samples in ChIP qRT-PCR. Negative control is MDA-MB-231 whole cell lysate, and Positive Control is MCF-7 whole cell lysate.

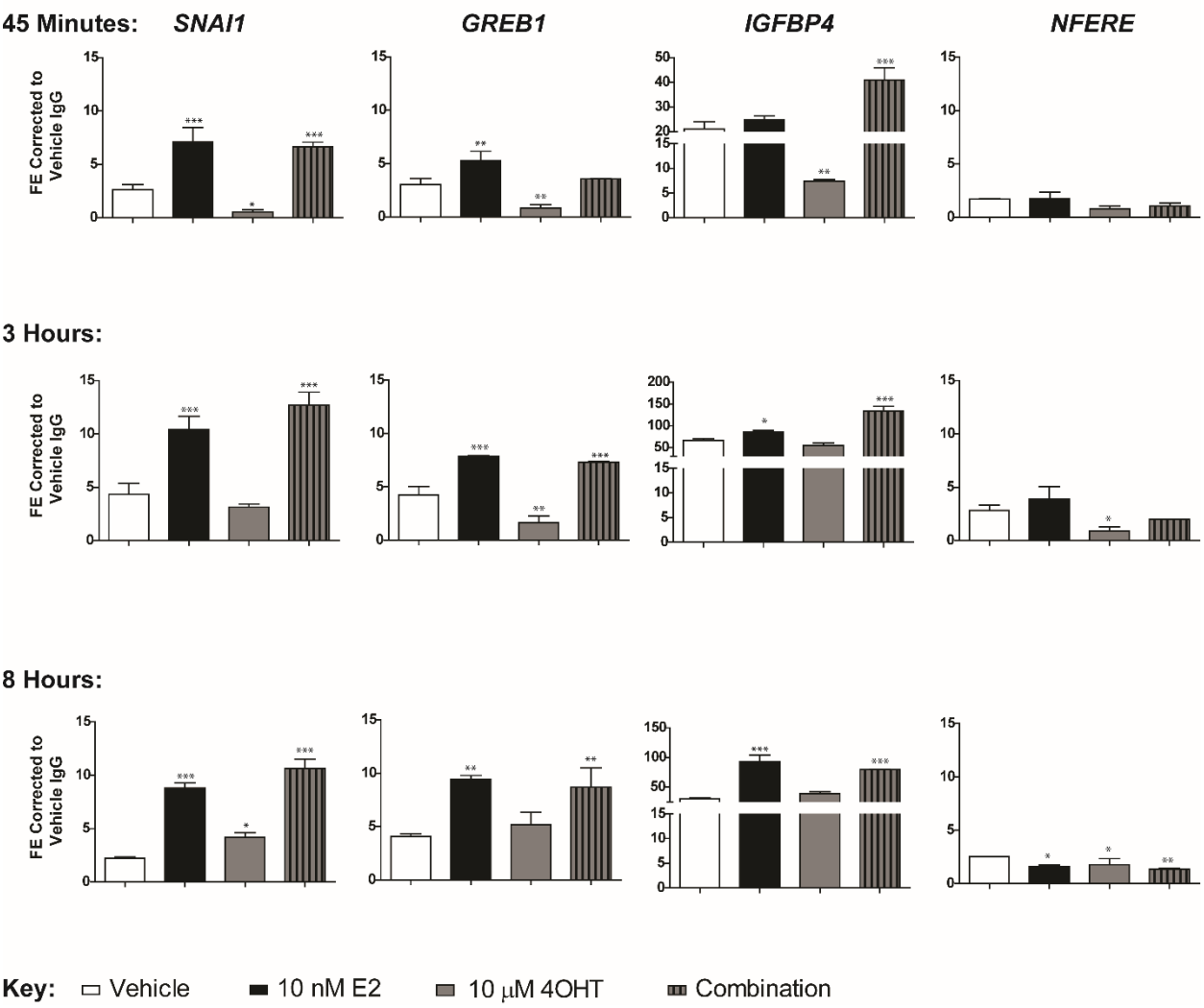

Figure 69: ERα ChIP qRT-PCR Time Course

MDA-MB-134-VI cells were treated to E2 deprivation followed by Vehicle (0.1% DMSO), 10 nM E2, 10 μM 4OHT, or combination treatments for 45 minutes, 3 hours, or 8 hours. ChIP qRT-PCR was performed for *SNAI1*, *GREB1*, and *IGFBP4* ERE conserved binding regions. *NFERE* was used as a negative control. Data represent one experiment with technical triplicates plated during the qRT-PCR ± STDEV. Asterisks depict significance compared to Fold Enrichment (FE) Vehicle after correction to Vehicle IgG for all samples with One Way ANOVA followed by Tukey's post-test (*$p < 0.05$, **$p < 0.005$, ***$p < 0.0005$).

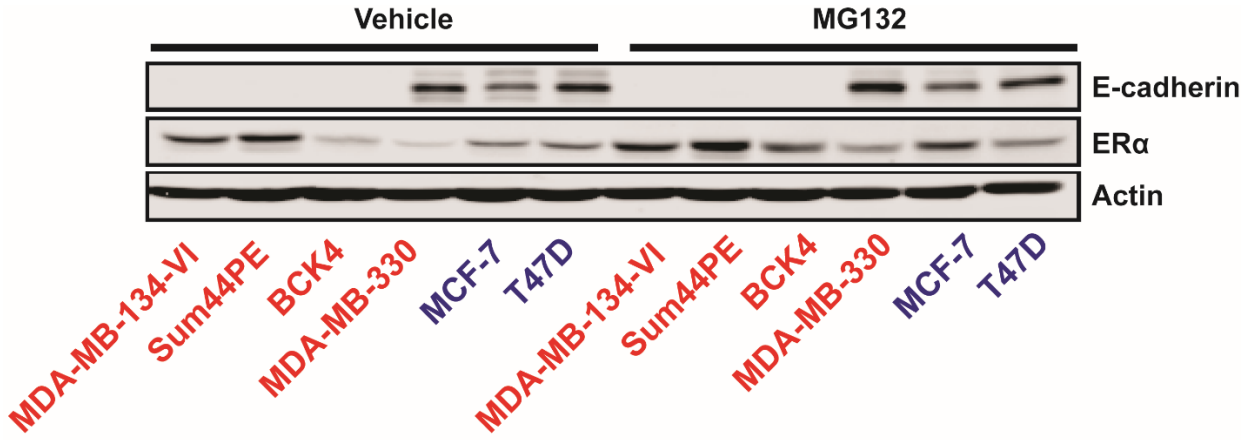

Figure 70: E-cadherin and ERα Protein Statuses of ILC and IDC Cell Lines Utilized in Experiments

Prior to probing for SNAIL and TWIST1 protein expressions, confirmation of E-cadherin and ERα statuses was performed in our panel of ILC and IDC cell lines by IB. A representative experiment is shown from three independently performed experiments treated ± 5 µM MG132 for 2 hours with 50 µg whole cell lysate/lane.

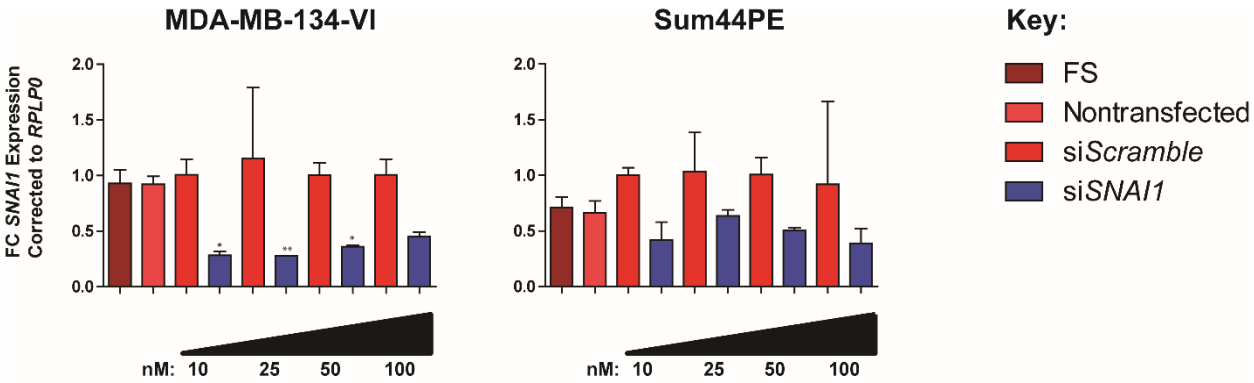

Figure 71: Transient *SNAI1* Knockdown Dose Response in ILC Cells

MDA-MB-134-VI and Sum44PE were subjected to reverse transfection of escalating doses of si*Scramble* or si*SNAI1*. Full Serum (FS) and Nontransfected cells served as additional controls. qRT-PCR for *SNAI1* was performed with technical triplicate samples ± STDEV, for a single experiment shown. Asterisks depict significance as determined by One Way ANOVA followed by Tukey's post-test with comparisons to each respective concentration-matched si*Scramble* (*$p < 0.05$, **$p < 0.005$, ***$p < 0.0005$).

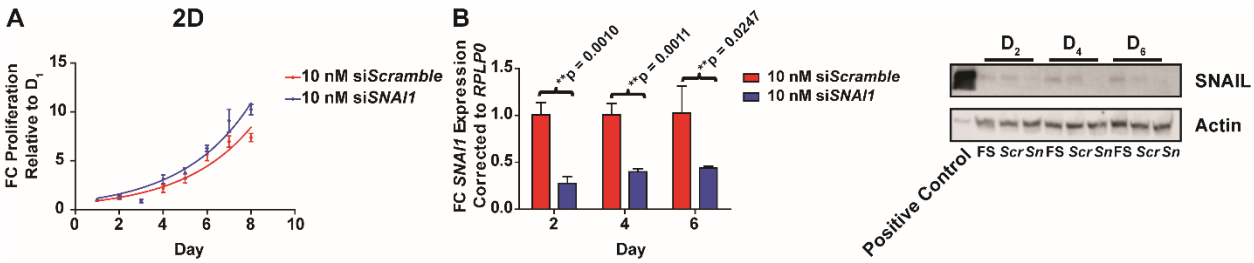

Figure 72: Transient *SNAI1* Knockdown 2D Proliferation Phenotype Is Present at Later Time Points, as Are mRNA and Protein Knockdown

MDA-MB-134-VI cells were transiently reverse transfected with 10 nM Scramble or *SNAI1* siRNA. (A) 2D proliferation was measured from $D_{1\text{-}8}$ with six technical replicates per time point/condition ± STDEV, normalized to D_1 values, and fitted with non-linear regression with comparison of rates performed (*p < 0.05, **p < 0.005, ***p < 0.0005). (B) qRT-PCR for *SNAI1* at $D_{2,4,6}$ was performed with technical triplicate samples ± STDEV. Students t-test was performed at each time point, with asterisks denoting significance (*p < 0.05, **p < 0.005, ***p < 0.0005). Data are representative of three independent experiments. Protein were isolated at the same time points to show levels of SNAIL in full serum (FS), Scramble siRNA (Scr), or *SNAI1* siRNA (Sn) treated cells relative to Actin internal control.

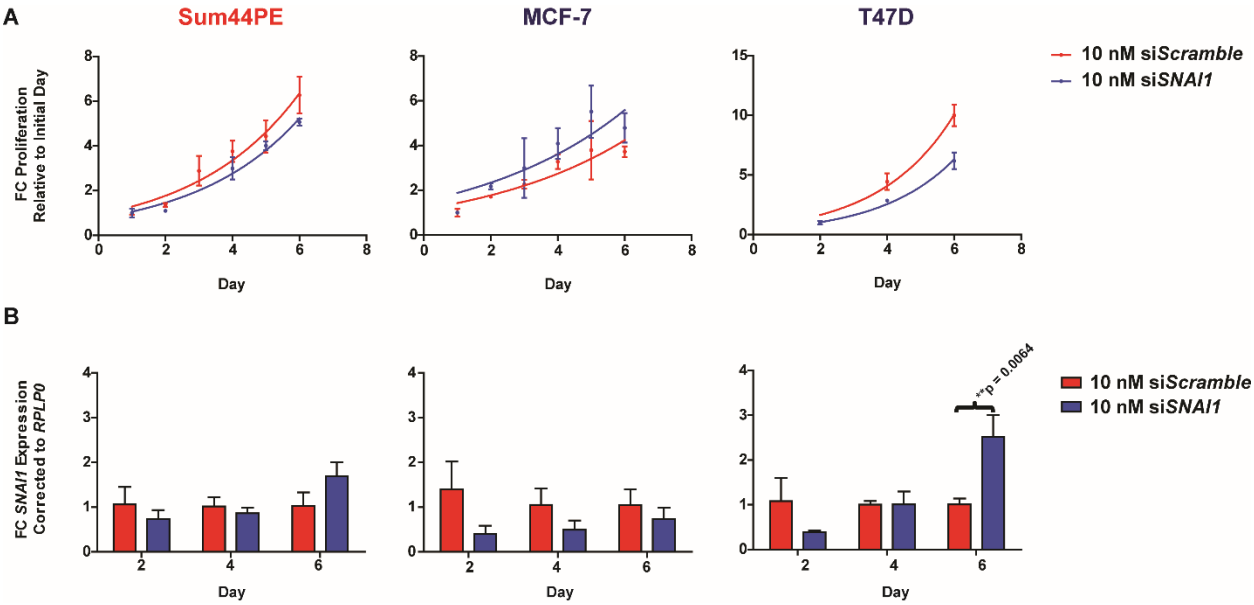

Figure 73: Transient *SNAI1* Knockdown Phenotypes are Not Stable or Repeatable in Sum44PE, MCF-7, or T47D, and Knockdown Rebounds

Sum44PE, MCF-7, and T47D were treated to the same experimental conditions for (A) 2D proliferation and (B) qRT-PCR as performed for MDA-MB-134-VI (see Figure 16). Representative data from single experiments of two attempts (Sum44PE, T47D) or of three attempts (MCF-7) are displayed with (A) six or (B) three replicate samples ± STDEV. Statistics were applied as previously (see Figure 16).

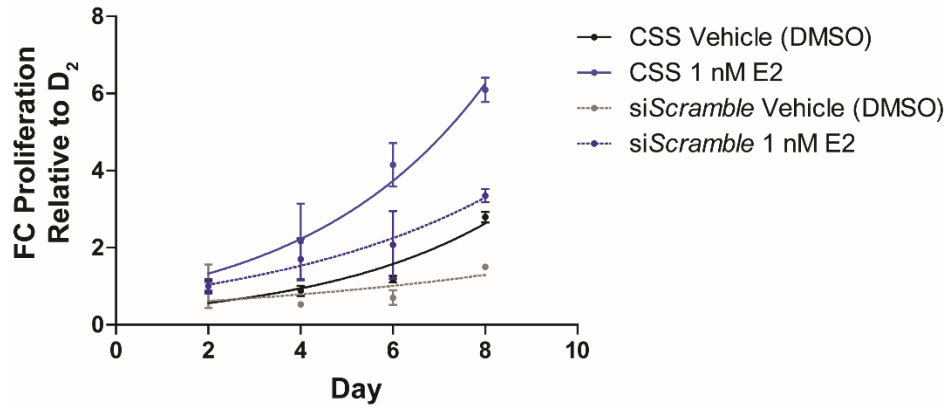

Figure 74: E2 Deprivation/si*RNA* Studies Caused Decreased Proliferation for si*Scramble* Cells
MDA-MB-134-VI cells were subjected to E2 deprivation, followed by reverse transfection with nothing (CSS) or si*Scramble* control si*RNA*. Cells were then treated to Vehicle (0.1% DMSO) or 1 nM E2 for 8 days. Data were analyzed as in Figure 17 with the same numbers of technical replicates and statistical considerations.

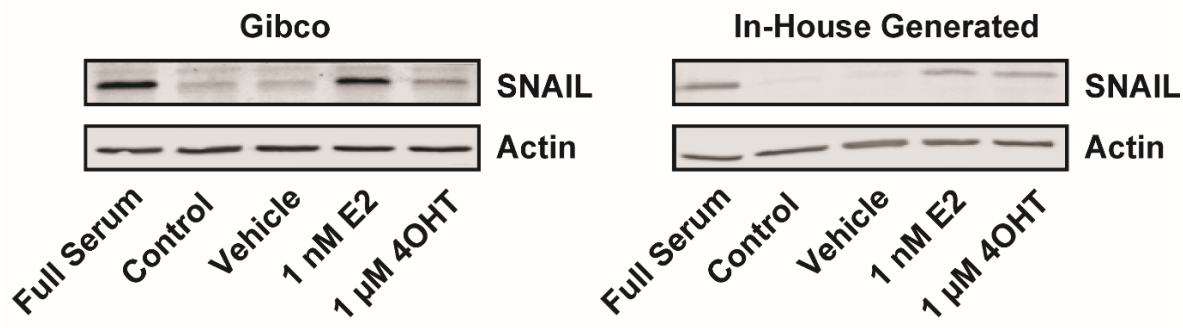

Figure 75: Different CSS Lots Were an Additional Source of Experimental Variation
Changes in CSS lot usage and results obtained were noted throughout this dissertation. Initial experiments utilized Gibco CSS, and use transitioned to in-house generated lots that varied with each batch, or Gemini. IBs (50 µg protein/lane) from representative comparison E2 deprivation experiments in MDA-MB-134-VI are shown above to highlight differences in responses obtained with same protocol, different sera.

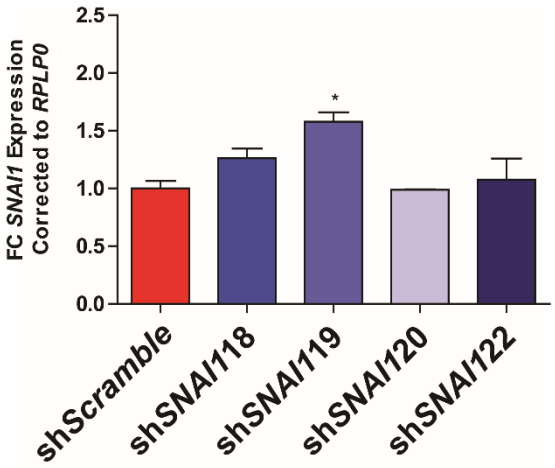

Figure 76: Lentiviral Stable Knockdown of SNAIL was Difficult to Maintain
qRT-PCR was performed on lentiviral stable SNAIL knockdown MDA-MB-134-VI cell lines for *SNAI1*, one passage out from the preliminary experiment (see Figure 18). Data are representative of a single experiment with technical duplicates ± STDEV normalized to sh*Scramble* control with One Way ANOVA followed by Tukey's post-test (*$p < 0.05$, **$p < 0.005$, ***$p < 0.0005$).

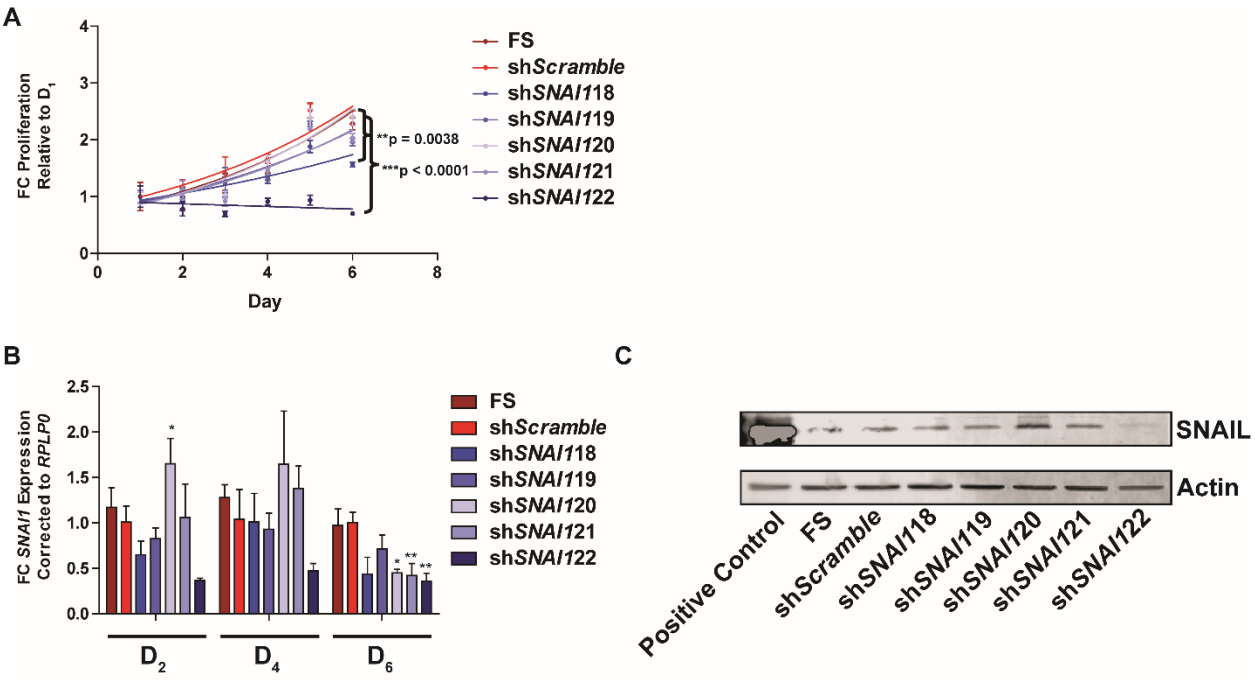

Figure 77: Transient Virus SNAIL Knockdown Panel Often Produced Phenotype and Expression Alterations That Did Not Match

The complete original lentiviral panel against *SNAI1* was utilized in the transient virus assay format to test effects on (A) 2D proliferation, (B) qRT-PCR of *SNAI1* at $D_{2,4,6}$, and (C) D_6 IB. Data were analyzed as previously and represent a single experiment containing (A) six technical replicates ± STDEV with non-linear regression and comparison of rates (*p < 0.05, **p < 0.005, ***p < 0.0005), or (B) triplicate samples normalized to sh*Scramble SNAI1* expression on each day ± STDEV followed by One Way ANOVA with Tukey's post-test (*p < 0.05, **p < 0.005, ***p < 0.0005).

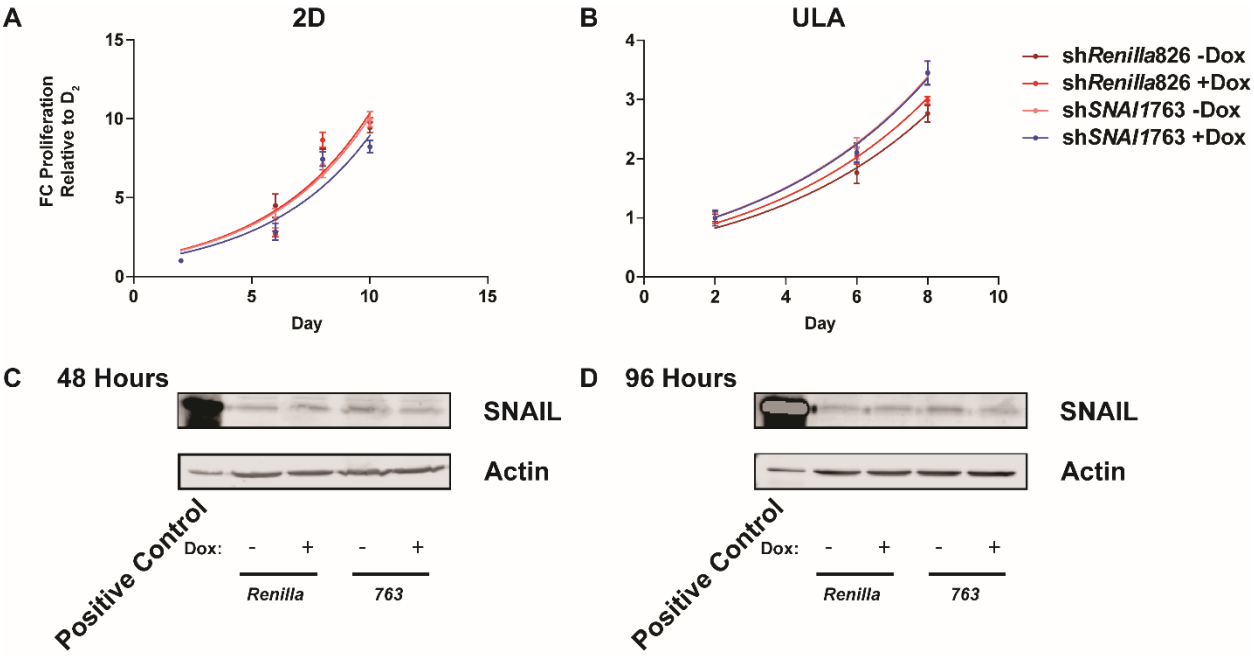

Figure 78: Inducible *SNAI1* Retroviral Knockdown System Generation Was Initially Unsuccessful

Upon acquisition of MDA-MB-134-VI inducible retroviral *SNAI1* knockdown cells, (A) 2D proliferation, (B) ULA proliferation, and (C) 48 Hour or (D) 96 Hour time point assays were plated. Cells were treated to ± 0.5 µg/mL Dox the morning after plating cells. Six technical replicates for each treatment/time point were utilized ± STDEV with normalization to D_2 and comparison of rates after non-linear regression fits (*$p < 0.05$, **$p < 0.005$, $p < 0.0005$).

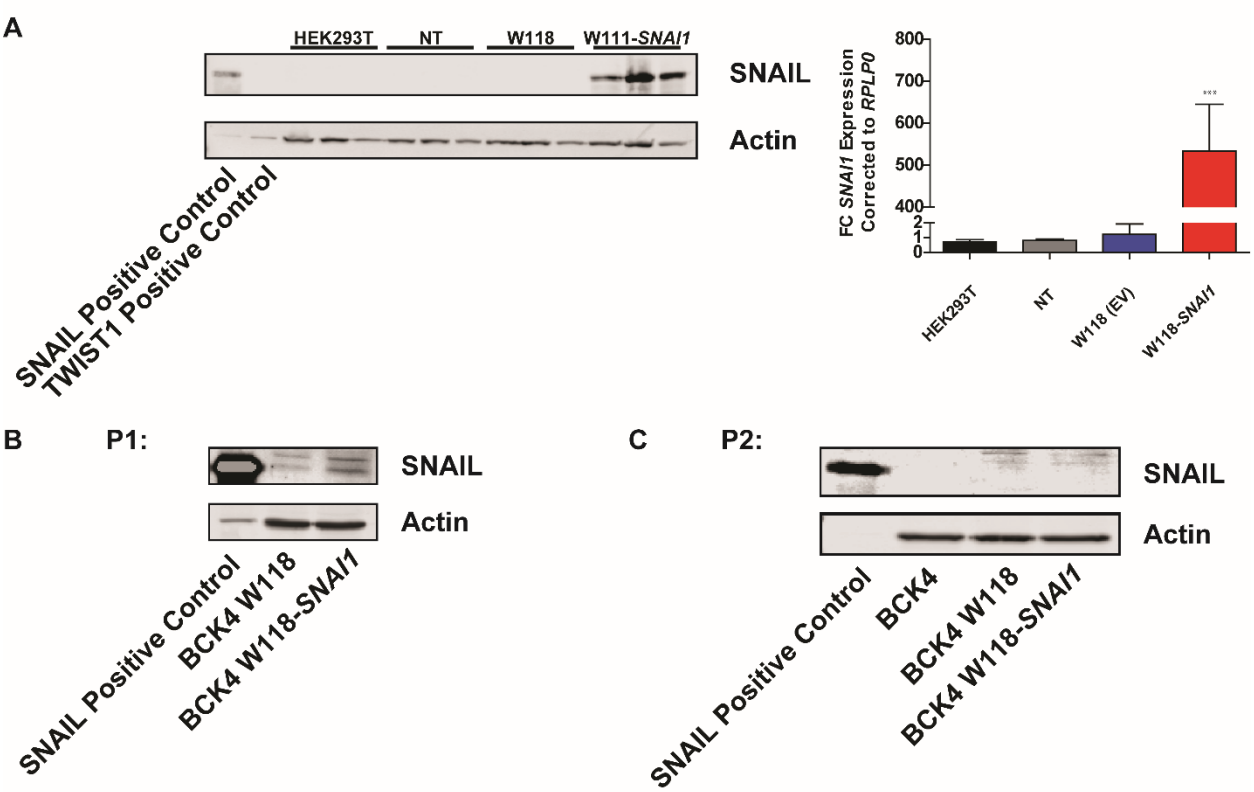

Figure 79: Lentiviral Stable *SNAI1* Overexpression Also Was Not Effectively Maintained
Prior to using the lentiviral plasmid for *SNAI1* overexpression in ILC cells, (A) Empty Vector (*EV*) W118 or W118-*SNAI1* were transfected into HEK293T cells and assessed by technical triplicates for both IB and qRT-PCR to assess SNAIL upregulation. qRT-PCR is displayed ± STDEV, normalized to *EV* control, and data compared with One Way ANOVA followed by Tukey's post-test (*$p < 0.05$, **$p < 0.005$, ***$p < 0.0005$). (B) BCK4 cells were stably infected with W118 or W118-*SNAI1* and measured for SNAIL overexpression by IB (50 µg/lane). (C) Lysates were assessed at the next passage by IB (50 µg/lane).

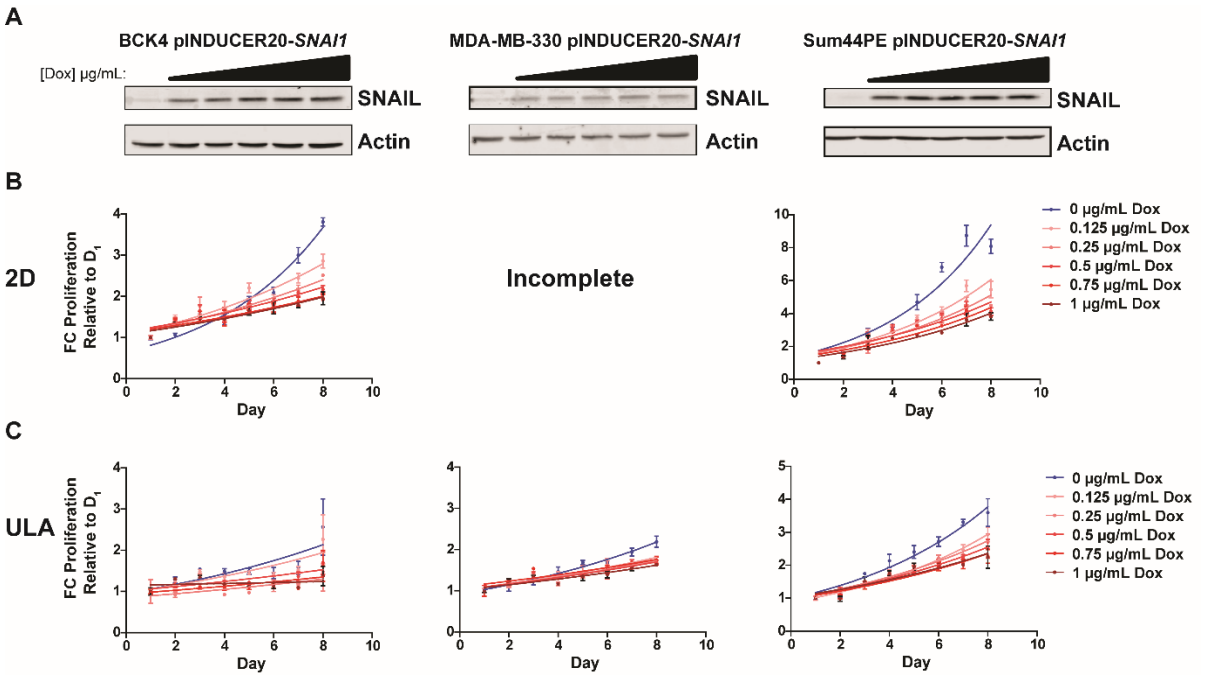

Figure 80: Dox Dose Responses in Inducible SNAIL Overexpression Coincide with Increased Proliferation in 2D, ULA

BCK4, MDA-MB-330, and Sum44PE pINDUCER20-*SNAI1* cells were plated for a Dox dose response. (A) IB for SNAIL was performed at the 48-hour time point with increasing doses of Dox loaded from left to right on each respective blot (25 µg/lane). (B) 2D and (C) ULA proliferation were assessed with increasing doses of Dox in technical triplicates ± STDEV for each respective treatment/time point with normalization to D_1 values and comparison of rates after non-linear regression fits (*p < 0.05, **p < 0.005, ***p < 0.0005).

Table 14: Dox Inducible *SNAI1* Dose Response p-Values from 2D, ULA Proliferation Assays

All comparisons are relative to -Dox	***2D***		***ULA***	
BCK4 pINDUCER20-*SNAI1*	**0.125 µg/mL:**	***p < 0.0001	**0.125 µg/mL:**	*NS* p = 0.6336
	0.25 µg/mL:	***p < 0.0001	**0.25 µg/mL:**	*NS* p = 0.1270
	0.5 µg/mL:	***p < 0.0001	**0.5 µg/mL:**	*NS* p = 0.0587
	0.75 µg/mL:	***p < 0.0001	**0.75 µg/mL:**	*NS* p = 0.0551
	1 µg/mL:	***p < 0.0001	**1 µg/mL:**	**p = 0.0009
MDA-MB-330 pINDUCER20-*SNAI1*	*Incomplete*		**0.125 µg/mL:**	***p = 0.0003
			0.25 µg/mL:	***p = 0.0003
			0.5 µg/mL:	***p < 0.0001
			0.75 µg/mL:	***p < 0.0001
			1 µg/mL:	***p < 0.0001
Sum44PE pINDUCER20-*SNAI1*	**0.125 µg/mL:**	*NS* p = 0.0559	**0.125 µg/mL:**	*NS* p = 0.2286
	0.25 µg/mL:	*p = 0.0092	**0.25 µg/mL:**	*p = 0.0086
	0.5 µg/mL:	**p = 0.0015	**0.5 µg/mL:**	*** p = 0.0003
	0.75 µg/mL:	**p = 0.0042	**0.75 µg/mL:**	*** p = 0.0002
	1 µg/mL:	*p = 0.0066	**1 µg/mL:**	*** p = 0.0002

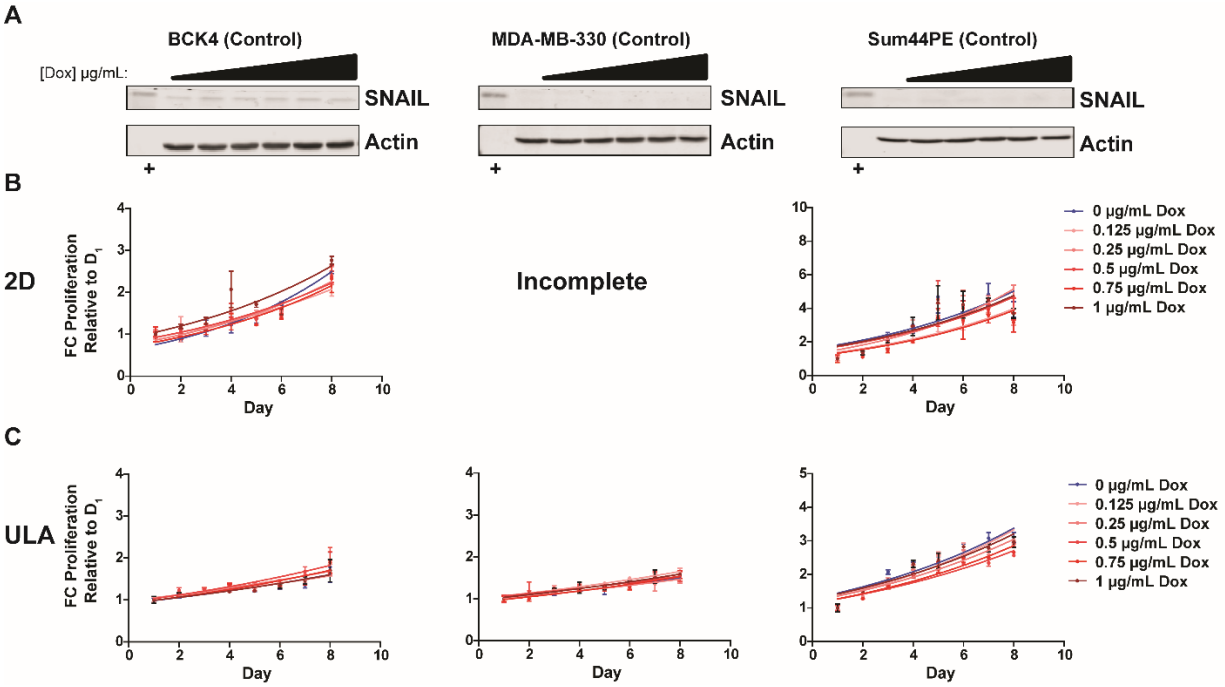

Figure 81: Dox Dose Responses in ILC Control Cells Show No Impact on Protein, Minimal Impacts on 2D, ULA Proliferation

BCK4, MDA-MB-330, and Sum44PE control cells were plated for a Dox dose response. (A) IB for SNAIL was performed at the 48-hour time point with increasing doses of Dox loaded from left to right on each respective blot (25 µg/lane). (B) 2D and (C) ULA proliferation were assessed with increasing doses of Dox in technical triplicates ± STDEV for each respective treatment/time point with normalization to D_1 values and comparison of rates after non-linear regression fits (*p < 0.05, **p < 0.005, ***p < 0.0005).

Table 15: ILC Control Dox Dose Response p-Values from 2D, ULA Proliferation Assays

All comparisons are relative to -Dox	***2D***		***ULA***	
BCK4 (Control)	**0.125 µg/mL:**	*p = 0.0078	**0.125 µg/mL:**	*NS* p = 0.3001
	0.25 µg/mL:	*NS* p = 0.0763	**0.25 µg/mL:**	*NS* p = 0.8810
	0.5 µg/mL:	*p = 0.0248	**0.5 µg/mL:**	*NS* p = 0.4060
	0.75 µg/mL:	*NS* p = 0.1507	**0.75 µg/mL:**	*NS* p = 0.5723
	1 µg/mL:	*NS* p = 0.1108	**1 µg/mL:**	*NS* p = 0.9442
MDA-MB-330 (Control)	*Incomplete*		**0.125 µg/mL:**	*NS* p = 0.4361
			0.25 µg/mL:	*NS* p = 0.5282
			0.5 µg/mL:	*NS* p = 0.5356
			0.75 µg/mL:	*NS* p = 0.3868
			1 µg/mL:	*NS* p = 0.5733
Sum44PE (Control)	**0.125 µg/mL:**	*NS* p = 0.8386	**0.125 µg/mL:**	*NS* p = 0.6714
	0.25 µg/mL:	*NS* p = 0.3626	**0.25 µg/mL:**	*NS* p = 0.7198
	0.5 µg/mL:	*NS* p = 0.9719	**0.5 µg/mL:**	*NS* p = 0.3725
	0.75 µg/mL:	*NS* p = 0.8240	**0.75 µg/mL:**	*NS* p = 0.6936
	1 µg/mL:	*NS* p = 0.9427	**1 µg/mL:**	*NS* p = 0.7605

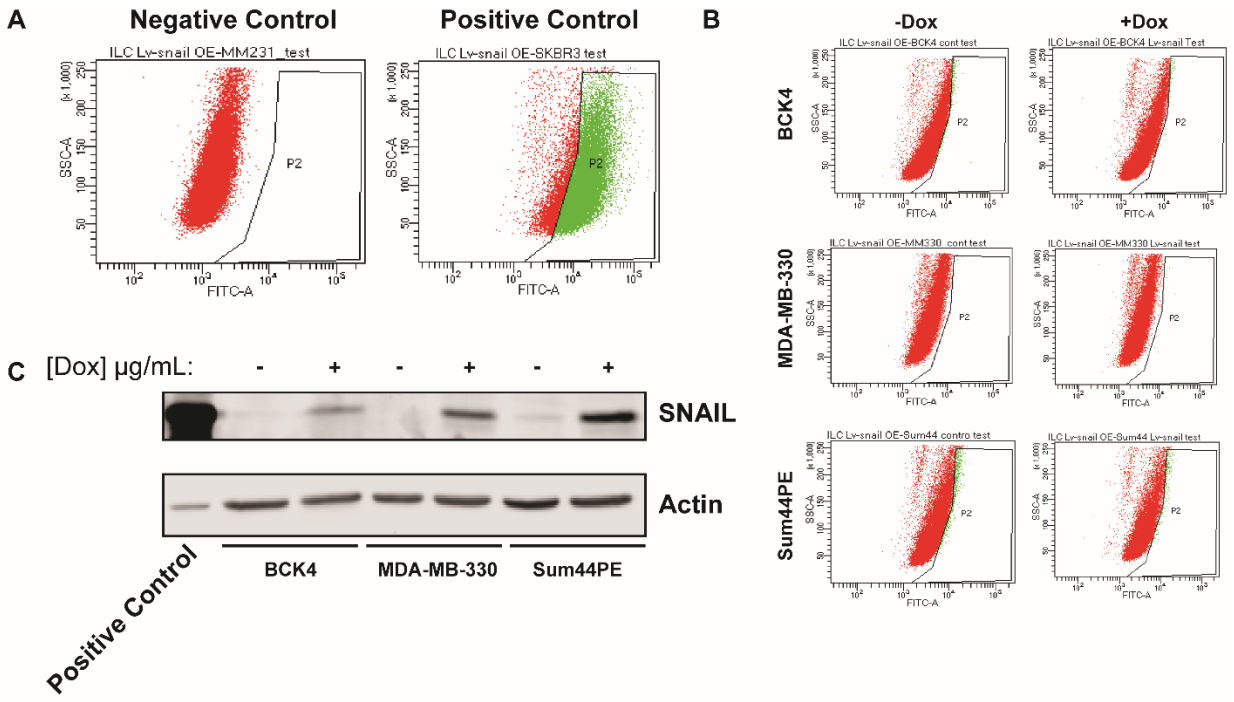

Figure 82: Inducible SNAIL ILC Cells Do Not Acquire ALDH$^+$ Phenotype with SNAIL Overexpression

ALDH Flow Cytometry assay was performed by Jian Chen, MS. (A) Negative (MDA-MB-231) and positive (SKBR3) control cell line ALDH profiles were collected. (B) Inducible SNAIL overexpression cells ± 0.5 µg/mL Dox were also assessed for ALDH profiles after 24 hours induction of SNAIL. (C) SNAIL protein was confirmed to be upregulated by IB (25 µg/lane). Data represent a single experiment.

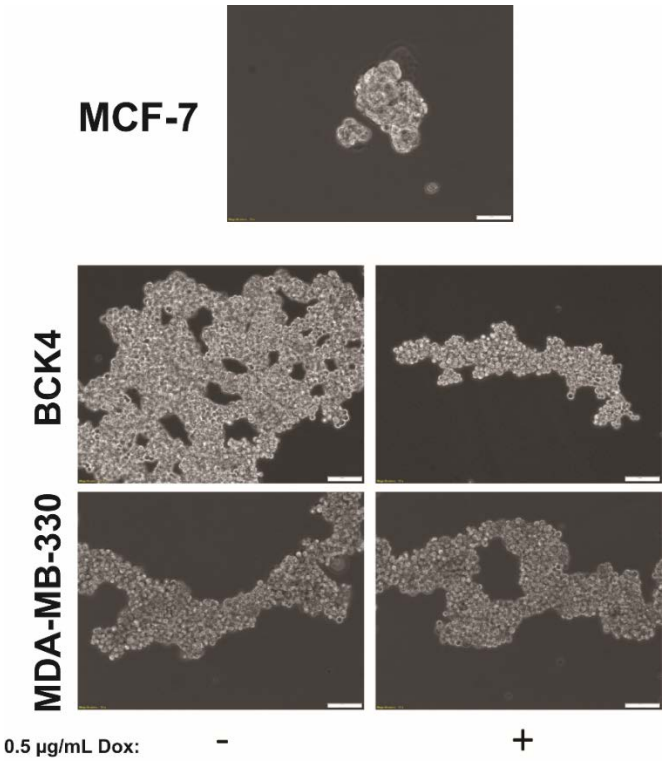

Figure 83: BCK4 and MDA-MB-330 Cells Do Not Form Proper Mammospheres
Inducible SNAIL overexpression ILC BCK4 and MDA-MB-330 cells were treated to Dox in a mammosphere assay. Phase contrast images are from D_{17} (20X magnification; scale bars represent 50 µm).

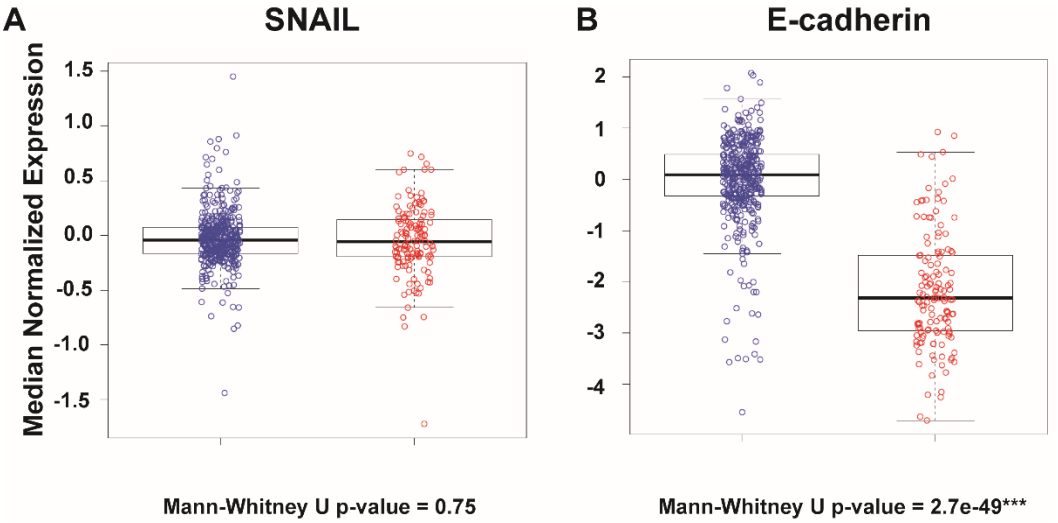

Figure 84: SNAIL Protein is Also Not Significantly Different Between ILC and IDC, But E-cadherin Is
RPPA from TCGA primary ILC (n = 137, red) and IDC (n = 417, blue) samples was analyzed for expression of (A) SNAIL and (B) E-cadherin. Mann-Whitney U p-values were applied to each data set. Data were analyzed in collaboration with Kevin Levine, BS.

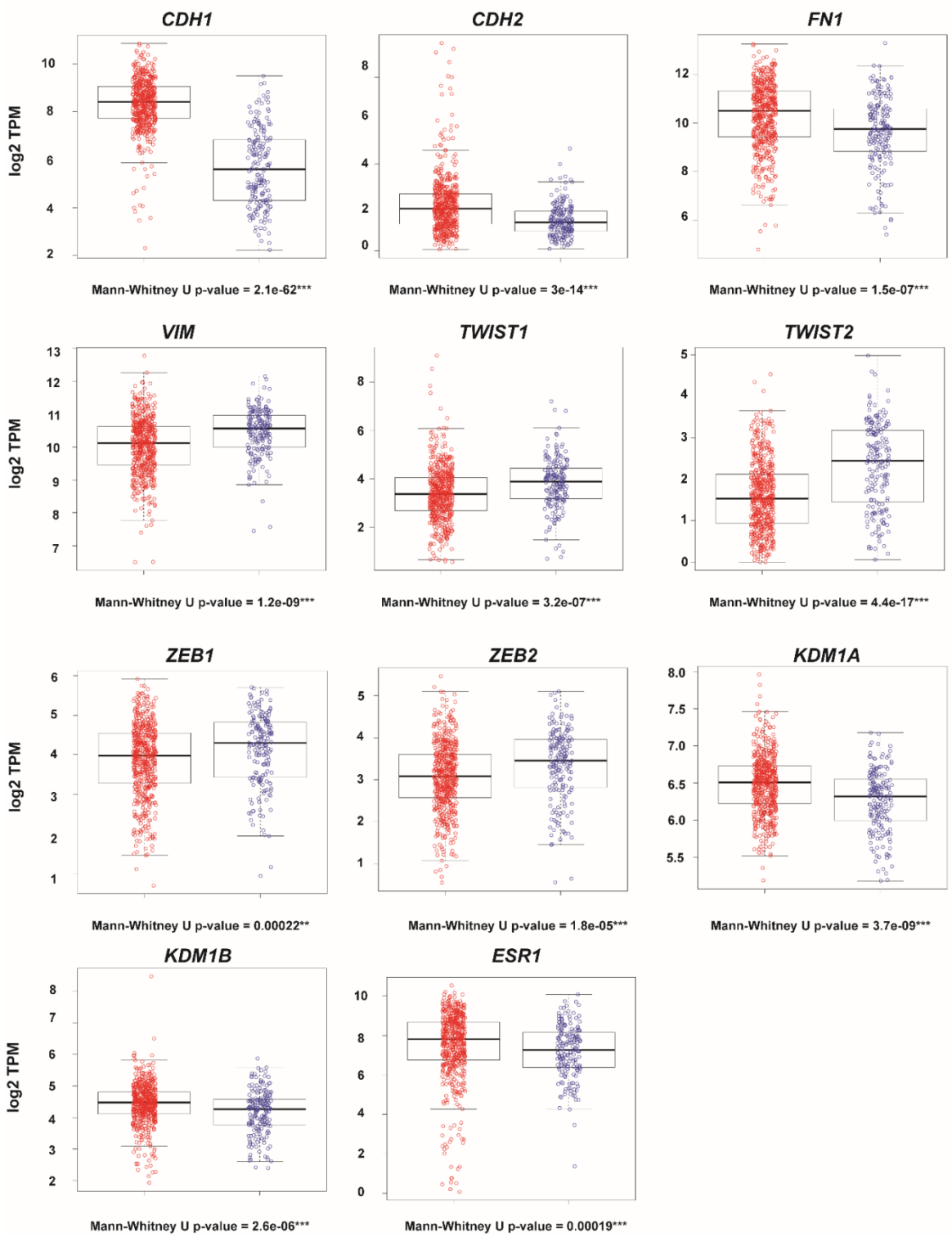

Figure 85: Overall EMT-TF Program is Downregulated in ILC as Compared to IDC Primary ERα Positive Lesions

TCGA ERα^{+} ILC (n= 184, red) versus IDC (n= 534, blue) lesions were probed for mRNA expressions of members of the EMT-TF panel. Mann-Whitney U p-values were applied to each data set. Analyses were performed in collaboration with Kevin Levine, BS.

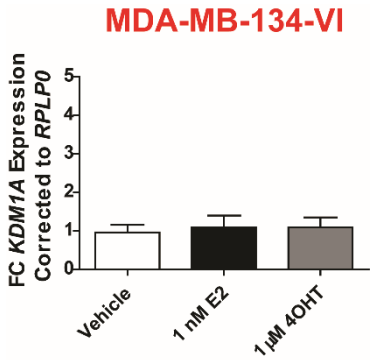

Figure 86: *KDM1A* is Not Regulated by ERα in MDA-MB-134-VI Cells
MDA-MB-134-VI cells were treated to E2 deprivation followed by Vehicle (0.1% DMSO), 1 nM E2, or 1 µM 4OHT for 8 hours. Data represent a single experiment with technical triplicates ± STDEV, normalized to the Vehicle with One Way ANOVA followed by Tukey's post-test (*p < 0.05, **p < 0.005, ***p < 0.0005).

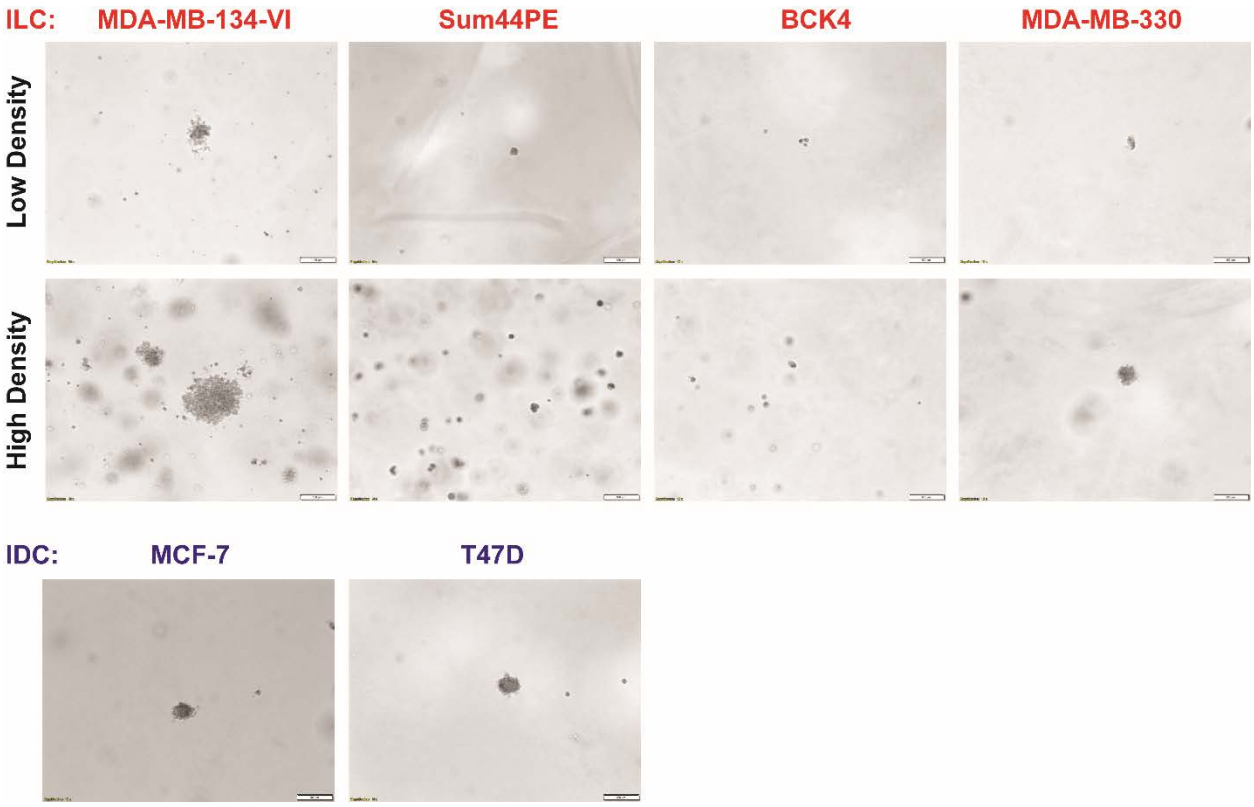

Figure 87: ILC Cells Form Discohesive Soft Agar Colonies as Compared to IDC Cells
ILC (red) and IDC (blue) cells were plated at the same density (10,000 cells/dish; marked as "low density for ILCs) or a higher density (100,000 cells/dish; marked as "high density for ILCs) in triplicate dishes for 28 days to monitor soft agar colony formation. Representative images were taken of colonies that were counted in each dish (10X magnification; bars represent 100 µm). Data represent a single experiment.

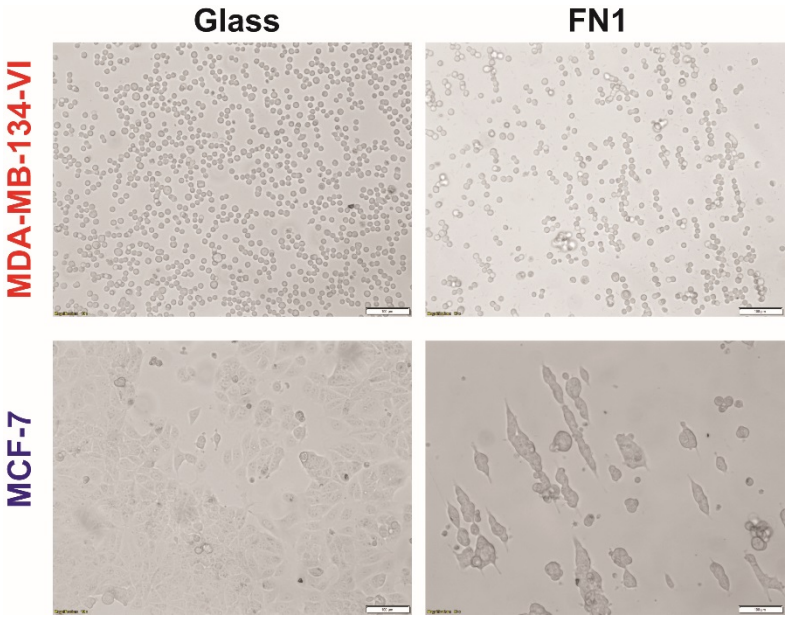

Figure 88: Preliminary Protein Micropatterning Experiment Was Successful for MDA-MB-134-VI and MCF-7 Cell Adhesion

MDA-MB-134-VI and MCF-7 cells were plated on 20 µm linear FN1-micropatterned (50 µg/mL), PDMS spin-coated coverslips at 200,000 cells/well in technical triplicate wells. Images were taken 24 hours post plating under phase contrast microscopy (10X magnification; bars represent 100 µm). Data represent the pilot study.

APPENDIX C

The following data are supplemental to Chapter 3 and assist in understanding of the WCRC-25 characterization.

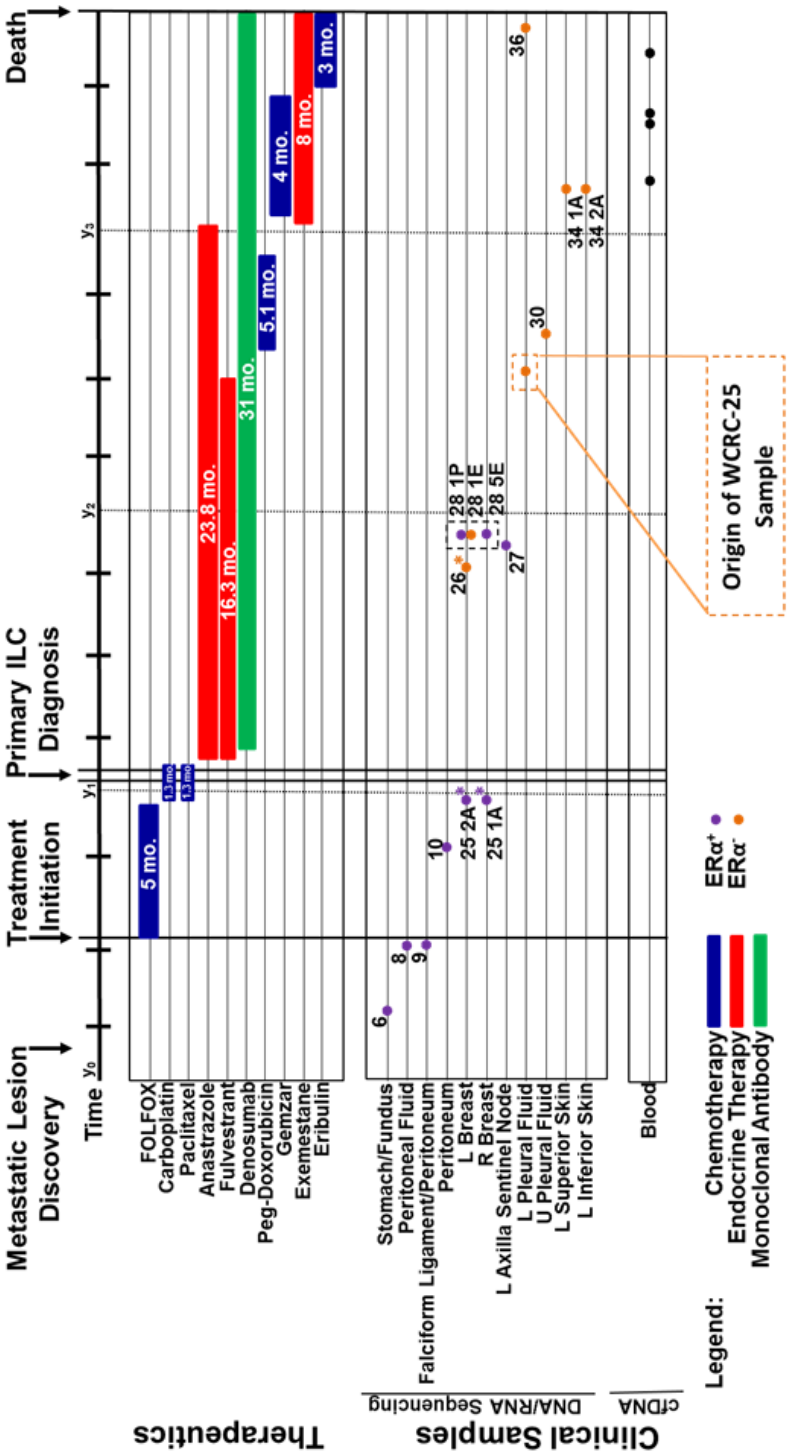

Figure 89: WCRC-25 Patient Clinical and Sample Acquisition Timeline with Numerical Descriptions of Samples

A compressed timeline (not to scale) of the WCRC-25 patient's clinical course is detailed above. De-identified clinical information was provided by Karthik Kota, MD. Samples pertinent to this project were listed. Asterisks (*) denote samples taken during biopsy. Dashed boxes around the breast samples indicate the time of double mastectomy. The figure was rotated for ease of visualization.

Table 16: Clinical Sample Overview for WCRC-25 Patient

Sample Name/Site	Sample Number	Months After Initial Diagnosis	ER	E-cad/p120
Stomach/Fundus	6	-9.1 (-2.3)	+ (*note: our section had no staining*)	-/cyto
Peritoneal Fluid	8	-7.1 (-0.25)	+	-/cyto
Falciform Ligament/Peritoneum	9	-7.1 (-0.25)	+	-/cyto
Peritoneum	10	-2.3 (4.5)	+	-/cyto
Right Breast Biopsy	25 1A	-1.3 (5.6)	+	*Uninterpretable*
Left Breast Biopsy$_1$	25 2A	-1.3 (5.6)	+	-/cyto
Left Breast Biopsy$_2$	26	8.2 (15)	-	-/cyto
Left Lymph Node	27	9.5 (16.4)	+	-/cyto
Right Breast Mastectomy	28 5E	9.8 (16.6)	+	-/cyto
Left Breast Mastectomy$_1$	28 1P	9.8 (16.6)	+	-/cyto
Left Breast Mastectomy$_2$	28 1E	9.8 (16.6)	-	-/cyto
Left Pleural Fluid$_1$/WCRC-25	29	16.3 (23.1)	- (*note: indicated from pathology report*)	-/cyto (*note: indicated from pathology report*)
Unknown Side Pleural Fluid	30	17.4 (24.3)	-	-/cyto
Left Superior Chest Skin	34 1A	24.1 (31)	-	-/cyto
Left Inferior Chest Skin	34 2A	24.1 (31)	-	-/cyto
Left Pleural Fluid$_2$	36	30.2 (37)	-	-/cyto
Blood$_1$	Draw 1	25.8 (32.7)	?	0.27% *CDH1* Q706*
Blood$_2$	Draw 2	27.2 (34.1)	?	?
Blood$_3$	Draw 3	27.7 (34.6)	?	?
Blood$_4$	Draw 4	29.8 (36.7)	?	8.28% *CDH1* Q706*

Sample names and numbers coordinate with Figure 39 and Appendix C Figure 89. Red font indicates months from initial ILC diagnosis. Black font in parentheses indicates months from initial gastric carcinoma diagnosis. Negative values mean prior to the first treatment regimen given for particular carcinoma (Anastrazole/Fulvestrant for ILC diagnosis; FOLFOX for gastric carcinoma diagnosis). Pathology calls are listed in the table as + for positive, - for negative, and cyto for cytoplasmic. A question mark means that the status was not tested. Mutational *CDH1* Q706* frequencies from ddPCR are listed for blood samples that have been tested.

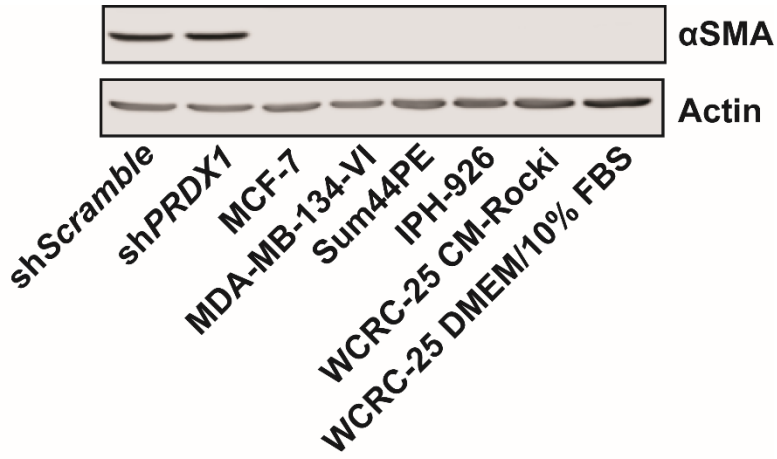

Figure 90: Stromal Marker αSMA is Not Expressed by WCRC-25
IB was performed with positive controls sh*Scramble* and sh*PRDX1* obtained from mouse stromal associated fibroblasts for αSMA and Actin internal control in a panel of IDC (MCF-7) and ILC cell lines. Data are representative of a single experiment with 40 µg/lane protein lysate.

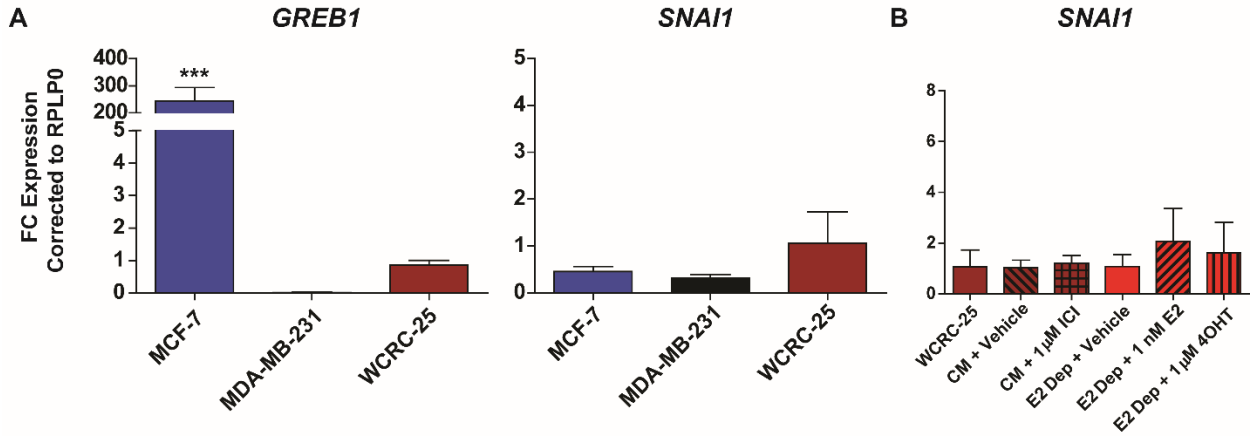

Figure 91: *GREB1* and *SNAI1* Are More Highly Expressed in WCRC-25 Than in MDA-MB-231; *SNAI1* is Mildly Induced by E2/4OHT in WCRC-25
(A) WCRC-25 cells were assessed by qRT-PCR for expression of ERα target genes *GREB1* and *SNAI1* against MCF-7 and MDA-MB-231 cells. (B) WCRC-25 cells were treated to 1 µM ICI or E2 deprivation followed by 1 nM E2 or 1 µM 4OHT with assessment of *SNAI1* expression alterations by qRT-PCR. Quantifications are representative of a single experiment with technical triplicates ± STDEV, normalized to WCRC-25 without treatment. Statistics were performed with One Way ANOVA followed by Tukey's post-test (*p < 0.05, **p < 0.005, ***p < 0.0005) with comparison to WCRC-25 untreated.

The following is a description of quality checks that were performed on WCRC-25 RNA Sequencing data:

After sequencing data were obtained, quality checks were performed to ensure interpretability of data. First, Phred scores were called to measure the base calling accuracy. A score of 30 defines 99.9% accuracy in base calling (errors only occur in 1 out of 1,000 bases called), a score of 40 defines 99.99% accuracy in base calling (errors only occur in 1 out of 10,000 bases called), and so on. Phred scores for this sequencing run were called at 37, giving great confidence to the accuracy of the sequencing calls made. Next, soft alignment clipping rates were measured. Soft alignment took into consideration that all reads did not necessarily align perfectly from 5' → 3' with the reference sequence. The rate at which the soft-clipped alignments occurred followed a distribution expected with increased reads. Measurement of insert sizes revealed that most inserts were between 100-200 base pairs, as expected from degraded FFPE RNA[282]. Next, GC content was assessed to determine if there was bias for low or high GC content reads, which could have influenced Illumina sequencing reads[283]. GC content was consistent for all samples circa 40%. The cumulative gene assignment diversity was next assessed, and hypothesized to be similar across all samples. However, the stomach sample taken early in the treatment course appeared to have a different trace than all other samples, and was thus considered to be a potential outlier in the study. Gene-body coverage was measured to determine that there was no bias in the preparation of samples, and subsequent reads, toward the 5' or 3' end[284]. Coverage was estimated near 50% for all samples, indicating no bias of reads toward either 5' or 3' end. Read mapping location rates were measured near 80% for unique genes, suggesting that the unique reads were mapped to unique regions of the reference or different gene regions. Strandedness was tested to assure that a bias did not exist for reads in either sense or antisense strand; no bias existed for either

strand in our data ser. Finally, the raw nucleotide rate comparison between cycles indicated read concordance between cycles (e.g. C with G in cycle 1 and G with C in cycle 2). The culmination of this quality control data gave confidence that the preparation of the library, quality of reads, and mapping of data were of high confidence for all samples run, with some concern noted about the stomach sample (Appendix C Figure 92).

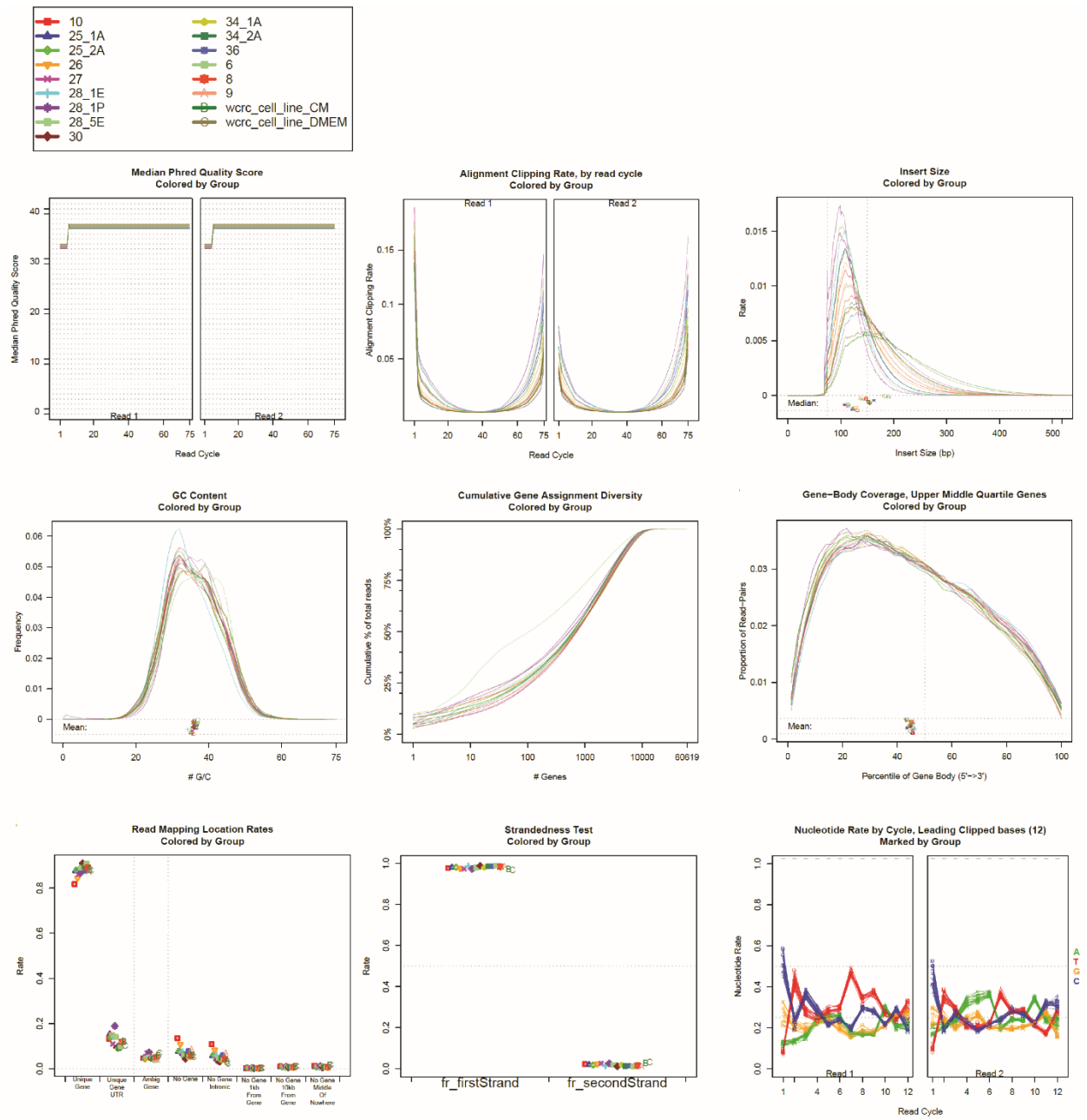

Figure 92: QoRTs Quality Control Plots from R Analyses for RNASeq
QoRTs plots were generated based on data and descriptions provided in main text to validate use of RNASeq from WCRC-25 patient.

BIBLIOGRAPHY

1. Siegel, R.L., K.D. Miller, and A. Jemal, *Cancer statistics, 2018.* CA Cancer J Clin, 2018. **68**(1): p. 7-30.

2. Siegel, R.L., K.D. Miller, and A. Jemal, *Cancer statistics, 2016.* CA Cancer J Clin, 2016. **66**(1): p. 7-30.

3. Colditz, G.A. and L.L. Peterson, *Obesity and Cancer: Evidence, Impact, and Future Directions.* Clin Chem, 2018. **64**(1): p. 154-162.

4. Renehan, A.G., M. Zwahlen, and M. Egger, *Adiposity and cancer risk: new mechanistic insights from epidemiology.* Nat Rev Cancer, 2015. **15**(8): p. 484-98.

5. Chlebowski, R.T., et al., *Breast Cancer After Use of Estrogen Plus Progestin and Estrogen Alone: Analyses of Data From 2 Women's Health Initiative Randomized Clinical Trials.* JAMA Oncol, 2015. **1**(3): p. 296-305.

6. Lukong, K.E., *Understanding breast cancer - The long and winding road.* BBA Clin, 2017. **7**: p. 64-77.

7. Higgins, M.J. and J. Baselga, *Targeted therapies for breast cancer.* J Clin Invest, 2011. **121**(10): p. 3797-803.

8. Masoud, V. and G. Pages, *Targeted therapies in breast cancer: New challenges to fight against resistance.* World J Clin Oncol, 2017. **8**(2): p. 120-134.

9. Akram, M., et al., *Awareness and current knowledge of breast cancer.* Biol Res, 2017. **50**(1): p. 33.

10. Rayter, Z., *History of breast cancer therapy*, in *Medical Therapy of Breast Cancer*, Z.M. Rayter, J., Editor. 2003, Cambridge University Press: Bristol Royal Infirmary, Bristol, UK. p. 10.

11. Sudhakar, A., *History of Cancer, Ancient and Modern Treatment Methods.* J Cancer Sci Ther, 2009. **1**(2): p. 1-4.

12. Koonin, E.V., *The origins of cellular life.* Antonie Van Leeuwenhoek, 2014. **106**(1): p. 27-41.

13. Byun, J.S. and K. Gardner, *Wounds that will not heal: pervasive cellular reprogramming in cancer.* Am J Pathol, 2013. **182**(4): p. 1055-64.

14. Olson, J.S., *Carcinogenesis*, in *The History of Cancer: An Annotated Bibliography*. 1989, Greenwood Press.

15. Clarke, J.H., *On the Parasitic Theory of Cancer*, in *The Therapeutics of Cancer*. 1994, B. Jain Publishers.

16. Wilkins, M.H., A.R. Stokes, and H.R. Wilson, *Molecular structure of deoxypentose nucleic acids.* Nature, 1953. **171**(4356): p. 738-40.

17. Franklin, R.E. and R.G. Gosling, *Evidence for 2-chain helix in crystalline structure of sodium deoxyribonucleate.* Nature, 1953. **172**(4369): p. 156-7.

18. Watson, J.D. and F.H. Crick, *Molecular structure of nucleic acids; a structure for deoxyribose nucleic acid.* Nature, 1953. **171**(4356): p. 737-8.

19. McGuire, K.P., *Breast Anatomy and Physiology*, in *Breast Disease: Diagnosis and Pathology*. 2015, Springer International Publishing. p. 14.

20. Bombonati, A. and D.C. Sgroi, *The molecular pathology of breast cancer progression.* J Pathol, 2011. **223**(2): p. 307-17.

21. Zhang, M., A.V. Lee, and J.M. Rosen, *The Cellular Origin and Evolution of Breast Cancer.* Cold Spring Harb Perspect Med, 2017. **7**(3).

22. Ingvarsson, S., *Molecular genetics of breast cancer progression.* Semin Cancer Biol, 1999. **9**(4): p. 277-88.

23. Stephens, P.J., et al., *The landscape of cancer genes and mutational processes in breast cancer.* Nature, 2012. **486**(7403): p. 400-4.

24. Nik-Zainal, S., et al., *Landscape of somatic mutations in 560 breast cancer whole-genome sequences.* Nature, 2016. **534**(7605): p. 47-54.

25. Pfeffer, C.M., B.N. Ho, and A.T.K. Singh, *The Evolution, Functions and Applications of the Breast Cancer Genes BRCA1 and BRCA2.* Cancer Genomics Proteomics, 2017. **14**(5): p. 293-298.

26. Gasco, M., S. Shami, and T. Crook, *The p53 pathway in breast cancer.* Breast Cancer Res, 2002. **4**(2): p. 70-6.

27. Dossus, L. and P.R. Benusiglio, *Lobular breast cancer: incidence and genetic and non-genetic risk factors.* Breast Cancer Res, 2015. **17**: p. 37.

28. Pecina-Slaus, N., *Tumor suppressor gene E-cadherin and its role in normal and malignant cells.* Cancer Cell Int, 2003. **3**(1): p. 17.

29. Onder, T.T., et al., *Loss of E-cadherin promotes metastasis via multiple downstream transcriptional pathways.* Cancer Res, 2008. **68**(10): p. 3645-54.

30. Chen, Z., et al., *Invasive lobular carcinoma of the breast: A special histological type compared with invasive ductal carcinoma.* PLoS One, 2017. **12**(9): p. e0182397.

31. Sommer, S. and S.A. Fuqua, *Estrogen receptor and breast cancer.* Semin Cancer Biol, 2001. **11**(5): p. 339-52.

32. Hayashi, S.I., et al., *The expression and function of estrogen receptor alpha and beta in human breast cancer and its clinical application.* Endocr Relat Cancer, 2003. **10**(2): p. 193-202.

33. Lee, H.R., T.H. Kim, and K.C. Choi, *Functions and physiological roles of two types of estrogen receptors, ERalpha and ERbeta, identified by estrogen receptor knockout mouse.* Lab Anim Res, 2012. **28**(2): p. 71-6.

34. Paterni, I., et al., *Estrogen receptors alpha (ERalpha) and beta (ERbeta): subtype-selective ligands and clinical potential.* Steroids, 2014. **90**: p. 13-29.

35. Pearce, S.T. and V.C. Jordan, *The biological role of estrogen receptors alpha and beta in cancer.* Crit Rev Oncol Hematol, 2004. **50**(1): p. 3-22.

36. Deroo, B.J. and K.S. Korach, *Estrogen receptors and human disease.* J Clin Invest, 2006. **116**(3): p. 561-70.

37. Marino, M., P. Galluzzo, and P. Ascenzi, *Estrogen signaling multiple pathways to impact gene transcription.* Curr Genomics, 2006. **7**(8): p. 497-508.

38. Carroll, J.S. and M. Brown, *Estrogen receptor target gene: an evolving concept.* Mol Endocrinol, 2006. **20**(8): p. 1707-14.

39. Vasquez, Y.M., *Estrogen-regulated transcription: Mammary gland and uterus.* Steroids, 2018. **133**: p. 82-86.

40. Pedram, A., et al., *Integration of the non-genomic and genomic actions of estrogen. Membrane-initiated signaling by steroid to transcription and cell biology.* J Biol Chem, 2002. **277**(52): p. 50768-75.

41. Doisneau-Sixou, S.F., et al., *Estrogen and antiestrogen regulation of cell cycle progression in breast cancer cells.* Endocr Relat Cancer, 2003. **10**(2): p. 179-86.

42. Liao, X.H., et al., *Estrogen receptor alpha mediates proliferation of breast cancer MCF-7 cells via a p21/PCNA/E2F1-dependent pathway.* Febs j, 2014. **281**(3): p. 927-42.

43. Santen, R.J., W. Yue, and J.P. Wang, *Estrogen metabolites and breast cancer.* Steroids, 2015. **99**(Pt A): p. 61-6.

44. Stanford, J.L., et al., *A case-control study of breast cancer stratified by estrogen receptor status.* Am J Epidemiol, 1987. **125**(2): p. 184-94.

45. Buerger, H., et al., *Different genetic pathways in the evolution of invasive breast cancer are associated with distinct morphological subtypes.* J Pathol, 1999. **189**(4): p. 521-6.

46. Perou, C.M., et al., *Molecular portraits of human breast tumours.* Nature, 2000. **406**(6797): p. 747-52.

47. Sorlie, T., et al., *Gene expression patterns of breast carcinomas distinguish tumor subclasses with clinical implications.* Proc Natl Acad Sci U S A, 2001. **98**(19): p. 10869-74.

48. *Comprehensive molecular portraits of human breast tumours.* Nature, 2012. **490**(7418): p. 61-70.

49. Perou, C.M., *Molecular stratification of triple-negative breast cancers.* Oncologist, 2010. **15 Suppl 5**: p. 39-48.

50. Wallden, B., et al., *Development and verification of the PAM50-based Prosigna breast cancer gene signature assay.* BMC Med Genomics, 2015. **8**: p. 54.

51. Rouzier, R., et al., *Breast cancer molecular subtypes respond differently to preoperative chemotherapy.* Clin Cancer Res, 2005. **11**(16): p. 5678-85.

52. Sorlie, T., *Introducing molecular subtyping of breast cancer into the clinic?* J Clin Oncol, 2009. **27**(8): p. 1153-4.

53. Prat, A. and C.M. Perou, *Deconstructing the molecular portraits of breast cancer.* Mol Oncol, 2011. **5**(1): p. 5-23.

54. Dai, X., et al., *Cancer Hallmarks, Biomarkers and Breast Cancer Molecular Subtypes.* J Cancer, 2016. **7**(10): p. 1281-94.

55. Malhotra, G.K., et al., *Histological, molecular and functional subtypes of breast cancers.* Cancer Biol Ther, 2010. **10**(10): p. 955-60.

56. Corben, A.D., *Pathology of invasive breast disease.* Surg Clin North Am, 2013. **93**(2): p. 363-92.

57. Makki, J., *Diversity of Breast Carcinoma: Histological Subtypes and Clinical Relevance.* Clin Med Insights Pathol, 2015. **8**: p. 23-31.

58. Weigelt, B., F.C. Geyer, and J.S. Reis-Filho, *Histological types of breast cancer: how special are they?* Mol Oncol, 2010. **4**(3): p. 192-208.

59. Fisher, E.R. and B. Fisher, *Lobular carcinoma of the breast: an overview.* Ann Surg, 1977. **185**(4): p. 377-85.

60. Arpino, G., et al., *Infiltrating lobular carcinoma of the breast: tumor characteristics and clinical outcome.* Breast Cancer Res, 2004. **6**(3): p. R149-56.

61. King, T.A. and J.S. Reis-Filho, *Lobular neoplasia.* Surg Oncol Clin N Am, 2014. **23**(3): p. 487-503.

62. van Roy, F. and G. Berx, *The cell-cell adhesion molecule E-cadherin.* Cell Mol Life Sci, 2008. **65**(23): p. 3756-88.

63. Berx, G. and F. Van Roy, *The E-cadherin/catenin complex: an important gatekeeper in breast cancer tumorigenesis and malignant progression.* Breast Cancer Res, 2001. **3**(5): p. 289-93.

64. Morrogh, M., et al., *Cadherin-catenin complex dissociation in lobular neoplasia of the breast.* Breast Cancer Res Treat, 2012. **132**(2): p. 641-52.

65. McCart Reed, A.E., et al., *Invasive lobular carcinoma of the breast: morphology, biomarkers and 'omics.* Breast Cancer Res, 2015. **17**: p. 12.

66. Dabbs, D.J., et al., *Lobular neoplasia of the breast revisited with emphasis on the role of E-cadherin immunohistochemistry.* Am J Surg Pathol, 2013. **37**(7): p. e1-11.

67. Ciriello, G., et al., *Comprehensive Molecular Portraits of Invasive Lobular Breast Cancer.* Cell, 2015. **163**(2): p. 506-19.

68. Johnson, K., D. Sarma, and E.S. Hwang, *Lobular breast cancer series: imaging.* Breast Cancer Res, 2015. **17**: p. 94.

69. Grubstein, A., et al., *Invasive Lobular Carcinoma of the Breast: Appearance on Digital Breast Tomosynthesis.* Breast Care (Basel), 2016. **11**(5): p. 359-362.

70. Chamming's, F., et al., *Imaging features and conspicuity of invasive lobular carcinomas on digital breast tomosynthesis.* Br J Radiol, 2017. **90**(1073): p. 20170128.

71. Sikora, M.J., et al., *Invasive lobular carcinoma of the breast: patient response to systemic endocrine therapy and hormone response in model systems.* Steroids, 2013. **78**(6): p. 568-75.

72. Mamtani, A. and T.A. King, *Lobular Breast Cancer: Different Disease, Different Algorithms?* Surg Oncol Clin N Am, 2018. **27**(1): p. 81-94.

73. Lehr, H.A., et al., *Cytokeratin 8 immunostaining pattern and E-cadherin expression distinguish lobular from ductal breast carcinoma.* Am J Clin Pathol, 2000. **114**(2): p. 190-6.

74. Klein, S., *Evaluation of palpable breast masses.* Am Fam Physician, 2005. **71**(9): p. 1731-8.

75. Moll, R., et al., *Differential loss of E-cadherin expression in infiltrating ductal and lobular breast carcinomas.* Am J Pathol, 1993. **143**(6): p. 1731-42.

76. Younis, L.K., H. El Sakka, and I. Haque, *The Prognostic Value of E-cadherin Expression in Breast Cancer.* Int J Health Sci (Qassim), 2007. **1**(1): p. 43-51.

77. Singhai, R., et al., *E-Cadherin as a diagnostic biomarker in breast cancer.* N Am J Med Sci, 2011. **3**(5): p. 227-33.

78. Shakoor, M.T., et al., *Unique presentations of invasive lobular breast cancer: a case series.* Int J Biomed Sci, 2014. **10**(4): p. 287-93.

79. James, J.J., et al., *Bone metastases from breast carcinoma: histopathological - radiological correlations and prognostic features.* Br J Cancer, 2003. **89**(4): p. 660-5.

80. Borst, M.J. and J.A. Ingold, *Metastatic patterns of invasive lobular versus invasive ductal carcinoma of the breast.* Surgery, 1993. **114**(4): p. 637-41; discussion 641-2.

81. Sobinsky, J.D., et al., *Unusual metastatic patterns of invasive lobular carcinoma of the breast.* Case Rep Oncol Med, 2013. **2013**: p. 986517.

82. Mathew, A., et al., *Distinct Pattern of Metastases in Patients with Invasive Lobular Carcinoma of the Breast.* Geburtshilfe Frauenheilkd, 2017. **77**(6): p. 660-666.

83. Hilleren, D.J., et al., *Invasive lobular carcinoma: mammographic findings in a 10-year experience.* Radiology, 1991. **178**(1): p. 149-54.

84. Le Gal, M., et al., *Mammographic features of 455 invasive lobular carcinomas.* Radiology, 1992. **185**(3): p. 705-8.

85. Krecke, K.N. and J.J. Gisvold, *Invasive lobular carcinoma of the breast: mammographic findings and extent of disease at diagnosis in 184 patients.* AJR Am J Roentgenol, 1993. **161**(5): p. 957-60.

86. Mandelson, M.T., et al., *Breast density as a predictor of mammographic detection: comparison of interval- and screen-detected cancers.* J Natl Cancer Inst, 2000. **92**(13): p. 1081-7.

87. Fodor, J., et al., *Comparison of mastectomy with breast-conserving surgery in invasive lobular carcinoma: 15-Year results.* Rep Pract Oncol Radiother, 2011. **16**(6): p. 227-31.

88. Berg, W.A., et al., *Diagnostic accuracy of mammography, clinical examination, US, and MR imaging in preoperative assessment of breast cancer.* Radiology, 2004. **233**(3): p. 830-49.

89. Anwar, I.F., et al., *Invasive lobular carcinoma of the breast: should this be regarded as a chronic disease?* Int J Surg, 2010. **8**(5): p. 346-52.

90. Dedes, K.J. and D. Fink, *Clinical presentation and surgical management of invasive lobular carcinoma of the breast.* Breast Dis, 2008. **30**: p. 31-7.

91. Koss, L.G., *The Breast*, in *Koss' Diagnostic Cytology and Its Histopathologic Bases*. 2006, Lippincott Williams and Wilkins.

92. Nishimura, R., et al., *Ki-67 as a prognostic marker according to breast cancer subtype and a predictor of recurrence time in primary breast cancer.* Exp Ther Med, 2010. **1**(5): p. 747-754.

93. Boelens, M.C., et al., *PTEN Loss in E-Cadherin-Deficient Mouse Mammary Epithelial Cells Rescues Apoptosis and Results in Development of Classical Invasive Lobular Carcinoma.* Cell Rep, 2016. **16**(8): p. 2087-2101.

94. Christgen, M., et al., *Oncogenic PIK3CA mutations in lobular breast cancer progression.* Genes Chromosomes Cancer, 2013. **52**(1): p. 69-80.

95. Li, C.I., D.J. Uribe, and J.R. Daling, *Clinical characteristics of different histologic types of breast cancer.* Br J Cancer, 2005. **93**(9): p. 1046-52.

96. Cho, S.H., J. Jeon, and S.I. Kim, *Personalized medicine in breast cancer: a systematic review.* J Breast Cancer, 2012. **15**(3): p. 265-72.

97. Tevaarwerk, A.J., K.B. Wisinski, and R.M. O'Regan, *Endocrine Therapy in Premenopausal Hormone Receptor-Positive Breast Cancer.* J Oncol Pract, 2016. **12**(11): p. 1148-1156.

98. Smith, I.E. and M. Dowsett, *Aromatase inhibitors in breast cancer.* N Engl J Med, 2003. **348**(24): p. 2431-42.

99. Boer, K., *Fulvestrant in advanced breast cancer: evidence to date and place in therapy.* Ther Adv Med Oncol, 2017. **9**(7): p. 465-479.

100. Puhalla, S., S. Bhattacharya, and N.E. Davidson, *Hormonal therapy in breast cancer: a model disease for the personalization of cancer care.* Mol Oncol, 2012. **6**(2): p. 222-36.

101. Dutertre, M. and C.L. Smith, *Molecular mechanisms of selective estrogen receptor modulator (SERM) action.* J Pharmacol Exp Ther, 2000. **295**(2): p. 431-7.

102. Lumachi, F., et al., *Endocrine therapy of breast cancer.* Curr Med Chem, 2011. **18**(4): p. 513-22.

103. Maximov, P.Y., T.M. Lee, and V.C. Jordan, *The discovery and development of selective estrogen receptor modulators (SERMs) for clinical practice.* Curr Clin Pharmacol, 2013. **8**(2): p. 135-55.

104. Vogel, C.L., et al., *Toremifene for breast cancer: a review of 20 years of data.* Clin Breast Cancer, 2014. **14**(1): p. 1-9.

105. Li, F., et al., *The selective estrogen receptor modulators in breast cancer prevention.* Cancer Chemother Pharmacol, 2016. **77**(5): p. 895-903.

106. Richardson, D.N., *The history of Nolvadex.* Drug Des Deliv, 1988. **3**(1): p. 1-14.

107. Traboulsi, T., et al., *Antiestrogens: structure-activity relationships and use in breast cancer treatment.* J Mol Endocrinol, 2017. **58**(1): p. R15-r31.

108. Cronin-Fenton, D.P., P. Damkier, and T.L. Lash, *Metabolism and transport of tamoxifen in relation to its effectiveness: new perspectives on an ongoing controversy.* Future Oncol, 2014. **10**(1): p. 107-22.

109. Wakeling, A.E. and S.R. Slater, *Estrogen-receptor binding and biologic activity of tamoxifen and its metabolites.* Cancer Treat Rep, 1980. **64**(6-7): p. 741-4.

110. McDonnell, D.P. and S.E. Wardell, *The molecular mechanisms underlying the pharmacological actions of ER modulators: implications for new drug discovery in breast cancer.* Curr Opin Pharmacol, 2010. **10**(6): p. 620-8.

111. Taylor, I.W., et al., *Effects of tamoxifen on cell cycle progression of synchronous MCF-7 human mammary carcinoma cells.* Cancer Res, 1983. **43**(9): p. 4007-10.

112. Li, W., et al., *Tamoxifen promotes apoptosis and inhibits invasion in estrogenpositive breast cancer MCF7 cells.* Mol Med Rep, 2017. **16**(1): p. 478-484.

113. Huang, B., M. Warner, and J.A. Gustafsson, *Estrogen receptors in breast carcinogenesis and endocrine therapy.* Mol Cell Endocrinol, 2015. **418 Pt 3**: p. 240-4.

114. Dhingra, K., *Antiestrogens--tamoxifen, SERMs and beyond.* Invest New Drugs, 1999. **17**(3): p. 285-311.

115. Barroso-Sousa, R. and O. Metzger-Filho, *Differences between invasive lobular and invasive ductal carcinoma of the breast: results and therapeutic implications.* Ther Adv Med Oncol, 2016. **8**(4): p. 261-6.

116. Smith, D.B., A. Howell, and J. Wagstaff, *Infiltrating lobular carcinoma of the breast: response to endocrine therapy and survival.* Eur J Cancer Clin Oncol, 1987. **23**(7): p. 979-82.

117. Jirstrom, K., et al., *Pathology parameters and adjuvant tamoxifen response in a randomised premenopausal breast cancer trial.* J Clin Pathol, 2005. **58**(11): p. 1135-42.

118. Rakha, E.A., et al., *Invasive lobular carcinoma of the breast: response to hormonal therapy and outcomes.* Eur J Cancer, 2008. **44**(1): p. 73-83.

119. Pestalozzi, B.C., et al., *Distinct clinical and prognostic features of infiltrating lobular carcinoma of the breast: combined results of 15 International Breast Cancer Study Group clinical trials.* J Clin Oncol, 2008. **26**(18): p. 3006-14.

120. Metzger Filho, O., et al., *Relative Effectiveness of Letrozole Compared With Tamoxifen for Patients With Lobular Carcinoma in the BIG 1-98 Trial.* J Clin Oncol, 2015. **33**(25): p. 2772-9.

121. Jankowitz, R.C. *Endocrine Response in Women With Invasive Lobular Breast Cancer*. [cited 2018 1 Jan 2018]; Available from: https://clinicaltrials.gov/ct2/show/NCT02206984?term=Jankowitz&cond=Lobular+Breast+Carcinoma&rank=1.

122. Institute, D.-F.C. *Palbociclib and Endocrine Therapy for LObular Breast Cancer Preoperative Study (PELOPS).* [cited 2018 1 Jan 2018]; Available from: https://clinicaltrials.gov/ct2/show/NCT02764541?term=PELOPS&cond=Lobular+Breast+Carcinoma&rank=1.

123. Ali, S., et al., *Molecular mechanisms and mode of tamoxifen resistance in breast cancer.* Bioinformation, 2016. **12**(3): p. 135-139.

124. Chang, M., *Tamoxifen resistance in breast cancer.* Biomol Ther (Seoul), 2012. **20**(3): p. 256-67.

125. Ring, A. and M. Dowsett, *Mechanisms of tamoxifen resistance.* Endocr Relat Cancer, 2004. **11**(4): p. 643-58.

126. Viedma-Rodriguez, R., et al., *Mechanisms associated with resistance to tamoxifen in estrogen receptor-positive breast cancer (review).* Oncol Rep, 2014. **32**(1): p. 3-15.

127. Girault, I., I. Bieche, and R. Lidereau, *Role of estrogen receptor alpha transcriptional coregulators in tamoxifen resistance in breast cancer.* Maturitas, 2006. **54**(4): p. 342-51.

128. Chen, I.C., et al., *Phosphatidylinositol-3 Kinase Inhibitors, Buparlisib and Alpelisib, Sensitize Estrogen Receptor-positive Breast Cancer Cells to Tamoxifen.* Sci Rep, 2017. **7**(1): p. 9842.

129. Bahreini, A., et al., *Mutation site and context dependent effects of ESR1 mutation in genome-edited breast cancer cell models.* Breast Cancer Res, 2017. **19**(1): p. 60.

130. Jiang, Y., et al., *Snail and Slug mediate tamoxifen resistance in breast cancer cells through activation of EGFR-ERK independent of epithelial-mesenchymal transition.* J Mol Cell Biol, 2014. **6**(4): p. 352-4.

131. Nawata, H., D. Bronzert, and M.E. Lippman, *Isolation and characterization of a tamoxifen-resistant cell line derived from MCF-7 human breast cancer cells.* J Biol Chem, 1981. **256**(10): p. 5016-21.

132. Sikora, M.J., et al., *Invasive lobular carcinoma cell lines are characterized by unique estrogen-mediated gene expression patterns and altered tamoxifen response.* Cancer Res, 2014. **74**(5): p. 1463-74.

133. Wakeling, A.E. and J. Bowler, *ICI 182,780, a new antioestrogen with clinical potential.* J Steroid Biochem Mol Biol, 1992. **43**(1-3): p. 173-7.

134. Mehta, R.S., et al., *Combination anastrozole and fulvestrant in metastatic breast cancer.* N Engl J Med, 2012. **367**(5): p. 435-44.

135. Robertson, J.F., et al., *Activity of fulvestrant 500 mg versus anastrozole 1 mg as first-line treatment for advanced breast cancer: results from the FIRST study.* J Clin Oncol, 2009. **27**(27): p. 4530-5.

136. Robertson, J.F.R., et al., *Fulvestrant 500 mg versus anastrozole 1 mg for hormone receptor-positive advanced breast cancer (FALCON): an international, randomised, double-blind, phase 3 trial.* Lancet, 2016. **388**(10063): p. 2997-3005.

137. Robertson, J.F., et al., *Pharmacokinetic profile of intramuscular fulvestrant in advanced breast cancer.* Clin Pharmacokinet, 2004. **43**(8): p. 529-38.

138. Osipo, C., et al., *Role for HER2/neu and HER3 in fulvestrant-resistant breast cancer.* Int J Oncol, 2007. **30**(2): p. 509-20.

139. McDonnell, D.P., S.E. Wardell, and J.D. Norris, *Oral Selective Estrogen Receptor Downregulators (SERDs), a Breakthrough Endocrine Therapy for Breast Cancer.* J Med Chem, 2015. **58**(12): p. 4883-7.

140. Kumler, I., et al., *Review of hormone-based treatments in postmenopausal patients with advanced breast cancer focusing on aromatase inhibitors and fulvestrant.* ESMO Open, 2016. **1**(4): p. e000062.

141. Howell, A., et al., *Results of the ATAC (Arimidex, Tamoxifen, Alone or in Combination) trial after completion of 5 years' adjuvant treatment for breast cancer.* Lancet, 2005. **365**(9453): p. 60-2.

142. Nourmoussavi, M., et al., *Ovarian ablation for premenopausal breast cancer: A review of treatment considerations and the impact of premature menopause.* Cancer Treat Rev, 2017. **55**: p. 26-35.

143. Conte, B., F. Poggio, and L. Del Mastro, *Luteininzing hormone releasing hormones analogs in combination with tamoxifen for the adjuvant treatment of premenopausal women with hormone receptor positive breast cancer.* Expert Opin Pharmacother, 2017. **18**(13): p. 1357-1362.

144. Institute of Cancer Research, U.K. *Trial of Perioperative Endocrine Therapy - Individualising Care (POETIC).* [cited 2018 1 Jan 2018]; Available from: https://clinicaltrials.gov/ct2/show/NCT02338310?term=POETIC&cond=Breast+Cancer&rank=1.

145. Tubiana-Hulin, M., et al., *Response to neoadjuvant chemotherapy in lobular and ductal breast carcinomas: a retrospective study on 860 patients from one institution.* Ann Oncol, 2006. **17**(8): p. 1228-33.

146. Katz, A., et al., *Primary systemic chemotherapy of invasive lobular carcinoma of the breast.* Lancet Oncol, 2007. **8**(1): p. 55-62.

147. Lips, E.H., et al., *Lobular histology and response to neoadjuvant chemotherapy in invasive breast cancer.* Breast Cancer Res Treat, 2012. **136**(1): p. 35-43.

148. Marmor, S., et al., *Relative effectiveness of adjuvant chemotherapy for invasive lobular compared with invasive ductal carcinoma of the breast.* Cancer, 2017. **123**(16): p. 3015-3021.

149. Xu, H., et al., *Recent advances of highly selective CDK4/6 inhibitors in breast cancer.* J Hematol Oncol, 2017. **10**(1): p. 97.

150. Finn, R.S., et al., *Palbociclib and Letrozole in Advanced Breast Cancer.* N Engl J Med, 2016. **375**(20): p. 1925-1936.

151. Massacesi, C., et al., *PI3K inhibitors as new cancer therapeutics: implications for clinical trial design.* Onco Targets Ther, 2016. **9**: p. 203-10.

152. Piccart, M., et al., *Everolimus plus exemestane for hormone-receptor-positive, human epidermal growth factor receptor-2-negative advanced breast cancer: overall survival results from BOLERO-2dagger.* Ann Oncol, 2014. **25**(12): p. 2357-62.

153. Chung, M.A., et al., *Optimal surgical treatment of invasive lobular carcinoma of the breast.* Ann Surg Oncol, 1997. **4**(7): p. 545-50.

154. Hussien, M., et al., *Surgical treatment for invasive lobular carcinoma of the breast.* Breast, 2003. **12**(1): p. 23-35.

155. Korhonen, T., H. Huhtala, and K. Holli, *A comparison of the biological and clinical features of invasive lobular and ductal carcinomas of the breast.* Breast Cancer Res Treat, 2004. **85**(1): p. 23-9.

156. Warneke, J., et al., *Lumpectomy and radiation treatment for invasive lobular carcinoma of the breast.* Am J Surg, 1996. **172**(5): p. 496-500.

157. Van Limbergen, E., et al., *Local control of operable breast cancer after radiotherapy alone.* Eur J Cancer, 1990. **26**(6): p. 674-9.

158. Poortmans, P.M., M. Bollet, and E. Van Limbergen, *Infiltrating lobular breast cancer: truly a separate entity! Consequences for radiation therapy.* Radiother Oncol, 2013. **106**(1): p. 1-4.

159. Voogd, A.C., et al., *Differences in risk factors for local and distant recurrence after breast-conserving therapy or mastectomy for stage I and II breast cancer: pooled results of two large European randomized trials.* J Clin Oncol, 2001. **19**(6): p. 1688-97.

160. Lamouille, S., J. Xu, and R. Derynck, *Molecular mechanisms of epithelial-mesenchymal transition.* Nat Rev Mol Cell Biol, 2014. **15**(3): p. 178-96.

161. Ye, X. and R.A. Weinberg, *Epithelial-Mesenchymal Plasticity: A Central Regulator of Cancer Progression.* Trends Cell Biol, 2015. **25**(11): p. 675-86.

162. Obrink, B., *Epithelial cell adhesion molecules.* Exp Cell Res, 1986. **163**(1): p. 1-21.

163. Kalluri, R. and R.A. Weinberg, *The basics of epithelial-mesenchymal transition.* J Clin Invest, 2009. **119**(6): p. 1420-8.

164. Canel, M., et al., *E-cadherin-integrin crosstalk in cancer invasion and metastasis.* J Cell Sci, 2013. **126**(Pt 2): p. 393-401.

165. Luqmani, Y.A. and N. Alam-Eldin, *Overcoming Resistance to Endocrine Therapy in Breast Cancer: New Approaches to a Nagging Problem.* Med Princ Pract, 2016. **25 Suppl 2**: p. 28-40.

166. Leung, E., et al., *Comparison of the effects of the PI3K/mTOR inhibitors NVP-BEZ235 and GSK2126458 on tamoxifen-resistant breast cancer cells.* Cancer Biol Ther, 2011. **11**(11): p. 938-46.

167. Joo, Y.K.*e.a.*, *Wnt pathway is affected by endocrine therapy in breast carcinomas.* Basic and Applied Pathology, 2011. **4**: p. 7.

168. Won, H.S., et al., *Inhibition of beta-Catenin to Overcome Endocrine Resistance in Tamoxifen-Resistant Breast Cancer Cell Line.* PLoS One, 2016. **11**(5): p. e0155983.

169. Theveneau, E. and R. Mayor, *Neural crest delamination and migration: from epithelium-to-mesenchyme transition to collective cell migration.* Dev Biol, 2012. **366**(1): p. 34-54.

170. Hugo, H., et al., *Epithelial--mesenchymal and mesenchymal--epithelial transitions in carcinoma progression.* J Cell Physiol, 2007. **213**(2): p. 374-83.

171. Pai, K., P. Baliga, and B.L. Shrestha, *E-cadherin expression: a diagnostic utility for differentiating breast carcinomas with ductal and lobular morphologies.* J Clin Diagn Res, 2013. **7**(5): p. 840-4.

172. Hiraguri, S., et al., *Mechanisms of inactivation of E-cadherin in breast cancer cell lines.* Cancer Res, 1998. **58**(9): p. 1972-7.

173. Da Silva, L., et al., *Aberrant expression of E-cadherin in lobular carcinomas of the breast.* Am J Surg Pathol, 2008. **32**(5): p. 773-83.

174. McCart Reed, A.E., et al., *An epithelial to mesenchymal transition programme does not usually drive the phenotype of invasive lobular carcinomas.* J Pathol, 2016. **238**(4): p. 489-94.

175. You, D., et al., *Fibronectin expression is upregulated by PI-3K/Akt activation in tamoxifen-resistant breast cancer cells.* BMB Rep, 2017. **50**(12): p. 615-620.

176. Liu, H., et al., *Tamoxifen-resistant breast cancer cells possess cancer stem-like cell properties.* Chin Med J (Engl), 2013. **126**(16): p. 3030-4.

177. Wang, Y., et al., *The Role of Snail in EMT and Tumorigenesis.* Curr Cancer Drug Targets, 2013. **13**(9): p. 963-972.

178. Ferrari-Amorotti, G., et al., *Inhibiting interactions of lysine demethylase LSD1 with snail/slug blocks cancer cell invasion.* Cancer Res, 2013. **73**(1): p. 235-45.

179. Dhasarathy, A., M. Kajita, and P.A. Wade, *The transcription factor snail mediates epithelial to mesenchymal transitions by repression of estrogen receptor-alpha.* Mol Endocrinol, 2007. **21**(12): p. 2907-18.

180. Yang, J., et al., *Twist, a master regulator of morphogenesis, plays an essential role in tumor metastasis.* Cell, 2004. **117**(7): p. 927-39.

181. Jambal, P., et al., *Estrogen switches pure mucinous breast cancer to invasive lobular carcinoma with mucinous features.* Breast Cancer Res Treat, 2013. **137**(2): p. 431-48.

182. Christgen, M., et al., *Comprehensive genetic and functional characterization of IPH-926: a novel CDH1-null tumour cell line from human lobular breast cancer.* J Pathol, 2009. **217**(5): p. 620-32.

183. Riggins, R.B., et al., *ERRgamma mediates tamoxifen resistance in novel models of invasive lobular breast cancer.* Cancer Res, 2008. **68**(21): p. 8908-17.

184. Cailleau, R., M. Olive, and Q.V. Cruciger, *Long-term human breast carcinoma cell lines of metastatic origin: preliminary characterization.* In Vitro, 1978. **14**(11): p. 911-5.

185. Sikora, M.J., et al., *WNT4 mediates estrogen receptor signaling and endocrine resistance in invasive lobular carcinoma cell lines.* Breast Cancer Res, 2016. **18**(1): p. 92.

186. Michaut, M., et al., *Integration of genomic, transcriptomic and proteomic data identifies two biologically distinct subtypes of invasive lobular breast cancer.* Sci Rep, 2016. **6**: p. 18517.

187. Ross-Innes, C.S., et al., *Differential oestrogen receptor binding is associated with clinical outcome in breast cancer.* Nature, 2012. **481**(7381): p. 389-93.

188. Robinson, J.T., et al., *Integrative genomics viewer.* Nat Biotechnol, 2011. **29**(1): p. 24-6.

189. Yu, Q., B.P. Zhou, and Y. Wu, *The regulation of snail: on the ubiquitin edge.* Cancer Cell Microenviron, 2017. **4**(2).

190. Das, A.T., L. Tenenbaum, and B. Berkhout, *Tet-On Systems For Doxycycline-inducible Gene Expression.* Curr Gene Ther, 2016. **16**(3): p. 156-67.

191. Alexeyev, M.F., et al., *A retro-lentiviral system for doxycycline-inducible gene expression and gene knockdown in cells with limited proliferative capacity.* Mol Biol Rep, 2010. **37**(4): p. 1987-91.

192. Hsu, P.D., E.S. Lander, and F. Zhang, *Development and applications of CRISPR-Cas9 for genome engineering.* Cell, 2014. **157**(6): p. 1262-78.

193. Vega, S., et al., *Snail blocks the cell cycle and confers resistance to cell death.* Genes Dev, 2004. **18**(10): p. 1131-43.

194. Lee, G.Y., et al., *Three-dimensional culture models of normal and malignant breast epithelial cells.* Nat Methods, 2007. **4**(4): p. 359-65.

195. Zhou, W., et al., *Snail contributes to the maintenance of stem cell-like phenotype cells in human pancreatic cancer.* PLoS One, 2014. **9**(1): p. e87409.

196. Ye, X., et al., *Distinct EMT programs control normal mammary stem cells and tumour-initiating cells.* Nature, 2015. **525**(7568): p. 256-60.

197. Moreb, J.S., *Aldehyde dehydrogenase as a marker for stem cells.* Curr Stem Cell Res Ther, 2008. **3**(4): p. 237-46.

198. Fillmore, C. and C. Kuperwasser, *Human breast cancer stem cell markers CD44 and CD24: enriching for cells with functional properties in mice or in man?* Breast Cancer Res, 2007. **9**(3): p. 303.

199. Manuel Iglesias, J., et al., *Mammosphere formation in breast carcinoma cell lines depends upon expression of E-cadherin.* PLoS One, 2013. **8**(10): p. e77281.

200. Muenst, S.*e.a.*, *Nuclear Expression of Snail Is an Independent Negative Prognostic Factor in Human Breast Cancer.* Disease Markers, 2013. **35**: p. 7.

201. Lin, T., et al., *Requirement of the histone demethylase LSD1 in Snai1-mediated transcriptional repression during epithelial-mesenchymal transition.* Oncogene, 2010. **29**(35): p. 4896-904.

202. Borowicz, S., et al., *The soft agar colony formation assay.* J Vis Exp, 2014(92): p. e51998.

203. Lau, M.T., C. Klausen, and P.C. Leung, *E-cadherin inhibits tumor cell growth by suppressing PI3K/Akt signaling via beta-catenin-Egr1-mediated PTEN expression.* Oncogene, 2011. **30**(24): p. 2753-66.

204. Christgen, M. and P. Derksen, *Lobular breast cancer: molecular basis, mouse and cellular models.* Breast Cancer Res, 2015. **17**: p. 16.

205. Haraguchi, M., M. Sato, and M. Ozawa, *CRISPR/Cas9n-Mediated Deletion of the Snail 1Gene (SNAI1) Reveals Its Role in Regulating Cell Morphology, Cell-Cell Interactions, and Gene Expression in Ovarian Cancer (RMG-1) Cells.* PLoS One, 2015. **10**(7): p. e0132260.

206. Lin, Y., et al., *The SNAG domain of Snail1 functions as a molecular hook for recruiting lysine-specific demethylase 1.* Embo j, 2010. **29**(11): p. 1803-16.

207. Maiques-Diaz, A. and T.C. Somervaille, *LSD1: biologic roles and therapeutic targeting.* Epigenomics, 2016. **8**(8): p. 1103-16.

208. Zheng, Y.C., et al., *Irreversible LSD1 Inhibitors: Application of Tranylcypromine and Its Derivatives in Cancer Treatment.* Curr Top Med Chem, 2016. **16**(19): p. 2179-88.

209. Hino, S., K. Kohrogi, and M. Nakao, *Histone demethylase LSD1 controls the phenotypic plasticity of cancer cells.* Cancer Sci, 2016. **107**(9): p. 1187-92.

210. Bennesch, M.A., et al., *LSD1 engages a corepressor complex for the activation of the estrogen receptor alpha by estrogen and cAMP.* Nucleic Acids Res, 2016. **44**(18): p. 8655-8670.

211. Gillet, J.P., S. Varma, and M.M. Gottesman, *The clinical relevance of cancer cell lines.* J Natl Cancer Inst, 2013. **105**(7): p. 452-8.

212. van Staveren, W.C., et al., *Human cancer cell lines: Experimental models for cancer cells in situ? For cancer stem cells?* Biochim Biophys Acta, 2009. **1795**(2): p. 92-103.

213. Maqsood, M.I., et al., *Immortality of cell lines: challenges and advantages of establishment.* Cell Biol Int, 2013. **37**(10): p. 1038-45.

214. Borrell, B., *How accurate are cancer cell lines?* Nature, 2010. **463**(7283): p. 858.

215. Nelson-Rees, W.A., D.W. Daniels, and R.R. Flandermeyer, *Cross-contamination of cells in culture.* Science, 1981. **212**(4493): p. 446-52.

216. Lucey, B.P., W.A. Nelson-Rees, and G.M. Hutchins, *Henrietta Lacks, HeLa cells, and cell culture contamination.* Arch Pathol Lab Med, 2009. **133**(9): p. 1463-7.

217. Geraghty, R.J., et al., *Guidelines for the use of cell lines in biomedical research.* Br J Cancer, 2014. **111**(6): p. 1021-46.

218. Gey. G. O., C., W. D., & Kubicek, M. T., *Tissue Culture Studies of the Proliferative Capacity of Cervical Carcinoma and Normal Epithelium.* Cancer Res, 1952. **12**: p. 2.

219. Ambrose, C.T., *The Tissue Culture Laboratory of Dr. George Otto Gey 60 yrs ago as recalled by a former student.* In Vitro Cell Dev Biol Anim, 2017. **53**(5): p. 467-473.

220. Hayflick, L., *THE LIMITED IN VITRO LIFETIME OF HUMAN DIPLOID CELL STRAINS.* Exp Cell Res, 1965. **37**: p. 614-36.

221. Sager, R., *Senescence as a mode of tumor suppression.* Environ Health Perspect, 1991. **93**: p. 59-62.

222. Campisi, J., *Aging, cellular senescence, and cancer.* Annu Rev Physiol, 2013. **75**: p. 685-705.

223. Sano, M.E.S., L. W., *The Behavior of Tumor Cells in Tissue Culture Subjected to Reduced Temperatures.* Cancer Res, 1942. **2**: p. 7.

224. Eagle, H., *Nutrition needs of mammalian cells in tissue culture.* Science, 1955. **122**(3168): p. 501-14.

225. Nema, R.K., S., *An animal cell culture: Advance technology for modern research.* Adv Biosci Biotechnol, 2012. **3**: p. 7.

226. Masters, J.R., *HeLa cells 50 years on: the good, the bad and the ugly.* Nat Rev Cancer, 2002. **2**(4): p. 315-9.

227. Beskow, L.M., *Lessons from HeLa Cells: The Ethics and Policy of Biospecimens.* Annu Rev Genomics Hum Genet, 2016. **17**: p. 395-417.

228. Caulfield, T. and B. Murdoch, *Genes, cells, and biobanks: Yes, there's still a consent problem.* PLoS Biol, 2017. **15**(7): p. e2002654.

229. Lasfargues, E.Y. and L. Ozzello, *Cultivation of human breast carcinomas.* J Natl Cancer Inst, 1958. **21**(6): p. 1131-47.

230. Lacroix, M. and G. Leclercq, *Relevance of breast cancer cell lines as models for breast tumours: an update.* Breast Cancer Res Treat, 2004. **83**(3): p. 249-89.

231. Neve, R.M., et al., *A collection of breast cancer cell lines for the study of functionally distinct cancer subtypes.* Cancer Cell, 2006. **10**(6): p. 515-27.

232. Kao, J., et al., *Molecular profiling of breast cancer cell lines defines relevant tumor models and provides a resource for cancer gene discovery.* PLoS One, 2009. **4**(7): p. e6146.

233. Dai, X., et al., *Breast Cancer Cell Line Classification and Its Relevance with Breast Tumor Subtyping.* J Cancer, 2017. **8**(16): p. 3131-3141.

234. Whitescarver, J., *Proceedings: Problems of in vitro culture of human mammary tumor cells.* J Invest Dermatol, 1974. **63**(1): p. 58-64.

235. Yao, T. and Y. Asayama, *Animal-cell culture media: History, characteristics, and current issues.* Reprod Med Biol, 2017. **16**(2): p. 99-117.

236. Cailleau, R., et al., *Breast tumor cell lines from pleural effusions.* J Natl Cancer Inst, 1974. **53**(3): p. 661-74.

237. Engel, L.W. and N.A. Young, *Human breast carcinoma cells in continuous culture: a review.* Cancer Res, 1978. **38**(11 Pt 2): p. 4327-39.

238. Reis-Filho, J.S., et al., *FGFR1 emerges as a potential therapeutic target for lobular breast carcinomas.* Clin Cancer Res, 2006. **12**(22): p. 6652-62.

239. Hollestelle, A., et al., *Loss of E-cadherin is not a necessity for epithelial to mesenchymal transition in human breast cancer.* Breast Cancer Res Treat, 2013. **138**(1): p. 47-57.

240. McLeskey, S.W., et al., *MDA-MB-134 breast carcinoma cells overexpress fibroblast growth factor (FGF) receptors and are growth-inhibited by FGF ligands.* Cancer Res, 1994. **54**(2): p. 523-30.

241. Behbod, F., et al., *An intraductal human-in-mouse transplantation model mimics the subtypes of ductal carcinoma in situ.* Breast Cancer Res, 2009. **11**(5): p. R66.

242. Kittrell, F., et al., *Mouse Mammary Intraductal (MIND) Method for Transplantation of Patient Derived Primary DCIS Cells and Cell Lines.* Bio Protoc, 2016. **6**(5).

243. Reddel, R.R., et al., *Differential sensitivity of human breast cancer cell lines to the growth-inhibitory effects of tamoxifen.* Cancer Res, 1985. **45**(4): p. 1525-31.

244. Reddel, R.R. and R.L. Sutherland, *Effects of pharmacological concentrations of estrogens on proliferation and cell cycle kinetics of human breast cancer cell lines in vitro.* Cancer Res, 1987. **47**(20): p. 5323-9.

245. Castles, C.G., et al., *Coexpression of wild-type and variant oestrogen receptor mRNAs in a panel of human breast cancer cell lines.* Br J Cancer, 1995. **71**(5): p. 974-80.

246. Hollestelle, A., et al., *Four human breast cancer cell lines with biallelic inactivating alpha-catenin gene mutations.* Breast Cancer Res Treat, 2010. **122**(1): p. 125-33.

247. Ethier, S.P., et al., *Differential isolation of normal luminal mammary epithelial cells and breast cancer cells from primary and metastatic sites using selective media.* Cancer Res, 1993. **53**(3): p. 627-35.

248. Turner, N., et al., *FGFR1 amplification drives endocrine therapy resistance and is a therapeutic target in breast cancer.* Cancer Res, 2010. **70**(5): p. 2085-94.

249. Harrell, J.C., T.M. Shroka, and B.M. Jacobsen, *Estrogen induces c-Kit and an aggressive phenotype in a model of invasive lobular breast cancer.* Oncogenesis, 2017. **6**(11): p. 396.

250. Christgen, M., et al., *IPH-926 lobular breast cancer cells are triple-negative but their microarray profile uncovers a luminal subtype.* Cancer Sci, 2013. **104**(12): p. 1726-30.

251. Micci, F., M.R. Teixeira, and S. Heim, *Complete cytogenetic characterization of the human breast cancer cell line MA11 combining G-banding, comparative genomic hybridization, multicolor fluorescence in situ hybridization, RxFISH, and chromosome-specific painting.* Cancer Genet Cytogenet, 2001. **131**(1): p. 25-30.

252. Gazdar, A.F., et al., *Characterization of paired tumor and non-tumor cell lines established from patients with breast cancer.* Int J Cancer, 1998. **78**(6): p. 766-74.

253. Dobrolecki, L.E., et al., *Patient-derived xenograft (PDX) models in basic and translational breast cancer research.* Cancer Metastasis Rev, 2016. **35**(4): p. 547-573

.
254. Liu, X., et al., *ROCK inhibitor and feeder cells induce the conditional reprogramming of epithelial cells.* Am J Pathol, 2012. **180**(2): p. 599-607.

255. Agarwal, S. and D.L. Rimm, *Making every cell like HeLa a giant step for cell culture.* Am J Pathol, 2012. **180**(2): p. 443-5.

256. Mao, Y., et al., *Stromal cells in tumor microenvironment and breast cancer.* Cancer Metastasis Rev, 2013. **32**(1-2): p. 303-15.

257. Jezierska-Drutel, A., S.A. Rosenzweig, and C.A. Neumann, *Role of oxidative stress and the microenvironment in breast cancer development and progression.* Adv Cancer Res, 2013. **119**: p. 107-25.

258. Choi, H.I., et al., *Peroxiredoxin 5 Protects TGF-beta Induced Fibrosis by Inhibiting Stat3 Activation in Rat Kidney Interstitial Fibroblast Cells.* PLoS One, 2016. **11**(2): p. e0149266.

259. Yan, D. and H. Dai, *[FOLFOX regimen in the patients with locally advanced or metastatic gastric cancer]*. Zhonghua Zhong Liu Za Zhi, 2009. **31**(3): p. 217-9.

260. Stathopoulos, G.P., et al., *Paclitaxel and carboplatin in pretreated advanced gastric cancer: a phase II study.* Oncol Rep, 2002. **9**(1): p. 89-92.

261. Brown-Glaberman, U. and A.T. Stopeck, *Impact of denosumab on bone mass in cancer patients.* Clin Pharmacol, 2013. **5**: p. 117-29.

262. Steger, G.G. and R. Bartsch, *Denosumab for the treatment of bone metastases in breast cancer: evidence and opinion.* Ther Adv Med Oncol, 2011. **3**(5): p. 233-43.

263. Trzpis, M., et al., *Epithelial cell adhesion molecule: more than a carcinoma marker and adhesion molecule.* Am J Pathol, 2007. **171**(2): p. 386-95.

264. Harigopal, M., et al., *Aberrant E-cadherin staining patterns in invasive mammary carcinoma.* World J Surg Oncol, 2005. **3**: p. 73.

265. Choi, Y.J., et al., *Interobserver variability and aberrant E-cadherin immunostaining of lobular neoplasia and infiltrating lobular carcinoma.* Mod Pathol, 2008. **21**(10): p. 1224-37.

266. Gusterson, B.A., et al., *Basal cytokeratins and their relationship to the cellular origin and functional classification of breast cancer.* Breast Cancer Res, 2005. **7**(4): p. 143-8.

267. Fadare, O., S.A. Wang, and D. Hileeto, *The expression of cytokeratin 5/6 in invasive lobular carcinoma of the breast: evidence of a basal-like subset?* Hum Pathol, 2008. **39**(3): p. 331-6.

268. Khilko, N., et al., *Invasive Lobular Carcinomas Do Not Express Basal Cytokeratin Markers CK5/6, CK14 and CK17.* Breast Cancer (Auckl), 2010. **4**: p. 49-55.

269. Engstrom, M.J., M. Valla, and A.M. Bofin, *Basal markers and prognosis in luminal breast cancer.* Breast Cancer Res Treat, 2017. **163**(2): p. 207-217.

270. Hug, N., D. Longman, and J.F. Caceres, *Mechanism and regulation of the nonsense-mediated decay pathway.* Nucleic Acids Res, 2016. **44**(4): p. 1483-95.

271. Shaw, J.A. and J. Stebbing, *Circulating free DNA in the management of breast cancer.* Ann Transl Med, 2014. **2**(1): p. 3.

272. Yersal, O. and S. Barutca, *Biological subtypes of breast cancer: Prognostic and therapeutic implications.* World J Clin Oncol, 2014. **5**(3): p. 412-24.

273. Dasari, S. and P.B. Tchounwou, *Cisplatin in cancer therapy: molecular mechanisms of action.* Eur J Pharmacol, 2014. **740**: p. 364-78.

274. Crowder, R.J., et al., *PIK3CA and PIK3CB inhibition produce synthetic lethality when combined with estrogen deprivation in estrogen receptor-positive breast cancer.* Cancer Res, 2009. **69**(9): p. 3955-62.

275. Pongas, G. and T. Fojo, *BEZ235: When Promising Science Meets Clinical Reality.* Oncologist, 2016. **21**(9): p. 1033-4.

276. Paoli, P., E. Giannoni, and P. Chiarugi, *Anoikis molecular pathways and its role in cancer progression.* Biochim Biophys Acta, 2013. **1833**(12): p. 3481-3498.

277. Liao, Y. and M.C. Hung, *Physiological regulation of Akt activity and stability.* Am J Transl Res, 2010. **2**(1): p. 19-42.

278. Vicier, C., et al., *Clinical development of mTOR inhibitors in breast cancer.* Breast Cancer Res, 2014. **16**(1): p. 203.

279. Mahmud, N., et al., *Metastatic lobular breast carcinoma mimicking primary signet ring adenocarcinoma in a patient with a suspected CDH1 mutation.* J Clin Oncol, 2015. **33**(4): p. e19-21.

280. Doria, M.T., et al., *Gastric metastasis as the first manifestation of an invasive lobular carcinoma of the breast.* Autops Case Rep, 2015. **5**(3): p. 49-53.

281. Groner, B. and A. Weiss, *Targeting survivin in cancer: novel drug development approaches.* BioDrugs, 2014. **28**(1): p. 27-39.

282. Adiconis, X., et al., *Comparative analysis of RNA sequencing methods for degraded or low-input samples.* Nat Methods, 2013. **10**(7): p. 623-9.

283. Benjamini, Y. and T.P. Speed, *Summarizing and correcting the GC content bias in high-throughput sequencing.* Nucleic Acids Res, 2012. **40**(10): p. e72.

284. Conesa, A., et al., *A survey of best practices for RNA-seq data analysis.* Genome Biol, 2016. **17**: p. 13.